An Investigation of Chromosomal Instability Survival Mechanisms in Cancer

Alvin Jun Xing Lee

University College London

and

Cancer Research UK London Research Institute

PhD Supervisor: Dr Charles Swanton

A thesis submitted for the degree of

Doctor of Philosophy

University College London

September 2011

Declaration

I, Alvin Lee, confirm that the work presented in this thesis is my own. Where information has been derived from other sources, I confirm that this has been indicated in the thesis.

Abstract

Chromosomal instability (CIN) describes ongoing numerical and structural chromosomal aberrations in cancer cells, leading to intra-tumour heterogeneity and is frequently associated with polyploidy and aneuploidy. CIN is a frequent event in solid tumours and previous evidence has implicated CIN with acquired multidrug resistance, intrinsic taxane resistance and poor patient prognosis. In this thesis, I have attempted to explore mechanisms required for the initiation of CIN and the tolerance of this pattern of genome instability.

Firstly, I have attempted to identify clinically relevant therapeutics that may have specific activity in CIN+ tumour cell lines. Focusing on a panel of colorectal cancer cell lines, classified as either CIN+ or CIN-, and treating them individually with kinase inhibitor and cytotoxic agent libraries, I demonstrated that CIN+ cell lines displayed significant intrinsic multidrug resistance. Next, I addressed if specific means to target CIN+ cells could be identified through pharmacological and RNA interference (RNAi) screens. No compounds were observed to be preferentially cytotoxic towards CIN+ cells in the pharmacological screen. A whole genome RNAi screen was performed to identify CIN+ specific survival pathways using isogenic cell line models of CIN. No genes were identified that conferred preferential cell death when silenced in CIN+ cells, despite sufficient statistical power to detect such targets. Using integrative genomics techniques and cell cycle data from this RNAi screen, I endeavoured to identify clinically relevant initiators of aneuploidy in colorectal cancer, that revealed both known and potential novel regulators of polyploidy.

Finally, I endeavoured to identify a mechanistic basis for the taxane-sensitising phenotype associated with the silencing of the ceramide transporter, CERT, which may reveal means to target CIN+ cells. I demonstrated that CERT silencing sensitises paclitaxel-treated cells to cell death in a LAMP2-dependent manner that is associated with autophagy flux and may target death of multinucleated cells specifically.

Acknowledgement

I would like to thank my PhD supervisor, Dr Charlie Swanton, for his guidance, enthusiasm, and mentorship. I would also like to thank him for taking me on as his first PhD student and for the amount of support he has given me throughout.

I thank my thesis committee, Dr Gordon Peters and Dr Sharon Tooze for their advice and supervision. I would also like to thank Prof. Julian Downward, Prof Ian Tomlinson and Dr Julie Cooper for supervision during the initial part of my PhD.

Thank you to all members of my laboratory, the Translational Cancer Therapeutics Laboratory, for help and support in experiments, discussions and writing – Andrew Rowan, Rebecca Burrell, David Endesfelder, Sarah McClelland, Marco Gerlinger, Claudio Santos and Nadeem Shaikh in particular have greatly contributed to the work presented here.

It would not have been possible to do this work without the support of the core services in the Cancer Research UK London Research Institute, the High-Throughput Screening Facility, Bioinformatics and Biostatistics (Philip East and Stuart Horswell in particular), the Equipment Park, Electron Microscopy and the FACS services. I would also like to take this opportunity to thank my many collaborators, whose work has been acknowledged in each relevant section.

I am grateful for the funding and research opportunity provided by Cancer Research UK. I would also like to thank the UCL MB PhD programme and Prof Gordon Stewart in particular, for his support and guidance.

Last but not least, I would like to thank my friends and family members who have supported me throughout.

Table of Contents

Abstract **3**
Acknowledgement **4**
Table of Contents **5**
Table of figures **8**
List of tables **11**
Abbreviations **12**
Chapter 1. Introduction **13**
1.1 Functional genomic approaches implicate CIN and CERT as pathways that may be exploited to limit drug resistance **13**
1.2 Regulation of chromosome segregation **16**
1.2.1 Entry into mitosis 17
1.2.2 The Anaphase Promoting Complex/Cyclosome (APC/C) 18
1.2.3 The Spindle Assembly Checkpoint (SAC) 19
1.2.4 The DNA damage checkpoint 22
1.3 Chromosomal Instability **22**
1.3.1 Polyploidy, tetraploidy, aneuploidy and CIN 24
1.3.2 Measuring Chromosomal Instability 26
1.3.3 Mechanisms contributing to CIN 27
1.3.4 Polyploidy and multinucleation as an intermediate state towards CIN 37
1.3.5 Adaptability of CIN/Aneuploid Cells 40
1.3.6 CIN and drug resistance 42
1.3.7 Extreme CIN and tumour suppression 45
1.3.8 CIN as a targetable phenotype 47
1.4 CERT and Ceramide mediated drug sensitivity **49**
1.4.1 CERT and Autophagy 51
1.4.2 Paclitaxel response and the lysosome 54
1.5 Conclusions **55**
Chapter 2. Materials and Methods **57**
2.1 Kinase inhibitor and cytotoxic agent screens to identify CIN survival mechanisms **57**
2.1.1 Cell lines 57
2.1.2 Calbiochem kinase inhibitor library and 5-FU screen 60
2.1.3 Anti-Cancer agent screen 61
2.1.4 Cell proliferation assay 61
2.1.5 Meta-Analysis of CIN outcome 61
2.1.6 Statistical methods 62
2.2 Whole genome RNAi screens for regulators of CIN survival and ploidy **63**
2.2.1 Cell culture and siRNA transfection protocol 63
2.2.2 Statistical normalisation of screening data 64
2.2.3 Statistical analysis of screen variance 65
2.2.4 Defining significant and consistent regions of copy number alteration in cell lines 66
2.2.5 Live cell imaging 67
2.3 CERT multidrug sensitisation pathway **67**

2.3.1 Cell culture and siRNA transfection protocol 67
2.3.2 Fluorescent ceramide transport analysis 68
2.3.3 Lipid extraction, liquid chromatography / mass spectrometry (LC/MS) analyses of ceramide 69
2.3.4 CERT microarray expression profiling 70
2.3.5 qPCR validation of microarray data 71
2.3.6 Drug response assays 73
2.3.7 LC3 immunoblotting 73
2.3.8 Immunofluorescence microscopy 75
2.3.9 Live cell imaging 76
2.3.10 Tissue Microarray cohort 76
2.3.11 Electron microscopy 78
2.3.12 CERT gene expression in breast cancer datasets 79
Chapter 3. Chromosomal instability confers intrinsic multidrug resistance 80
3.1 Introduction 80
3.2 Results 80
3.2.1 Classification of CIN+ cell lines and relationship with ploidy status and Structural Chromosomal Complexity 80
3.2.2 CIN+ status is associated with intrinsic multidrug resistance 84
3.2.3 Somatic mutation status and drug sensitivity 92
3.2.4 Isogenic CIN+ CRC cell lines display intrinsic multidrug resistance 95
3.2.5 CIN+ not tetraploidy is associated with multidrug resistance 101
3.2.6 CIN+ CRC cell lines do not demonstrate increased sensitivity towards AICAR and 17-AAG 105
3.2.7 Relationship between CIN status and benefit from cytotoxic therapy 111
3.3 Discussion 118
3.4 Conclusion 120
Chapter 4. Unbiased whole-genome RNAi screens to identify survival mechanism in CIN+ cancer 122
4.1 Introduction 122
4.2 Results 124
4.2.1 Optimisation of screening parameters 124
4.2.2 The screen 131
4.2.3 Validation of candidate genes for on-target effects 134
4.2.4 Validation of candidate genes for differential lethality effects 136
4.2.5 Reselection of candidate genes and validation 141
4.2.6 Statistical analysis of noise within the system and reproducibility of results 146
4.2.7 Retrospective power analysis of whole genome RNAi screen 149
4.3 Discussion 151
4.3.1 Summary of screen results 151
4.3.2 Estimation of noise component in genome wide siRNA screen and validation experiments 153
4.3.3 Suitability of siRNA screening approach for synthetic lethality 153
4.3.4 Suitability of HCT116 *MAD2+/-* cell line as a model of CIN+ synthetic lethality 155
4.3.5 The CIN model system and the technical challenges of siRNA screening may lead to yield poor validation rate 156

4.3.6 Comparison with screens performed in yeast to identify polyploidy and aneuploidy survival regulators 157
4.4 Conclusion 158
Chapter 5. Identification of novel ploidy regulators with relevance to CIN+ Colorectal Cancer 159
5.1 Introduction 159
5.2 Results 160
5.2.1 Whole Genome RNAi screen identifies potential tumour relevant genes that are involved in the generation or maintenance of polyploidy 160
5.2.2 Validation of candidate genes for on-target effects 166
5.2.3 Live cell microscopy analysis reveals potential mechanisms for the generation of polyploid cells 168
5.3 Discussion 175
5.4 Conclusion 179
Chapter 6. CERT predicts chemotherapy benefit and mediates cytotoxic and polyploid-specific cancer cell death through autophagy induction ... 180
6.1 Introduction 180
6.2 Results 181
6.2.1 CERT depletion results in ceramide accumulation 181
6.2.2 Transcriptomic analysis reveals a CERT-specific response 184
6.2.3 CERT depletion induces LAMP2 which is required for paclitaxel cell death 188
6.2.4 Ceramide treatment on the background of CERT silencing induces a specific transcriptional response 191
6.2.5 CERT depletion and paclitaxel exposure initiates an autophagy response . 191
6.2.6 CERT-mediated paclitaxel sensitisation is LAMP2 dependent 196
6.2.7 CERT depletion induces localisation of LAMP2/LC3 and the accumulation of lysosomal structures in the presence of paclitaxel 198
6.2.8 Relationship of paclitaxel response with autophagy gene expression 203
6.2.9 CERT depletion promotes mitotic catastrophe that is LAMP2 dependent . 205
6.2.10 CERT is overexpressed in HER2+ primary breast cancer 207
6.2.11 CERT depletion sensitises HER2+ breast cancer cell lines to cytotoxics and induces autophagic flux 213
6.2.12 CERT expression is associated with survival outcome in patients with primary breast cancer treated with adjuvant chemotherapy. 218
6.3 Discussion 223
6.4 Conclusion 226
Chapter 7. Discussion 227
Chapter 8. Appendix 233
8.1 RNAi-mediated functional analysis of pathways influencing cancer cell drug resistance 233
8.2 Chromosomal instability confers intrinsic multidrug resistance 234
8.3 Chromosomal instability determines taxane response 235
8.4 CERT predicts chemotherapy benefit and mediates cytotoxic and polyploid-specific cancer cell death through autophagy induction 236
8.5 Concordance of exon array and real-time PCR assessment of gene expression following cancer cell cytotoxic drug exposure 237
Reference List 238

Table of figures

Figure 1 Types of kinetochore-microtubule attachments and activation of the SAC 21
Figure 2 Ploidy and CIN 25
Figure 3 Premature sister chromatid seperation 29
Figure 4 Multipolar spindle formation leads to merotely.....35
Figure 5 Merotely leads to errors in chromosome segregation 36
Figure 6 Errors in cell division may result in polyploid cell formation 39
Figure 7 Maturation of autophagosomes and fusion with lysosomes to form autolysosomes 53
Figure 8 Ploidy and structural chromosomal complexity analysis of cell lines 83
Figure 9 10 CIN+ CRC cell lines were treated with 160 kinase inhibitors at 10μM and 1μM for 72 hours.....86
Figure 10 18 CIN+ and 9 CIN- CRC cell lines were treated with 160 kinase inhibitors at 10μM for 72 hours.....87
Figure 11 Heatmap of 18 CIN+ and 9 CIN- CRC cell lines were treated with 160 kinase inhibitors at 10μM for 72 hours 88
Figure 12 Analysis of impact of proliferation rate on response to kinase inhibitors. 91
Figure 13 Analysis of somatic mutation status and response to kinase inhibitors 94
Figure 14 Isogenic CIN+ and CIN- cell lines were treated with kinase inhibitors 97
Figure 15 Isogenic CIN+ and CIN- cell lines were treated with cytotoxic agent panel..98
Figure 16 Heatmap of isogenic CIN+ and CIN- cell lines were treated with cytotoxic agent panel.....99
Figure 17 Microsatellite PCR fragment analysis (marker 15_XVII) 100
Figure 18 Isogenic tetraploid and diploid HCT116 cell lines were treated with kinase inhibitors.....103
Figure 19 Histograms showing distribution of number of markers per cell corresponding to Chromosome 2 and 15 in TC4 and TC9 104
Figure 20 Boxplots of CIN+ and CIN- CRC cell lines individually treated with 5 concentrations of 17-AAG or AICAR 107
Figure 21 Graphs of mean relative cell numbers in HCT116 diploid parental and *MAD2+/-* cell lines after treatment with 17-AAG or AICAR 108
Figure 22 Graphs of mean relative cell number in DC8, TC4 and TC9 cell lines after treatment with 17-AAG, AICAR or a combination of both.....109
Figure 23 Graphs of mean relative cell number in CRC cell lines that overlapped between two studies 110
Figure 24 Analysis of drug sensitivity of isogenic CIN+ cell lines to clinically relevant cytotoxics 113
Figure 25 Fixed effects meta-analysis of studies reporting the relationship between CIN and overall survival 114
Figure 26 Fixed effects meta-analysis of studies reporting the relationship between CIN and progression-free survival 115
Figure 27 Analysis on impact of CIN on patient survival.....116
Figure 28 Analysis on impact of CIN on benefit from adjuvant chemotherapy 117
Figure 29 Pre-screen optimisation.....126
Figure 30 Drug response following BUB1B silencing in HCT116 cells 128

Figure 31 Silencing kinetochore components in HCT116 diploid parental and *MAD2+/-* cell lines....130
Figure 32 Screen overview, and candidate gene selection....133
Figure 33 Heatmap of candidate gene validation....135
Figure 34 Assessment of differential lethality in HCT116 *MAD2+/-* cell line and diploid parental cell line....137
Figure 35 Assessment of differential lethality of the 17 candidate genes in non-isogenic CIN+ and CIN- cell lines....140
Figure 36 Reselection of candidate genes and assessment for differential viability effects. Error bars represent standard deviations across replicate wells....144
Figure 37 Further assessment of candidate genes for differential viability effects....145
Figure 38 Usage of mixture models to assess noise factors....148
Figure 39 Retrospective power analysis of whole genome RNAi Screen and average cell number in control transfected cells....150
Figure 40 Workflow of candidate gene selection and validation....152
Figure 41 Cell cycle profile data from whole genome siRNA screens and overlapped with DNA copy number data in CIN+ CRC cell lines....164
Figure 42 Validation of candidate genes for off-target effects....167
Figure 43 Representative time-lapse phase-contrast images following CD52 silencing in HCT116 cells....169
Figure 44 Graphs of percentage cells entering mitosis and time spent in mitosis....172
Figure 45 Percentage of mitotic errors in cells following candidate gene silencing....173
Figure 46 Representative images of mitotic errors....174
Figure 47 Workflow of candidate genes selection and validation....176
Figure 48 Validation of siRNA transfection and measurements of ceramide content of cells....183
Figure 49 CERT gene expression signature....186
Figure 50 qPCR validation of microarray data....187
Figure 51 Investigation of pathways mediating paclitaxel-induced cell death following CERT silencing....189
Figure 52 siCERT and ceramide mediates an autophagy transcriptional response....193
Figure 53 LC3I/II western blot analysis following CERT and LAMP2 silencing for 48h and 24h of paclitaxel exposure....194
Figure 54 LC3I/II western blot analysis following siCON or CERT silencing for 48h and 24h of paclitaxel exposure in the presence of leupeptin protease inhibitor....195
Figure 55 Autophagy response precedes apoptotic activity following CERT silencing and paclitaxel treatment....197
Figure 56 CERT depletion results in increased LAMP2 spot intensity as measured using immunofluorescence microscopy....199
Figure 57 Representative transmission electron micrographs (TEM) of siCON/paclitaxel and siCERT/paclitaxel cells....201
Figure 58 Electron dense structures appearing following CERT silencing were quantified....202
Figure 59 Assessment of relationship of paclitaxel response with autophagy gene expression....204
Figure 60 Live cell imaging and single cell fate analysis following CERT silencing and paclitaxel treatment....206
Figure 61 CERT mRNAis overexpressed in HER2+ primary breast cancer....208

Figure 62 CERT protein expression in TMA Cohort.....209
Figure 63 Representative IHC images for CERT expression.....212
Figure 64 CERT silencing sensitises HER2+ breast cancer cell lines to various drugs and induces autophagic flux changes. 215
Figure 65 CERT silencing induces changes in autophagic flux in HCC1954 cells and sensitisation that is LAMP2-dependent in response to drug treatment.....216
Figure 66 CERT expression is associated with survival outcome in patients with primary breast cancer treated with adjuvant chemotherapy.....220

List of tables

Table 1 Table of mutations in mitotic checkpoint genes.....30
Table 2 Table of mutations in kinetochore-associated genes.....32
Table 3 Table of colorectal cancer cell lines used.....59
Table 4 List of Taqman probes used 72
Table 5 Cell lines used in this study.....82
Table 6 Table of inhibitors that preferentially target CIN- cell lines over CIN+ cell lines 90
Table 7 Demographic data of patients in breast cancer TMA cohort 211
Table 8 Multivariate analysis of prognostic predictors including CERT expression in breast cancer TMA cohort.....222

Abbreviations

CC	Correlation coefficient
CERT	Ceramide Transporter Protein
CIN	Chromosomal Instability
CLP	Sanger Institute Cancer Cell Line Project
COSMIC	Sanger Institute Catalogue Of Somatic Mutations In Cancer
ER	Endoplasmic Reticulum
GII	Genome Integrity Index
LOH	Loss of heterozygosity
MIN	Microsatellite Instability
MS	Mass Spectrometry
PICNIC	Predicting Integral Copy Numbers In Cancer
qPCR	Quantitative Polymerase Chain Reaction
RNAi	RNA Interference
SAC	Spindle Assembly Checkpoint
siRNA	Short Interfering RNA
SCCS	Structural Chromosomal Complexity Score
SNP	Single Nucleotide Polymorphism

Chapter 1. Introduction

This thesis concerns an investigation of chromosomal instability (CIN) survival mechanisms in cancer. Significant intra-tumour genetic heterogeneity is associated with the cancer cell population *in vivo* (1, 2). Genomic instability mechanisms provide means for the acquisition of genetic variation within the cancer cell population. One such mechanism of genomic instability is CIN, which describes an increased rate of ongoing numerical and structural chromosomal changes within cells (3, 4).

In this chapter, the CIN phenotype and its potential relationship with cancer multidrug resistance will be discussed. Expanding upon this, evidence suggesting that CIN may present a targetable phenotype in the treatment of cancer will be reviewed. Additionally, I will review evidence from our laboratory concerning the involvement of CERT, a ceramide transporter protein, in the mediation of multidrug sensitisation and introduce the possibility that CERT targeting may be exploitable in cancer medicine in order to limit drug resistance and conceivably target CIN cells.

Sections of this chapter have been published in review form (5) and as a first author primary research article in (6) (See Appendix 8.1 and 8.2).

1.1 Functional genomic approaches implicate CIN and CERT as pathways that may be exploited to limit drug resistance

One of the major challenges in cancer treatment is drug resistance as it limits the efficacy of cytotoxics used in cancer management (7). Following the widespread introduction of RNA interference (RNAi) technology, several methods have been

developed to enable short- or long-term target silencing in cultured cells in the laboratory (8), enabling the functional annotation of the human genome. RNAi allows for the silencing of genes in a “one by one” approach to assess the phenotypic effects of each gene on drug sensitivity.

Synthetic small interfering RNA (siRNA) duplexes are commonly used in RNAi experiments. siRNAs are most commonly introduced into the cell using cationic lipid transfection agents that allow the human cell to take up the nucleic acids. The RISC (‘RNA-induced silencing complex’) enzyme complex recognises the siRNA and the antisense portion of the siRNA guides the RISC to its complementary mRNA strand. If it is a partial match, translation is blocked. This partial match is normally associated with microRNA (miRNA) processing and may explain the off-target gene silencing effects of siRNAs. If a complementary match with the anti-sense strand occurs, the siRNA is cleaved. Potential off-target effects can also occur in this pathway if the sense strand of the siRNA duplex is incorporated into the RISC instead of the antisense strand. Both partial and complementary match of the RISC with mRNA result in decreased levels of that mRNA and a corresponding decrease in the levels of protein expression.

Several high-throughput RNAi screens have implicated hundreds of genes capable of inducing drug resistance in tumour cells, indicating the complexity of the problem (5) and suggesting that targeting individual genes to overcome drug resistance in cancer is unlikely to succeed due to the polygenic nature of this process. The complexity of multidrug resistance may provide an explanation for the lack of clinical evidence for the

role of MDR transporters in acquired multidrug-resistance of cancers (9) and the failure of Phase III trials targeting P-glycoprotein (Pgp; an ABC transporter) (10).

Targeting pathways that are involved in multidrug resistance or its acquisition may be a strategy to overcome the polygenic problem of drug resistance. Aneuploidy has been previously shown to be permissive for the rapid evolution of multidrug resistance (11). An RNAi screen for regulators of multidrug sensitivity targeting all kinases (kinome library 779 siRNAs) and ceramide pathway regulators (ceramidome library 50 siRNAs) in the HCT116 (colorectal cancer), MDA-MB-231 (breast cancer) and A549 (non-small cell lung cancer) cell lines was previously performed by our laboratory (12). It was demonstrated that a common effect of all siRNAs promoting resistance to paclitaxel (a taxane drug that stabilises microtubules) was a reduction in the accumulation of drug-treated cells at the mitotic checkpoint, supporting the concept that spindle checkpoint disruption promotes paclitaxel antagonism (12, 13). Most siRNAs promoting resistance also induced the appearance of polyploid cells, multinucleation and centrosomal abnormalities without drug treatment, indicating the link between pathways maintaining chromosomal stability and drug resistance. Further examining the link between CIN and intrinsic taxane resistance, my laboratory demonstrated that CIN cancer cells overexpress a set of genes termed the microtubule-stabilising (MTS) gene signature (14) (see Appendix 8.3), and this enables the cells to survive the down-regulation of these genes resulting from MTS treatment. Given the association between CIN and taxane resistance and that CIN may be permissive for the acquisition of multidrug resistance, I reasoned that targeting CIN may be a means to limit drug resistance in the clinical setting. To this end, I sought to further understand CIN survival mechanisms in cancer and the pathways regulating the generation and maintenance of CIN.

The ceramide transporter CERT was identified in the same kinome and ceramidome screen to potentiate multidrug sensitivity to paclitaxel, doxorubicin, cisplatin and 5-FU (fluorouracil) when silenced by RNAi (12), indicating another pathway that could be targeted to limit multidrug resistance in cancer. Given the taxane sensitising affects mediated following CERT silencing and taxane resistance demonstrated by CIN+ cells, I reasoned that a clearer understanding of the process through which cells are sensitised following CERT silencing might identify means through which CIN+ cells might be more efficiently targeted.

1.2 Regulation of chromosome segregation

CIN reflects improper cell division, where mechanisms ensuring the fidelity of proper chromosome segregation are compromised during cellular division and are propagated in subsequent generations of cell division. The eukaryotic cell division cycle can be divided into four phases, Gap 1 (G1), Synthesis (S), Gap 2 (G2) and Mitosis (M) (15). M phase can be further divided into prophase, prometaphase, metaphase, anaphase and telophase. G1, S and G2 together make up the interphase period of the cell. During interphase, chromosomes are decondensed (16). A period of cell growth occurs during G1 followed by DNA replication in S phase. DNA replication in S phase results in the generation of paired sister chromatids consisting of two identical chromosomes, joined at a structure called the centromere and held together by a protein complex termed Cohesin (17, 18). During G2, the cell undergoes a phase of cell growth again. Finally in M phase, the chromosomes condense and the cell begins to divide as mitosis occurs, separating sister chromatids of chromosomes into two daughter nuclei. The completion

of cell division is achieved following cytokinesis, where daughter nuclei are separated into two separate daughter cells along with equally divided cytoplasm.

1.2.1 Entry into mitosis

Entry into mitosis is regulated by the G2/M checkpoint. CDK1 is the key regulator during this period of the cell cycle and is itself tightly regulated. During G2, Myt1 and Wee1 suppress mitotic entry via the inhibitory Thr14 and Tyr15 phosphorylation of CDK1 (19). This checkpoint allows for the completion of cell growth and also enables the repair of DNA damage errors, prior to the commencement of cell division.

Activation of CDK1 requires both activating phosphorylation and the removal of inhibitory phosphorylation. The phosphorylation of the Thr161 residue (20) by CAK (CDK-Activating Kinase) (21) allows the formation of the Cyclin B/CDK1 complex (also known as Maturation Promoting Factor (MPF))(22). Formation of the Cyclin B/CDK1 complex leads to the activation of CDC25 phosphatase that functions to remove the inhibitory phosphorylation of CDK1 (23). In mammals this is accomplished by CDC25a and CDC25b isoforms of this protein (24). CDK1 mediates phosphorylation of Condensin, (25) allowing the chromosomes to condense, and also the phosphorylation of Lamins, leading to nuclear envelope breakdown (NEB) (26) and thus allowing spindle fibres access to the chromosomes to form attachments.

Each sister chromatid has a kinetochore consisting of an inner protein plate and an outer protein plate that forms the site for kinetochore-microtubule attachments (27). Following NEB, microtubules from centrosomes at opposite poles of the cell seek out randomly to capture the kinetochores (28). Some microtubules that do not attach to

kinetochores attach instead to microtubules originating from the opposing centrosome to form the mitotic spindle (29). Those that fail to attach eventually depolymerise (30). The kinetochore-microtubule attachments coupled with polymerisation and depolymerisation of microtubules, provides the pulling force necessary to later separate the chromosome's two chromatids to the opposite ends of the cells (31).

1.2.2 The Anaphase Promoting Complex/Cyclosome (APC/C)

The Anaphase Promoting Complex/Cyclosome (APC/C) is an E3 ubiquitin ligase complex (32). It plays a role in two transitions between phases during mitosis, namely during the metaphase to anaphase transition and during the anaphase to telophase transition. The specificity of its roles is regulated by its interaction with CDC20 and CDH1. During the metaphase to anaphase transition, the APC/C associates with CDC20 to target Securin, the negative regulator of Separase, for degradation (32). Separase functions to cleave Cohesin, and this allows for the loss of sister-chromatid cohesion (33).

The APC/C is also involved in exit from mitosis. Following anaphase, exit from mitosis is regulated by two networks, the Cdc Fourteen Early Anaphase Release (FEAR) and the Mitotic Exit Network (MEN) (34). These networks act to release CDC14, which is normally bound to and inhibited by Cfi/Net1. An active CDC14 proceeds to dephosphorylate CDH1, allowing CDH1 to bind to and activate the APC/C. The APC/C-CDH1 complex targets Cyclin B for degradation, and thus inactivates CDK1, triggering an exit from mitosis (35).

The APC/C and CDC20 interaction is itself regulated to prevent premature chromosome segregation. One checkpoint regulating this is the Spindle Assembly Checkpoint (SAC).

1.2.3 The Spindle Assembly Checkpoint (SAC)

The SAC is a pathway that acts during mitosis and is active during metaphase to prevent entry into anaphase by ensuring the proper bi-orientation of sister chromatids and thus preventing the missegregation of chromosomes. Bi-orientation of sister chromatids occur when each kinetochore is attached to microtubules originating from opposing spindle poles (28). Sister chromatids with improper orientation fail to generate proper tension and this results in the removal of kinetochore-microtubule attachments by Aurora B Kinase (AURKB) (36). Aurora B acts to remove erroneous attachments recursively (37) by phosphorylating kinetochore components (38) until all sister chromatids are properly bi-orientated on the bipolar spindle. Examples of improper kinetochore-microtubule attachments include merotelic attachments, when one kinetochore is attached to microtubules from both spindle poles, and syntelic attachments, where both sister kinetochores are attached to microtubules from the same spindle pole (39).

When Aurora B removes kinetochore-microtubule attachments, the unattached kinetochores recruit MAD1 that in turn is required for the recruitment of MAD2 (40) (41). MAD2, BUBR1 and BUB3 bind to CDC20 to form the mitotic checkpoint complex (MCC), which is the main mediator of this checkpoint and is a potent inhibitor of the APC/C (42). In mammalian cells, BUB1 and Aurora B appear to promote the binding of the MCC to the APC/C (43). Following kinetochore-microtubule attachments, MAD2 localisation decreases (41), and this may act to satisfy the SAC.

The proper generation of tension across kinetochores may also act to inactivate the SAC (44). This may explain why merotelic attachments, appear to be sufficient to deplete MAD2 and satisfy the SAC (45) as tension is still generated across the kinetochore via attachments to both spindle poles (Figure 1).

Drugs such as taxanes promote mitotic arrest through the activation of the SAC, however, mitotic slippage describing an escape from mitosis under the continued presence of conditions that normally activate the SAC, may occur (27) and cells can then enter a multinucleated interphase (46).

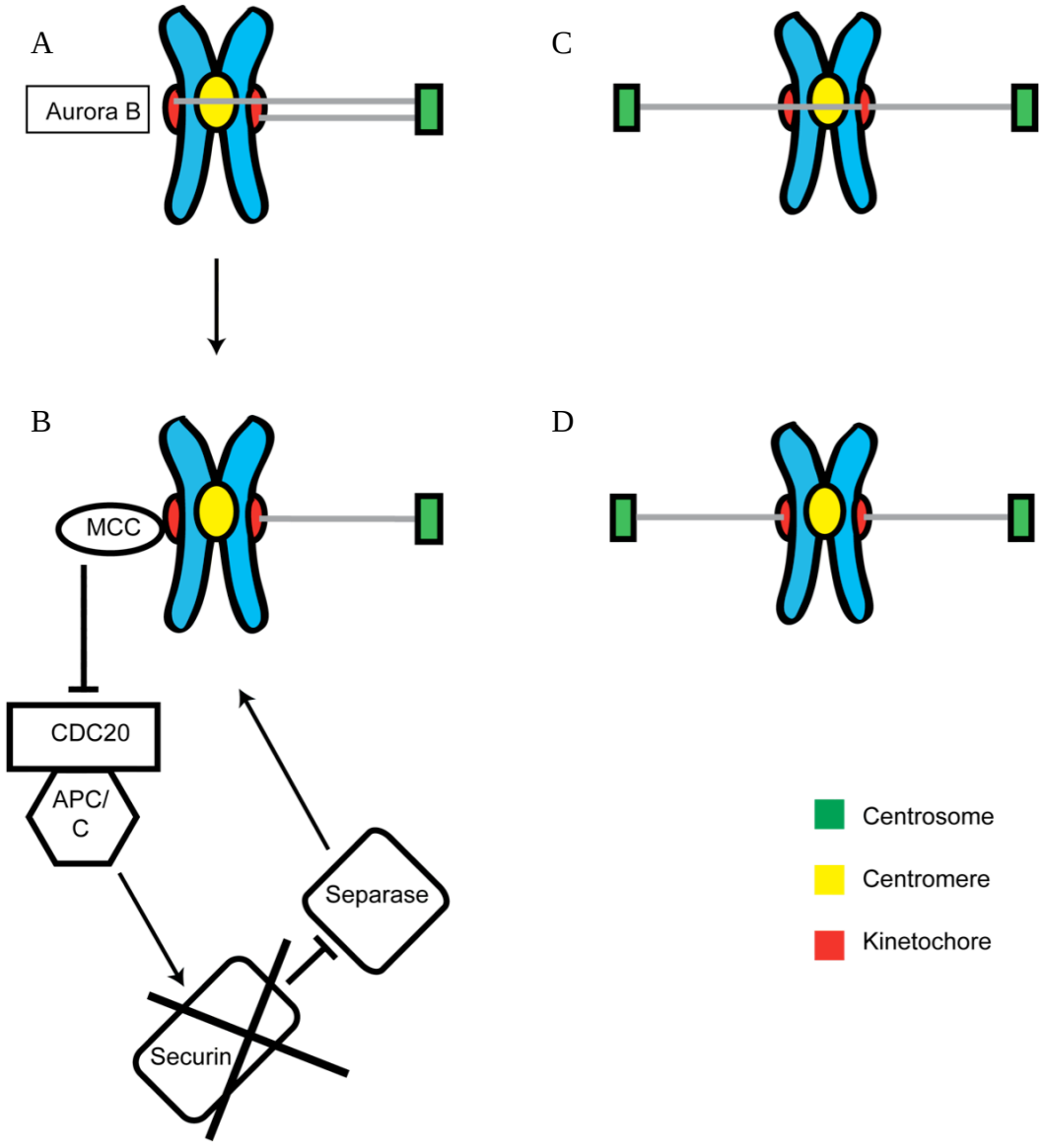

Figure 1 Types of kinetochore-microtubule attachments and activation of the SAC
A) Both kinetochores are attached to the microtubules from the same centrosome, leading to a syntelic attachment, this results in improper sister chromatid orientation and failure to generate tension across the kinetochore. Aurora B is recruited to detach the kinetochore-microtubule attachments.
B) Unattached kinetochores result in the activation of the SAC via the recruitment of MCC components to the kinetochores. This inhibits the ability of the APC/C-CDC20 complex to degrade Securin and release Separase that cleaves the cohesin complex holding the sister chromatids together.
C) Merotelic attachments, where one kinetochore is attached to microtubules from both spindle poles fail to activate the SAC.
D) Correct kinetochore-microtubule attachment result in bi-orientated sister chromatids.

1.2.4 The DNA damage checkpoint

The DNA damage checkpoint can act to prevent progression through mitosis. In response to DNA damage, CHK1 and CHK2 can be activated by ATM and ATR (47). CHK1 negatively phosphorylates CDC25 (48) and may prevent the removal of inhibitory phosphorylation of CDK1 (48) and thus preventing progress into mitosis (49). CHK1 may also phosphorylate Securin and prevent the degradation of Securin by the APC/C-CDC20 complex (49). Further supporting a role for DNA damage checkpoints in regulating metaphase to anaphase transition, in yeast cells CHK2 acts to interfere with Securin and CDC20 interactions (50), thus preventing the separation of sister chromatids.

1.3 Chromosomal Instability

The number and structure of chromosomes in each cell can be perturbed in human cancer due to CIN, a form of genomic instability. Human cancer is associated with at least two distinct patterns of genomic instability, CIN or microsatellite instability (MIN), and most human colorectal cancers (CRC) can be classified as demonstrating one or the other (51). The more common form of genomic instability in CRC is CIN, resulting in ongoing numerical and structural chromosomal aberrations in cancer cells, leading to intra-tumour heterogeneity (3, 4). CIN can be classified as numerical (gains and losses of whole chromosomes) or structural CIN (chromosomal rearrangements such as translocations and deletions) and commonly both occur simultaneously (52). As a consequence, cancer cells demonstrating a CIN phenotype are frequently aneuploid or

polyploid. Aberrations in chromosome number and structure are often interlinked in CIN+ cancer. This has been confirmed by Roschke and colleagues who have demonstrated a high correlation of modal chromosome number with numerical chromosomal complexity (a measure of gains and losses of whole chromosomes) and a weak but significant correlation of modal chromosomal number with structural chromosomal complexity (a measure of chromosome translocations, deletions, duplications, insertions, inversions, or homogeneously staining regions). In addition, a moderate correlation between structural and numerical complexity was reported (4).

The less common pattern of genomic instability in cancer is MIN caused by a deficiency in the mismatch repair apparatus. Due to the accumulation of replication errors, MIN results in length variation of microsatellites (or short tandem repeat sequences) in DNA. The majority of MIN+ CRC cell lines are near-diploid (53, 54) and chromosomally stable (CIN-).

In contrast, CIN+ CRC cell lines are aneuploid and display a higher frequency of chromosomal missegregation errors during each mitosis relative to diploid cells (3). In human cancer, CIN+ is widely inferred through the measurement of tumour DNA ploidy using flow cytometry (55); normal diploid cells are defined by a DNA index of 1.0 (56) and thus an increase in DNA index infers polyploidy or aneuploidy. Approximately 60% of human CRC are CIN+ and 15% are near-diploid MIN+. 25% of human CRC appears to be neither MIN+ nor CIN+, however, the insensitivity of flow cytometry to detect small changes in ploidy or to detect structural chromosomal aberrations may lead to tumours wrongly classified as CIN- (55, 57).

1.3.1 Polyploidy, tetraploidy, aneuploidy and CIN

Most eukaryotic cells are diploid (2n), containing 2 sets of homologous chromosomes. The terms CIN and polyploidy/aneuploidy are frequently but incorrectly interchanged. CIN describes a dynamic state where the number or structure of chromosomes changes at high rate per cell division, and so gross genetic differences are frequently observed between different cells within the same tumour. Tetraploidy refers to the specific state of double the number of chromosomes present in the diploid cell (4n). Polyploidy describes the state of an exact multiplication of the haploid (n) chromosome and aneuploidy describes a non-exact multiplication of the haploid chromosome number. A consequence of this is that whilst CIN+ cells are aneuploid and sometimes polyploid, aneuploidy and polyploidy are not synonymous with CIN (Figure 2).

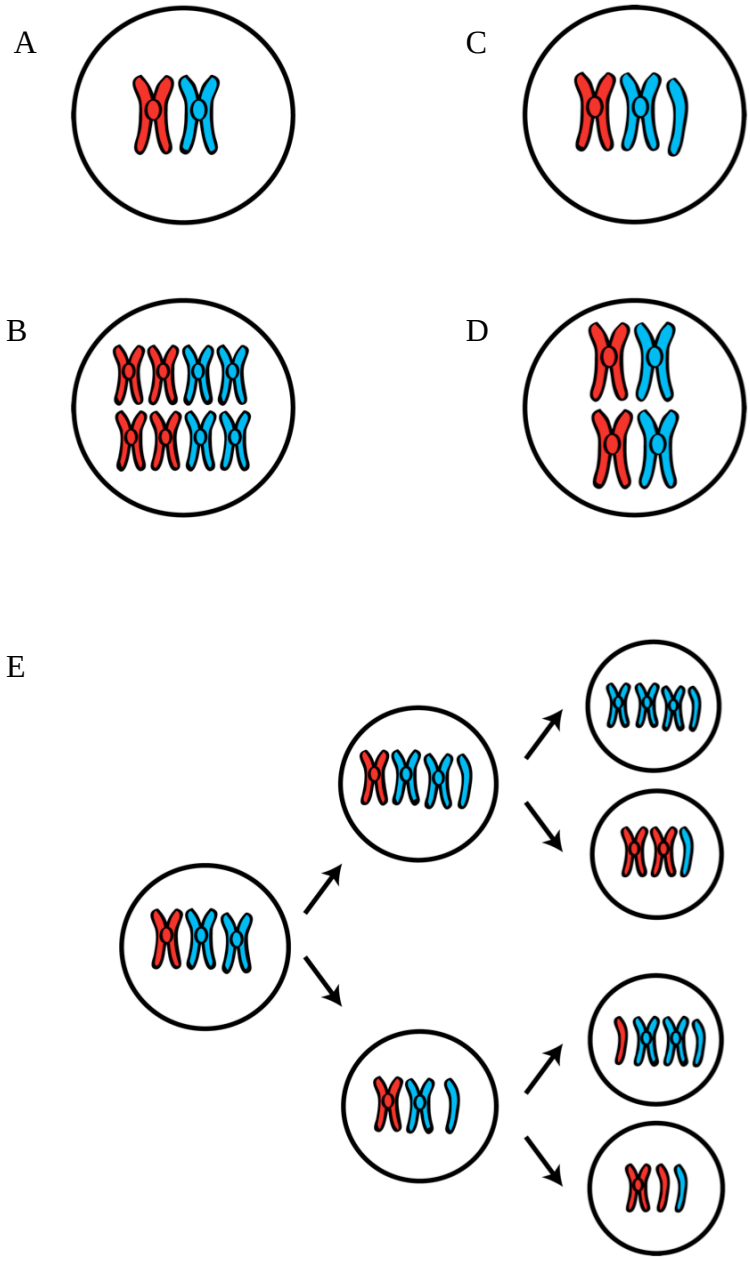

Figure 2 Ploidy and CIN
A) An example diploid cell with 2 chromosomes (2n).
B) Polyploidy describes the state of an exact multiplication of the haploid (n) chromosome.
C) Aneuploidy describes a non-exact multiplication of the haploid chromosome number
D) Tetraploidy is a special case of polyploidy, describing an exact duplication of the 2n chromosome number.
E) CIN describes a dynamic state where the number or structure of chromosomes changes at high rate per cell division, resulting in a heterogeneous daughter cell population.

1.3.2 Measuring Chromosomal Instability

It is challenging to obtain true scores of CIN, especially *in vivo*, as it requires the measurement of rate of change of whole chromosome number or structure across a cell population. Most proxy methods of scoring CIN are static measures that take a "snapshot" at a certain point in time that measure the number of chromosomes, chromosome complexity and genetic diversity in a supposedly clonal population.

Flow cytometry is commonly used to measure the DNA content of cancer cells and by extension, estimate the ploidy (55). The stemline scatter index (SSI) derived by flow cytometry experiments provides a clonal heterogeneity score that allows for the classification of tumours into diploid and aneuploid stable or unstable states (58).

Other established methods of scoring CIN include labour intensive methods such Spectral Karyotyping (SKY) and centromeric Fluorescence In situ Hybridisation (FISH). SKY allows for scoring of modal chromosomal number, structural or numerical complexity and heterogeneity of chromosomal number between cells (4). The number of chromosomes can be counted using centromeric FISH, and a description of aneuploidy and chromosomal numerical heterogeneity may be obtained.

Vast amounts of array Comparative Genomic Hybridisation (aCGH), Single Nucleotide Polymorphism (SNP) and gene expression microarray data are available on various platforms, which can be used to derive surrogate measures of aneuploidy or CIN (4, 58-62). Recently developed algorithms for the analysis of biallelic SNP arrays allow for the estimation of ploidy levels, loss of heterozygosity (LOH) events and the degree of

chromosomal structural instability and the location of aberrant chromosomal regions (63) (64).

Surrogate measures of aneuploidy based on expression microarray data include scores such as the CIN70 gene signature (59, 60), a gene signature reflecting total functional aneuploidy (tFA, a measure of the total level of chromosomal aberrations in a given tumour). The expression of this gene set correlates with SKY, SNP based structural complexity scores, and SSI derived from flow cytometry (60). A relationship of chromosomal instability scored by SSI with prognostic breast cancer gene expression signatures such as MammaPrint and Oncotype DX has been reported, suggesting that prognostic gene expression signatures are linked to CIN (65).

1.3.3 Mechanisms contributing to CIN

CIN+ cancer cells missegregate chromosomes and exhibit visible segregation errors during anaphase (66), such as anaphase bridges and lagging chromosomes. Various mechanisms have been proposed to contribute to CIN in cancer, reflecting an increase in chromosome missegregation events or a failure of checkpoints to detect or address problems in cell division.

Aberrant regulation of pathways involved in mitosis such as the APC/C and Cyclin B pathways may impact upon progression through the cell cycle and proper chromosomal segregation (67, 68). Mutations of APC/C subunits have been shown to delay mitotic exit and result in aberrant Cyclin B expression (67). In yeast models, Cyclin B overexpression was associated with gains and losses of chromosomes leading to aneuploidy and the failure to activate the SAC (68).

It has been shown that disrupting components of the SAC may lead to the generation of CIN (Figure 3). Evidence for this includes loss of function experiments of SAC genes including BUB1, by mutation in CIN CRC cell lines (69), the induction of a CIN phenotype in HCT116 non-CIN CRC cells by deletion of one allele of *MAD2* (70), and impairment of the mitotic checkpoint by a truncating mutation of MAD1L1 (71). Supporting this, mutations and aberrant expression of SAC genes have been found in some tumours *in vivo* (69, 72). The overexpression or depletion of SAC genes such as *MAD2* or *BUBR1* can induce chromosome segregation errors and failure to arrest cells in mitosis in response to mitotic arresting drugs (73-75) that lead to aberrant chromosome structure or number. However *in vitro* demonstrations have shown that many CIN+ cell lines have a functional SAC (66, 76, 77), suggesting that there must exist alternative mechanisms that generate CIN in the majority of tumours. Furthermore, mutations of mitotic checkpoint proteins appear to be rare in solid tumours (Table 1, analysis based on data from the Sanger Catalogue of Somatic Mutations in Cancer (COSMIC) database, (78)). Further analysis of data from the Sanger COSMIC database indicates that mutations in human kinetochore proteins (as defined in (79)) are also rare, indicating that mutations of the kinetochore-microtubule interface are unlikely to be the main contributor of CIN in human solid cancers (Table 2, analysis provided by David Endesfelder).

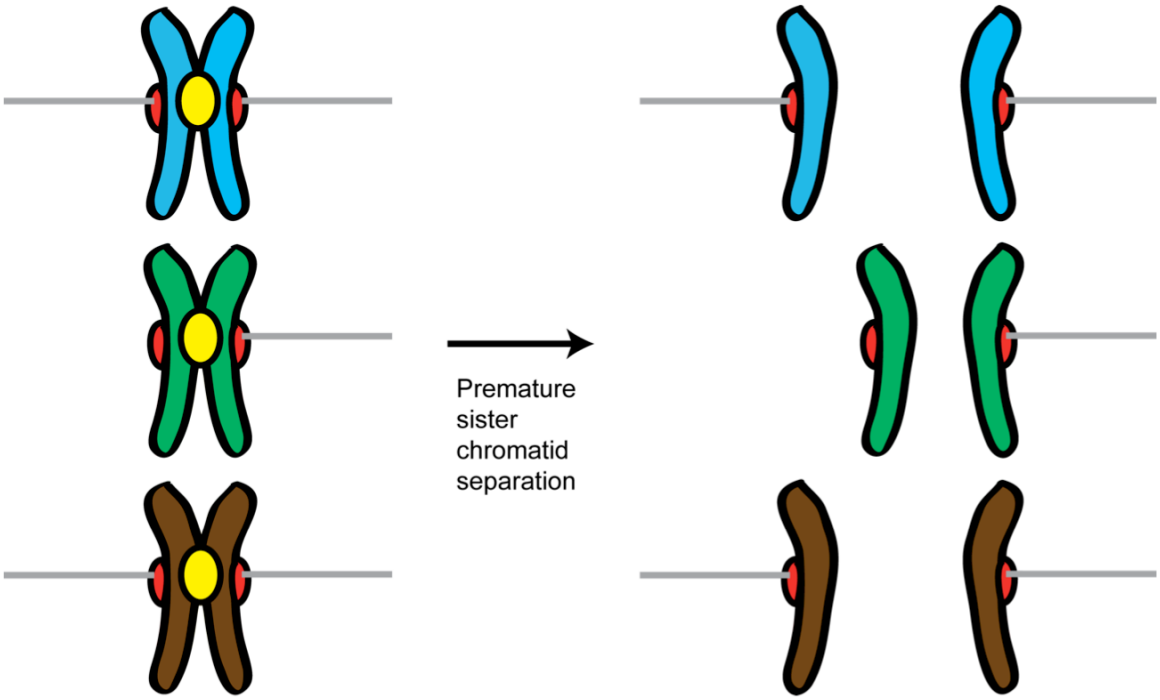

Figure 3 Premature sister chromatid seperation
Circumvention of the SAC and downstream pathways may lead to CIN due to premature sister chromatid separation before all kinetochores are attached to microtubules

	BUB1	BUB3	BUBR1	CDC20	MAD1	MAD2
Breast	0(27)	0(11)	0(27)	0(11)	0(11)	0(11)
CNS	0(31)	0(23)	0(455)	0(23)	0(23)	0(23)
Haematopoietic and lymphoid tissue	0(27)	0(0)	0(27)	0(0)	0(0)	0(0)
Kidney	1(116)	0(101)	1(116)	0(101)	0(101)	0(101)
Large Intestine	0(42)	0(12)	0(42)	0(12)	0(12)	0(12)
Lung	0(226)	0(12)	0(226)	0(12)	0(11)	0(12)
Ovary	1(27)	1(1)	1(27)	0(0)	0(0)	0(0)
Pancreas	0(1)	0(1)	0(1)	0(1)	0(1)	0(1)
Pleura	0(1)	0(1)	0(1)	0(1)	0(1)	0(1)
Skin	0(6)	0(6)	0(6)	0(6)	0(6)	0(6)
Stomach	0(20)	0(0)	0(20)	0(0)	0(0)	0(0)
Testis	0(13)	0(0)	0(13)	0(0)	0(0)	0(0)
Upper Aerodigestive Tract	0(3)	0(3)	0(19)	0(3)	0(3)	0(3)
Urinary Tract	0(2)	0(2)	0(2)	0(2)	0(2)	0(2)

Table 1 Table of mutations in mitotic checkpoint genes
Mutation data provided by the Sanger Institute (78) Numbers in brackets indicate the number of samples in which mutation data is available for.

	Breast	CNS	haematopoietic and	Kidney	Large Intestine	Lung	Ovary	Pancreas	Pleura	Skin	Stomach	Testis	Upper Aerodigestive	Urinary Tract	Salivary Gland	Liver
CENP-A	0(11)	0(1)	0(0)	0(101)	0(12)	0(12)	0(0)	0(1)	0(1)	0(6)	0(0)	0(0)	0(3)	0(2)	0(0)	0(0)
CENP-B	0(11)	0(23)	0(0)	0(101)	0(12)	0(12)	0(0)	0(1)	0(1)	0(6)	0(0)	0(0)	0(3)	0(2)	0(0)	0(0)
CENP-C	0(11)	0(23)	0(0)	0(101)	0(12)	1(12)	0(0)	0(1)	0(1)	0(6)	0(0)	0(0)	0(3)	1(2)	0(0)	0(0)
CENP-H	0(48)	0(22)	0(0)	0(0)	1(37)	0(0)	0(0)	0(0)	0(0)	0(0)	0(0)	0(0)	0(0)	0(0)	0(0)	0(0)
CENP-I	0(11)	0(23)	0(0)	0(5)	0(12)	0(11)	0(0)	0(1)	0(1)	1(6)	0(0)	0(0)	0(3)	0(2)	0(0)	0(0)
CENP-K	0(11)	0(22)	0(0)	0(0)	0(11)	0(0)	0(0)	0(0)	0(0)	0(0)	0(0)	0(0)	0(0)	0(0)	0(0)	0(0)
CENP-50/	0(11)	0(22)	0(0)	0(0)	0(11)	0(0)	0(0)	0(0)	0(0)	0(0)	0(0)	0(0)	0(0)	0(0)	0(0)	0(0)
CENP-O	0(11)	0(22)	0(0)	0(0)	0(11)	0(0)	1(1)	0(0)	0(0)	0(0)	0(0)	0(0)	0(0)	0(0)	0(0)	0(0)
CENP-P	0(0)	0(0)	0(0)	0(0)	0(0)	0(0)	2(2)	0(0)	0(0)	0(0)	0(0)	0(0)	0(16)	0(0)	0(9)	0(0)
CENP-Q	0(11)	0(22)	0(0)	0(0)	0(11)	0(0)	2(2)	0(0)	0(0)	0(0)	0(0)	0(0)	0(0)	0(0)	0(0)	0(0)
CENPR/	0(11)	0(22)	0(0)	0(0)	0(11)	0(0)	0(0)	0(0)	0(0)	0(0)	0(0)	0(0)	0(0)	0(0)	0(0)	0(0)
CENP-L	0(11)	0(22)	0(0)	0(0)	0(11)	0(0)	0(0)	0(0)	0(0)	0(0)	0(0)	0(0)	0(0)	0(0)	0(0)	0(0)
CENP-M	0(11)	0(22)	0(0)	0(0)	0(11)	0(0)	0(0)	0(0)	0(0)	0(0)	0(0)	0(0)	0(0)	0(0)	0(0)	0(0)
CENP-N	0(11)	0(22)	0(0)	0(0)	0(11)	0(0)	0(0)	0(0)	0(0)	0(0)	0(0)	0(0)	0(0)	0(0)	0(0)	0(0)
CENP-T	0(11)	0(22)	0(0)	0(0)	0(11)	0(0)	0(0)	0(0)	0(0)	0(0)	0(0)	0(0)	0(0)	0(0)	0(0)	0(0)
CENP-S/APITD1	0(11)	0(22)	0(0)	0(0)	0(11)	0(0)	1(1)	0(0)	0(0)	0(0)	0(0)	0(0)	0(0)	0(0)	0(0)	0(0)
MIS18A	0(11)	0(22)	0(0)	0(0)	0(11)	0(0)	0(0)	0(0)	0(0)	0(0)	0(0)	0(0)	0(0)	0(0)	0(0)	0(0)
MIS18B/ OIP5	0(11)	0(22)	0(0)	0(0)	0(11)	0(0)	0(0)	0(0)	0(0)	0(0)	0(0)	0(0)	0(0)	0(0)	0(0)	0(0)
KNL2	0(11)	0(22)	0(0)	0(0)	0(11)	0(0)	0(0)	0(0)	0(0)	0(0)	0(0)	0(0)	0(0)	0(0)	0(0)	0(0)
MIS12	0(11)	0(22)	0(0)	0(0)	0(11)	0(0)	0(0)	0(0)	0(0)	0(0)	0(0)	0(0)	0(0)	0(0)	0(0)	0(0)
DSN1	0(11)	0(22)	0(0)	0(0)	0(11)	0(0)	2(2)	0(0)	0(0)	0(0)	0(0)	0(0)	0(0)	0(0)	0(0)	0(0)
NSL1	0(11)	0(22)	0(0)	0(0)	0(11)	0(0)	0(0)	0(0)	0(0)	0(0)	0(0)	0(0)	0(0)	0(0)	0(0)	0(0)
NDC80	0(11)	0(22)	0(0)	0(0)	0(11)	0(0)	1(1)	0(0)	0(0)	0(0)	0(0)	0(0)	0(0)	0(0)	0(0)	0(0)
NUF2	0(11)	0(23)	0(0)	0(101)	0(12)	0(12)	3(3)	0(1)	0(1)	0(6)	0(0)	0(0)	0(3)	0(2)	0(0)	0(0)
SPC25	0(0)	1(23)	0(0)	0(101)	0(12)	0(11)	0(0)	0(1)	0(1)	0(6)	0(0)	0(0)	0(3)	0(2)	0(0)	0(0)
KNL1/CASC5	0(0)	1(23)	0(0)	0(101)	0(12)	0(11)	0(0)	0(1)	0(1)	0(6)	0(0)	0(0)	0(3)	0(2)	0(0)	0(0)
ZWINT	0(11)	0(23)	0(0)	0(101)	0(12)	0(12)	0(0)	0(1)	0(1)	0(6)	0(0)	0(0)	0(3)	0(2)	0(0)	0(0)
ROD/KNTC1	0(11)	1(23)	0(0)	3(412)	0(12)	1(12)	5(5)	0(1)	0(1)	0(6)	0(0)	0(0)	0(3)	0(2)	0(0)	0(0)
ZW10	0(11)	1(23)	0(0)	0(101)	0(12)	0(12)	0(0)	0(1)	0(1)	0(6)	0(0)	0(0)	0(3)	0(2)	0(0)	0(0)
ZWILCH	0(11)	0(22)	0(0)	0(0)	0(11)	0(0)	1(1)	0(0)	0(0)	0(0)	0(0)	0(0)	0(0)	0(0)	0(0)	0(0)
CENP-F	0(32)	3(446)	0(0)	0(0)	2(35)	0(0)	6(6)	0(0)	0(0)	0(0)	0(0)	0(0)	0(0)	0(0)	0(0)	0(0)
SPINDLY/	0(11)	0(22)	0(0)	0(0)	0(11)	0(0)	1(1)	0(0)	0(0)	0(0)	0(0)	0(0)	0(0)	0(0)	0(0)	1(1)
DYNEIN	0(11)	0(22)	0(0)	0(0)	0(11)	0(0)	0(0)	0(0)	0(0)	0(0)	0(0)	0(0)	0(0)	0(0)	0(0)	0(0)
NDE1	0(11)	0(22)	0(0)	0(0)	0(11)	0(0)	1(1)	0(0)	0(0)	0(0)	0(0)	0(0)	0(0)	0(0)	0(0)	0(0)
NDEL1	0(11)	0(22)	0(0)	0(0)	0(11)	0(0)	0(0)	0(0)	0(0)	0(0)	0(0)	0(0)	0(0)	0(0)	0(0)	0(0)
NUDC	0(11)	0(22)	0(0)	0(0)	0(11)	0(0)	1(1)	0(0)	0(0)	0(0)	0(0)	0(0)	0(0)	0(0)	0(0)	0(0)
LIS1/	0(11)	0(22)	0(0)	0(0)	0(11)	0(0)	0(0)	0(0)	0(0)	0(0)	0(0)	0(0)	0(0)	0(0)	0(0)	0(0)

SKA1	0(11)	0(22)	0(0)	0(0)	0(11)	0(0)	0(0)	0(0)	0(0)	0(0)	0(0)	0(0)	0(0)	0(0)	0(0)	0(0)
SKA2/ FAM33A	0(11)	0(22)	0(0)	0(0)	0(11)	0(0)	0(0)	0(0)	0(0)	0(0)	0(0)	0(0)	0(0)	0(0)	0(0)	0(0)
CLASP1	0(11)	1(22)	0(0)	0(0)	0(11)	0(0)	0(0)	0(0)	0(0)	0(0)	0(0)	0(0)	0(0)	0(0)	0(0)	0(0)
CLIP170	1(48)	0(22)	0(0)	0(0)	0(37)	0(0)	2(2)	0(0)	0(0)	0(0)	0(0)	0(0)	0(0)	0(0)	0(0)	0(0)
EB1/MAPRE1	0(11)	0(22)	0(0)	0(0)	0(11)	0(0)	0(0)	0(0)	0(0)	0(0)	0(0)	0(0)	0(0)	0(0)	0(0)	0(0)
TOG/CKAP5	0(11)	0(22)	0(0)	0(0)	0(11)	0(0)	1(1)	0(0)	0(0)	0(0)	0(0)	0(0)	0(0)	0(0)	0(0)	0(0)
KIF2A	0(11)	0(23)	0(0)	0(101)	0(12)	0(12)	0(0)	0(1)	0(1)	0(6)	0(0)	0(0)	0(3)	0(2)	0(0)	0(0)
KIF18A	0(22)	0(0)	0(0)	0(11)	0(0)	0(0)	2(2)	0(0)	0(0)	0(0)	0(0)	0(0)	0(0)	0(0)	0(0)	0(0)
CENP-E	2(32)	0(23)	0(0)	0(101)	0(36)	0(12)	5(5)	0(1)	0(1)	0(6)	0(0)	0(0)	0(3)	0(2)	0(0)	0(0)
AURKB	1(27)	1(455)	0(27)	0(116)	0(42)	1(226)	0(26)	0(1)	0(1)	0(6)	0(20)	0(13)	0(19)	0(2)	0(9)	0(0)
INCENP	0(11)	0(23)	0(0)	0(101)	0(12)	1(12)	0(0)	0(1)	0(1)	0(6)	0(0)	0(0)	0(3)	0(2)	0(0)	0(0)
SURVIVIN	0(11)	0(447)	0(0)	1(101)	0(12)	0(12)	0(0)	0(1)	0(1)	0(6)	0(0)	0(0)	0(3)	0(2)	0(0)	0(0)
CDCA8	0(11)	1(22)	0(0)	0(0)	0(11)	0(0)	0(0)	0(0)	0(0)	0(0)	0(0)	0(0)	0(0)	0(0)	0(0)	0(0)
TD60/RCC2	0(11)	0(22)	0(0)	0(0)	0(11)	0(0)	0(0)	0(0)	0(0)	0(0)	0(0)	0(0)	0(0)	0(0)	0(0)	0(0)
SGO1/SGOL1	0(11)	0(22)	0(0)	0(0)	0(11)	0(0)	0(0)	0(0)	0(0)	0(0)	0(0)	0(0)	0(0)	0(0)	0(0)	0(0)
SGO2/SGOL2	0(11)	0(22)	0(0)	0(0)	0(11)	0(0)	2(2)	0(0)	0(0)	0(0)	0(0)	0(0)	0(0)	0(0)	0(0)	0(0)
PPP1CC	0(11)	1(447)	0(0)	0(101)	0(12)	0(11)	0(0)	0(1)	0(1)	0(6)	0(0)	0(0)	0(3)	0(2)	0(0)	0(0)
PLK1	0(27)	0(31)	0(27)	0(28)	0(42)	1(37)	0(26)	0(1)	0(1)	0(6)	0(20)	0(13)	0(3)	0(2)	0(0)	0(0)
NUP107	0(11)	0(447)	0(0)	0(101)	0(12)	0(11)	0(0)	0(1)	0(1)	0(6)	0(0)	0(0)	0(3)	0(2)	0(0)	0(0)
NUP85	0(11)	0(23)	0(0)	0(101)	0(12)	0(11)	1(1)	0(1)	0(1)	0(6)	0(0)	0(0)	0(3)	0(2)	0(0)	0(0)
NUP133	2(48)	0(23)	0(0)	0(101)	0(38)	0(11)	1(1)	0(1)	0(1)	0(6)	0(0)	0(0)	0(3)	0(2)	0(0)	0(0)
NUP160/ NUP120	0(11)	1(23)	0(0)	0(101)	0(12)	0(11)	4(4)	0(1)	0(1)	0(6)	0(0)	0(0)	0(3)	0(2)	0(0)	0(0)
NUP96/ NUP98	2(48)	1(23)	0(0)	1(101)	0(38)	0(11)	1(1)	0(1)	0(1)	0(6)	0(0)	0(0)	0(3)	0(2)	0(0)	0(0)
NUP37	0(11)	0(23)	0(0)	0(101)	0(12)	0(11)	1(1)	0(1)	0(1)	0(6)	0(0)	0(0)	0(3)	0(2)	0(0)	0(0)
NUP43	0(11)	0(23)	0(0)	0(101)	0(12)	0(11)	0(0)	0(1)	0(1)	0(6)	0(0)	0(0)	0(3)	0(2)	0(0)	0(0)
SEC13	0(11)	0(22)	0(0)	0(0)	0(11)	0(0)	1(1)	0(0)	0(0)	0(0)	0(0)	0(0)	0(0)	0(0)	0(0)	0(0)
SEH1/SEH1L	0(11)	0(22)	0(0)	0(0)	0(11)	0(0)	0(0)	0(0)	0(0)	0(0)	0(0)	0(0)	0(0)	0(0)	0(0)	0(0)
ELYS/AHCTF1	0(11)	0(22)	0(0)	0(0)	0(11)	0(0)	5(5)	0(0)	0(0)	0(0)	0(0)	0(0)	0(0)	0(0)	0(0)	0(0)
CRM1/XPO1	0(11)	1(23)	0(0)	0(101)	0(12)	0(11)	1(1)	0(1)	0(1)	0(6)	0(0)	0(0)	0(3)	0(2)	0(0)	0(0)
RANBP2	0(11)	0(23)	0(0)	0(101)	0(12)	0(11)	0(0)	1(2)	0(1)	0(6)	0(0)	0(0)	0(3)	0(2)	0(0)	0(0)
RANGAP1	0(11)	0(22)	0(0)	0(0)	0(11)	0(0)	0(0)	0(0)	0(0)	0(0)	0(0)	0(0)	0(0)	0(0)	0(0)	0(0)

Table 2 Table of mutations in kinetochore-associated genes
Mutation data provided by the Sanger Institute (78) Numbers in brackets indicate the number of samples in which mutation data is available for.

Downstream of the SAC, defects in sister chromatid cohesion such as those resulting from the deletion of the *PTTG1* gene (encoding Securin) (80) can also result in chromosomal missegregation and loss of chromosomes. However, in human cancers such as breast cancer, Securin appears to be overexpressed (81) and *in vitro* experiments with non-degradable Securin have shown that inhibition of chromosome segregation occurs, resulting in aneuploid cells (82). These experiments suggest that an optimal level of Securin is required to maintain proper chromosomal segregation.

Extra centrosomes are frequently found in cancer cells (83), and are associated with increasing levels of CIN (84). Aurora A overexpression in cell lines has been shown to lead to centrosome amplification and aneuploidy (85-87). Confirming this, overexpression of Aurora A in mouse models demonstrated centrosome amplification, tetraploidy and premature chromosome segregation (88). Further supporting a role for Aurora A in promoting centrosome amplification and CIN, aneuploidy in gastric tumours has been reported to be correlated with Aurora A amplification (85).

It has been suggested that extra centrosomes contribute to CIN by allowing the formation of multipolar spindles that then allow multipolar cell divisions to occur. However, Ganem and colleagues have shown that in experiments where extra centrosomes are introduced into diploid cells, the daughter cells of the multipolar divisions are not viable (89). Instead, they suggest that extra centrosomes generate CIN by promoting an increase in chromosome missegregation by generating a 'multipolar spindle intermediate' that promotes centrosome clustering leading to a subsequent increase in the incidence of merotelic attachments (Figure 4). Further evidence for the formation of bipolar spindles following multipolar spindle formation was provided by

Duncan and colleagues who reported that in polyploid hepatocytes, a high frequency of multipolar metaphases were observed but most cell divisions were bipolar (90). Additionally, hyperstable microtubules leading to spindle abnormalities (91) can promote an increase in merotelic attachments. Merotelic attachments may contribute to CIN, as too many abnormal kinetochore-microtubule attachments may be formed that may overwhelm the Aurora B Kinase pathway that normally functions to correct these misattachments. As the SAC is not activated, anaphase onset is not delayed, leading to an increase in the incidence of aneuploidy through increased chromosomal missegregation events due to an increase in lagging chromosomes (Figure 5). Supporting this, Thompson and Compton have shown that inducing transient monopolar spindle formation using a small molecular inhibitor of Eg5, a mitotic kinesin (92), increases the rate of chromosome missegregation in cancer cells.

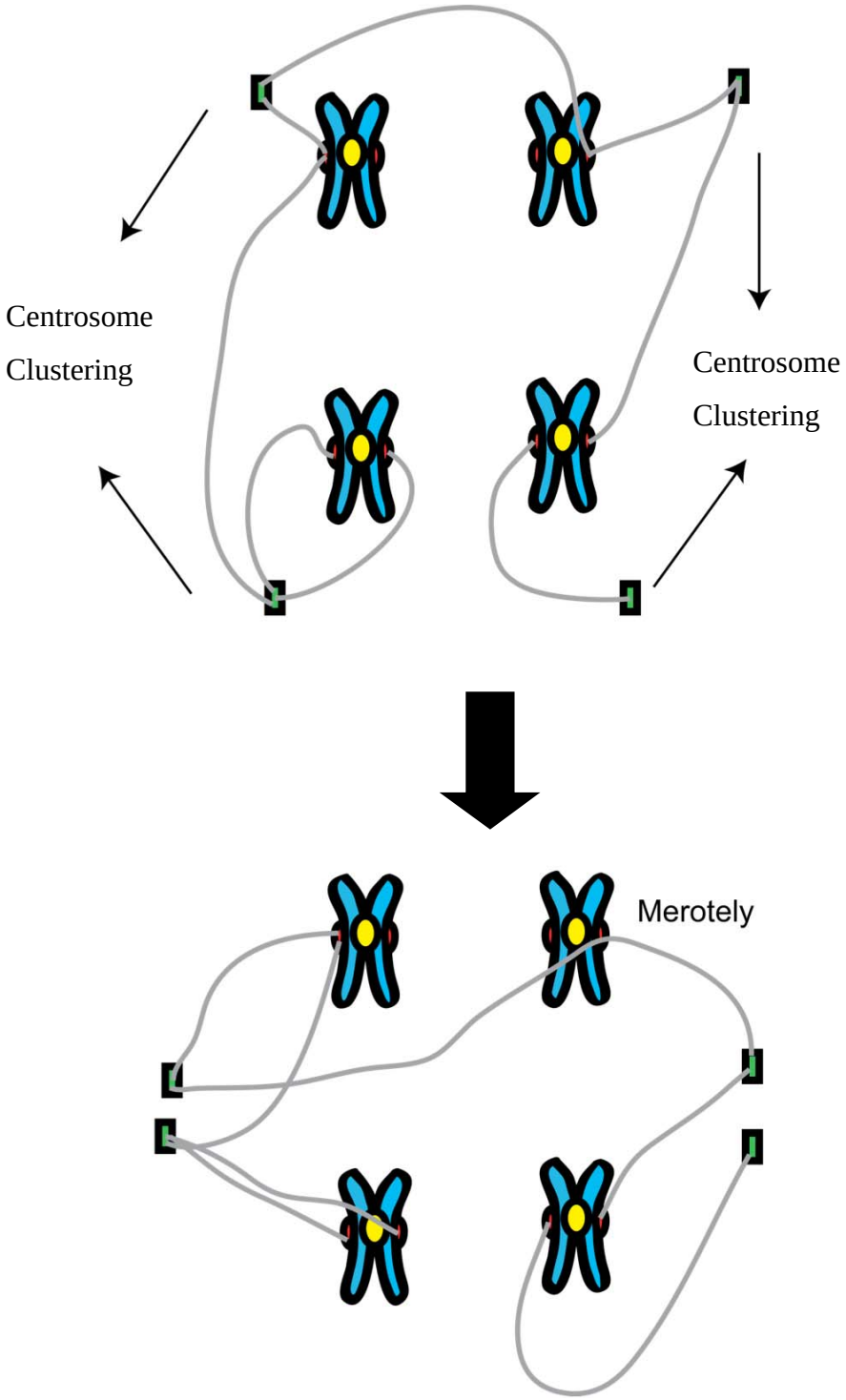

Figure 4 Multipolar spindle formation leads to merotely
Multipolar spindle formation resulting from extra centrosomes may lead to an increase in merotelic attachments following centrosome clustering and reorganisation into a bipolar spindle

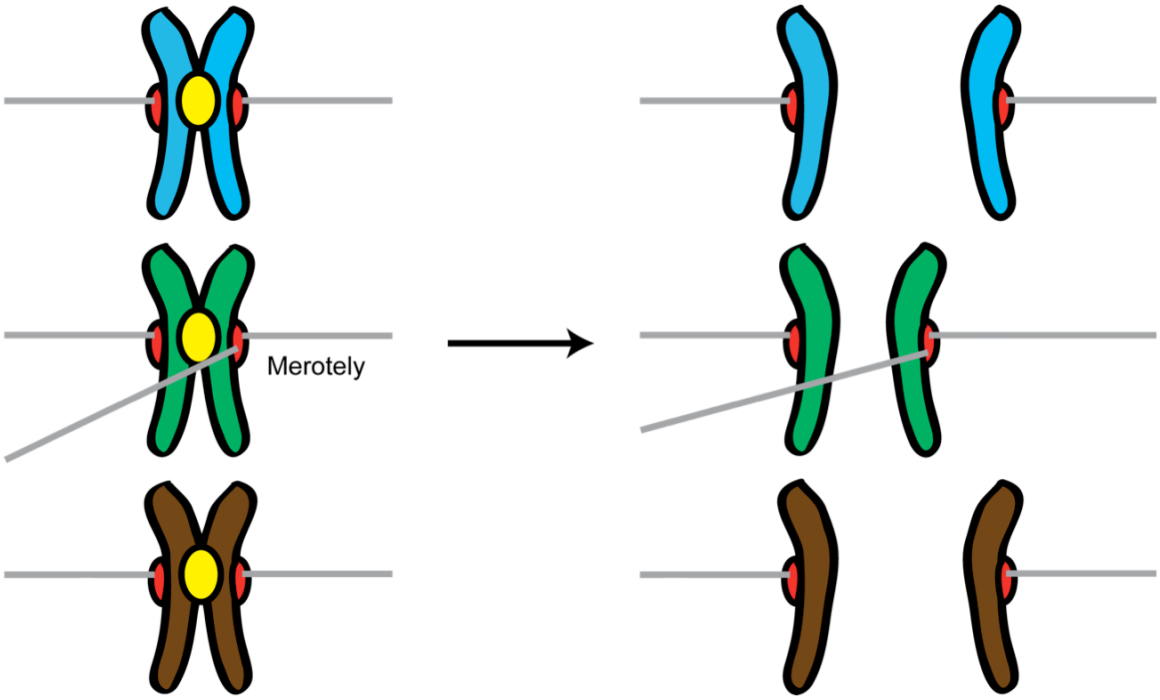

Figure 5 Merotely leads to errors in chromosome segregation
Merotelic attachments may increase the number of lagging chromosomes and anaphase bridges, leading to errors in chromosome segregation

1.3.4 Polyploidy and multinucleation as an intermediate state towards CIN

Polyploidy, tetraploidy and aneuploidy may appear to be a consequence of CIN due to missegregation of chromosomes. However, these phenotypes may also contribute to the development of CIN. Yeast studies suggest that tetraploidy leads to an increase in merotelic attachments due to altered spatial dimensions of the volume and size of the cell with respect to spindle length (93). Furthermore, tetraploidy may induce the loss of individual chromosomes in cells at rates much higher than that of triploid or diploid cells (94). However, this observation could indicate an increased rate of regression to the diploid state rather than a sustainable elevated rate of CIN.

Cytokinesis defects may lead to the generation of multinucleate cells with increasing ploidy (95-97) and these multinucleated cells demonstrate features of CIN. Shi and colleagues demonstrated that in human cancer cells, diploid cells can undergo a normal bipolar mitosis but fail to complete cytokinesis (98) leading to the generation of tetraploid binucleate daughter cells. These cells demonstrated an increase in missegregation of chromosomes 8 and 12 of between 83 and 166 fold times that of diploid cells. Supporting the view that multinucleation is associated with CIN, aberrant expression of mitotic kinases such as AURKB have been found to induce the formation of multinucleated cells that eventually become polyploid or aneuploid following fusion of the nuclei (99) (Figure 6). Fujiwara and colleagues have shown that tetraploid binucleate p53-null mouse mammary epithelial cells display an increase in the frequency of whole-chromosome aneuploidy compared to their diploid counterparts (increased loss of chromosomes) and higher levels of gross chromosome

rearrangements (as shown using SKY) (100). Failure of cytokinesis may result in daughter cells with extra chromosomes and the formation of multipolar spindle intermediates with increased merotelic attachments (89). Experiments with binucleate mouse hepatocytes demonstrate that the daughter cells demonstrate significant aneuploidy with multipolar spindle formation and defects in chromosome segregation (90).

Taken together, these studies indicate that polyploidy/aneuploidy may contribute to CIN and that multinucleation is also associated with CIN. In this thesis, I have attempted to identify regulators of ploidy in human CRC as these pathways may have relevance to the generation or maintenance of CIN+ *in vivo*.

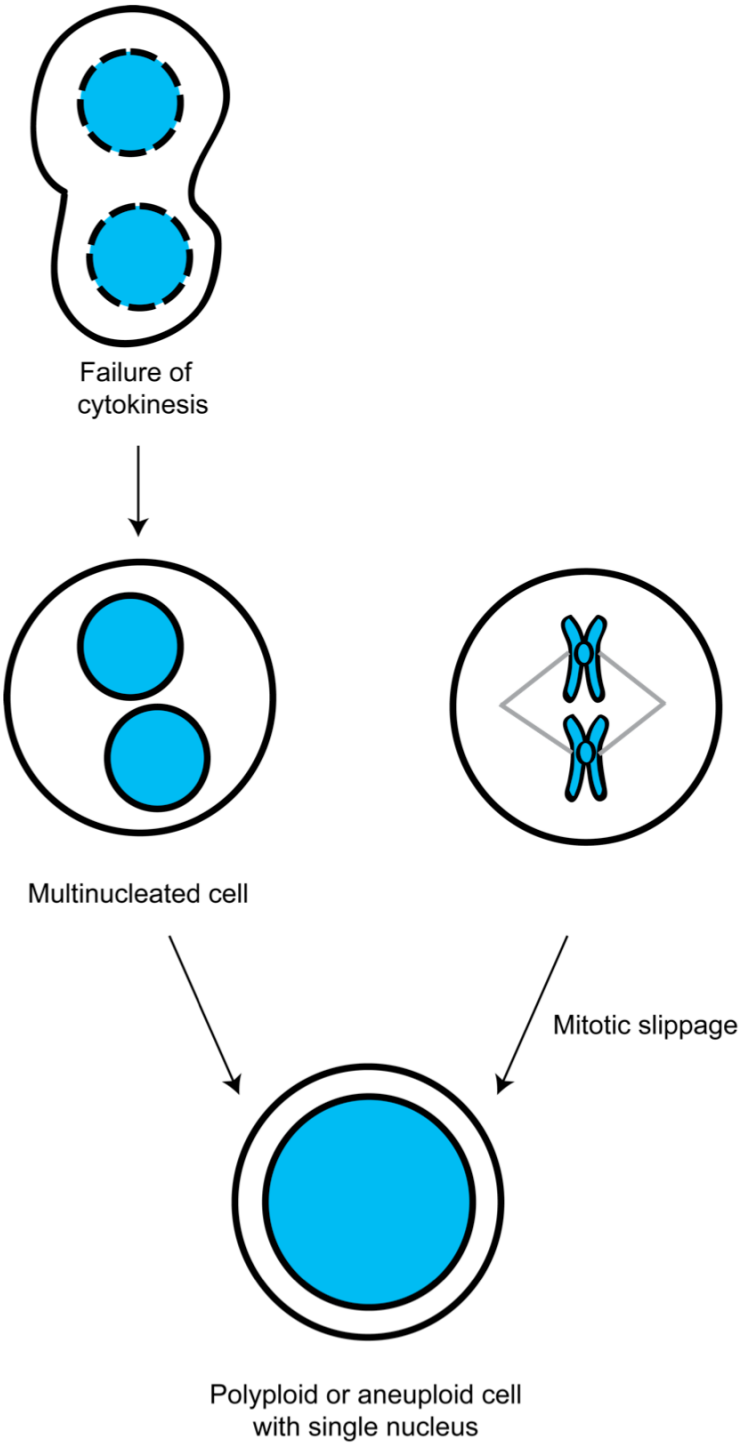

Figure 6 Errors in cell division may result in polyploid cell formation
Cytokinesis failure may cause the formation of polyploid binucleate cells and subsequent nuclei fusion may result in an aneuploid or polyploid cell with a single nucleus. Mitotic slippage may also result in polyploid cells.

1.3.5 Adaptability of CIN/Aneuploid Cells

Increasing evidence suggests that CIN is associated with poor prognosis in solid tumours (55, 59, 101). It has been suggested that adverse outcome associated with CIN may be related to increased tumour cell heterogeneity driving the ability of tumours to adapt to environmental stresses (102-104). However, while an increased level of CIN may be beneficial in driving adaption, more extreme levels of CIN and concomitant severe genetic disruption may compromise fitness, suggesting that an "optimal" level of CIN for carcinogenesis may exist (51, 60, 102, 105).

In Darwinian evolution, mutations allow new variants to arise in a population and in the face of a selection pressure, individuals with advantageous characteristics will be selected for. Nowell proposed that genomic instability within cancer cells allows for the generation and selection of cancer cell clones with a selective advantage (106). CIN within cancer cells may therefore drive evolution by natural selection within the tumour environment due to large-scale heritable chromosomal variations resulting from intra-tumoural genetic heterogeneity. The evolution of cancer clones is likely to occur at random (107), and the CIN cancer cell population may have an advantage in the face of selection pressure by allowing the rapid generation of new and potentially advantageous genotypes. An optimal level of CIN (51) leading to genetic alterations required to negotiate selection barriers during tumour progression might explain the selection for aneuploid tumours and the high frequency of karyotypic instability in solid tumours. The high number of tumours displaying aneuploidy and CIN (55) appears to lend weight to this hypothesis.

Consistent with this hypothesis, transient initiation of CIN, following the brief induction of MAD2 expression in activated-KRAS initiated mouse lung tumour models, is associated with a high frequency of tumour recurrence following withdrawal of the KRAS oncogenic stimulus (75). Weaver and colleagues demonstrated that in mouse models, increased chromosome missegregation caused by decreasing the levels of CENPE provoked an increase in levels of spontaneous tumours of the spleen and lung (108). In humans, patients with a rare recessive syndrome called mosaic variegated aneuploidy (MVA) display an increased predisposition to early onset cancer. This has been linked to monoallelic or biallelic mutations resulting in a decrease in levels of normal BUBR1 (109).

Further supporting this view is evidence suggesting that CIN+ cells may be able to restore or gain phenotypes through divergent mechanisms (110). This may include increasing the gene expression of other proteins via copy number changes or the creation of fusion proteins. In experiments performed by Rancati and colleagues, yeast cells were depleted of a protein normally required for cytokinesis, *MYO1*. The deletion of this gene in the cells resulted in many strains of yeast that were either aneuploid or polyploid with a resulting change in gene expression that correlated with the change in number of chromosomes. Electron microscopy analysis of 10 of the *MYO1* deficient cell lines revealed that cytokinesis was restored through 3 morphologically different mechanisms that were non-MYO1 dependent. Further analysis of gene expression changes within these cell lines revealed that 2 of the morphological changes were associated with changes in ribosomal biogenesis and the other was correlated with cell wall biogenesis. This work suggests CIN may allow for the restoration of cellular functions via mechanisms that bypass the original genetic defect.

1.3.6 CIN and drug resistance

The development of drug resistance is a process that may be catalysed by on-going chromosomal re-arrangements in CIN tumours. Duesberg and colleagues demonstrated that aneuploid cancer cells can acquire accelerated drug resistance *in vitro* in the face of drug selection pressures (11). In their experiments, they investigated the response of aneuploid and diploid Chinese hamster cells to diverse drugs including puromycin, cytosine arabinoside, colcemid, and methotrexate. The cells were grown in the presence of drug, and they were able to generate drug resistant clones in the aneuploid cells but none from the diploid cells. Additionally, they demonstrated that cells selected to be resistant to one drug were cross-resistant to other drugs.

My laboratory has proposed that CIN is associated with taxane resistance both *in vitro* and *in vivo* (12, 14). Taxanes hyper-stabilise microtubules by altering microtubule dynamics via increased polymerisation of microtubules (111), leading to the activation of the SAC. Cells arrest in mitosis (112) and subsequently undergo cell death, or they can undergo mitotic slippage, escaping the mitotic arrest. Cell death during a mitotic arrest or after a mitotic slippage to form a multinucleated interphase cell is termed mitotic catastrophe (46).

Microtubule inhibitors are known to induce polyploidy in checkpoint-deficient or taxane-resistant cells (69, 113, 114), which has prompted the suggestion that polyploidy in response to paclitaxel may be a useful indicator of drug resistance (114). The kinome RNAi screen from our lab extended these observations and suggested that genes that are permissive for polyploidy, when targeted by RNAi, influence pathways that taxanes depend upon for cellular cytotoxicity, and that polyploidy or CIN prior to drug treatment may serve as a marker for *de novo* taxane resistance. Conversely, taxane

treatment may select for a higher frequency of CIN in residual tumour. Taxane treatment may result in selection of a population of cells with partial checkpoint dysfunction that is still sufficient to support long-term growth and survival (as prolonged disruption of the spindle checkpoint is not tolerated by cancer cells because of critical chromosome loss) (115).

A common theme emerged from both the paclitaxel kinome screen in three cell lines performed by our laboratory (12) and a whole-genome paclitaxel screen performed by Whitehurst and colleagues (116) with respect to the relationship between mitotic arrest and paclitaxel efficacy. Enhancers of paclitaxel cytotoxicity (upon siRNA knockdown) identified in both screens – CERT (ceramide transporter protein), ACRBP (acrosin-binding protein) and TUBGCP2 (tubulin, gamma complex associated protein 2) – were capable of augmenting a paclitaxel-induced mitotic arrest, growth inhibition or caspase activity. Intriguingly, the mitotic response to the paclitaxel-sensitisers ACRBP and TUBGCP2 was dependent on the cell line, indicating the uncoupling of spindle-checkpoint-induced cell cycle arrest with downstream apoptotic pathways. In the H2126 NSCLC cell lines, gene silencing of ACRBP and TUBGCP2 resulted in enhanced inhibition of proliferation with paclitaxel, whereas the depletion of these genes in H1155 cells enhanced caspase activation induced by paclitaxel. The authors suggest that tumours with a weakened spindle checkpoint may become more dependent on the aberrant expression of genes such as ACRBP that increase the robustness of the spindle assembly checkpoint, thus allowing for efficient mitotic progression.

RNAi has also been used to validate the role of the microtubule stabilising protein TAU (117) as a paclitaxel-resistance factor (118). Gene expression data from tumours

removed from 82 patients with stage I–III breast cancer prior to paclitaxel treatment were analysed. TAU was one of the most significantly differentially expressed genes in patients with pathological complete response compared with patients with residual disease. Lower TAU mRNA expression was found in patients with pathological complete response. When ZR75.1 and MCF-7 cancer cell lines were transfected with siRNA targeting TAU, cell viability was decreased after treatment with paclitaxel compared with control-transfected cells. TAU siRNA-transfected cells also appeared to take up more paclitaxel. Further data suggested that TAU competes with paclitaxel for binding with microtubules, and therefore results in poorer efficacy of paclitaxel treatment.

Carter and colleagues demonstrated the existence of gene expression signature that correlated with CIN, termed the CIN70 signature (59). Expanding upon this and further examining the link between CIN and intrinsic taxane resistance, my laboratory proposed that CIN cancer cells *in vivo* overexpress a set of genes termed the microtubule-stabilising (MTS) gene signature (14), that enables them to survive down-regulation of these genes following MTS treatment. A similar type of signature was not seen with the non-MTS cytotoxic, 5-FU. In cancer cell lines, MTS treatment resulted in this gene signature being down-regulated in CIN- CRC cell lines but not CIN+ CRC cell lines. Silencing these genes using siRNA resulted in an increase in paclitaxel sensitivity. Together, the CIN70 and MTS gene signature work are significant as they propose that there exists stable gene expression changes that are common across CIN+ cancers and that these stable gene expression changes can contribute to drug resistance.

Taken together, this implied 1) that pathways associated with maintaining chromosomal stability may contribute to sensitivity to paclitaxel and other microtubule targeting drugs 2) that pathways required for response to taxane treatment are de-regulated in CIN tumours and that CIN cancer cells may overexpress certain genes allowing them to better tolerate multiple cellular stresses, including cytotoxic treatment.

1.3.7 Extreme CIN and tumour suppression

The potential advantage conferred by genomic instability must be balanced against disadvantageous consequences of diversity resulting from the generation of large numbers of cells with deleterious variants. Muller (119) proposed that in a population new variants can occur at many different loci. Without genetic recombination, the combinations of two variants can only occur if the second one occurs in the offspring of the first. In the presence of a selection pressure, many new occurring variants are lost. Genetic material that is permanently lost cannot be regained in a population without recombination and this would result in a “ratchet” effect that would cause disadvantageous mutants to accumulate within the population and decrease the overall fitness of the population. The synergism where random genetic drift overwhelms the ability of natural selection to eradicate incoming deleterious mutations is known as mutational meltdown (120) and leads to eventual extinction of the population.

One explanation as to why CIN+ tumours may not relapse by themselves in a manner similar to mutational meltdown may be that the tumour environment constantly exerts a selection pressure and deleterious variants are eliminated from the population before they are allowed to accumulate and remain fixed in the population. This may be similar to that observed in P-endosymbiont bacteria (121). As discussed previously, Rancati and colleagues provided evidence that CIN+ permits cells to restore lost functions by

altering other pathways (110). Additionally, it is conceivable that CIN cancer cells may duplicate genes in order to guard against potential loss of these genes, or that variants with these genomic duplications may be at a selective advantage in the presence of an external selection pressure.

However, there is increasing support for the concept that increasing the level of chromosomal instability may be lethal towards cancer cells. Weaver and colleagues have postulated in their animal models that excessive chromosomal instability leads to tumour lethality (108) as the karyotype that generated the tumour is lost following further chromosomal missegregation and this was likened to mutational meltdown. In this case, CIN was acting both as a tumour initiator but excessive CIN acted as a tumour suppressor, supporting the idea that an optimal level of CIN is required to initiate cancer. Janssen and colleagues (74) proposed that reducing the protein levels of BUBR1 and MPS1 in combination with low doses of paclitaxel increases the level of missegregation errors to a lethal degree. Consistent with that, Kops and colleagues (122) demonstrated that increasing chromosome losses by deactivating the mitotic checkpoint via siRNA knockdown of MAD2 and BUBR1 was lethal for cancer cells and that a weakened checkpoint might have negative effects on proliferation. This leads to the suggestion that the exacerbation of tumour genome instability may be a target for therapeutic intervention by overwhelming the cancer cell population with deleterious variants.

Recently, our laboratory has demonstrated that there exists a non-monotonic relationship between CIN and clinical outcome for a variety of cancer types (60). According to this model, patients with tumours demonstrating an intermediate level of

CIN show a poorer prognosis compared to patients with extreme levels of CIN (60, 105). This may be due to a higher degree of on-going chromosomal alterations in cells with extreme CIN that are not tolerated by the tumour cells analogous to bacterial population genetics models of mutational meltdown and animal models demonstrating a tumour suppressor role for CIN.

These studies suggest that an optimal level of CIN may provide an evolutionary advantage but an excessive level, coupled with external stressors such as drug treatment may be deleterious to the CIN cancer cell population. The addition of chemotherapy as an additional selection pressure to cancer cells with a high level of CIN may accelerate cancer cell population implosion similar to Muller's ratchet. More provocatively, it raises the question whether cytotoxic treatment can act as a selection pressure to drive tumour cells from a lower to an intermediate CIN state enhancing tumour biological aggressiveness and worsening patient outcome.

1.3.8 CIN as a targetable phenotype

Roschke and colleagues have demonstrated the existence of anticancer compounds that may specifically target karyotypically complex cancer cells (123), indicating that it may be possible to target CIN+ cancer cells specifically. Various experiments have suggested that there may be adaptations acquired by a CIN+ cell in order to tolerate and maintain the CIN state. Normal mammalian cells appear to poorly tolerate the aneuploid state. In humans, trisomies involving chromosomes 13, 18 and 21 are the only three that are tolerated in humans up to birth (124). These three chromosomes encode the smallest number of transcripts suggesting that normal cells poorly tolerate the increase in gene dosage brought about by an increase in number of chromosomes. Furthermore, studies in aneuploid mouse embryonic fibroblasts (125) and primary foreskin fibroblasts from

Down's syndrome patients show reduced proliferation rates compared to normal fibroblasts (126). This suggests that CIN+ acquire additional adaptations to enable them to cope with the increase in genetic content.

Experiments performed in yeast model systems have enabled us to gain insight into the adaptations acquired by aneuploid cells in order to tolerate aneuploidy. Polyploid yeast are dependent for survival upon increased expression of genes involved in pathways such as sister chromatid cohesion and mitotic spindle function (93). Torres and colleagues demonstrated that strains of aneuploid yeast show delayed cell cycle transition, an increase in glucose uptake, and a gene expression pattern characteristic of the environmental stress response (127). Despite the proliferative disadvantage that aneuploid cells had under general conditions, Pavelka and colleagues showed that under stressful conditions, such as changes in temperature or the additions of drugs to the media, aneuploid cell lines did not experience as large an anti-proliferative effect as the euploid cell lines (128).

Following on from the experiments performed by Torres and colleagues, recently Tang and colleagues (129) demonstrated that CRC cancer cells lines with increased ploidy display increased sensitivity towards 17-AAG and AICAR compared to CRC cell lines with a near-diploid karyotype. This may be due to an increased demand for energy and dependence upon protein-folding in cells with an increase in ploidy. Additionally, non-cancer cells with increased ploidy were more susceptible to chloroquine, an inhibitor of autophagy, suggesting an increased dependency on the autophagic pathway that may result from an increase in cellular size and protein production. However, the findings

with chloroquine were not replicated when the authors compared aneuploid cancer cells to diploid cells.

The discovery of the CIN70 gene signature, (59) that is overexpressed in cancer cells with high levels of aneuploidy, suggest that there indeed exist common pathways that are deregulated across CIN+ tumours of various types. Regulators of chromosome segregation were present in the gene signature, including *AURKB, CDC20* and *MAD2* suggesting that CIN cancer cells may have a greater dependency on pathways involved in chromosome duplication and segregation, similar to that observed in experiments involving polyploid yeast (93).

Taken together, these observations indicate there CIN+ cells certainly require adaptations and that there are pathways that are commonly deregulated in CIN+ tumour cells of differing tissue origins. Therefore, this suggests that karyotypic instability may be specifically targeted in human cancer. Targeting CIN survival regulators may also limit cytotoxicity to surrounding normal non-CIN tissue, thus limiting side effects. In my thesis, I have sought to identify survival pathways that CIN+ specific.

1.4 CERT and Ceramide mediated drug sensitivity

The ceramide pathway has been implicated in the cellular response to cytotoxic chemotherapy and enzymes that impair ceramide accumulation in response to drug exposure have been associated with multidrug resistance (130). Ceramide is a bioactive lipid belonging to the sphingolipid group that is pro-apoptotic (131) although the mechanisms have been difficult to define completely (132). The identification of small molecules that may potentiate the generation of ceramide in specific cellular compartments within cancer cells may have therapeutic potential to augment

chemosensitivity (133). In the previously described RNAi screen for regulators of multidrug sensitivity performed by our lab (12), the ceramide transporter CERT was the strongest hit potentiating multidrug sensitivity to paclitaxel, doxorubicin, cisplatin and 5-FU (fluorouracil) when silenced by RNAi. CERT was relatively over-expressed in paclitaxel-resistant ovarian cancer and was one of six genes included in a functional metagene that was found by our laboratory to be predictive of combination-chemotherapy drug sensitivity in breast cancer (134).

CERT is a splice variant of Goodpasture antigen-binding protein that functions to transport ceramide from the endoplasmic reticulum (ER) to the Golgi apparatus where it is then converted to sphingomyelin (SM) in an ATP-dependent non-vesicular manner (135). The CERT protein contains a pleckstrin homology (PH) domain (136), that allows it to recognise PI4P and localise to the Golgi, and a (StAR)-related (START) domain (137) that allows the binding of long-chain ceramides (C14-C20 ceramide) (135). A FFAT motif exists between these two domains on CERT and this allows it to interact with the VAP proteins located on the ER. However, there also exists non-CERT mediated transport of ceramide from the ER to Golgi in the form of vesicular transport where ceramide is then converted to glucosylceramide instead of SM (135, 138, 139).

Disruption of the CERT-mediated transport pathway may lead to cell death due to the accumulation of ceramide in the ER where it is unable to be converted into SM, potentially augmenting a ceramide-induced cell death response. Several cytotoxic agents have been shown to promote ceramide accumulation, resulting from increased de novo synthesis or sphingomyelinase activity. Consistent with alterations in endoplasmic reticulum physiology due to the accumulation of ceramide, depletion of CERT by RNAi

together with paclitaxel treatment leads to the synergistic induction of endoplasmic stress, as measured by the increase in phosphorylated PERK (protein-kinase-like endoplasmic reticulum kinase). Despite the association of CERT depletion with taxane sensitivity and ER stress activation, the molecular pathways responsible for downstream cell death signalling remain unclear.

Consistent with an integral role for the ceramide pathway in influencing multidrug response, several enzymes in this pathway, including glucosylceramide synthase, dihydroceramide synthase, sphingosine kinase and acid ceramidase, have been shown to alter sensitivity to several common cytotoxics (140-144)

1.4.1 CERT and Autophagy

A clearer understanding of the molecular pathways responsible for cell death following CERT depletion and drug exposure may offer a broader understanding of cytotoxic response and offer therapeutic opportunities to delay the acquisition of drug resistance. Ceramide has previously been shown to induce autophagy (145). This may be the result of an increase in ER-stress due to the unfolded protein response (UPR) as misfolded proteins that accumulate in the ER can induce autophagy (146, 147). Ceramide may also induce starvation induced autophagy as ceramide can induce the down-regulation of nutrient transporter proteins (148) leading to cells not being able to efficiently use extracellular nutrients.

Autophagy is a dynamic regulated pathway where cytoplasmic material (that can contain organelles and proteins) is delivered to lysosomes for degradation. Induction signals for autophagy result in the formation of the phagophore that engulfs the cytosolic material that is to be degraded (149) This then leads to the formation of

autophagosome. Many Atg proteins are involved in the formation of the autophagosome, a double-membraned organelle, (Atg1–10, Atg12–14, Atg16–18, Atg29 and Atg31). In mammalian cells, Beclin can induce autophagy and this is potentiated by UVRAG. LC3 is found on the inner membrane of the autophagosome and is a commonly used marker of autophagy induction. A step-wise maturation of the autophagosomes then occurs via fusion with endosomes, forming amphisomes. These then fuse with lysosomes to form autolysosomes (150) to degrade the contents of the autophagosomes (Figure 7). Autophagy can play both a protective and detrimental role in cell survival (151) and autophagic cell death following autophagy induction has been proposed (152).

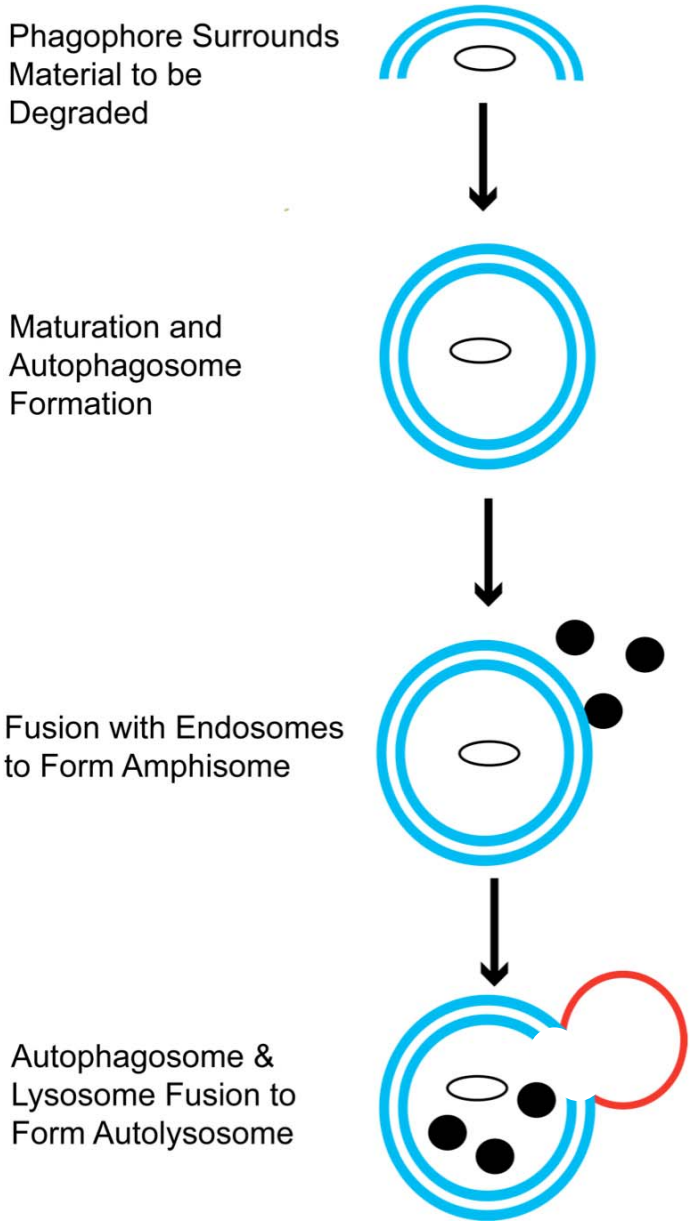

Figure 7 Maturation of autophagosomes and fusion with lysosomes to form autolysosomes

1.4.2 Paclitaxel response and the lysosome

Microtubule-stabilising agents are known to trigger activation of the protease cathepsin B and its release from the lysosome. Furthermore cathepsin B inhibition antagonises microtubule-stabilising agents (153) and lysosome-destabilising agents demonstrate synergistic cytotoxicity with either vincristine or paclitaxel (154). Two screens have identified other lysosomal regulators that influence paclitaxel response. The Gauchers disease gene product, GBA1, was identified by our laboratory in the screen of ceramide regulators as a candidate paclitaxel-resistance gene following silencing by siRNA (12). GBA1 protein level is induced at 12–18 h following paclitaxel treatment, coincident with maximal mitotic arrest of HCT-116 cells. The vacuolar ATPase subunit ATP6V0D2 was also identified as an enhancer of paclitaxel cytotoxicity following gene silencing in the genome wide screen by Whitehurst and colleagues for genes regulating paclitaxel sensitivity (116). In a pharmacological validation strategy, inhibition of the vacuolar ATPase with a synthetic lysosomal ATPase inhibitor, RTA-203, together with low-dose paclitaxel treatment, significantly reduced the viability of H1155 NSCLC cells. Targeting glucosylceramide synthase, an enzyme involved in the conversion of ceramide to glucosylceramide at the lysosomes, has been shown to promote sensitivity to doxorubicin, vinblastine and paclitaxel with a concomitant fall in expression of ABCB1 (144).

Data indicating that the down-regulation of CERT may increase levels of ceramide, an autophagy inducer, and that cell death following paclitaxel treatment may be influenced by lysosomal activity together suggest that the autophagy-lysosomal pathway may play a role in sensitising cells to taxanes following CERT silencing. In this thesis I have

attempted to elucidate how CERT silencing results in the sensitisation of cancer cells to paclitaxel and other cancer cytotoxics using integrative functional genomics techniques

1.5 Conclusions

CIN is a complex multifactorial phenotype that may arise following errors in the machinery maintaining proper cellular division. Additional adjustments are required for the cell to tolerate the CIN state and chromosome missegregation and this may be reflected in an increased dependency on pathways regulating glucose utilisation, protein folding and autophagy.

The polygenic nature of multidrug resistance as illustrated by functional genomic studies, combined with the ability of the tumour population to silence gene expression through epigenetic means (155) or activate gene expression through increased gene dosage triggered by chromosome reassortment in aneuploid tumours (156), may explain the relative ease with which tumour populations acquire resistance to non-cross-resistant cytotoxics as treatment lines advance in solid tumours. CIN+ cells are intrinsically resistant to microtubule targeting drugs and functional genomic approaches reveal that resistance to microtubule targeting agents is mediated by the down-regulation of genes maintaining chromosomal stability. Attempts to limit cytotoxic resistance and improve patient survival with ‘non-cross-resistant’ agents are likely to produce only modest benefits unless strategies can be identified to target the underlying genetic propensity of the cancer cell to rapidly disrupt the expression of large numbers of genes potentially involved in multidrug resistance pathways.

In this thesis, I have addressed four questions that attempt to explore the underlying basis for the initiation and the tolerance of CIN:

1. Is CIN associated with intrinsic resistance to other clinically relevant drugs?
2. Can specific means to target CIN+ cells be identified through pharmacological and whole genome RNA interference screens?
3. Can clinically relevant initiators of aneuploidy be identified through integrative functional genomics techniques?
4. Can a molecular basis for CERT-mediated paclitaxel sensitisation be defined that might support the targeting of CIN+ cells?

Chapter 2. Materials and Methods

2.1 Kinase inhibitor and cytotoxic agent screens to identify CIN survival mechanisms

2.1.1 Cell lines

All cells were incubated at 37 ºC with 10% CO2 in Dulbecco's Modified Eagle Medium (D-MEM) (1X), liquid (High Glucose) with L-Glutamine from Gibco (Invitrogen) and supplemented with 1:10000 of Penicillin-Streptomycin (catalogue no. P4333, 10000 units penicillin, 10 mg Streptomycin) from Sigma.

27 CRC cell lines previously characterised for numerical/structural CIN, MIN status (3, 157-159) were used (Table 3).

Publicly available somatic mutation data from the Sanger Institute Cancer Cell Line Project (CLP) and COSMIC database (78) was used. 15 CIN+ and 6 CIN- cell lines used in my analysis were present within the CLP database. A total of 20 out of the 61 genes resequenced in the project were found to have somatic mutations in at least 1 of those 21 cell lines. Additional information regarding the somatic mutation status of *APC*, *CTNNB1*, *KRAS*, *MLH1*, *PIK3CA* and *TP53* were obtained from both published (160-163) and internal laboratory data.

Isogenic HCT116 *MAD2+/-* cell lines (164) and HCT116 *PTTG1-/-* cell lines (80) were donated courtesy of Drs Benezra and Vogelstein respectively.

To generate tetraploid HCT116 cells, naturally occurring tetraploid cells were isolated from the parental cell line and single cell sorted using flow cytometry. Clonal FISH was performed with Centromere Enumeration Probes (CEP) against Centromere 2 and 15.

Cell Line
C32
COLO205
COLO678
DLD1
GP2D
HCA7
HCI-H508
HCI-H747
HCT116
HCT15
HDC57
HT55
LS1034
LS174T
RKO
SKCO1
SW1116
SW1222
SW1417
SW1463
SW403
SW48
SW620
SW837
SW948
T84
VACO5

Table 3 Table of colorectal cancer cell lines used

2.1.2 Calbiochem kinase inhibitor library and 5-FU screen

Calbiochem Kinase Inhibitor Libraries I and II (EMD Biosciences) containing 160 inhibitors were used. Comprehensive data for these inhibitors including references documenting target inhibition or downstream signalling cascade inactivation can be found on the manufacturer's website (165).

Cells were plated into 96-well tissue culture microplates at an initial seeding density of 4000 cells/well. After 24 hours, cells were treated with the inhibitors at a final concentration of 10μM/well. This concentration was selected following drug titration test analysis to give an optimal range of mean relative surviving cells following inhibitor treatment across all cell lines. After 72 hours of treatment, cell viability was assayed using the Celltiter-Blue Cell Viability Assay (Promega). The assay reagent was added at a 1:5 dilution and cells were incubated at 37 ºC for 1 hour before recording fluorescence (560(20)Ex/590(10)Em) using an Envision plate reader. The readout for each inhibitor treated well was normalised to vehicle control wells. For the HCT116 *MAD2* isogenic cell lines, a final inhibitor concentration of 1μM/well was used to allow for a larger range of number of surviving cells across all inhibitors.

5-FU (Sigma) was used at both 1μM and 10μM for a treatment length of 72 hours. The 27 CRC cell lines were plated and assayed using the same conditions and methods as above.

2.1.3 Anti-Cancer agent screen

Biolog Anti-Cancer Agent Microplates M11-M14 consisting of 92 anti-cancer agents at 4 increasing concentrations between 0.1 µM and 25µM per agent were used. Cells were plated at an initial seeding density of 5000 cells/well. After 72 hours, Biolog Redox Dye Mix MA was added at a 1:6 dilution and cells incubated for 6 hours at 37 ºC. The number of surviving cells per well was assayed using an Envision plate reader to detect absorbance at 590nm and normalised to the negative control wells.

2.1.4 Cell proliferation assay

The proliferation rate of all 9 CIN- and 18 CIN+ CRC cell lines was measured using the IncuCyte Long-term Cell Imaging System. Cell lines were plated in 96-well plates at an initial plating density of 4000 cells/well and phase contrast images were obtained 2-hourly over 70 hours allowing measurements of cell monolayer confluence. Outliers were removed manually and growth curves were fitted by splines with the R package *grofit* (166) with smoothing parameter *smooth.gc = 0.7.*

2.1.5 Meta-Analysis of CIN outcome

Axel Walther performed the analysis presented in this section.

Survival data were summarised using a log hazard ratio for comparison between CIN+ and CIN- groups. Data from individual studies were extracted using the methods described by *(167)* and pooled to generate the summary statistic and confidence intervals using a fixed-effects model with inverse variance weighting. All meta-analyses were performed using Stata 10.1 (Stata Corp, College Station, TX).

2.1.6 Statistical methods

In this section, I was assisted by David Endesfelder.

All tests were performed as two-sided unless otherwise mentioned. To remove outliers, drugs resulting in relative number of cells >1.4 compared to vehicle control were eliminated from analysis. A Kolmogorov-Smirnov test was performed to test for overall differences in the distribution of relative cell numbers following inhibitor treatment between CIN+ and CIN- cell lines. Inhibitors that showed a fraction of surviving cells > 0.8 in > 75 % of the cell lines were excluded from the analysis. For comparisons of 2 cell lines, drugs resulting in relative number of cells >0.8 in both cell lines were removed from analysis. A Wilcoxon signed-rank test was used to test for differences between CIN+ and CIN- cells (for each concentration of drug in Biolog microplates). For the Biolog microplates, each concentration of drug was used in duplicate; therefore the replicates which showed the least difference in cell number between the 2 cell lines was used for further analysis.

The maximal slope of the growth curve (*mu*) for each cell line was used to test if the difference in drug sensitivity between CIN+ and CIN- colorectal cancer cell lines were not solely due to different proliferation rates. CIN+ and CIN- cell lines with $mu < 1$ were tested with a one-sided Wilcoxon-Mann-Whitney test. Next, the influence of the proliferation rates of each cell line was corrected. A linear regression model for all cell lines with $mu < 1$ was estimated, where *mu* was used as the independent variable and the mean fraction of surviving cells over all inhibitors as the dependent variable. The residuals of this analysis were tested for significant differences between CIN+ and CIN- with a one-sided Wilcoxon-Mann-Whitney-Test (168). An analysis of covariance model

with interactions was applied, where the mean fraction of surviving cells over all inhibitors was used as the dependent variable, *mu* as the linear independent and CIN status as the factor variable. The interaction term was utilised to test for significant differences in slopes between CIN+ and CIN- cell lines.

To test for significant differences in sensitivity to thymidylate synthase inhibitors comparing HCT116 diploid parental to *PTTG1-/-* or *MAD2+/-* cells, the influence of different concentrations was corrected by estimating a linear regression model for near linear correlations between concentration and sensitivity or a one-way ANOVA otherwise. In each case the concentration was used as the independent variable and the resulting residuals were tested for differences between CIN+ and CIN- cells with a Wilcoxon-Mann-Whitney test.

2.2 Whole genome RNAi screens for regulators of CIN survival and ploidy

2.2.1 Cell culture and siRNA transfection protocol

The same conditions were used to transfect the HCT116 diploid parental and *MAD2+/-* cells. All cells were incubated at 37 ºC with 10% CO2 in Dulbecco's Modified Eagle Medium (D-MEM) (1X), liquid (High Glucose) with L-Glutamine from Gibco (Invitrogen) and supplemented with 1:10000 of Penicillin-Streptomycin (catalogue no. P4333, 10000 units penicillin, 10 mg Streptomycin) from Sigma. The cell lines were used coutesy of Dr Benezra (164).

The Dharmacon whole genome siRNA library targeting 21222 genes in triplicate was used. The screen was performed using 96-well tissue microplates with a final

concentration of siRNA of 37.5nM and 0.3µl/well of Lipofectamine RNAiMAX (Invitrogen). The microplates were plated with 0.1% Poly-L-Lysine (Sigma) diluted 1:8 in PBS prior to cell culture.

The whole genome siRNA library was resuspended in 10µl of HBSS (Invitrogen) and pre-aliquoted into 96-well microplates. On the day of the screen, 0.3µl of Lipofectamine RNAiMAX diluted in 10µl of Optimem-I (Invitrogen) was added to each well. The mixture was allowed to incubate at room temperature for 15 minutes. 4000 cells in 80µl media were added to each well. The plates were incubated for 72 hours at 37ºC and 10% CO2. Following this, the medium was aspirated from each well and 150µl of a -20ºC 80% Ethanol solution was added as a fixative. All plates were stored at -20ºC prior to analysis. DAPI (Roche) was used to label the DNA. DAPI staining was performed as follows: Each well was washed three times using 35µl of PBS each time. 35µl of a DAPI in PBS solution (1µg/ml) was added to each well. Plates were incubated for 30 minutes at room temperature. The DAPI solution was then aspirated and 35µl of PBS was added to each well prior to sealing the plates. The plates were scanned on an Acumen ex3 laser scanning cytometer to measure cell number and cell cycle profile.

2.2.2 Statistical normalisation of screening data

Becky Saunders performed the analysis described in this section.

For analysis of cell number data from the whole genome RNAi screens, cell number was normalised as follows: Normalised value = log (well value / plate median value) to provide a normal distribution. A z-score for each well was calculated by dividing the normalised well plate value by the plate median absolute deviation (MAD). The median

z-score across triplicate wells was then calculated to provide the final z-score for each candidate gene.

For the analysis of cell cycle profile data from the whole genome RNAi screens, to allow comparison of z-scores obtained from the HCT116 diploid parental screen with other whole genome screens in fibrosarcoma (HT1080), lung cancer (PC9) and renal cancer (RCC4) cell lines, the >4n data for the HCT116 diploid parental cell line was renormalised as follows: Normalised well = (well value - plate median value) / screen MAD.

2.2.3 Statistical analysis of screen variance

This section was performed by Stuart Horswell.

Raw (absolute) count data were normalized for plate and possible edge effects by fitting a linear model with row/column interaction terms and an independent "plate" factor. Initially a Poisson model was used, but as this provided evidence of over-dispersion, the dispersion parameter was estimated and a negative binomial model was applied instead. Model fitting was performed using the "glm" function in base R, with dispersion parameter estimated using glm.nb and the negative binomial family implemented using the negative.binomial family, both from the MASS package.

Residuals were extracted from these models and are subsequently referred to as "normalised" data. The fitting of mixture models was performed using the lme function from package nlme, with siRNA nested within MAD2 status for the random effects, and siRNA, MAD2 status and siRNA * MAD2 status interaction as the fixed terms. A

retrospective power analysis was performed using the critical values obtained from a z-score analysis of the data from the mixture models.

All analyses were performed using R.

2.2.4 Defining significant and consistent regions of copy number alteration in cell lines

The following analysis steps was performed by David Endesfelder

The analysis was performed using R. First, minimum consistent regions of genomic alteration were identified across all cell lines. Next, each of these regions was assessed for gain in DNA copy number. Since many CIN cell lines are near triploid or tetraploid, using a diploid baseline (copy number = 2) would result in most of the genome being computed as gained. Therefore to select for genomic regions altered specifically relative to the background ploidy of the cell line, ploidy status was estimated for each cell line using the median copy number over all SNP probes. Each region in each cell line was then defined as either gained (copy number > ploidy baseline) and normalised to the ploidy baseline of the cell line or not gained and set to 0. Then each region was assessed for loss in the same manner.

To test for statistical significance between CIN+ and CIN- cell lines a d-score for each lost and gained region was computed by calculating the mean normalised copy number across CIN+ and CIN- cell lines, thereby accounting for both amplitude and frequency of genomic aberrations. A Significance Analysis of Microarrays was then performed with a modified two-sample t-statistic. In comparison to a standard two-sample t-statistic, SAM includes an additional parameter which decreases the influence of high

sample variance. This was empirically set to 0.5 which results in a balanced weighting of frequency and amplitude.

To detect significant regions, 10000 random class label permutations were performed and all regions with a q-value < 0.05 were defined as significantly gained or lost. To ensure the selection of genes consistently altered across aneuploid tumours, any genomic change not seen across >50% of the tumours was excluded from further analysis. Regions were then mapped to genes using BioMart.

2.2.5 Live cell imaging

For live cell imaging H2B-mRFP HCT-116 cells were monitored at 37ºC and 5% CO_2 in LabTech II (LabTech) chambers. Cells were plated into chamber slides for reverse transfection. Images were acquired every 3 min for 8 h using a 40x oil NA 1.3 objective on an Olympus Deltavision Personal microscope (API) equipped with a DAPI-FITC-Rhod/TR-CY5 (Chroma) filter set and environmental chamber.

2.3 CERT multidrug sensitisation pathway

2.3.1 Cell culture and siRNA transfection protocol

All cells were incubated at 37 ºC with 10% CO2 in Dulbecco's Modified Eagle Medium (D-MEM) (1X), liquid (High Glucose) with L-Glutamine from Gibco (Invitrogen) and supplemented with 1:10000 of Penicillin-Streptomycin (catalogue no. P4333, 10000 units penicillin, 10 mg Streptomycin) from Sigma. Where siRNA transfection was performed, the media was not supplemented with Penicillin-Streptomycin.

Cell lines used include HCT116 and the HER2+ breast cancer cell lines BT474, HCC1954 and SKBR3. The GFP-LC3 HEK293 cell line was used courtesy of Dr Sharon Tooze.

All siRNAs were obtained from Dharmacon and siRNA transfections were performed using reverse transfection methods with Lipofectamine RNAiMax reagent (Invitrogen) at 0.3µl per well of a 96-well plate or 2µl per well of a 6-well plate and with a final concentration of siRNA of 37.5nM. For siRNA transfections in 96-well plates, a final volume of 100µl with 4000 cells per well was used. Both siRNA and transfection reagent were made up to 10µl each in Optimem-I from Gibco (Invitrogen). After 5 minutes incubation at room temperature, both mixtures were added together and vortexed. The mixed solution was allowed to incubate for at least 20 minutes at room temperature. Cells were trypsinised and resuspended in tissue culture medium. The Optimem-I mix and medium containing cells were added to the each well to make up the final volume for 100µl. For siRNA transfections in 6-well plates, a similar protocol to that of the 96-well plates was used, but scaled up proportionally to a final volume of 1.5ml with 300000 cells per well. Both siRNA and transfection reagent were made up to 200µl each in Optimem-I when using 6-well plates.

2.3.2 Fluorescent ceramide transport analysis

Dr Charles Swanton performed the analysis described in this section.

HCT116 cells were seeded the day before the experiment on 25-mm diameter coverslips at a density of 2×10^5 cells. On the day of the experiment the coverslip was placed into a chamber and the cells were washed in modified Krebs-Ringer buffer and incubated on

ice for 20 min with 0.05 µm BODIPY® FL C5-ceramide and excess dye was removed by washing with modified Krebs-Ringer buffer. The coverslip was then mounted on a heated stage after replacing the medium with fresh medium at 37 °C. The distribution of ceramide was analyzed after 20 minutes using an inverted Zeiss LSM-510 scanning laser confocal microscope (Thornwood, NY).

2.3.3 Lipid extraction, liquid chromatography / mass spectrometry (LC/MS) analyses of ceramide

Liquid Chromatography / Mass Spectrometry were performed by Stefka Spassieva and Lina Obeid.

Briefly, cell pellets were fortified with internal standard (C_{13}/C_{16} ceramide, C_{17}/C_{16} ceramide, and $C_{17}/C_{24:1}$) and lipids were extracted with 2 ml ethyl acetate/isopropanol/water (60/30/10 v/v) solvent, dried under a stream of nitrogen, and re-suspended into 150 µl 1 mM NH_4COOH in 0.2% HCOOH in methanol. The MS analyses of endogenous ceramide species were performed on a Thermo Finnigan TSQ Quantum triple quadrupole mass spectrometer, operating in a Multiple Reaction Monitoring positive ionization mode. Lipid extracts were gradient eluted from the BDS Hypersil C8, 150 x 3.2 mm, 3-µm particle size column, with a 1.0 mM methanolic ammonium formate/2 mM aqueous ammonium formate mobile phase system. Peaks corresponding to the target analytes and internal standards were collected and processed with Xcalibur software. Quantitative analyses were based on the calibration curves generated by spiking an artificial matrix with known amounts of the target analyte synthetic standards and an equal amount of the internal standard. The target analyte/internal standard peak areas ratios were plotted against analyte concentration.

The target analyte/internal standard peak area ratios from the samples were similarly normalized to the internal standard and compared to the calibration curves, using a linear regression model. The phosphate contents of the lipid extracts were used to normalize the MS measurements of ceramides. The phosphate contents of the lipid extracts were measured with a standard curve analysis and a colorimetric assay of ashed phosphate.

2.3.4 CERT microarray expression profiling

Philip East performed the analysis described in this section

HCT116 cells were transfected with either siCON or siCERT and treated in triplicate with paclitaxel, C6-ceramide, or vehicle control for 8h for use on HuEx-1_0-st-v2 exon arrays (Affymetrix).

The HuEx-1_0-st-v2 exon arrays were processed using RMA (169) to generate gene level signal estimates for core level probesets. The arrays were normalised using quantile normalisation and antigenomic probes used to model the background. Quantification was run using apt-1.10.0 from Affymetrix. Prior to statistical analysis genes showing low variance across all samples were removed (coefficient of variance < 0.05) along with those with a consistently low signal in all samples (< 10^{th} percentile in all but 1 or less samples). All Affymetrix control probe sets were excluded from further analysis. Condition dependent gene changes were selected using a linear model where the standard errors were corrected using empirical Bayes shrinkage. Statistically significant genes were selected using a nestedF procedure run across applied contrasts (fdr < 0.05). Analysis was carried out in Bioconductor using Limma (170).

2.3.4.1 Enriched functional signatures

Metacore from GeneGo Inc. was used to identify any enriched biological signatures within the CERT depleted dependent gene changes in the presence of Ceramide. Differential genes (fdr < 0.05, no prior filtering) were tested against Metacore's process networks using the HuEx-1_0-st-v2 array as background. To refine this analysis a more comprehensive autophagy gene set was constructed from Metacore's process network set and its autophagy Map. This autophagy gene set was mapped back to the array data and tested for enrichment in CERT dependent gene changes (p-value < 0.05). The autophagy gene set was also tested using GSEA running 10000 permutations on the gene names and using a modified t-statistic to rank the genes (171, 172).

2.3.5 qPCR validation of microarray data

cDNA from the same samples used in the exon array analysis were used in Taqman Arrays (Applied Biosystems). 30 to 1000ng of cDNA was made up to 50µl using RNAase free water. The sample was then added to 50µl TaqMan® Universal PCR Master Mix (2×) (Applied Biosystems) in a 1.5ml microcentrifuge tube and vortexed. 100µl of the vortexed mix was added to each Taqman Array fill reservoir and centrifuged according to manufacturer's instructions to distribute cDNA samples within the Taqman Array card. Cards were then sealed using the provided card sealer and the qPCR reaction was run on an Applied Biosystems 7900HT instrument according to the Taqman Array protocol. The Taqman probes that were used are listed in Table 4.

18S-Hs99999901_s1	GBA-Hs00164683_m1
AADACL1-Hs00736941_m1	HPS5-Hs00200565_m1
ACADM-Hs00163494_m1	JUN-Hs00277190_s1
ATF1-Hs00270896_m1	KIF20A-Hs00194882_m1
ATF2-Hs00153179_m1	KLF6-Hs00154550_m1
AURKA-Hs01597773_mH	LAMP2-Hs00174474_m1
BDNF-Hs00538277_m1	MARVELD2-Hs00376394_m1
BNIP3L-Hs00188949_m1	MDK-Hs00171064_m1
BUB3-Hs00190920_m1	MRS2L-Hs00252895_m1
CASP4-Hs01031947_m1	MT1A-Hs00831826_s1
CCNE2-Hs00180319_m1	MTO1-Hs00201667_m1
CDC20-Hs00415851_g1	NEFL-Hs00196245_m1
CENPH-Hs00224722_m1	NR4A2-Hs00428691_m1
COL4A3BP-Hs00178615_m1	PBX1-Hs00231228_m1
COL4A3BP-Hs00178621_m1	PDIA6-Hs00194922_m1
CPA4-Hs00275311_m1	PTTG1IP-Hs00188967_m1
CREB3L2-Hs00811200_m1	SCML1-Hs00232467_m1
CYP24A1-Hs00167999_m1	SCML2-Hs00232330_m1
DDIT3-Hs00358796_g1	SPRR2D-Hs00863465_m1
EIF2AK3-Hs00178128_m1	TGFBR3-Hs00234257_m1
ENAH-Hs00430216_m1	TRIB3-Hs00221754_m1
FOXL2-Hs00846401_s1	TRIB3-Hs01082394_m1
FYCO1-Hs00225888_m1	WDFY1-Hs00604732_m1
GAPDH-Hs00266705_g1	WIPI1-Hs00215872_m1

Table 4 List of Taqman probes used

2.3.6 Drug response assays

Cells were plated into 96-well tissue culture microplates at an initial seeding density of 4000 cells/well for siRNA reverse transfection. After 48 hours of paclitaxel (Sigma) or vehicle control (DMSO, Sigma) treatment, cell viability was assayed using the Celltiter-Blue Cell Viability Assay (Promega). The assay reagent was added at a 1:5 dilution and cells were incubated at 37 ºC for 1 hour before recording fluorescence (560(20)Ex/590(10)Em) using an Envision plate reader.

2.3.7 LC3 immunoblotting

Cells were plated into 6-well tissue culture microplates at an initial seeding density of 300000 cells/well for siRNA reverse transfection. Cells were then harvested at 24h after paclitaxel or vehicle control treatment or at other specified timepoints. Where relevant, the protease inhibitor leupeptin (Sigma Aldrich) was used at a final concentration of 1µg/ml. As a positive control for the induction of autophagy, 1.5ml of Earle's Balanced Salt Solution (EBSS) was added to each well, following the aspiration of media and three 5-minute washes with PBS. Cells were harvested 2 hours following the addition of EBSS.

2.3.7.1 Lysate harvesting

6-well microplates were placed on ice and cell culture medium was aspirated followed by 3 washes with PBS. Final aspiration was performed and TNTE buffer (20mM Tris-HCl; 150mM NaCl; 0.3% Triton X-100; 5mM EDTA; pH 7.5) was added at 150µl per well and cells were harvested using a cell scraper. 150µl of lysate were added to a 1.5ml

tube and centrifuged for 5 minutes at >10000rpm. 130µl of the supernatant was aliquoted to a fresh tube. The supernatant was used immediately for immunoblotting.

2.3.7.2 Immunoblotting protocol

All reagents used were from Invitrogen unless otherwise stated. 30µl of lysate was aliquoted into a fresh 1.5ml tube containing 10µl of NuPAGE LDS Sample Buffer (4X) and 4% beta-mercaptoethanol (Sigma). Samples were heated on a heating block at 65ºC for 2 minutes. 35µl of the heated sample was loaded per well in a 1.5 mm, 10 well NuPAGE Novex 4-12% Bis-Tris Gel. 1x MES running buffer was used for gel electrophoresis at a voltage of 200V for 45 minutes. Upon completion of gel electrophoresis, the gel was washed for 5 minutes in 2x Transfer Buffer (with 10% methanol) prior to sandwiching in between chromatography paper (pre-soaked for 10 minutes with 2x Transfer Buffer with methanol) and a PVDF membrane (GE Healthcare) (presoaked in methanol for 10 seconds) for transfer of proteins. A semi-dry transfer was performed for 30 minutes at a constant 15V.

Upon completion of the semi-dry transfer, the PVDF membrane was washed for 5 minutes with TBS, followed by blocking of non-specific binding by incubating the membrane for 1 hour in a 5% non-fat Milk in TBS solution at room temperature. This was followed by three 5-minute washes in TBS prior to incubating with primary anti-LC3 mouse antibodies (Nanotools) at a dilution of 1:250 in the milk in TBS solution overnight at 4ºC.

The membrane was washed three times in TBS for 10 minutes each prior to incubating with HRP-conjugated secondary antibodies (GE Healthcare) at dilution of 1:10000 in

the milk solution at room temperature. The membrane was washed three times in TBS for 10 minutes each, prior to adding ECL reagents (GE Healthcare) for detection of the HRP-conjugated antibody.

2.3.8 Immunofluorescence microscopy

Cells were transfected in 6-well plates containing glass cover slips. The 6-well plate siRNA transfection protocol was used. Cells were fixed using PTEMF (20 mM PIPES (pH 6.8), 10 mM EGTA, 1 mM MgCl2, 0.2% Triton X-100 and 4% formaldehyde) at room temperature for 10 minutes. Primary antibodies were diluted as follows in PBS + 3% BSA; anti-LAMP2 (Abcam) 1/1000 and cover slips were incubated for one hour in the antibody solution. Following three 5-minute washes with PBS, cross-adsorbed secondary antibodies were used (Molecular probes) in PBS + 3% BSA. Cover slips were incubated for one hour at room temperature in the secondary antibody solution followed by three 5-minute washes with PBS. To visualise the cell nuclei, cover slips were then incubated in a 1µg/ml DAPI (Rosche) in PBS solution for 30 minutes at room temperature. Three 5-minute washes with PBS were then performed. The cover slip was dried before being mounted on a glass slide.

3D image stacks were acquired in 0.2 µm steps using a 100x oil NA 1.4 objective on an Olympus Deltavision Personal microscope (API) equipped with a DAPI-FITC-Rhod/TR-CY5 filter set (Chroma) and a Coolsnap HQ camera. The 3D image stacks were deconvolved with SoftWorx (API).

For quantification of LAMP2 spot intensity, cells were plated into 96-well tissue culture microplates at an initial seeding density of 4000 cells/well for siRNA reverse

transfection. After 48 hours of paclitaxel treatment, cells were fixed using 80% ethanol at -20ºC for 1 hour. Primary and secondary antibodies were used following the same protocol as in the previous section. Cytoplasmic spot intensity was measured using a Cellomics Arrayscan high-throughput imaging system.

2.3.9 Live cell imaging

For live cell imaging H2B-mRFP HCT-116 cells were monitored at 37ºC and 5% CO_2 in LabTech II (LabTech) chambers. Cells were plated into chamber slides for reverse transfection using the same protocol as transfection for 6-well plates but scaled down proportionally by 4 times. Cells were then treated with paclitaxel or vehicle control. Images were acquired every 10 minutes for 48h using a 40x oil NA 1.3 objective on an Olympus Deltavision Personal microscope (API) equipped with a DAPI-FITC-Rhod/TR-CY5 (Chroma) filter set and environmental chamber.

2.3.10 Tissue Microarray cohort

Patricia Gorman and Rebecca Roylance performed the analysis described in this section.

Archival paraffin-embedded breast cancer tissue was obtained from 356 patients diagnosed at Leeds Teaching Hospitals NHS Trust between 1983-1997. Tissue microarrays (TMAs) were constructed containing cores, 0.6mm in diameter and 4μm in thickness, selected from representative tumour areas as determined by a consultant breast histopathologist (AMH) from H&E stained sections. Full clinico-pathological data was available. The majority of chemotherapy treated patients were given CMF (cyclophosphamide, methotrexate and Fluorouracil 5-FU) or FEC (Fluorouracil 5-FU,

epirubicin and cyclophosphamide) treatment. Ethical approval was obtained (Leeds East **06/Q1206/180**).

Briefly, following deparaffinisation an antigen retrieval step was performed. This was done using the automated Ventana system and Tris buffer (Ventana Medical Systems, Inc). Tissue sections were incubated with CERT rabbit polyclonal antibody (Bethyl laboratories. Inc) dilution 1:3500 for 1 hour. Appropriate biotinylated secondary antibodies were used followed by streptavidin–biotin–peroxidase complex. Peroxidase was localised using diaminobenzidine, with counterstaining with Mayers haematoxyin. Negative controls were the omission of primary antibody. A known positive control was used with each batch of staining. Slides were viewed by two independent scorers blinded to each others findings.

CERT localised to the cytoplasm. Scoring was performed of both the percentage and intensity of staining using a scale of 0-3, with 0 = tumours with no staining whatsoever; 1 = tumours with rare scattered positive staining; 2 = tumours with moderate to strong staining but with some cells showing no readily detected staining; and 3 = tumours with strong staining, uniformly visualized over the whole section. A quickscore (percentage of cells staining positive x intensity) was quantified (173).

Survival analysis was performed by David Endesfelder and Jil Sander.

Survival analysis was performed with a univariate cox-proportional hazard regression model and a log-rank statistic was used for significance testing. A maximally selected rank statistic (174) was used on all 356 patients to detect a CERT expression quickscore threshold for separating good from poor prognosis. The R-package maxstat (175) was

used to derive the reported threshold of 175. To test for differences of CERT expression. A maximally selected rank statistic (174) was used on all 356 patients to detect a CERT expression quickscore threshold separating good from poor prognosis. A significant result of the maximally selected rank statistic suggests that a threshold separating good from poor prognosis exists. Based on this threshold (quickscore = 175), CERT expression was grouped into high and low expression for the whole dataset. Survival analysis was performed with a univariate cox-proportional hazard regression and a log-rank statistic was used for significance testing between the CERT high and CERT low groups. To test for differences of CERT expression levels between HER2+ and double-negative breast cancers (ER-/HER2-) a two-sided t-test was used.

2.3.11 Electron microscopy

Cells were grown on 13mm glass coverslips in 6-well tissue culture microplates. HCT-116 cells were transfected with siCERT or siCON using the standard protocol for 6-well tissue microplates. Following 48h of siRNA transfection, cells were treated with 25nM paclitaxel or vehicle control for 24h. Cells were fixed with 2.5% glutaraldehyde/ 4% paraformaldehyde in 0.1M Phosphate Buffer (PB) for one hour. The samples were passed on to the Electron Microscopy Facility where samples were post-fixed in reduced osmium tetroxide, stained with tannic acid, dehydrated step-wise to 100% ethanol and embedded in epon. Sections (~70nm) were cut using a Leica Ultracut UCT ultramicrotome and post-stained with lead citrate before viewing in a Tecnai G2 Spirit 120kV transmission electron microscope (FEI Company) using Ultrascan and Orius CCD cameras (Gatan UK).

2.3.12 CERT gene expression in breast cancer datasets

Nicolai Juul Birkbak performed the analysis of microarray datasets.

Raw microarray expression data for 12 publicly available breast cancer cohorts were used ((176-187) and GSE2109). Kruskal Wallis tests were performed to test for expression differences.

Chapter 3. Chromosomal instability confers intrinsic multidrug resistance

3.1 Introduction

In the Introduction, I discussed the association of CIN with acquired drug resistance (11) and intrinsic taxane resistance *in vitro* and *in vivo* (14). Furthermore, in patients with solid tumours, CIN is associated with poor prognosis (55, 59, 101). In this chapter, I discuss my attempts to 1) test the hypothesis that CIN cancer cells are intrinsically multidrug resistant, and 2) identify pathways that are essential for the survival of CIN+ cancer cells compared to CIN- cancer cells.

Kinase inhibitor and cytotoxic libraries were used in an attempt to identify agents that might be preferentially lethal towards CIN+ cells. The majority of this work has been published as a joint first author paper (6) (see Appendix 8.2) and was done mainly in collaboration with David Endesfelder who assisted in copy number analysis and statistical analysis. Section 3.2.7, examining the link of the CIN+ phenotype with patient outcome in clinical datasets was done in collaboration with Dr Axel Walther.

3.2 Results

3.2.1 Classification of CIN+ cell lines and relationship with ploidy status and Structural Chromosomal Complexity

9 CIN- and 18 CIN+ CRC cell lines (Table 5) were selected for use in the study. The CIN status for these cell lines had been previously described in terms of numerical and structural chromosomal aberrations (3, 157-159).

In order to confirm the utility of published approaches for defining the CIN status of the cell lines and to confirm the CIN+ or CIN- status of these cell lines, where SNP Array data was available, ploidy status of the cell lines were estimated using weighted mean integer copy numbers derived from the PICNIC (Predicting Integral Copy Numbers In Cancer) algorithm (63) (Figure 1A). Ploidy estimates classified cells as CIN+ if they surpassed a threshold of ploidy >2.2 (corresponding to an estimated DNA index of 1.1). Modal chromosomal number as determined previously using high quality metaphase spreads (157, 158) correlated well with ploidy estimates derived from weighted mean PICNIC copy number analysis using the SNP Array data (Pearson's CC=0.94, Pearson's correlation test $p<0.0001$) (Figure 1B). These data support the utility of SNP Array data for estimating cell line ploidy status and are consistent with ploidy estimates by traditional measures, confirming the CIN status of cell lines used in this analysis.

Next the relationship between CIN status and structural chromosomal complexity was addressed using a summary Structural Chromosomal Complexity Score (SCCS) derived from the SNP Array datasets. This SCCS was determined by summarising (i) the number of breakpoints, (ii) loss of heterozygosity (LOH) events as predicted using PICNIC (63) and (iii) the Genome Integrity Index (GII) (61), into a single value for each cell line (Figure 1C). There was a highly significant correlation between ploidy status and the SCCS (Pearson's CC =0.746, $p=0.0002$). Taken together, these analyses confirm that cells classified as CIN+ have significantly greater ploidy and structural chromosomal complexity compared to CIN- cells.

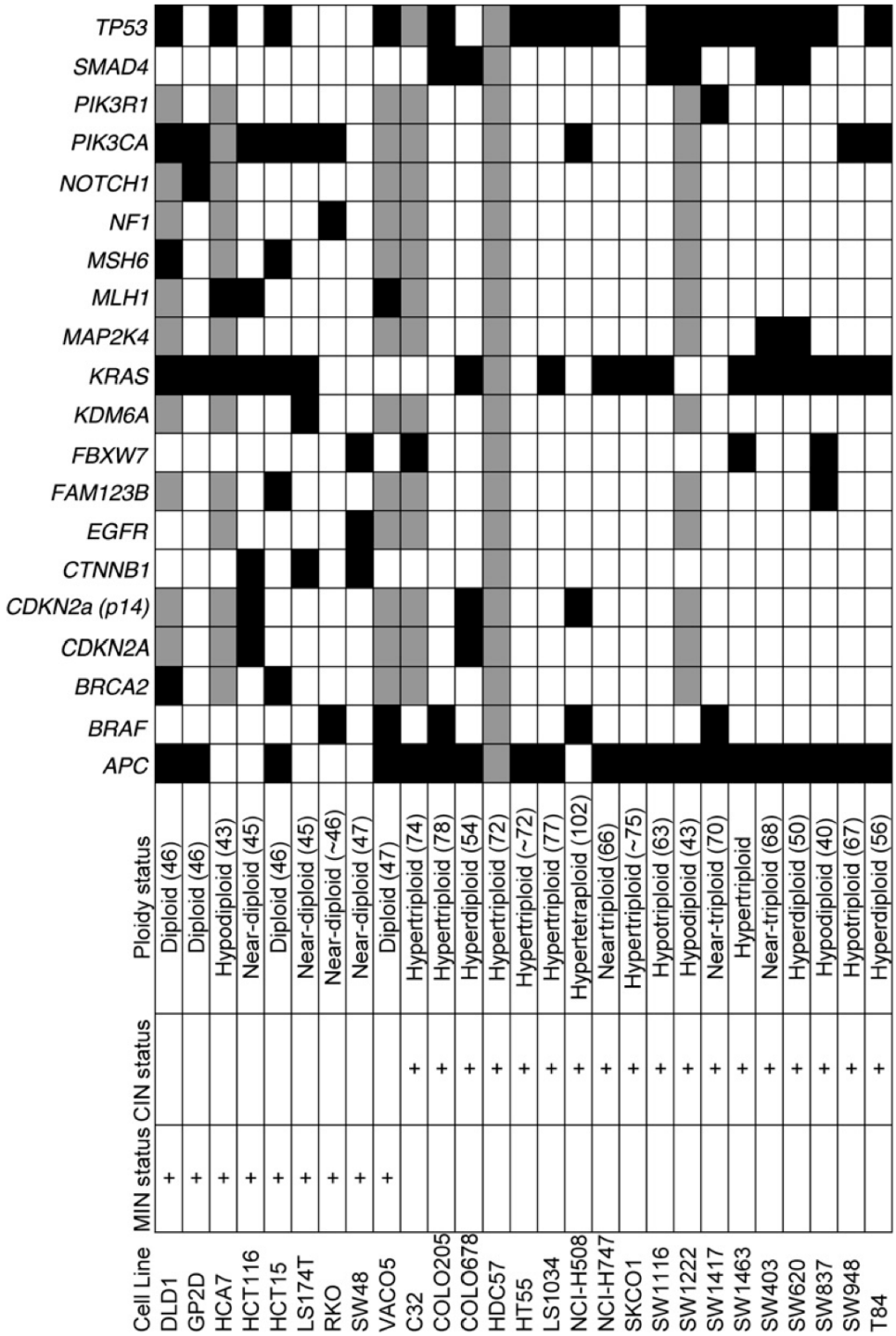

Table 5 Cell lines used in this study
CIN, MIN, ploidy and mutation status of the cell lines used in this study. Black indicates presence of a mutation, white indicates absence and grey indicates that the mutation status is unknown.

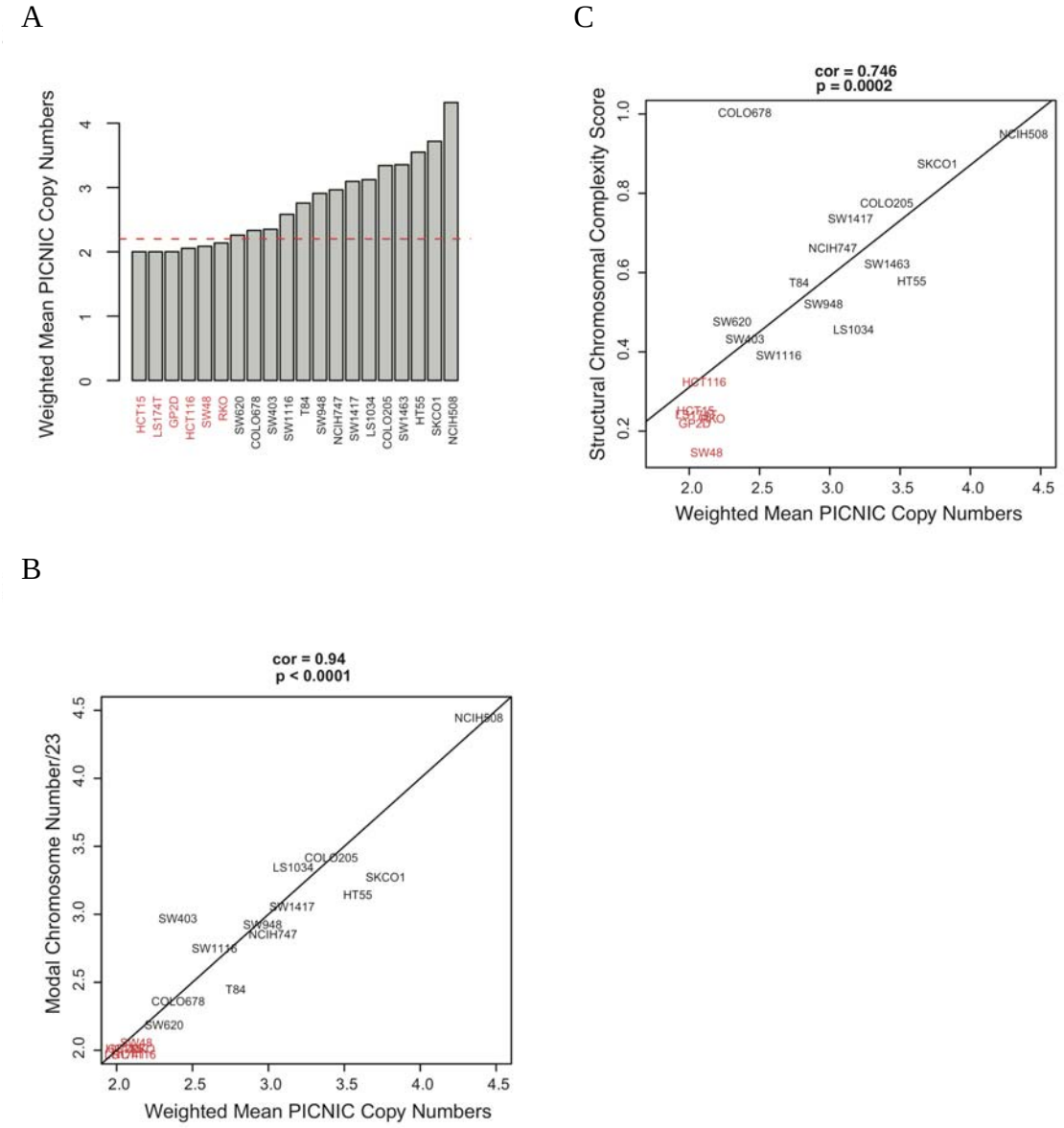

Figure 8 Ploidy and structural chromosomal complexity analysis of cell lines
A) Barplot of the ploidy status of 20 CRC cell lines determined using mean copy number PICNIC analysis of SNP Array data. Red line indicates ploidy value threshold of 2.2. CIN+ cell lines in black text and CIN- cell lines in red text throughout.
B) Correlation of modal chromosomal numbers and weighted mean copy numbers of the cell lines as determined by PICNIC. Pearson's CC=0.94, p<0.0001.
C) Correlation of Structural Chromosomal Complexity Score with ploidy as determined by weighted mean copy number PICNIC analysis of SNP Array data. Pearson's CC=0.746, p=0.0002.

3.2.2 CIN+ status is associated with intrinsic multidrug resistance

Next, I wanted to determine whether a specific kinase inhibitor could be identified to selectively target CIN+ cell lines. A small molecule library (Calbiochem Kinase Inhibitor Library I and II) that included 160 inhibitors was used to treat the 18 CIN+ and 9 CIN- cell lines. Preliminary drug titration experiments revealed that the majority of the CIN+ cell lines were resistant to concentrations up to 1μM (Figure 9) and therefore 10μM was selected as the optimal drug concentration for cell growth inhibition across the majority of cell lines in order to attempt to identify drugs that were specifically active in CIN+ cells. No specific inhibitor or inhibitor family was found to be preferentially active in CIN+ cell lines compared to CIN- cell lines. In contrast, CIN+ cancer cell lines were significantly more resistant to the inhibitors (Kolmogorov-Smirnov test, $p<0.0001$) (Figure 10, Figure 11). Following correction for multiple testing hypotheses, 45 inhibitors were identified which demonstrated significantly greater activity in CIN- cell lines compared to CIN+ cell lines (Table 6) and 15 out of this 45 kinase inhibitors primarily target the CDK family. The relative resistance of CIN+ cell lines to these CDK inhibitors may be due to overexpression of cell cycle regulatory genes such as CDK1 in CIN+ cancer cells (59).

To address whether the variation in drug sensitivity between the CIN+ and CIN- cell lines was attributable to differences in proliferation rate, the maximum growth rate (maximal slope (*mu*) of growth curve) was calculated for each cell line. The CIN+ and CIN- cell lines displayed significantly different slopes in regression lines (t-test, $p = 0.007$) with the CIN- cell lines demonstrating a higher proliferation rate compared to the CIN+ cell lines (Wilcoxon-Mann-Whitney test, $p = 0.003$). These data are consistent with previous studies suggesting that aneuploidy (125) (126) or chromosomal

segregation defects (188) (66) have a negative impact on cellular proliferation rate. A significant correlation was observed between increased sensitivity to the inhibitors at higher proliferation rates for CIN+ cell lines (Pearson's CC = 0.61, p = 0.007). In contrast, no such correlation was observed between proliferation rate and drug sensitivity in CIN- cell lines (Pearson's CC = 0.24, p = 0.55) (Figure 12A). Neither ploidy index nor the SCCS showed a significant correlation with proliferation rate.

I next wanted to ask whether CIN+ and CIN- cell lines with similar proliferation rates displayed differential drug sensitivity. Cell lines with *mu* of the growth curve < 1, indicating a lower proliferative rate, were examined (22 out of 27 cell lines). CIN+ cell lines remained multidrug resistant compared to CIN- cell lines within this group (one-sided Wilcoxon-Mann-Whitney test p = 0.013). Next, a more conservative statistical approach was used to normalise the proliferation rate of each individual cell line within this group. CIN+ cell lines remained significantly more drug resistant compared to CIN- cell lines (one-sided Wilcoxon-Mann-Whitney test, p = 0.049) after this correction (Figure 12B). These data suggest that at similar growth rates, CIN+ cell lines remain more drug resistant compared to CIN- cell lines, indicating that proliferation rate is unlikely to be the main determinant of drug sensitivity.

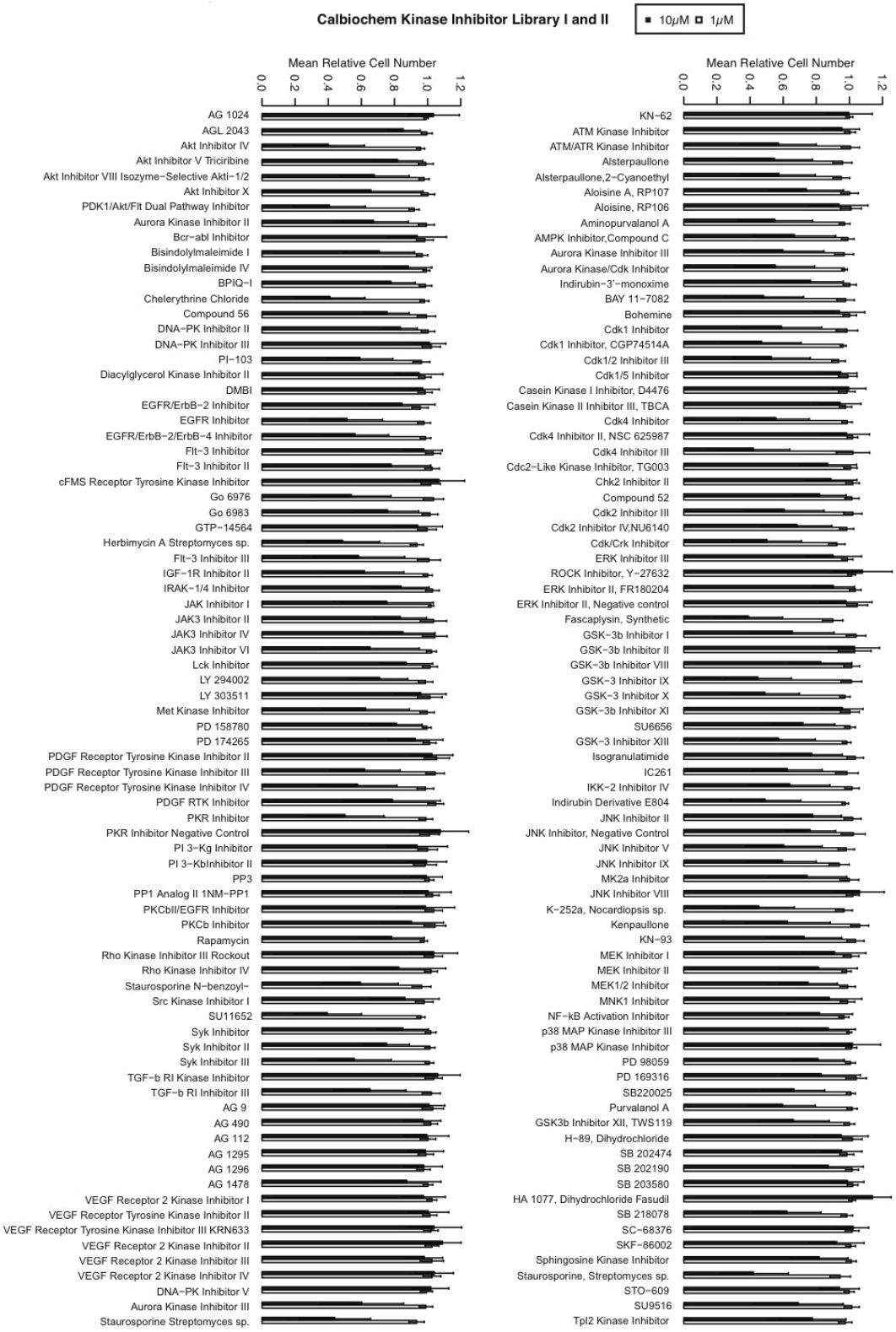

Figure 9 10 CIN+ CRC cell lines were treated with 160 kinase inhibitors at 10μM and 1μM for 72 hours.
Barplot shows mean cell number across all cell lines following each inhibitor treatment. The CIN+ cell lines appear to be largely resistant to inhibitor treatment at 1μM.

A

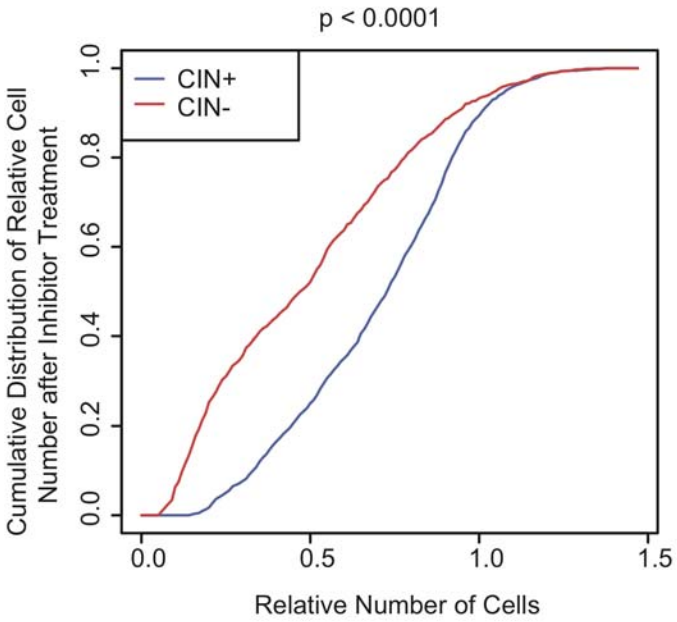

B

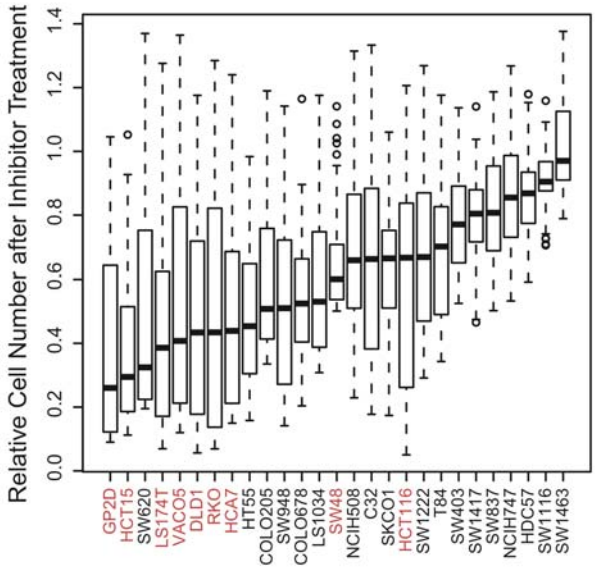

Figure 10 18 CIN+ and 9 CIN- CRC cell lines were treated with 160 kinase inhibitors at 10μM for 72 hours
A) A higher fraction of cells survive inhibitor treatment in CIN+ cell lines compared to CIN- cell lines. ($p<0.0001$).
B) Boxplot of median cell number following inhibitor treatment across all inhibitors for all cell lines. The length of the whiskers was limited by maximal=1.5 times the IQR in this boxplot and throughout.

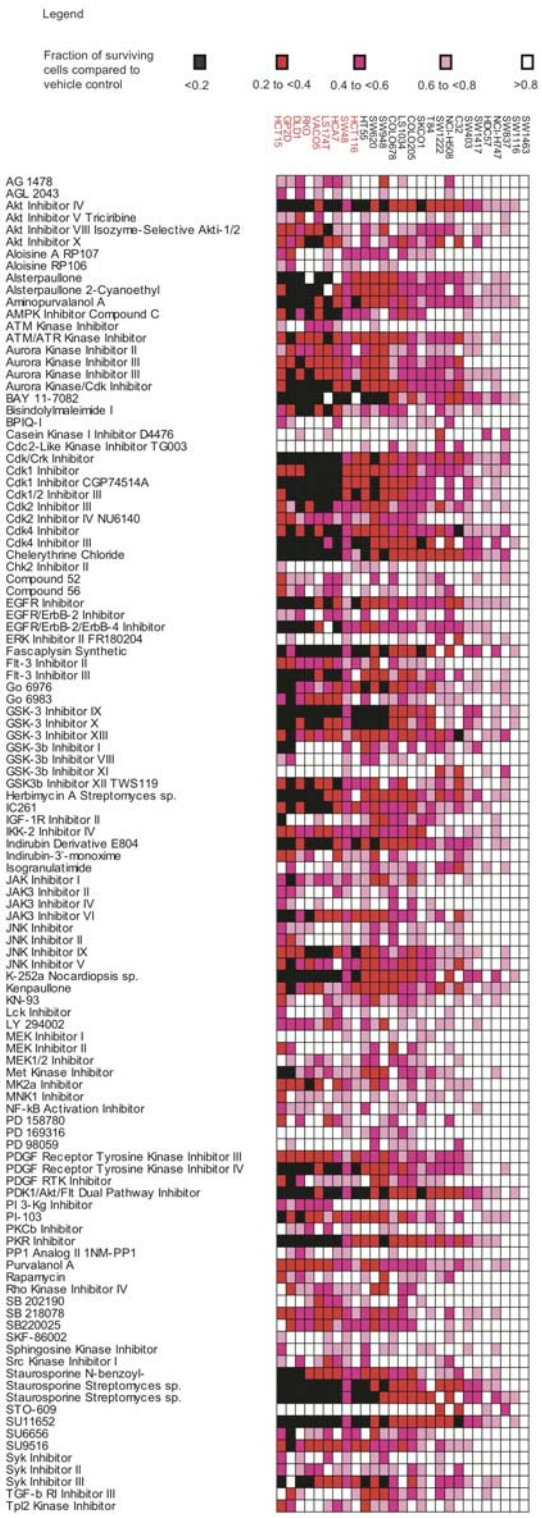

Figure 11 Heatmap of 18 CIN+ and 9 CIN- CRC cell lines were treated with 160 kinase inhibitors at 10μM for 72 hours

Heatmap shows the relative numbers of surviving cells following inhibitor treatment across the cell lines (Inhibitors that have minimal impact on cell growth defined as a surviving cell fraction of >0.8 in >75% of the cell lines tested have been excluded).

Inhibitor Name	Median fraction of surviving cells CIN+	Median fraction of surviving cells CIN-	Adjusted P-Value (Bonferroni-Holm)
Akt Inhibitor IV	0.33	0.11	0.0205
Alsterpaullone	0.55	0.18	0.0163
Alsterpaullone,2-Cyanoethyl	0.50	0.20	0.0128
Aminopurvalanol A	0.48	0.13	0.0033
AMPK Inhibitor,Compound C	0.64	0.21	0.0011
ATM/ATR Kinase Inhibitor	0.54	0.27	0.0128
Aurora Kinase Inhibitor III	0.56	0.23	0.0304
Aurora Kinase Inhibitor III	0.56	0.21	0.0304
Aurora Kinase/Cdk Inhibitor	0.53	0.17	0.0043
Bisindolylmaleimide I	0.69	0.21	0.0043
Cdk/Crk Inhibitor	0.42	0.14	0.0057
Cdk1 Inhibitor	0.58	0.20	0.0033
Cdk1 Inhibitor, CGP74514A	0.40	0.12	0.0043
Cdk1/2 Inhibitor III	0.44	0.14	0.0033
Cdk2 Inhibitor III	0.60	0.27	0.0057
Cdk4 Inhibitor	0.51	0.18	0.0033
Cdk4 Inhibitor III	0.37	0.14	0.0366
Compound 52	0.86	0.55	0.0366
EGFR Inhibitor	0.47	0.16	0.0074
EGFR/ErbB-2/ErbB-4 Inhibitor	0.51	0.16	0.0205
Fascaplysin, Synthetic	0.34	0.13	0.0247
Flt-3 Inhibitor II	0.76	0.41	0.0033
Flt-3 Inhibitor III	0.55	0.15	0.0366
Go 6983	0.75	0.31	0.0304
GSK-3 Inhibitor IX	0.37	0.12	0.0043
GSK-3 Inhibitor X	0.52	0.16	0.0128
GSK3b Inhibitor XII, TWS119	0.66	0.25	0.0057
IC261	0.66	0.20	0.0016
Indirubin Derivative E804	0.42	0.16	0.0247
JAK3 Inhibitor VI	0.61	0.25	0.0205
JNK Inhibitor IX	0.57	0.16	0.0011
K-252a, Nocardiopsis sp.	0.38	0.14	0.0043
PDGF Receptor Tyrosine Kinase Inhibitor III	0.53	0.30	0.0205
PDGF Receptor Tyrosine Kinase Inhibitor IV	0.48	0.16	0.0033

PDK1/Akt/Flt Dual Pathway Inhibitor	0.34	0.12	0.0205
PI 3-Kg Inhibitor	0.96	0.50	0.0247
PKR Inhibitor	0.44	0.15	0.0074
PP1 Analog II 1NM-PP1	1.00	0.73	0.0033
Purvalanol A	0.58	0.30	0.0163
Staurosporine N-benzoyl-	0.59	0.32	0.0304
Staurosporine Streptomyces sp.	0.37	0.11	0.0163
Staurosporine, Streptomyces sp.	0.34	0.13	0.0057
SU11652	0.33	0.11	0.0205
SU9516	0.66	0.29	0.0033
Syk Inhibitor III	0.62	0.19	0.0443

Table 6 Table of inhibitors that preferentially target CIN- cell lines over CIN+ cell lines

A

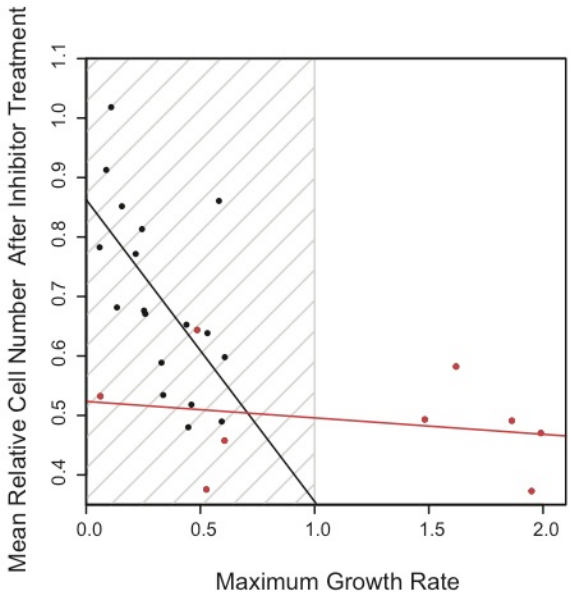

B

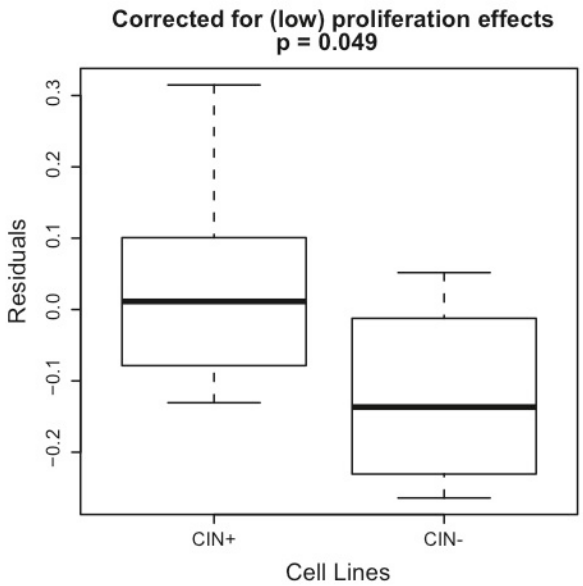

Figure 12 Analysis of impact of proliferation rate on response to kinase inhibitors.
A) Mean relative surviving cell number following kinase inhibitor treatment was plotted against *mu* for each cell line. CIN+ cell lines in black and CIN- cell lines in red. Shaded area indicates cell lines with mu <1.
B) At similar low proliferation rates (mu<1), CIN+ cell lines were more resistant to kinase inhibitor treatment compared to the CIN- cell lines when corrected for the influence of proliferation rate (p = 0.049).

3.2.3 Somatic mutation status and drug sensitivity

Next I asked whether distinct tumour cell line somatic mutations might be the underlying determinant of drug resistance rather than genomic instability status. Publicly available somatic mutation data from the Sanger Institute Cancer Cell Line Project (CLP) and COSMIC database (78) was used. 15 CIN+ and 6 CIN- cell lines used in my analysis were present within the CLP database and a total of 20 out of the 61 genes resequenced in the project were found to have somatic mutations in at least 1 of those 21 cell lines. I investigated whether the somatic mutation status of the 20 genes (as listed in Table 5) was associated with either altered sensitivity to inhibitors grouped according to target kinase family (Aurora kinases, AKT, CDK, EGFR, FLT-3, GSK-3, JAK3, JNK, MEK, PDGFR, PI3K and SYK) or to all inhibitors combined. Comparison of drug sensitivity response in mutated and wild-type cell lines was not performed for 7 out of the 20 genes due to insufficient numbers of cell lines with mutations in either the wild-type or mutated group leading to insufficient statistical power.

PIK3CA mutation was the only somatic mutation significantly associated with altered sensitivity to inhibitors grouped according to target kinase families (*PIK3CA* mutation associated with increased sensitivity to inhibitors targeting AKT, Aurora kinases, EGFR, PDGFR and PI3K, Wilcoxon-Mann-Whitney-Test, corrected $p = 0.003$, $p = 0.038$, $p = 0.016$, $p = 0.038$ and $p = 0.004$ respectively) (Figure 13A). No evidence for a specific association with either *PIK3CA* exon 9 or exon 20 mutation status and drug sensitivity was found. Notably, *PIK3CA* mutations were more likely to occur in CIN- than CIN+ cell lines ($p=0.0066$, Fisher's exact test).

No single somatic mutation was associated with altered sensitivity to all inhibitors. Next, data for somatic mutation status and CIN status were pooled. When corrected for multiple testing with Benjamini-Hochberg under the assumption that the tests are either positively correlated or independent (189), CIN+ status was the only parameter significantly associated with multidrug resistance (corrected $p = 0.01$) (Figure 13B). Taken together, these data suggest that the association of *PIK3CA* mutation with CIN- status may confound the interpretation of the association of *PIK3CA* mutation status with sensitivity to specific inhibitors and may simply reflect the intrinsic drug sensitivity of CIN- cells.

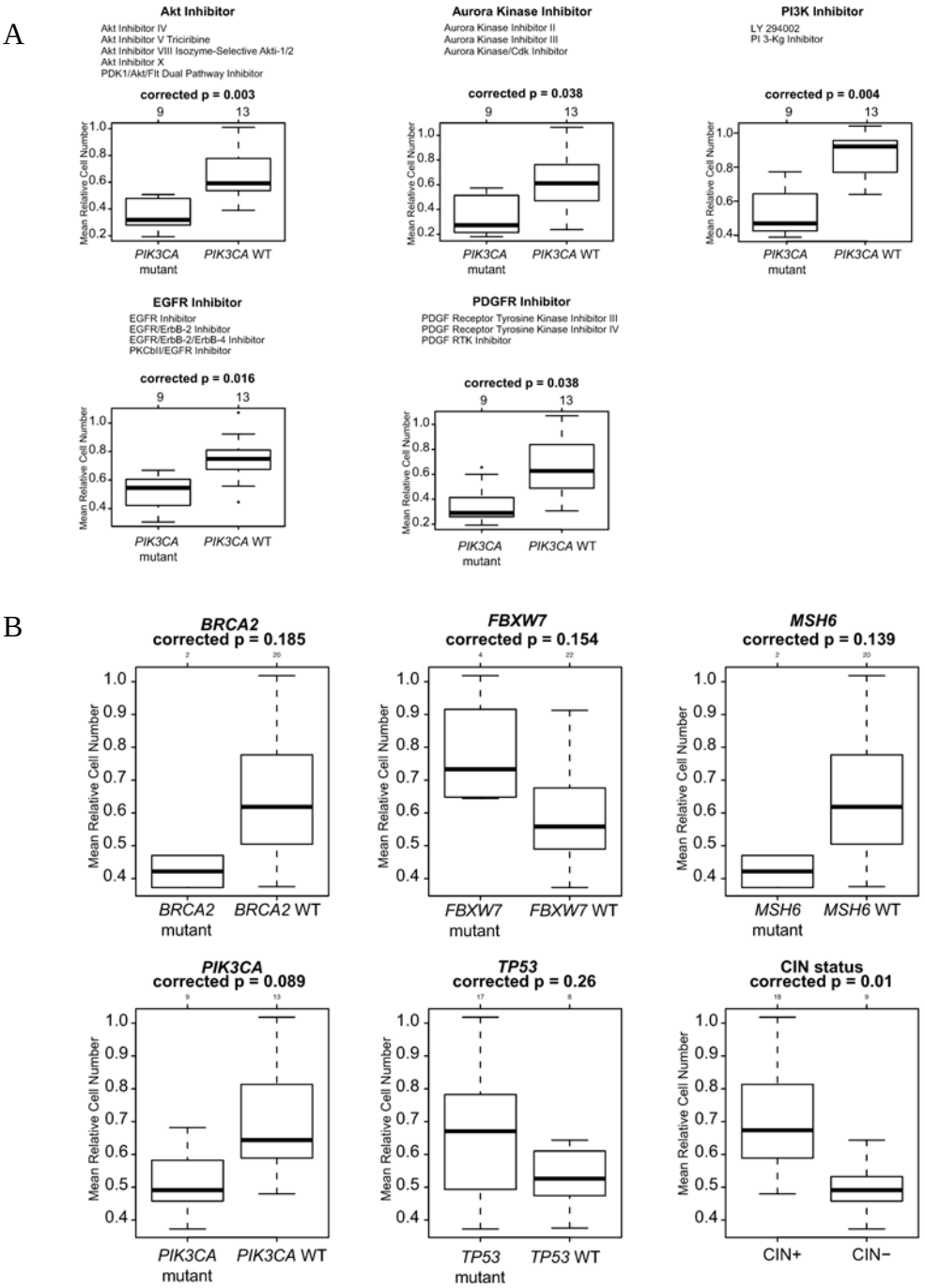

Figure 13 Analysis of somatic mutation status and response to kinase inhibitors
A) PIK3CA mutation was the only somatic mutation significantly associated with increased sensitivity to inhibitors grouped according to the target kinase families: AKT, Aurora kinase, EGFR, PDGFR and PI3K (Wilcoxon-Mann-Whitney-Test).
B) CIN+ status appeared to be associated significantly (corrected p=0.01) with altered drug sensitivity across all kinase inhibitors when tested together with mutation status of 13 other genes and corrected for multiple testing. Only genes where mutation status was associated with an alteration in drug sensitivity with p-value<0.6 have been shown.

3.2.4 Isogenic CIN+ CRC cell lines display intrinsic multidrug resistance

In order to support a direct role for the contribution of CIN to the multidrug resistant phenotype, drug sensitivity was assessed in isogenic CRC models of CIN. The HCT116 *MAD2+/-* cell line has one allele of the SAC gene, *MAD2*, deleted by homologous recombination, resulting in numerical CIN relative to its diploid parental cell line (164). The isogenic HCT116 *MAD2+/-* cell line and its parental diploid cell line were treated with the kinase inhibitors. The *MAD2+/-* cell line was found to be more resistant overall compared to the parental diploid cell line (one-sided Wilcoxon signed-rank test, p=0.001) (Figure 14A, B) and this was consistent with the non-isogenic cell line drug sensitivity data. No single inhibitor appeared to specifically target the HCT116 *MAD2 +/-* cell line.

In order to further test the association of CIN with intrinsic drug resistance to drugs other than kinase inhibitors, the HCT116 *MAD2+/-* and another CIN+ isogenic cell line, HCT116 *PTTG1-/-* (encoding for Securin), were challenged together with their isogenic parental diploid HCT116 cell lines with the Biolog cytotoxic library containing 92 anti-cancer cytotoxic agents. Consistent with the data from the kinase inhibitors, both the CIN+ *MAD2+/-* and *PTTG1-/-* cells were significantly more resistant (one-sided Wilcoxon signed-rank test, $p<0.001$, except $p=0.035$ at the lowest concentration of drug for *PTTG1 -/-*) to a diverse range of anti-cancer agents compared to the parental diploid cell lines (Figure 15, Figure 16). However, the magnitude of difference in relative cell number between the *PTTG1-/-* and diploid parental cells was small despite being statistically significant.

Importantly both the HCT116 *MAD2+/-* and parental diploid cell lines continue to display MIN+ (Figure 17), indicating that MIN status is unlikely to sufficiently explain the altered drug sensitivity in the CIN+ isogenic models. These data suggest that CIN+ status, initiated by ongoing chromosome missegregation events driven by loss of two distinct proteins controlling mitotic fidelity, is the dominant phenotype associated with altered drug sensitivity.

A

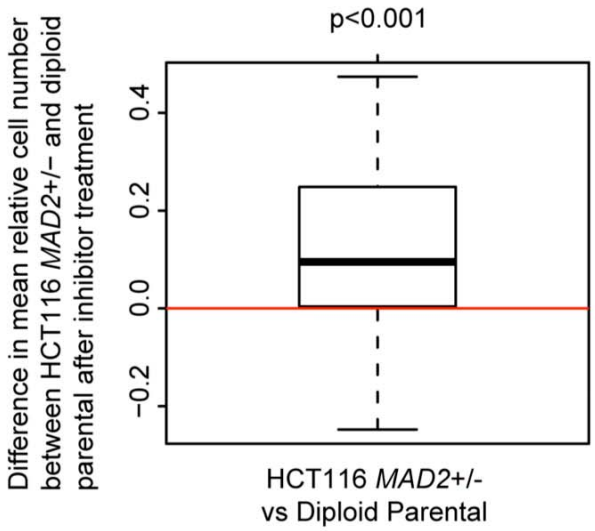

B

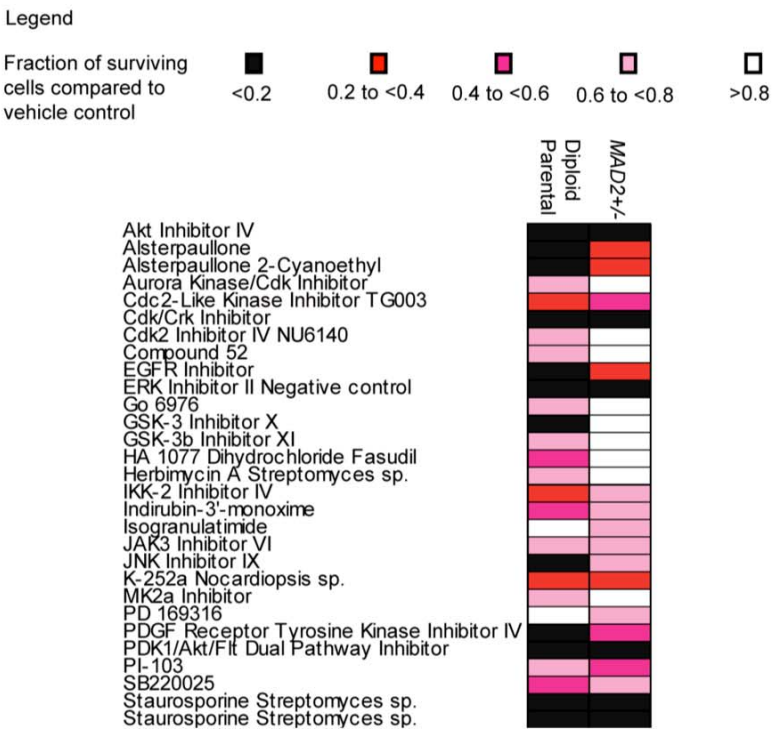

Figure 14 Isogenic CIN+ and CIN- cell lines were treated with kinase inhibitors
A) Boxplot showing that following treatment with kinase inhibitors, there appeared to be a higher surviving fraction of cells in the HCT116 *MAD2+/-* cell line compared to its parental diploid cell line ($p<0.001$) following treatment with each equivalent inhibitor.
B) Heatmap showing the relative numbers of surviving cells following the inhibitor treatments compared to vehicle control across the HCT116 *MAD2+/-* and parental diploid cell lines (Inhibitors that show a surviving cell fraction of >0.8 in both cell lines have been excluded).

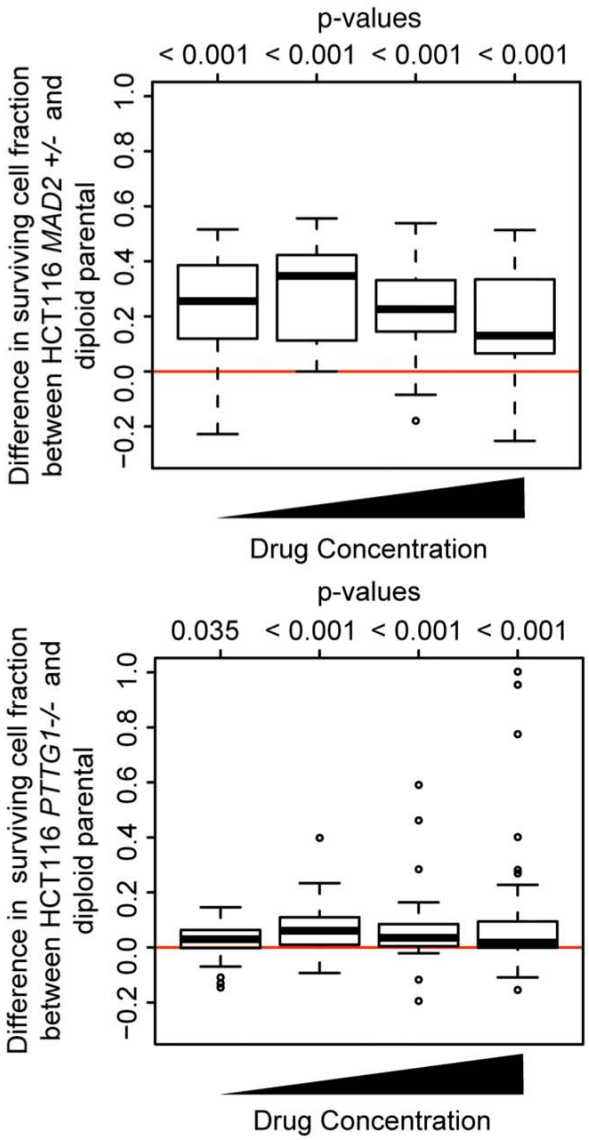

Figure 15 Isogenic CIN+ and CIN- cell lines were treated with cytotoxic agent panel Biolog M11-M14 drug microplates were used at 4 increasing concentrations per drug (0.1µM to 25µM) to treat HCT116 *MAD2+/-* and PTTG1 -/- and their parental diploid cell lines for 72 hours. The boxplot shows difference in relative surviving cell number across all drugs at each of the four concentrations, comparing *MAD2+/-* and PTTG1 -/- cells to their specific isogenic parental cells. Significant p-values suggest higher resistance in *MAD2+/-* or *PTTG1-/-* cells compared to their parental diploid cells.

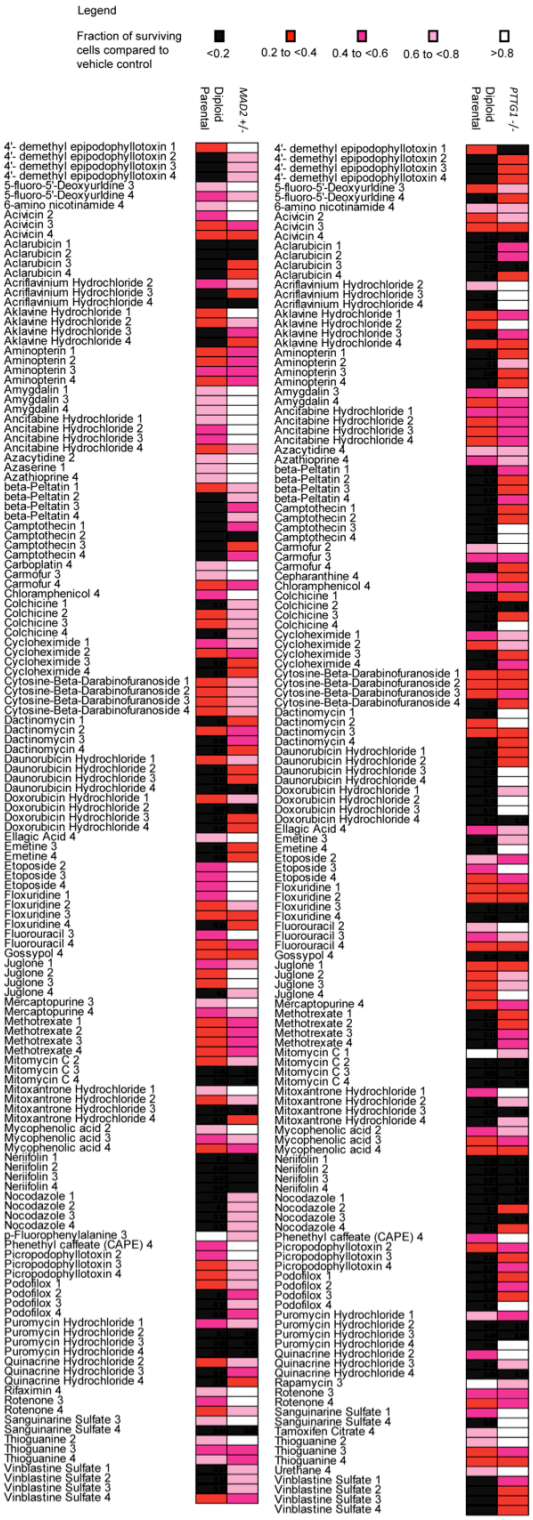

Figure 16 Heatmap of isogenic CIN+ and CIN- cell lines were treated with cytotoxic agent panel

Heatmap of surviving fraction of cells compared to negative control in HCT116 *MAD2+/-*, PTTG1 -/- and their parental diploid cell lines treated with Biolog drug microplates. Drugs resulting in a surviving cellular fraction of >0.8 compared to negative control in both isogenic cell lines were excluded.

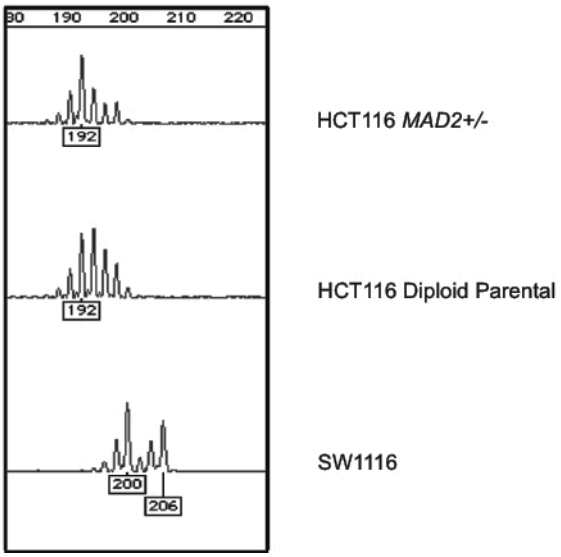

Figure 17 Microsatellite PCR fragment analysis (marker 15_XVII)
A similar profile for HCT116 *Mad2+/-* and diploid parental HCT116 was observed. SW1116 is a representative MIN- cell line for comparison.

3.2.5 CIN+ not tetraploidy is associated with multidrug resistance

CIN+ CRC cell lines missegregate chromosomes at a high rate, in contrast to CIN- CRC cells that have a lower frequency of mitotic errors (3, 51). In addition, CIN- cells fail to tolerate the propagation of CIN when chromosome segregation errors are artificially induced by drug treatment (66), suggesting that sustaining CIN in a cell population may require a specialised survival phenotype. The majority of CIN+ CRC cell lines used in this study are triploid or tetraploid. I therefore considered whether altered ploidy status rather than ongoing CIN might be associated with enhanced drug resistance. Clonal tetraploid and diploid HCT116 cells were treated with the kinase inhibitors. There was no significant difference in the relative number of surviving cells following drug treatment between HCT116 Tetraploid Clone 4 (TC4) cell line and Diploid Clone 8 (DC8) cell line. However, Tetraploid Clone 9 (TC9) was significantly more resistant compared to the DC8 cell line (Wilcoxon signed-rank test, $p<0.001$) (Figure 18A). Further investigation by clonal FISH (Figure 18B) revealed that TC9 had a more heterogeneous karyotype compared to TC4 cell lines with a significantly higher proportion of cells that deviated from the mode of four copies of both Chromosomes 2 and 15 (Fisher's exact test, $p=0.05$) (Figure 19). This implies that karyotypic heterogeneity rather than increased ploidy might be responsible for increased drug resistance compared to karyotypically stable diploid cells. I cannot formally exclude the possibility that acquired mutations present in the drug resistant tetraploid clone that may have permitted the spontaneous tetraploid phenotype may primarily be responsible for increased drug resistance.

Taken together with the isogenic cell line data presented here, where CIN is artificially induced through loss of one allele of *MAD2* or both copies of *PTTG1*, these results support the contribution of CIN rather than increased ploidy status or MIN in conferring altered drug sensitivity.

A

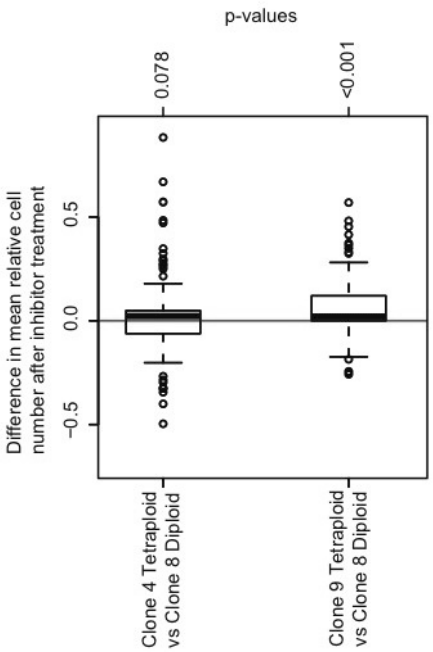

B

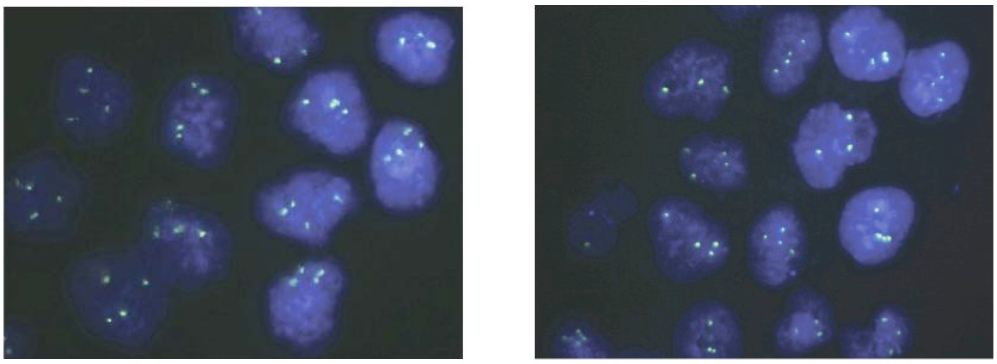

Tetraploid Clone 4 Tetraploid Clone 9

Figure 18 Isogenic tetraploid and diploid HCT116 cell lines were treated with kinase inhibitors

A) Boxplot of relative surviving cell numbers comparing HCT116 Tetraploid Clone 4 (TC4) and Diploid Clone 8 (DC8) cell lines, and Tetraploid Clone 9 (TC9) with DC8 cell lines. The TC9 cell line was significantly more resistant compared to DC8 ($p<0.001$). The difference in drug sensitivity between TC4 and DC8 was not significant ($p=0.078$).

B) Representative FISH images for TC4 and TC9. Probes against Chromosome 15 in green.

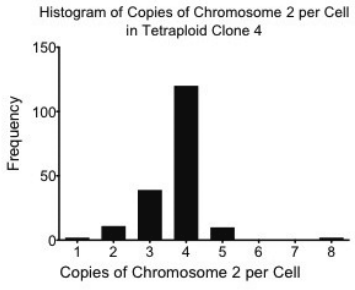

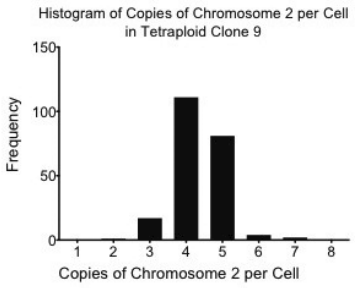

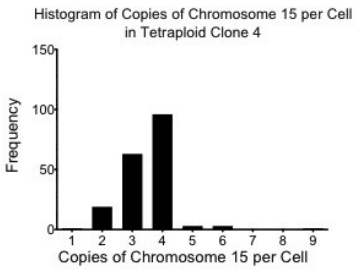

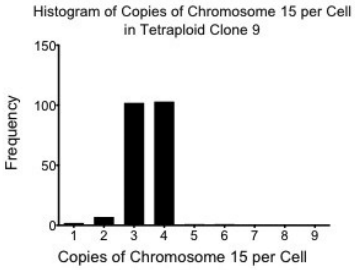

	% Cells with 4 copies of both Chr 2 and 15	% Cells with number of copies ≠4 of either Chr 2 or Chr 15
Clone 4	37	63
Clone 9	28	72

Fisher's Exact Test, p=0.05

Figure 19 Histograms showing distribution of number of markers per cell corresponding to Chromosome 2 and 15 in TC4 and TC9
TC9 had a statistically significant higher proportion of cells that deviated from having 4 copies of both Chromosome 2 and 15 (p=0.05) compared to TC4.

3.2.6 CIN+ CRC cell lines do not demonstrate increased sensitivity towards AICAR and 17-AAG

It has been reported that AICAR (5-aminoimidazole-4-carboxamide riboside), a cell-permeable precursor of ZMP (an AMP analogue), which allosterically activates AMP-activated protein kinase (AMPK), thereby mimicking energy stress, and 17-AAG (17-allylamino-17-demethoxy-geldanamycin), that inhibits the chaperone Hsp90, may selectively target aneuploid cells over diploid ones for death, due to an induction of energy and proteotoxic stress (129). In their study, Tang and colleagues then went on to observe preferential death in five (CACO2, HT29, SW403, SW480, SW620) aneuploid (CIN+) cancer cell lines compared to five (HCT116, HCT15, DLD1, SW48, LOVO) diploid or near-diploid MIN+ (CIN-) CRC cell lines when treated with these compounds.

I next wanted to investigate if I could replicate their observations in a larger panel of CRC cell lines. 14 CIN+ cell lines (C32, COLO205, COLO678, HDC57, HT55, LS1034, SKCO1, SW403, SW480, SW620, SW837, SW1222 AND T84) and 8 CIN- cell lines (DLD1, GP2D, HCA7, HCT15, LS174T, RKO, SW48 and VACO5) were treated with 5 concentrations of 17-AAG ranging from 5-1000nM and 5 concentrations of AICAR ranging from 100-1000μM (Figure 20). At the 2 highest concentrations of 17-AAG used and at all concentrations of AICAR used apart from 100 and 750μM, the CIN+ cell lines showed a statistically significant increase in mean relative surviving cell number compared to the CIN- cell lines ($p<0.05$, Mann-Whitney U test).

The HCT116 diploid parental and *MAD2+/-* cell lines were also treated with 17-AAG (5 concentrations ranging from 5-1000nM) and AICAR (5 concentrations ranging from

1-100μM) (Figure 21). I was not able to observe a significant difference in sensitivity at each concentration of drug for both cell lines.

Finally, DC8, TC4 and TC9 cell lines were treated with 5 concentrations of 17-AAG ranging from 5-1000nM, 5 concentrations of AICAR ranging from 100-1000μM, and a combination of 200μM AICAR with 0, 50, 100, or 200nM 17-AAG (Figure 22). I was not able to observe a significant difference in mean relative surviving cell number between these cell lines, despite the increase in ploidy of the tetraploid clones.

Restricting analysis to cell lines that overlapped between the study by Tang and colleagues and my experiments (CIN+ : SW403, SW480, SW620 and CIN- : HCT116, HCT15, DLD1, SW48), I was unable to observe a significant difference in cell viability between the CIN+ and CIN- cell lines following treatment with either 17-AAG or AICAR (Figure 23)

Therefore, in the panel of CIN+ and CIN- CRC cell lines, and in the isogenic MAD2 and tetraploid/diploid cell lines, I was unable to observe preferential death in CIN+ or cell lines with increased ploidy.

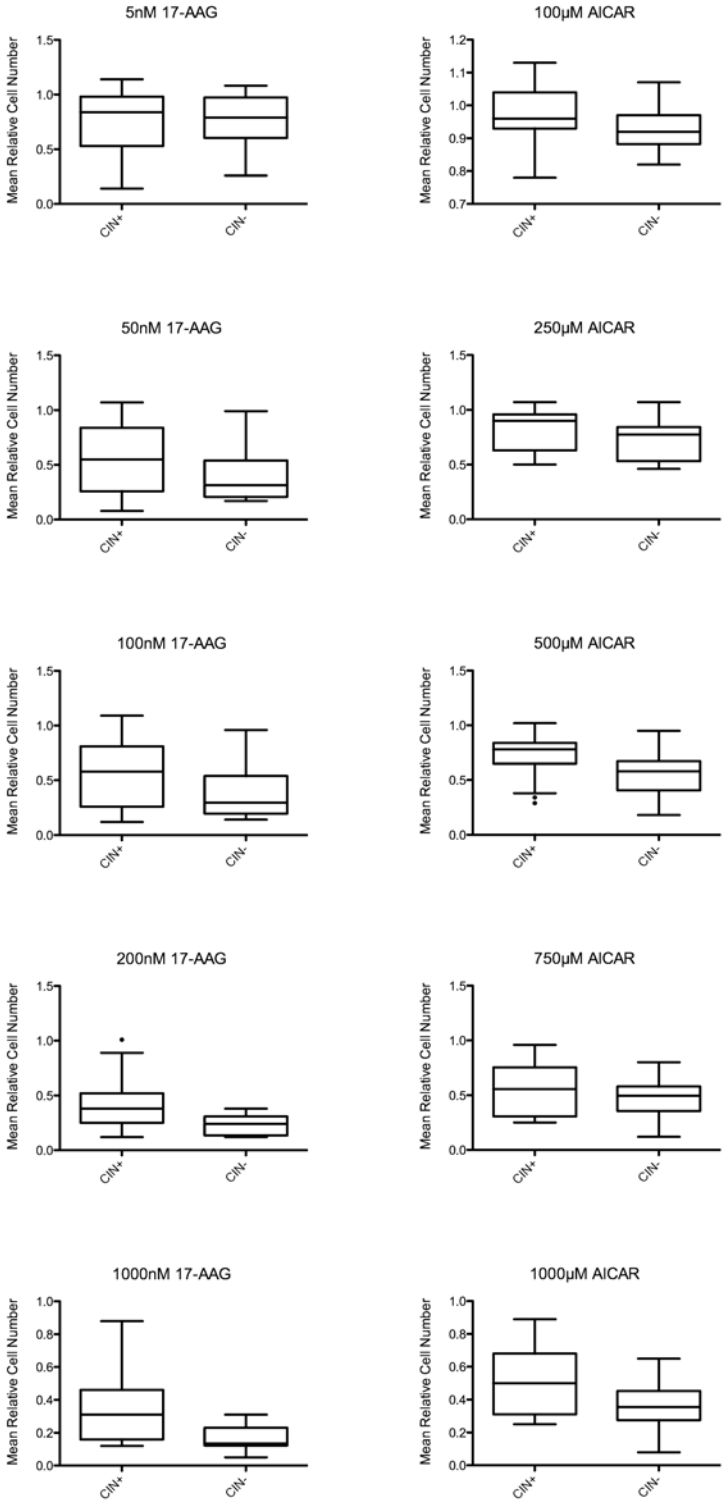

Figure 20 Boxplots of CIN+ and CIN- CRC cell lines individually treated with 5 concentrations of 17-AAG or AICAR

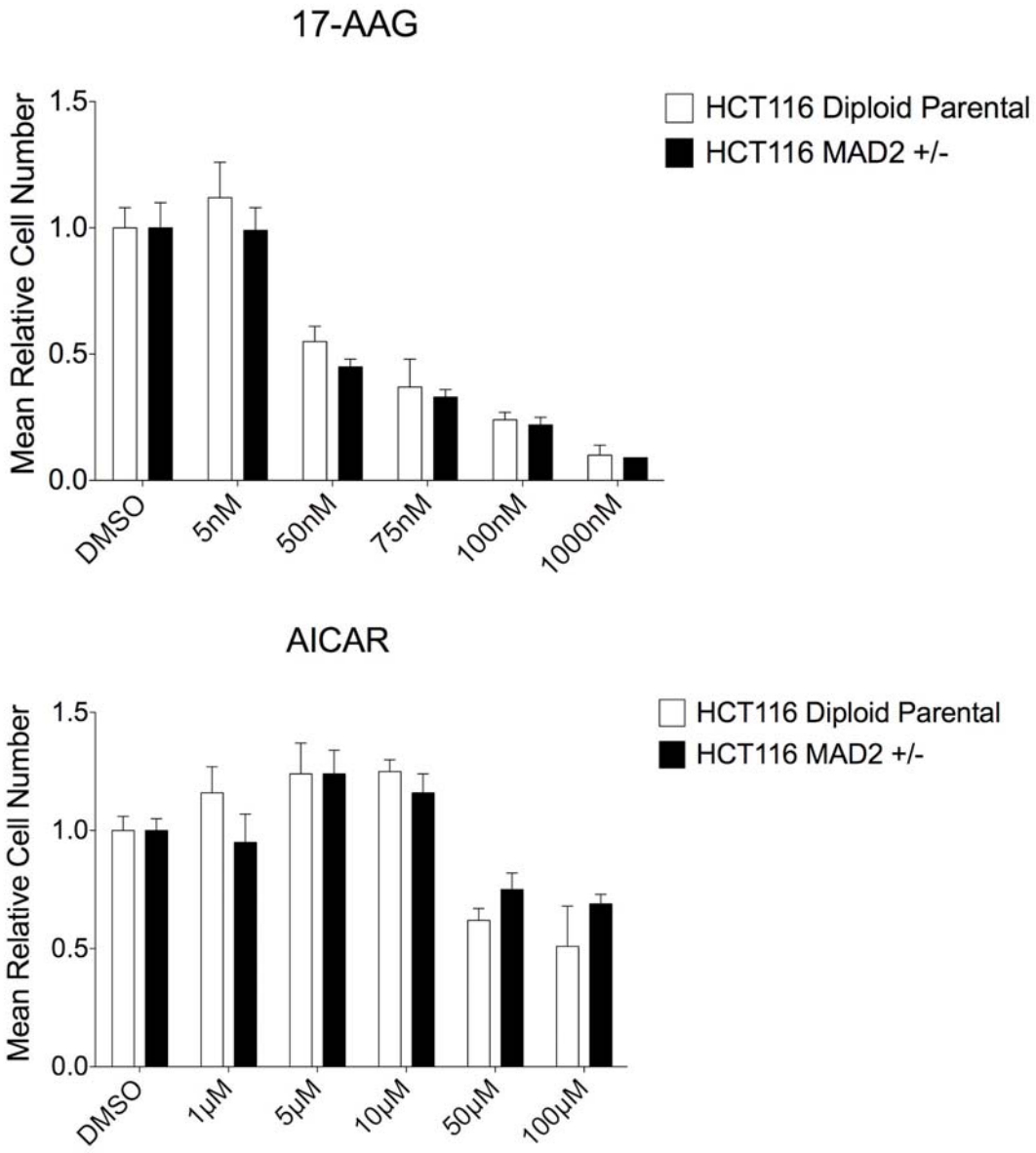

Figure 21 Graphs of mean relative cell numbers in HCT116 diploid parental and *MAD2+/-* cell lines after treatment with 17-AAG or AICAR

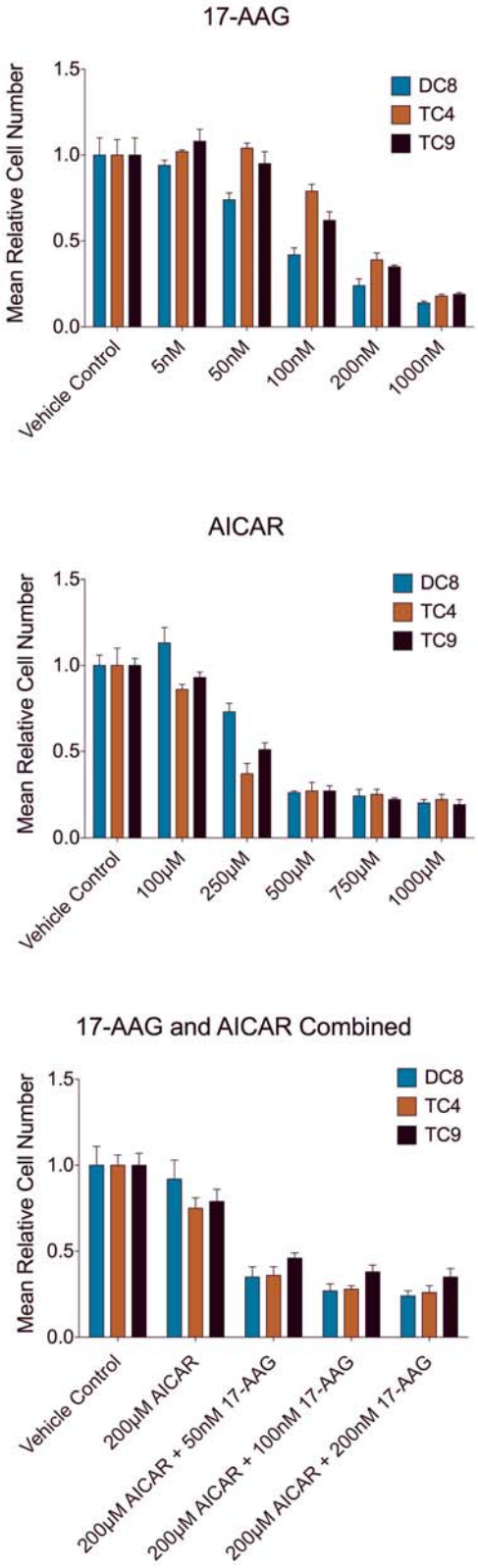

Figure 22 Graphs of mean relative cell number in DC8, TC4 and TC9 cell lines after treatment with 17-AAG, AICAR or a combination of both

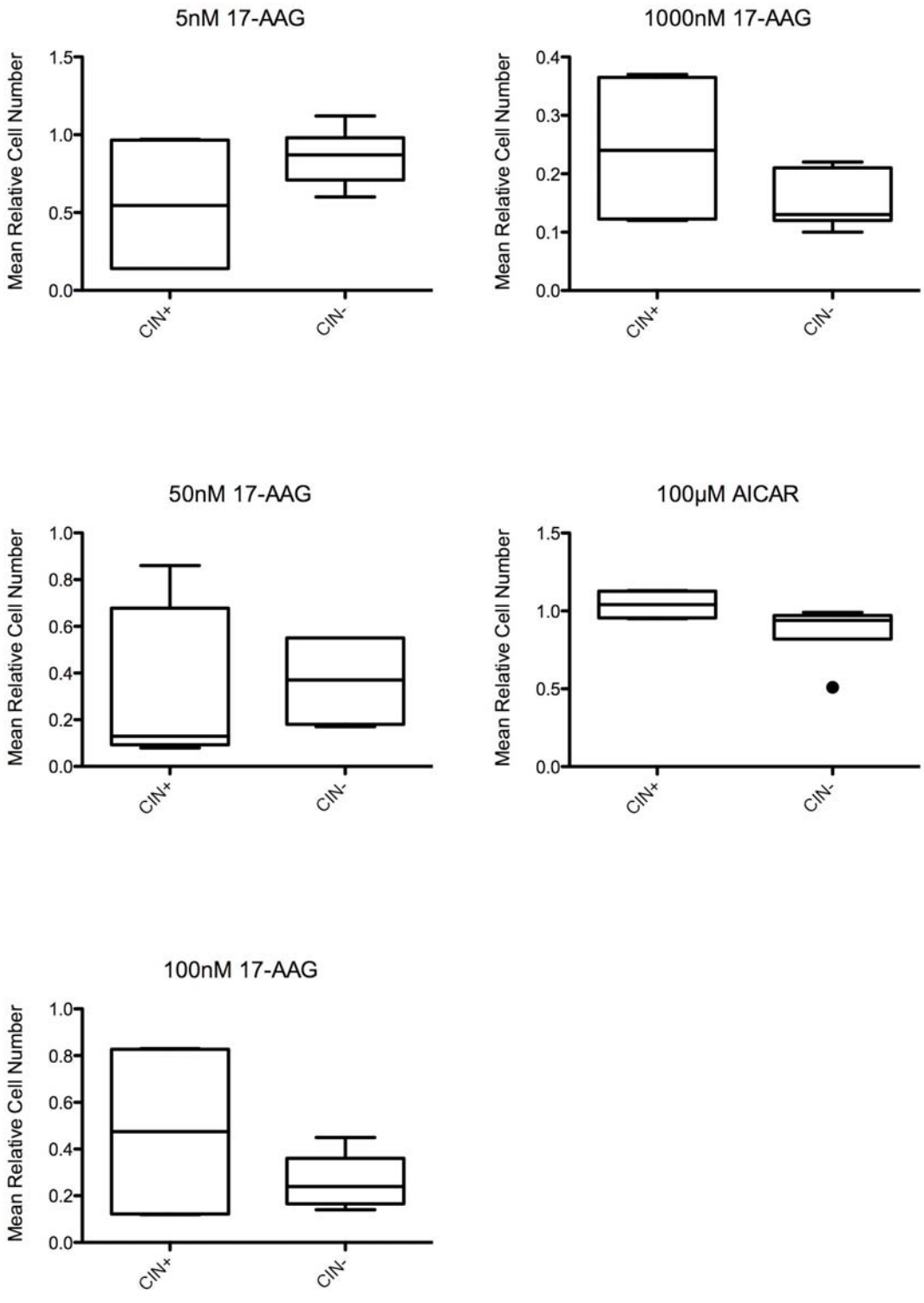

Figure 23 Graphs of mean relative cell number in CRC cell lines that overlapped between two studies
CIN+ cell lines (SW403, SW480, SW620) and CIN- cell lines (HCT116, HCT15, DLD1, SW48) were individually treated with 17-AAG or AICAR.

3.2.7 Relationship between CIN status and benefit from cytotoxic therapy

Meta-analysis of clinical datasets in this section has been contributed by Dr Axel Walther.

Published clinical data support the view that CIN+ CRC is associated with a worse prognosis compared to CIN- tumours (55) and data presented here suggest that CIN+ cell lines display intrinsic multidrug resistance. Conceivably the poorer prognosis of CIN+ disease may relate in part to intrinsic thymidylate synthase inhibitor drug resistance, cytotoxics commonly used in the adjuvant treatment of CRC. Using the panel of CIN+ and CIN- CRC cell lines, I next wanted to investigate if the CIN+ CRC cell lines displayed intrinsic resistance to clinically relevant drugs. Consistent with this hypothesis, isogenic CIN+ cells are significantly more resistant to the majority of thymidylate synthase inhibitors tested, including 5-FU, and methotrexate, a dihydrofolate reductase inhibitor. Non-isogenic CIN+ cells also appeared to be more resistant to 5-FU compared to CIN- cell lines, at physiological concentrations (as measured by peak plasma concentration, approximately between 200nM and 5μM)(190, 191) (Figure 24).

Next, using clinical datasets, I wanted to know if CIN+ status might be associated with poorer outcome following adjuvant therapy with 5-FU-based regimens. A meta-analysis of studies examining the relationship between CIN and prognosis in locoregional (non-metastatic) CRC revealed that CIN+ disease (defined as aneuploidy/polyploidy measured by flow cytometry) confers a worse overall survival (30 studies) (Figure 25) and progression-free survival (15 studies) (Figure 26) compared to patients with diploid

CRC. Similarly, if only patients who received chemotherapy were included (2 studies) (192) (193), CIN+ status is associated with a worse overall survival (Figure 27).

Two studies explored the predictive value of CIN (192, 194) in patients with locoregional CRC who received either adjuvant chemotherapy or no chemotherapy following surgery (Figure 28). Patients with diploid CRC appear to benefit from 5-FU based therapy (N=262, HR=0.61; 95% CI 0.40-0.94, p=0.024; I^2=0%, p=0.467) compared with untreated diploid controls, whereas there was no significant difference between treated and untreated CIN+ CRC (N=303, HR=0.81; 95% CI 0.57-1.16, p=0.250; I^2=0%, p= 0.932) despite the similar number of patients involved in the study. The combined analysis of all patients suggests a benefit following 5-FU treatment comparable to that reported in the literature for genetically unselected patients (195). Whilst these studies are limited, they are consistent with the view that patients with CIN+ CRC derive less benefit from 5-FU based adjuvant cytotoxic chemotherapy than patients with diploid CRC.

A

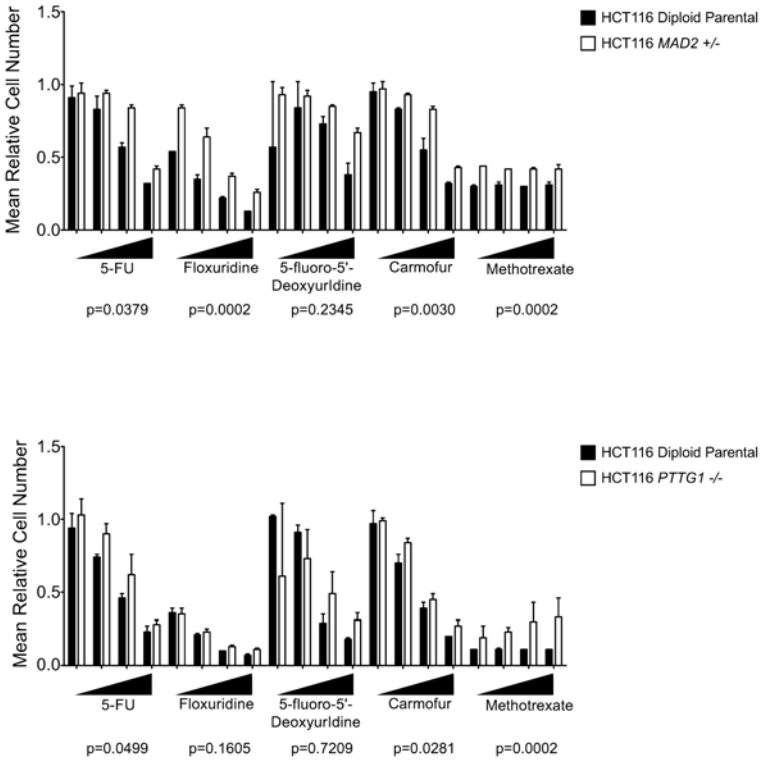

B

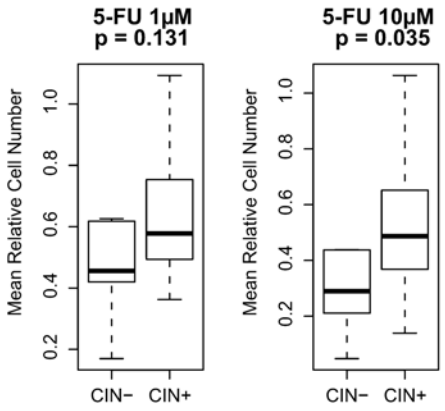

Figure 24 Analysis of drug sensitivity of isogenic CIN+ cell lines to clinically relevant cytotoxics

A) HCT116 *MAD2+/-* and PTTG1 -/- cell lines appeared to be more resistant compared to their parental diploid cell lines when treated for 72h with clinically relevant cytotoxics at a range of concentrations from 0.1µM to 25µM present on the Biolog Microplates. Boxplot shows mean cell number relative to negative control at each concentration of drug used. Significant p-values suggest higher resistance in *MAD2+/-* or *PTTG1-/-* cells compared to their parental diploid cells.

B) 18 CIN+ and 9 CIN- cells were treated with 1µM and 10µM of 5-FU for 72 hours. CIN+ cell lines appeared to be significantly more resistant compared to CIN- cell lines (p=0.035, Wilcoxon-Mann-Whitney-Test) at 10µM of 5-FU.

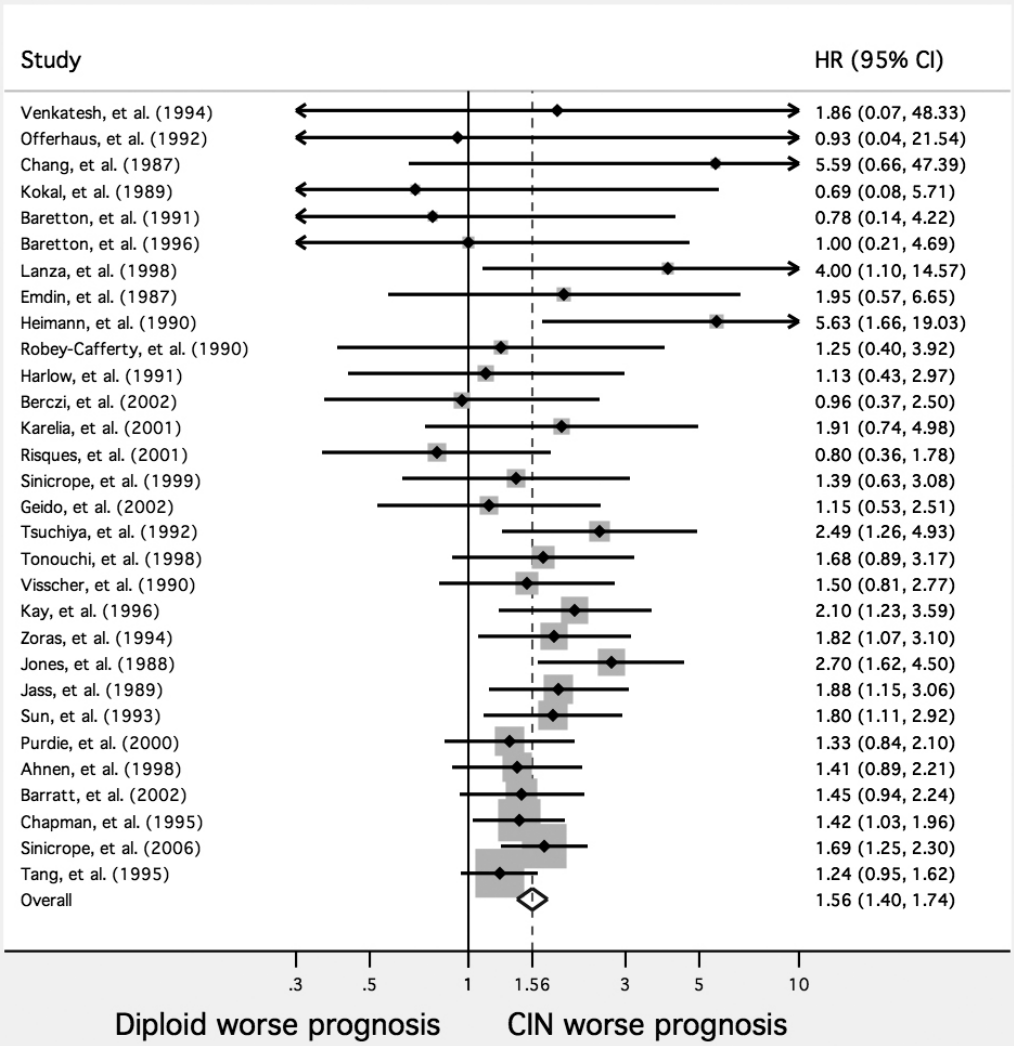

Figure 25 Fixed effects meta-analysis of studies reporting the relationship between CIN and overall survival

Fixed effects meta-analysis of studies reporting the relationship between CIN and overall survival: p= 2.22E-16, I^2=0%. Only studies reporting data on stage 1 - 3 are included (192-194, 196-222).

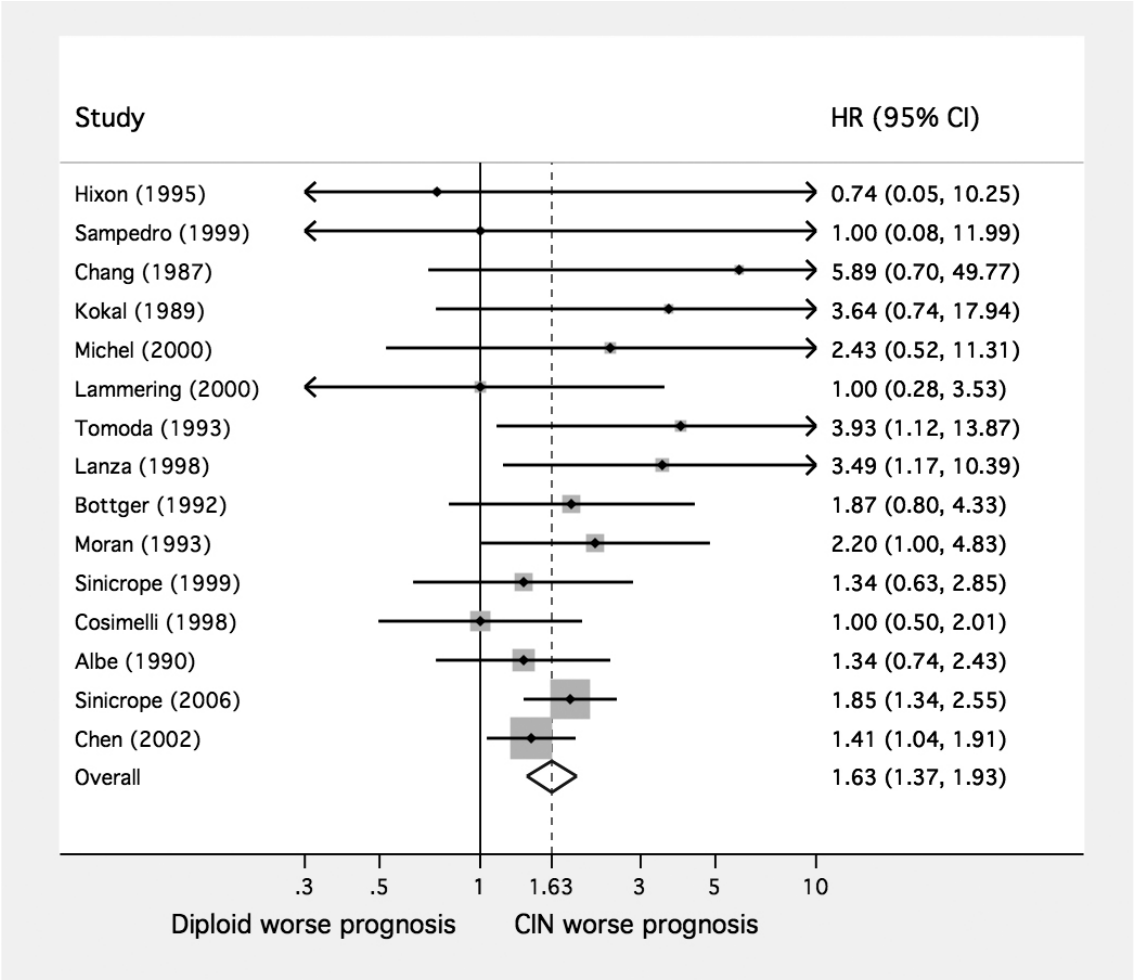

Figure 26 Fixed effects meta-analysis of studies reporting the relationship between CIN and progression-free survival

Fixed effects meta-analysis of studies reporting the relationship between CIN and progression-free survival: p= 3.29E-08, I^2= %. Only studies reporting data on stage 1 - 3 are included (193, 198, 208, 209, 214, 223-232).

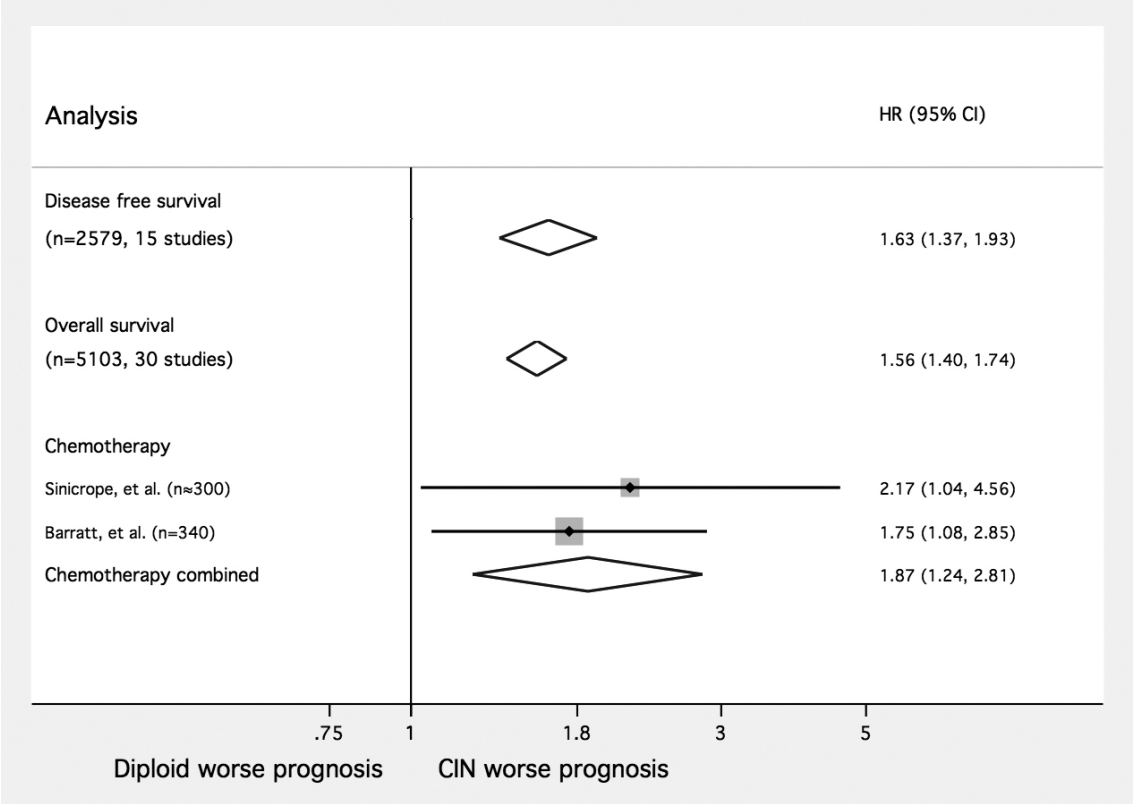

Figure 27 Analysis on impact of CIN on patient survival
Impact of CIN on disease free survival, overall survival, and those receiving adjuvant chemotherapy in locoregional CRC. Overall CIN+ appears to confer a worse prognosis compared to diploid.

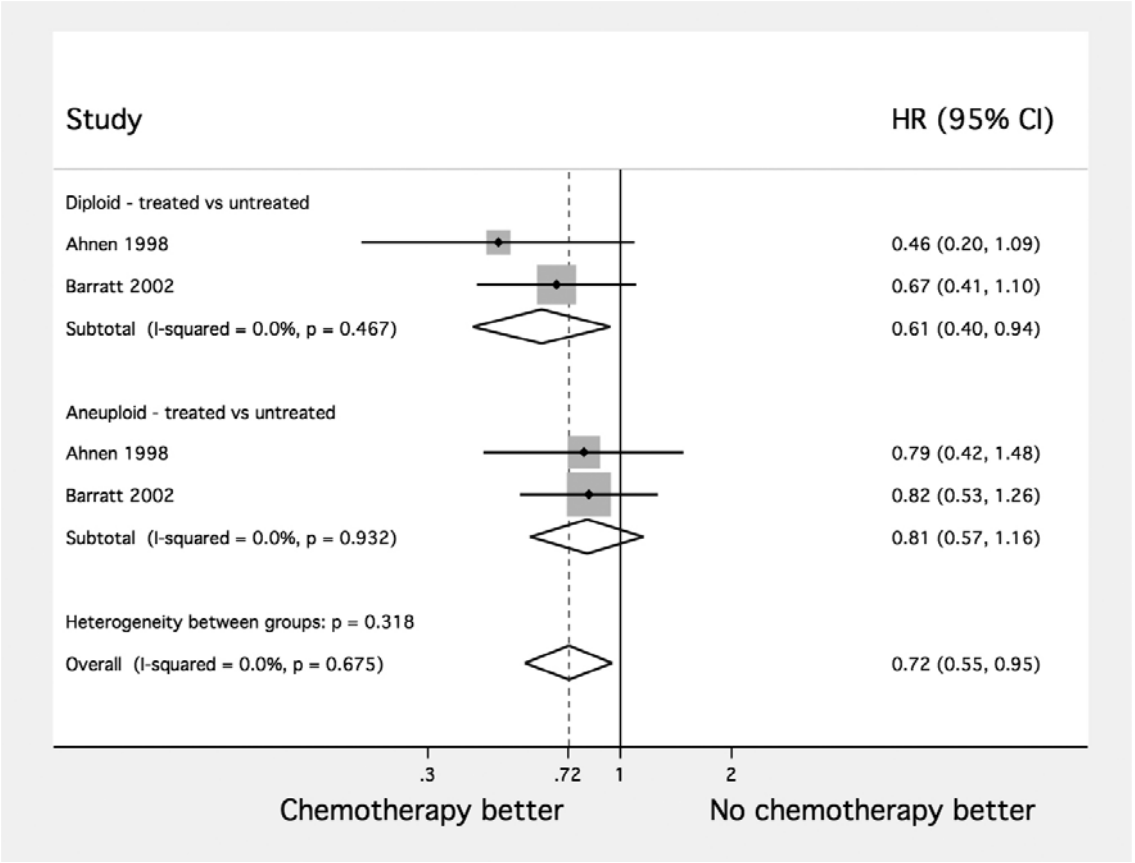

Figure 28 Analysis on impact of CIN on benefit from adjuvant chemotherapy
Benefit derived from adjuvant 5-FU in patients with (near) diploid (top) and CIN+ (middle) CRC. Patients with diploid CRC appear to benefit more from chemotherapy compared to patients with CIN+ tumours. Combined analysis of CIN+ and diploid patients shows similar magnitude of benefit as would be expected from literature (bottom) (195).

3.3 Discussion

In this analysis I have provided evidence that CIN+ CRC cell lines display intrinsic multidrug resistance compared to CIN- cell lines. No specific kinase inhibitor was identified that resulted in preferential lethality of the CIN+ cell lines. I cannot exclude the potential for off-target effects at the concentrations of kinase inhibitors used in this analysis, however the same conditions were applied to the CIN- cells and therefore off-target phenomena are unlikely to change the conclusions of this work. Furthermore, in the isogenic systems, I observed significant drug resistance in the CIN+ cell lines relative to their isogenic parental CIN- pairs at almost all concentrations of cytotoxics tested (ranging from 0.1μM to 25μM). Intriguingly, work with the isogenic CIN+ and tetraploid cell lines suggest that the primary association is between multidrug resistance and CIN+ rather than polyploidy.

I was unable to produce results that agreed with the observation by Amon and colleagues (129) that CRC cancer cells lines with increased ploidy demonstrate increased sensitivity towards 17-AAG and AICAR compared to CRC cell lines with a near-diploid karyotype. I speculate that one explanation for this may be the limited genetic diversity of the panel of CRC cell lines used in their study (5 CIN+ and 5 CIN-) compared to my analysis using 14 CIN+ and 8 CIN- cell lines. Furthermore, 2 of the CIN- cell lines that they used, HCT15 and DLD1, are likely to have originated from the same patient (based on DNA fingerprinting analysis) (233, 234). Similarly, 2 of the CIN+ cell lines they used, SW480 and SW620, originated from the same patient (235), further limiting the genetic diversity of their cell line panel. Moreover, I failed to

observe a difference in sensitivity in the isogenic models of CIN and tetraploidy compared to the parental diploid cells, further disagreeing with their observations.

It has been previously demonstrated that aneuploid cell lines can acquire multidrug resistance at an accelerated rate (156) that may be driven by cancer cell heterogeneity resulting from multiple chromosomal reassortments in aneuploid cells. The short time course of my experiments in comparison to this study suggests that multidrug resistance that I observed is likely to be an intrinsic property of CIN+ cells rather than a process that is acquired in the cell lines over multiple generations. I speculate that either basal population heterogeneity in CIN+ cell lines is sufficiently diverse to confer a cell viability advantage following drug exposure or there is a specific CIN+ survival phenotype that initiates a tolerance of ongoing chromosomal rearrangements that is also associated with multidrug resistance.

There is increasing evidence in support of a CIN+ survival phenotype and putative molecular coordinators of this property. Cell death after mitotic arrest may result from transcriptional inhibition due to condensed chromatin, precipitating the degradation of short-lived mRNA encoding pro-survival proteins (46). CIN+ cells may overexpress these pro-survival genes compared to diploid cells (14) that may drive the resistance of CIN+ cells to a mitotic arrest triggered by taxanes. Jeganathan and colleagues have demonstrated that tolerance of chromosome missegregation events can be conferred by a hypomorphic *BUB1* allele in mouse embryonic fibroblasts (236). Recently, Thompson and Compton have demonstrated that chromosome missegregation in diploid human cells triggers an increase in nuclear p53 and that p53 null cells are able to tolerate chromosome missegregation events enabling the propagation of aneuploid genomes

(237). A higher proportion of the CIN+ cell lines used in my study have mutant p53 in comparison to the CIN- cell lines (where p53 mutation status is known, 3 out of 8 CIN- cell lines and 14 out of 17 CIN+ cell lines). However when data for somatic mutation status and CIN status was pooled, CIN+ status was the only parameter significantly associated with resistance to these inhibitors.

Therefore, evidence exists for the coordination of apoptotic/cell death pathways following chromosome missegregation events. Conceivably, common molecular pathways regulating cell death following a chromosome missegregation event may become disrupted in CIN+ cells, simultaneously triggering tolerance of chromosome re-assortments and, as an indirect consequence, resistance to drug exposure.

3.4 Conclusion

The observations that CIN+ cancer cell lines appear to be less sensitive to a range of anti-cancer agents compared to diploid cells and that poorer patient outcome follows cytotoxic treatment of CIN+ tumours compared to diploid counterparts, strongly suggest the need to consider tumour stratification according to CIN status in the design of clinical trials testing novel anti-cancer agents in CRC. This is particularly relevant to the advanced CRC setting where the incidence of CIN+ is greater than in early stage disease. Stratifying drug response according to CIN status may limit the risk of early drug attrition and heighten the chance of identifying responder populations in patients with diploid tumours. Importantly, these data indicate that specifically targeting cancer cells with CIN+ status using currently available kinase inhibitors appears challenging. An improved understanding of the mechanisms associated with the generation and

survival of CIN+ CRC will be important to drive the development of new therapeutic approaches in order to improve patient outcome in this high risk disease subtype.

With this in mind, I next used whole genome RNAi functional genomics approaches in an effort to identify CIN+ survival pathways and mechanisms responsible for the initiation or maintenance of this CIN+ phenotype.

Chapter 4. Unbiased whole-genome RNAi screens to identify survival mechanism in CIN+ cancer

4.1 Introduction

One common application of RNAi technology in cancer research is in genome wide RNAi screens to identify genes whose loss of function results in synthetic lethality, where the combination of loss of function of the gene with the particular genotype of interest results in a decrease in cell viability compared to an isogenic cancer cell without that genotype of interest (238-240).

In the previous chapter, I have shown that CIN+ cancer cell lines appear to be less sensitive to a range of anti-cancer agents including kinase inhibitors and cancer cytotoxics compared to diploid cells. There may be two potential explanations for this observation 1) basal population heterogeneity in CIN+ cell lines is sufficiently diverse to confer a Darwinian-like cell viability adaptive advantage following drug exposure or 2) a specific CIN+ survival phenotype is associated with a tolerance of ongoing chromosomal rearrangements (66, 236) that indirectly impacts upon drug sensitivity, initiating multi-drug resistance.

As discussed in section 1.3.8, experiments conducted using yeast model systems have shown that polyploid yeast are dependent for survival upon increased expression of genes involved in pathways such as sister chromatid cohesion and mitotic spindle function (93). Furthermore, Torres and colleagues have shown that strains of aneuploid yeast show delayed cell cycle transition, an increase in glucose uptake, and a gene expression pattern characteristic of the environmental stress response (127). In the

previous section, I observed that CIN+ colorectal cancer (CRC) cell lines on average display a lower proliferative rate compared to CIN- CRC cell lines. These experiments suggest that there are specialised adaptations and possible compromises required to sustain aneuploidy or polyploidy. Additionally, as discussed in the previous chapter, Tang and colleagues demonstrated that CIN+ CRC cell lines might be more susceptible to inhibitors of protein folding (17-AAG) and activators of AMPK (AICAR). However, I was unable to obtain similar results using our panel of non-isogenic CIN+ and CIN- CRC cell lines, and our isogenic models of CIN and tetraploidy.

I reasoned that mammalian CIN+ cancer cells have acquired adaptations to tolerate a polyploid or aneuploid state similar to that observed in yeast cells and that these adaptations may be exploitable to limit the survival of CIN+ cells specifically. Specific therapeutic targeting of CIN+ tumour cells may also reduce side effects associated with treatment by limiting cytotoxicity towards normal diploid cells. To this end, I used a functional genomics approach to identify regulators of CIN+ survival in human cancer, by performing unbiased whole genome RNAi screens in the HCT116 (diploid) cell line and its isogenic HCT116 *MAD2+/-* cell line. *MAD2* heterozygosity is sufficient to induce CIN in (164). The high-throughput RNAi study presented in this chapter has been performed with extensive support from the High-Throughput Screening Facility (Michael Howell, Ming Jiang, Rachael Instrell and Becky Saunders) in this Institute. Section 4.2.6, analysing the variance within the whole genome RNAi screen and subsequent validation experiments has been completed in collaboration with Stuart D. Horswell who performed the statistical analysis.

4.2 Results

The CRC cell line HCT116 and its isogenic CIN+ cell line were chosen for the screen. The HCT116 cell line is a non-CIN cell line with microsatellite instability (MIN) and a near diploid modal chromosomal number (6). An isogenic clone of HCT116 with one allele of *MAD2* (a component of the spindle assembly checkpoint (SAC)) deleted by homologous recombination (164) was the CIN+ counterpart of the HCT116 cell line used for the screen. This cell line displays some of the phenotypes proposed to be associated with CIN, such as premature sister chromatid separation (80), failure to arrest appropriately in the presence of mitotic inhibitors (73-75), an increase in aneuploidy (3, 52) as scored by clonal FISH, and an increased rate of chromosomal loss compared to the parental diploid cell line.

4.2.1 Optimisation of screening parameters

Various parameters were assessed prior to the whole genome RNAi screen to optimise the dynamic range and reproducibility of our results in measuring cell number and cell cycle profile parameters (subG1, G1, S, 4n and >4n) following 72h of siRNA transfection. The Acumen eX3 laser scanning cytometer instrument was used. This instrument is equipped with scanning lasers with excitation and emission wavelengths compatible with fluorescent probes. Images are then acquired through a wide field objective across the bottom of a microplate, with a resolution equivalent to a 20x microscope objective (241). DAPI was used to stain cellular DNA content fluorescently for use with the instrument.

Positive control siRNAs resulting in distinct cell cycle phenotypes were used in the optimisation of the conditions for the screen. The controls included TOP2A siRNA, which results in an increase in the >4n population of cells, and PLK1 siRNA, which reduces cell viability. Various parameters for the plating of the cells were tested in order to optimise the balance between initial seeding cell density (so as to minimise errors due to low numbers of cells) and the dynamic range of both the cell cycle profile and numbers of surviving cells. The parameters that were analysed were poly-L-lysine concentration (to promote cell adhesion and prevent loss of cells during washing and fixing of cells prior to DAPI staining) and initial cell plating density. Twenty-three transfection reagents were also assessed at various concentrations and a range of siRNA concentrations to identify the optimal transfection with minimal cytotoxicity associated with non-targeting control and transfection reagent only and maximal dynamic range of phenotype following silencing of positive control genes (eg >4n induction by siTOP2A and decrease in cell viability following siPLK1). Various fixative agents were assessed in an effort to identify one that would give the best quality in terms of the cell cycle profile readout. Cell cycle profile identification was tested with propidium iodide (PI) and DAPI at various concentrations. The conditions were optimised for both 96-well and 384-well plate formats. The 96-well format was chosen for the final screen was due to its better reproducibility of results. Figure 29 demonstrates the good dynamic range and small variance between replicates following transfection with control siRNAs in the HCT116 diploid parental cell line.

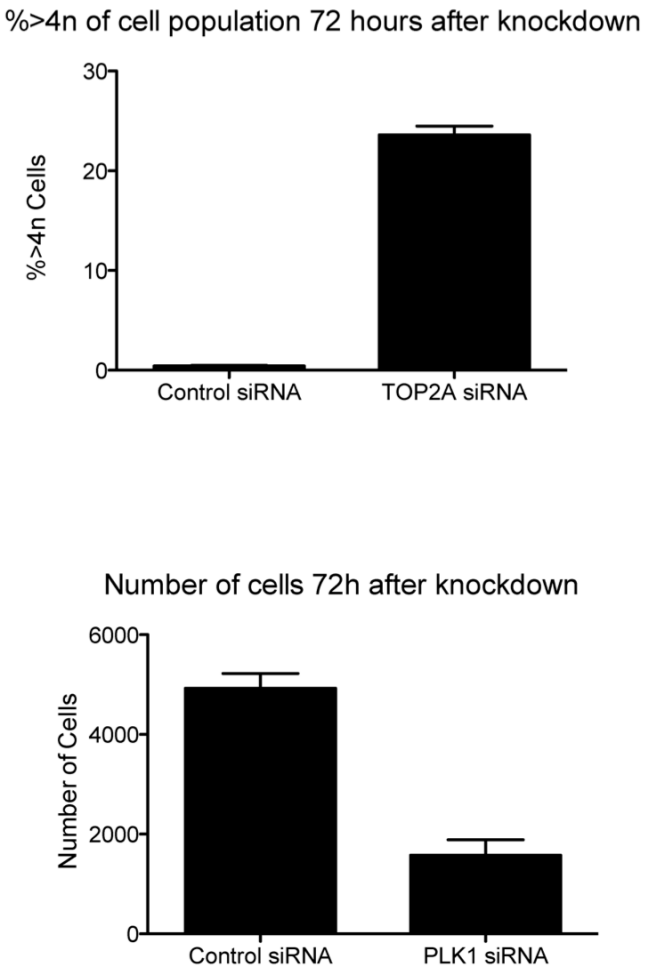

Figure 29 Pre-screen optimisation

Percentage of cells with >4n DNA content (top) and cell number (bottom) 72h after siRNA knockdown using positive control siRNAs under optimal transfection conditions. Error bars represent standard deviations across replicate wells.

I wanted to identify a positive control that selectively killed CIN+ cells in advance of the screens. From the previous chapter, I have shown that the *MAD2+/-* cells are resistant to multiple drugs with no single agent being able to selectively target this cell line over its diploid parental counterpart. This excluded the use of any of the kinase inhibitors or cytotoxic agents that we used in the previous chapter. However, I was concerned that the resistance of *MAD2+/-* cells to multiple drugs with differing mechanisms of action may have resulted from a cloning artefact subsequent to the homologous recombination step required to generate these cells. In order to exclude this possibility, I silenced the *BUB1B* gene, a component of the SAC, in the HCT116 wild type cells in order to investigate whether this observation was specific to SAC disruption. In this investigation, I used 5 drugs with different mechanisms of action at concentrations ranging from 0.1μM to 20μM. The drugs were Dactinomycin, Ancitabine, Podophyllotoxin, Doxorubicin and Flavopiridol. The *BUB1B* silenced cells were more resistant to these drugs compared to the control silenced cells (Figure 30) reinforcing the observation that deficiency in SAC components can promote multidrug resistance. Possible explanations for why *BUB1B* silencing confers drug resistance may include: 1) The silencing of *BUB1B* selects for a sub-population of cells that are able to tolerate a compromised SAC, and thus are able to better tolerate other stresses such as drug treatment. 2) *BUB1B* silencing results in CIN and the generation of a heterogeneous population of cells. However, this is unlikely to fully explain the drug resistance phenotype observed due to the short time duration of the experiments. 3) a functioning SAC triggers cell death pathways following drug treatment and *BUB1B* silencing overcomes this.

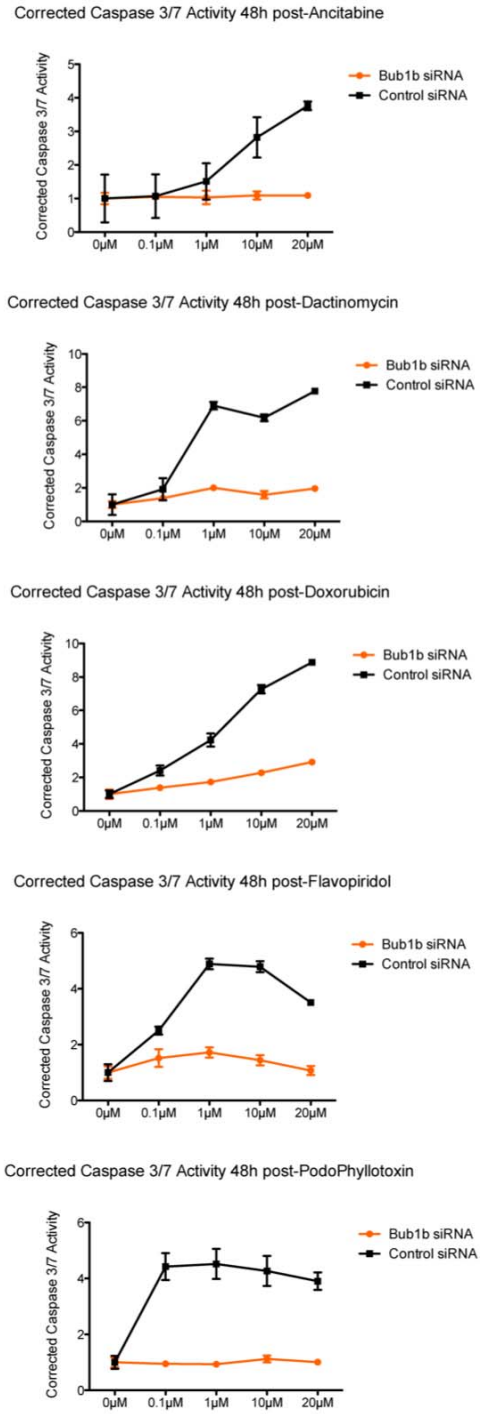

Figure 30 Drug response following BUB1B silencing in HCT116 cells
Graph of relative corrected Caspase 3/7 activity in HCT116 cells after transfection with siCON or siBUB1B for 48h followed by 48h of exposure to Ancitabine, Dactinomycin, Doxorubicin, Flavopiridol or PodoPhyllotoxin at 4 concentrations ranging from 0.1µM to 20µM.

The drug screens did not reveal a positive control that was selectively lethal in CIN+ cells. Since silencing of kinetochore components has been shown to result in an increase in mitotic catastrophe in SAC-compromised cells (242) I reasoned that a small-scale cell viability screen with siRNAs against 27 different kinetochore components in the HCT116 *MAD2+/-* and diploid parental HCT116 cells might reveal a positive control. I was unable to identify any siRNA that resulted in preferential lethality within the CIN+ cell lines at a magnitude that could confidently be replicated in a whole genome RNAi screen (Figure 31). Therefore I was unable to selectively identify genes that induce preferential lethality of CIN+ isogenic cells in advance of the screen.

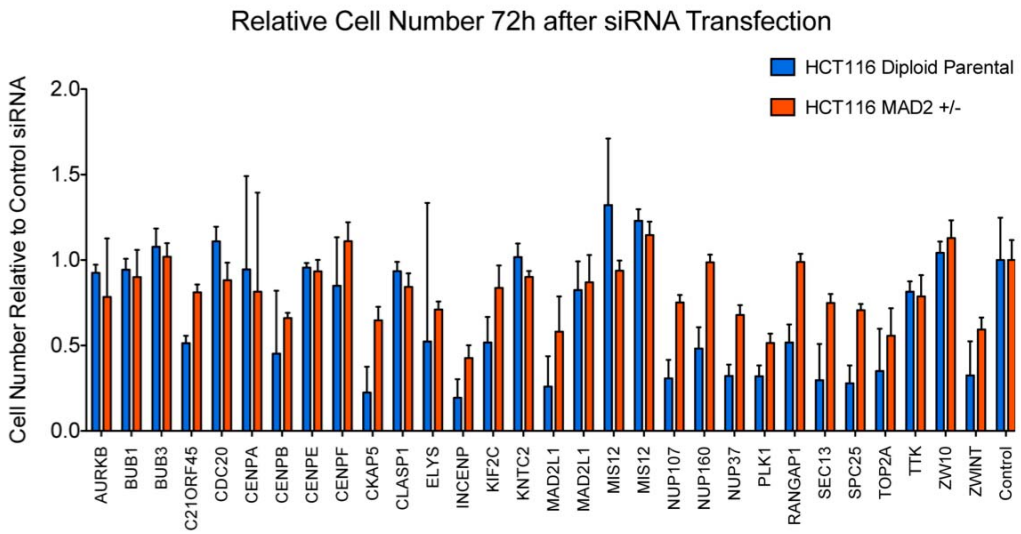

Figure 31 Silencing kinetochore components in HCT116 diploid parental and *MAD2+/-* cell lines
Relative cell number after 72h of knockdown with siRNAs targeting kinetochore components in HCT116 diploid parental and *MAD2+/-* cell lines.

4.2.2 The screen

The HCT116 parental diploid cell line and *MAD2+/-* isogenic cell line were transfected with the Dharmacon whole genome siRNA library targeting 21222 genes in triplicate (267 96-well plates in triplicate) (Figure 32A). This high throughput screen allowed me to address whether loss of function of any of these genes caused a greater reduction in cell viability in the *MAD2+/-* cell line compared to its diploid parental cell line. Both cell lines were transfected in 96-well plates and were fixed 72 hours after transfection. Plates were then stained with DAPI, to allow us to quantify the number of surviving cells following siRNA transfection. Data was normalised and analysed as described in material and methods. 10 plates from the screen in the HCT116 *MAD2+/-* cell line were excluded from analysis due to errors in the readouts of the DAPI staining on these plates.

Z-scores (a score measuring standard deviations from the mean for normalised data) for cell number were obtained from this normalised data for cell number following siRNA transfection. Z-scores for non-targeting control siRNA (siCON) and non-targeting non-RISC-processed control siRNA (RISC-FREE) transfected cells tended to lie slightly right of the median z-score value for cell number in both *MAD2+/-* and diploid parental cell lines (Figure 32B). The shifting of negative controls to the right of the normalised cell number curve does not contradict previous observations in other whole genome siRNA screens (243) and may indicate that the majority of siRNAs have negative cell viability effects when transfected into these cell lines.

To select candidate genes whose loss of function results in a preferential decrease in the viability of the *MAD2* deficient cell line, I overlapped siRNAs that resulted in a maximal cell number z-score of -2 in the MAD2 deficient cell line and whose z-score was at least 2 less compared to thee corresponding HCT116 diploid parental screen (Figure 32C). I was able to identify 69 candidate genes for follow up whose loss of function may be preferentially lethal to CIN+ cancer cells.

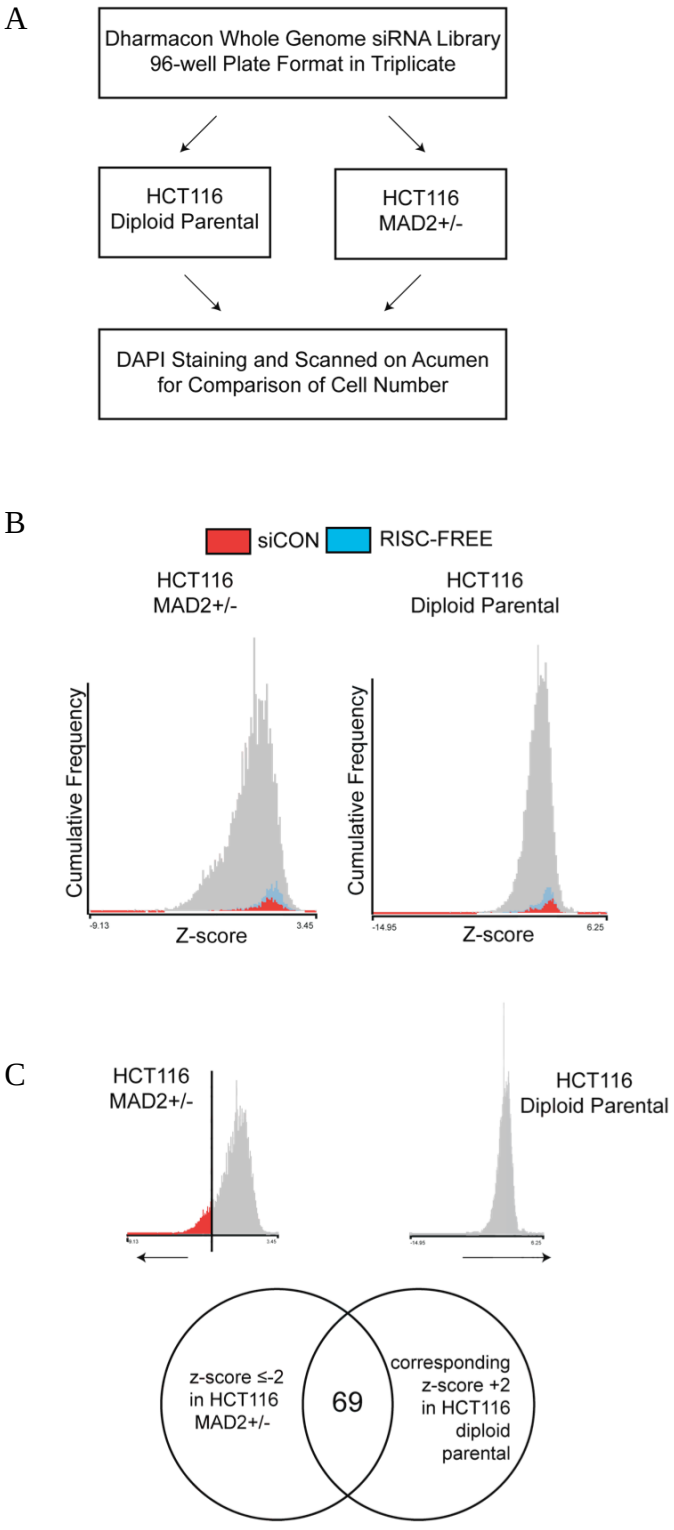

Figure 32 Screen overview, and candidate gene selection
A) Workflow diagram of screen.
B) Distribution of cell number z-scores in HCT116 *MAD2+/-* cell line (left) and diploid parental cell line (right). siCON values are highlighted in red and RISC-FREE in blue.
C) Diagram of criteria for selection of candidate genes for follow-up.

4.2.3 Validation of candidate genes for on-target effects

siRNAs may not only silence a target gene but may also suppress the expression of other genes through off-target effects. I wanted to assess these candidate genes for off-target effects prior to validating preferential lethality in CIN+ cancer cell lines. To address this, I first repeated the high throughput screen assay in the HCT116 *MAD2+/-* cell line using the four individual siRNAs that make up the Dharmacon SmartPool siRNAs for each gene of interest. 69 candidate genes were reassayed (Figure 33). The number of surviving cells for each siRNA was normalised to non-targeting control siRNAs and expressed as a percentage of control value (POC). I was unable to standardise cell number values to derive z-scores for these candidate genes as I was reassaying a smaller number of candidate genes compared to the genome-wide screen and this was a biased list in terms of impact on cellular viability. The results enabled me to select 17 candidate genes that resulted in a reduction of cell number in HCT116 *MAD2+/-* to ≤66% of control siRNA as both an average of the 4 individual siRNAs that make up the pool and also in at least 2 out of 4 individual siRNAs for follow-up experiments.

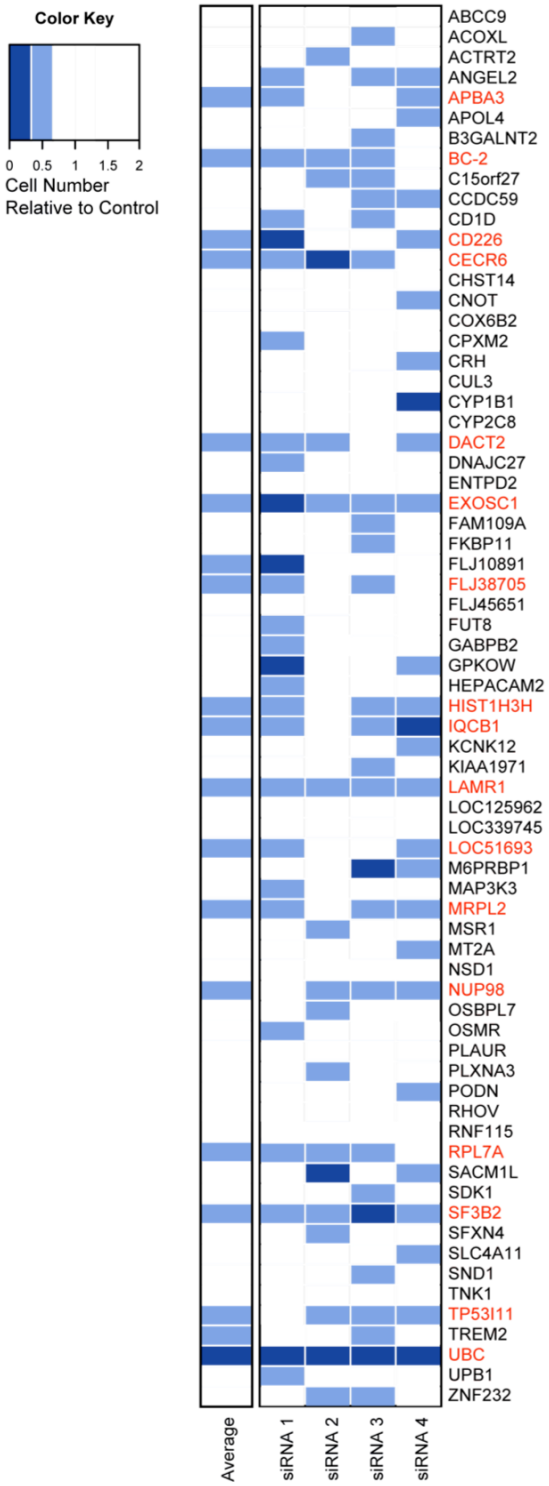

Figure 33 Heatmap of candidate gene validation
Performed in HCT116 *MAD2+/-* single cell line to exclude off-target effects for cell viability. Genes highlighted in red were selected for further validation.

4.2.4 Validation of candidate genes for differential lethality effects

I next wanted to determine whether these candidate CIN+ synthetic lethal genes would induce a greater decrease in viability in CIN+ cell lines compared to CIN- cell lines. The 17 candidate genes selected in the previous section were rescreened 3 times in the HCT116 *MAD2+/-* and diploid parental cell line. Unfortunately, I was unable to validate any of these genes as consistently being able to preferentially decrease cell viability in the HCT116 *MAD2+/-* cell line compared to its parental diploid cell line (Figure 34A).

In an attempt to try to capture cell death at different time points following gene silencing, the experiment was repeated at three different endpoint times (Figure 34B) but similar results were obtained.

Finally, most of the 17 candidate genes that we reassayed caused a reduction of cell viability of at least 50% in both cell lines when silenced. Such a magnitude of cell death in both cell lines may have been masking a differential lethality effect. The initial whole genome RNAi screen was performed using siRNA at a final concentration of 37.5nM. I therefore repeated the assay with 18.75nM of siRNA, to attempt to establish if a reduction in magnitude of gene knockdown and toxicity of siRNA transfection may reveal a difference in magnitude of cell death between the two cell lines (Figure 34C). Although there was a reduction in magnitude of cell death, we were still unable to observe consistent preferential lethality effects in the *MAD2+/-* cell line.

A

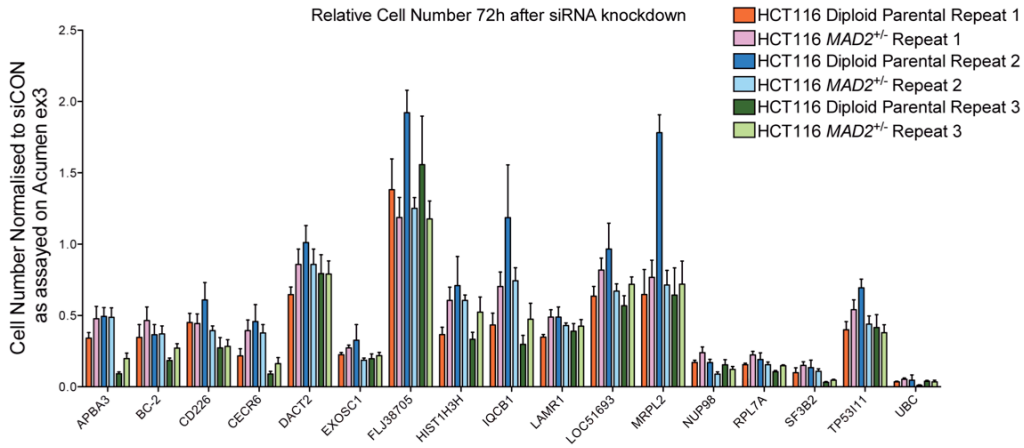

B

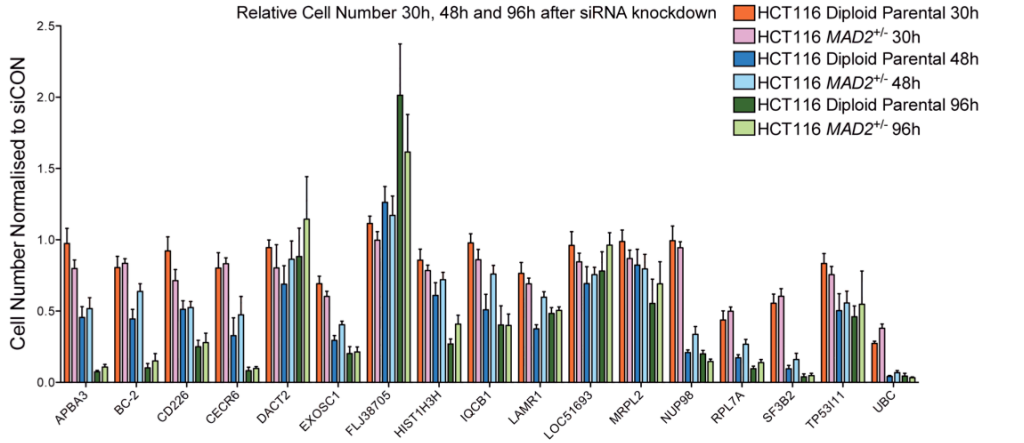

C

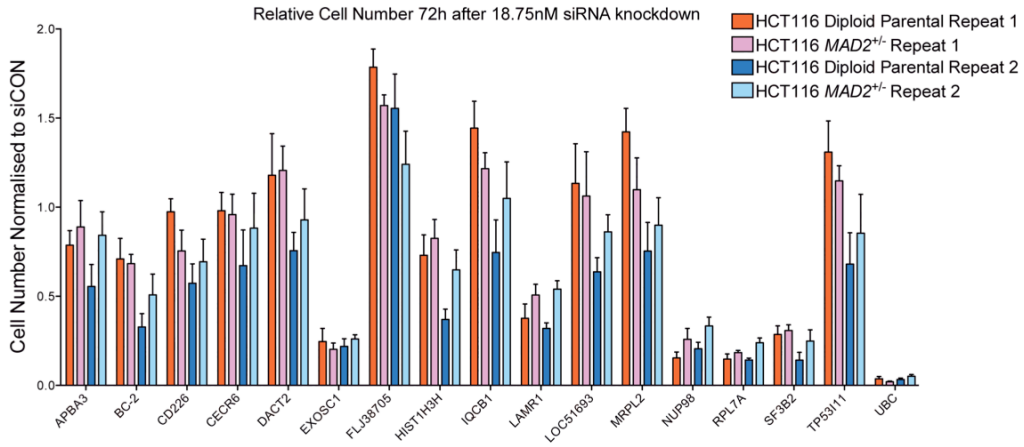

Figure 34 Assessment of differential lethality in HCT116 *MAD2+/-* cell line and diploid parental cell line

Error bars represent standard deviations across replicate wells.
A) Graph of relative cell number 72h after siRNA transfection. Experiment was repeated three times in both cell lines. Bars are arranged for each siRNA as three pairs of corresponding experiments in HCT116 diploid parental and *MAD2+/-* cell lines (labelled in graph as repeat 1, 2 or 3).
B) Graph of relative cell number 30h, 48 and 96h after siRNA transfection. Experiment was repeated three times in both cell lines. Bars are arranged for each siRNA as three pairs of corresponding time point experiments in HCT116 diploid parental and *MAD2+/-* cell lines (labelled in graph as 30h, 48h or 96h).
C) Graph of relative cell number 72h after siRNA transfection at a reduced final concentration of 18.75nM. Experiment was repeated twice in both cell lines. Bars are arranged for each siRNA as two pairs of corresponding experiments in HCT116 diploid parental and *MAD2+/-* cell lines (labelled in graph as repeat 1 or 2).

These 17 candidate genes were also rescreened in a non-isogenic panel of 7 CIN+ and 6 CIN- cell lines. The CIN+ cell lines used were C70, COLO205, HRA19, HT29, HT55, SKCO1 and SW620. The CIN- cell lines were DLD1, GP2D, HCA7, RKO, SW48 and VACO5. However, in agreement with results in the isogenic cell lines, depletion of these candidate genes did not appear to result in a significant difference in cell death in the CIN+ cells compared to CIN- cells (Figure 35A and B).

A

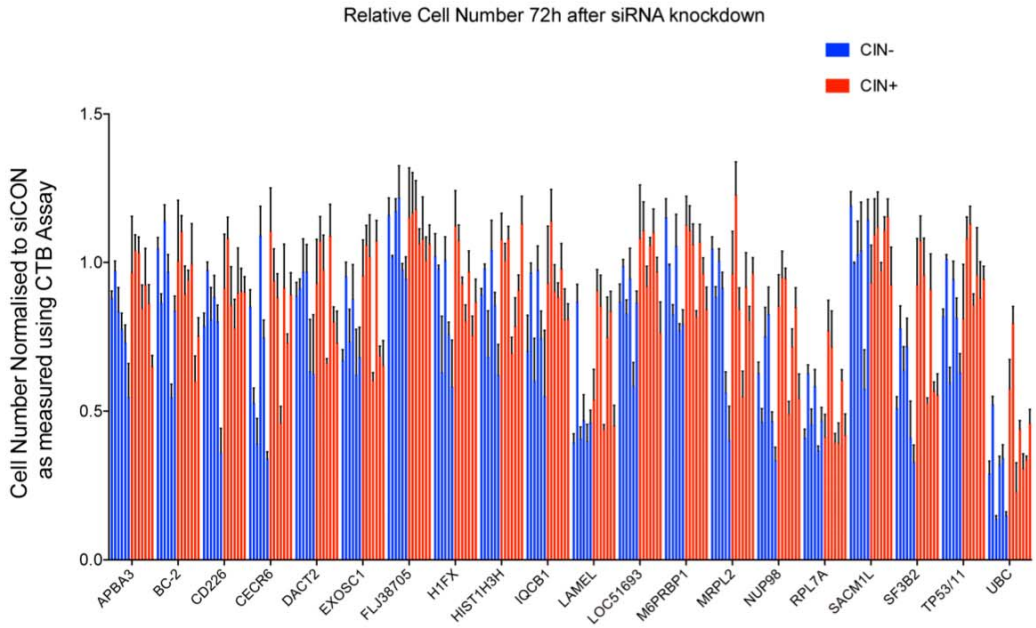

B

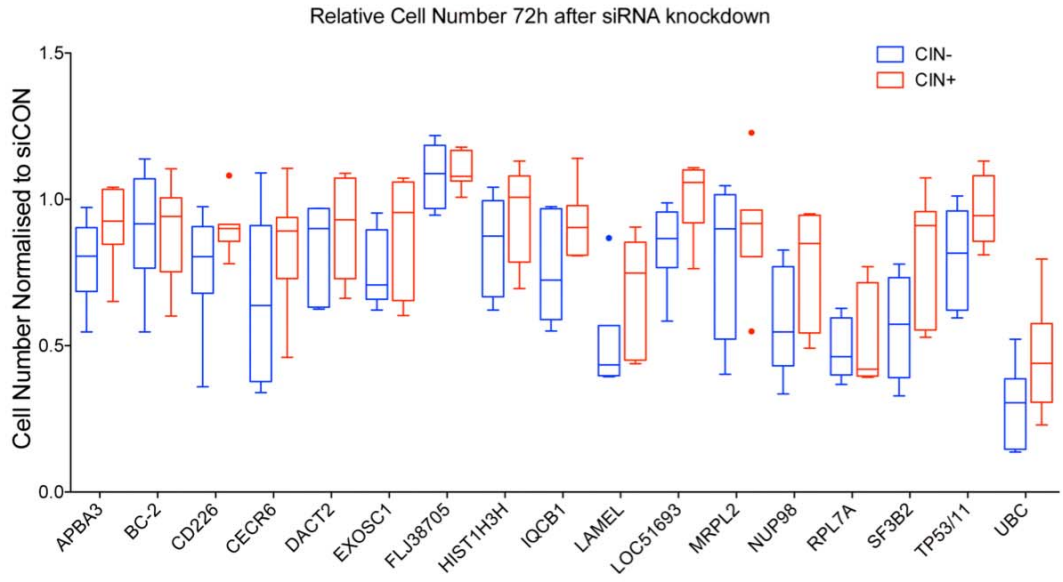

Figure 35 Assessment of differential lethality of the 17 candidate genes in non-isogenic CIN+ and CIN- cell lines
Error bars represent standard deviations across replicate wells.
A) Graph of relative cell number 72h after siRNA transfection. Each bar represents a single individual cell line.
B) Boxplot of relative cell number 72h after siRNA transfection in CIN+ and CIN- cell lines. Whiskers limted by 1.5x interquartile range.

4.2.5 Reselection of candidate genes and validation

I was concerned that the inability to consistently validate candidate genes as being preferentially lethal towards CIN+ cells was due to a flaw in the selection process of our candidate genes. An alternate method for selecting candidate genes that are required for the survival of HCT116 *MAD2+/-* cells was used. Instead of comparing the cell number z-scores with the HCT116 diploid parental cell line, z-scores from the HCT116 *MAD2+/-* screen was compared with three other whole genome RNAi screens assayed in the Institute using the same methods as this HCT116 screen These other screens were performed using cell lines of a different tissue origin; fibrosarcoma (HT1080), non-small cell lung cancer (PC9) and renal cancer (RCC4). The rationale for this selection method was 1) As candidate genes were selected using a differential z-score approach, there was potential to not select a candidate gene if there was an error in the readout for the parental diploid cell line. An error in a single replicate may affect the mean surviving cell number, and thus affect the z-score. 2) Comparing across 4 screens performed in different cell lines may result in more specific candidate gene selection and this reduces the number of false positives and will hopefully reveal candidate genes that are specifically lethal towards HCT116 *MAD2+/-* cells when silenced. However, I acknowledge that these genes may not be specifically lethal towards CIN+ cell lines but may be a result of other specific lethalities such as colon-specific or MIN+ specific lethality.

Candidate genes were selected on a criteria of z-score <-2.5 in the *MAD2+/-* screen and non-significant z-scores (>-2 and <2) in the three other whole genome RNAi screens (Figure 36A). I obtained a list of 75 additional candidate genes having excluded candidate genes that had already been selected using the previous method.

These 75 candidate genes were next screened in the HCT116 diploid parental and *MAD2+/-* cell lines to validate their effects on cell viability and to assess for differential lethality effects (Figure 36B). I performed this screen of the 75 genes twice in each cell line. On both occasions, just under a fifth of the 75 candidate genes resulted in a reduction of cell number to ≤66% of control siRNA when silenced in both cell lines. This was a slightly lower validation rate compared to the 69 candidate genes selected on the basis of z-score comparison with the HCT116 diploid parental cell line, where 17 genes resulted in a reduction of cell number to ≤66% of control siRNA when silenced in the HCT116 *MAD2+/-* cell line (24.6% validation). The magnitude of cell death resulting from silencing of these 75 genes appeared to vary between experiments, however the positive control siRNA, KIF11, reliably resulted in at least an 80% reduction of cell viability in both cell lines for each repeat of the experiment. This suggested that the effects of siRNAs causing a strong reduction in cell viability are unlikely to be masked by variation arising from performing the experiment on separate occasions.

However, only some of the 75 candidate genes caused a similar magnitude of decrease in cell viability on the two different occasions the two cell lines were screened. Furthermore, only silencing of three genes, *AAAS*, *CD37* and *PPHLN1* resulted in an greater decrease of cell viability of at least 20% in the HCT116 *MAD2+/-* cell line compared to the diploid parental cell line on both occasions. These genes were selected for further validation experiments. OCIA was not selected as it appeared to cause an increase in cell proliferation rate in the diploid parental cell line compared to control siRNA transfected cells. I next attempted to validate these candidate genes on a further three occasions as being preferentially lethal in the HCT116 *MAD2+/-* cell line

compared to its diploid parental cell line. Again, I was unable to confidently validate candidate genes as being consistently selectively lethal towards CIN+ cells (Figure 37).

A

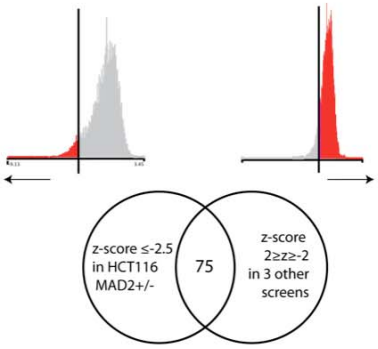

B

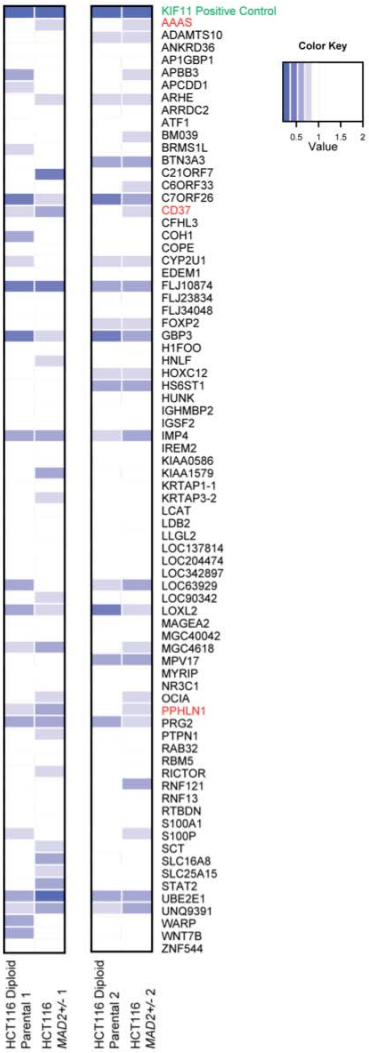

Figure 36 Reselection of candidate genes and assessment for differential viability effects. Error bars represent standard deviations across replicate wells
A) Diagram of candidate gene selection criteria.
B) Heatmap of relative cell number 72h after siRNA transfection in HCT116 diploid parental and *MAD2+/-* cell line. Experiment was repeated 2 times. KIF11 (positive control) highlighted in green. Candidate genes selected for follow up highlighted in red.

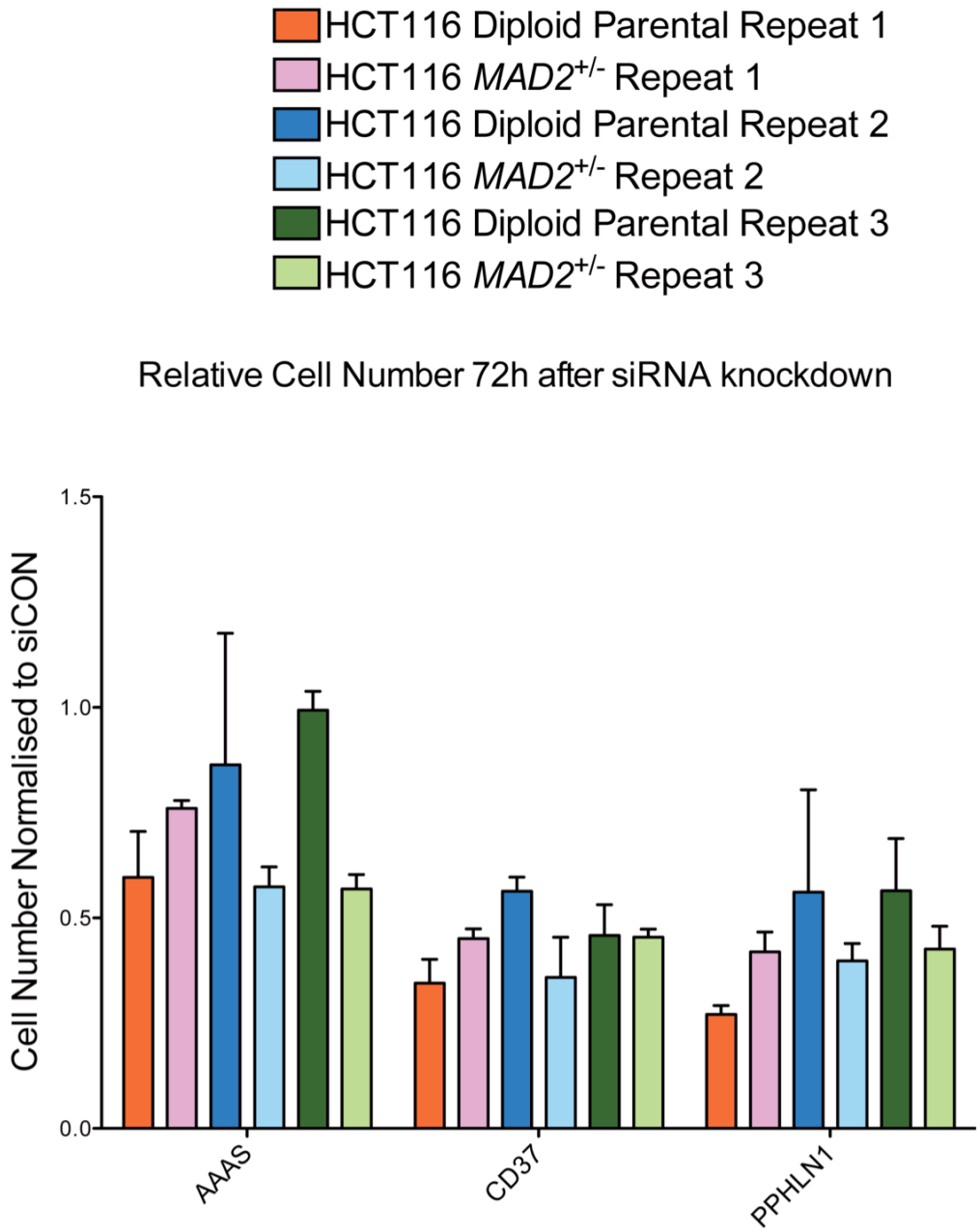

Figure 37 Further assessment of candidate genes for differential viability effects
Graph of relative cell number 72h after siRNA transfection in HCT116 diploid parental and *MAD2+/-* cell lines. Experiment was repeated three times in both cell lines. Bars are arranged for each siRNA as pairs of the three experiments.

4.2.6 Statistical analysis of noise within the system and reproducibility of results

The statistical analysis presented in this section has been performed by Stuart D. Horswell.

I was unable to validate any candidate gene as being consistently able to induce preferential cell death in the *MAD2+/-* cell line despite selecting candidate genes using two different methods. I was concerned that the level of variance within our system was affecting the reproducibility of our results and hoped that statistical models could be used to estimate the levels of variance within the screen in order to better understand the reasons why the screen may have failed and to estimate the power of the screen to detect synthetic lethal candidate genes.

To this end, mixed effects models were used to estimate the levels of variance contributed by various component within the system. The mixed effects model decomposes the overall variation observed in the data by estimating the contribution of each variable to the total variation. Any residual or "unaccounted for" variation is inferred to be noise that may be systemic. For our system, this involved defining the variables within our system, fitting separate models for each of these predictor variables and finally using well-defined algorithms to estimate the “noise” term associated with each predictor (244, 245).

The variables within this system were defined as *MAD2* status, siRNA and replicates for each siRNA (triplicate per siRNA). The ‘unknown’ noise component within the system was defined as θ. Cell count data was fitted into the model and was analysed in groupings of 5 and 15 plates (Figure 38A and B). The θ-noise component in all

groupings contributed approximately 30 to 50% of the variance within the system. This noise component was extremely similar in magnitude (but not identical) to the variance contributed by the siRNA component and therefore may have resulted in the ‘masking’ of the effects on cell viability of the various siRNAs.

A

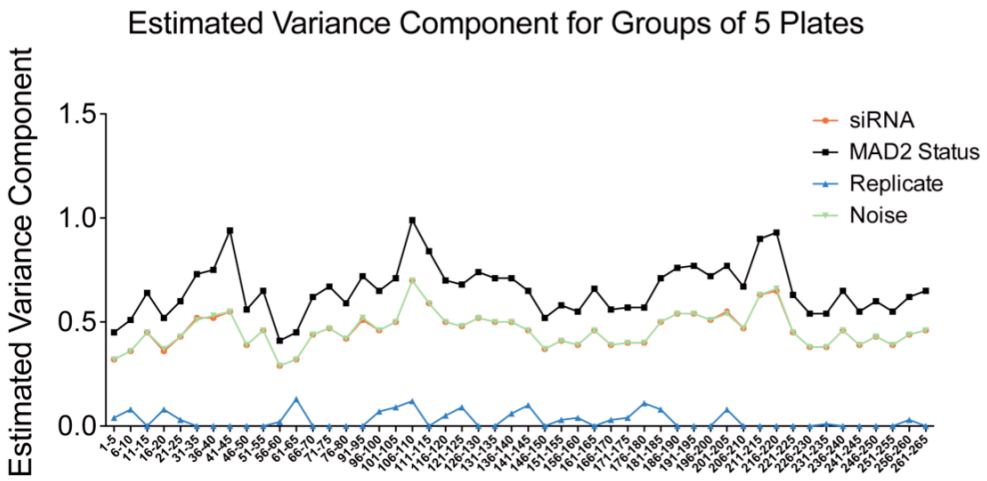

B

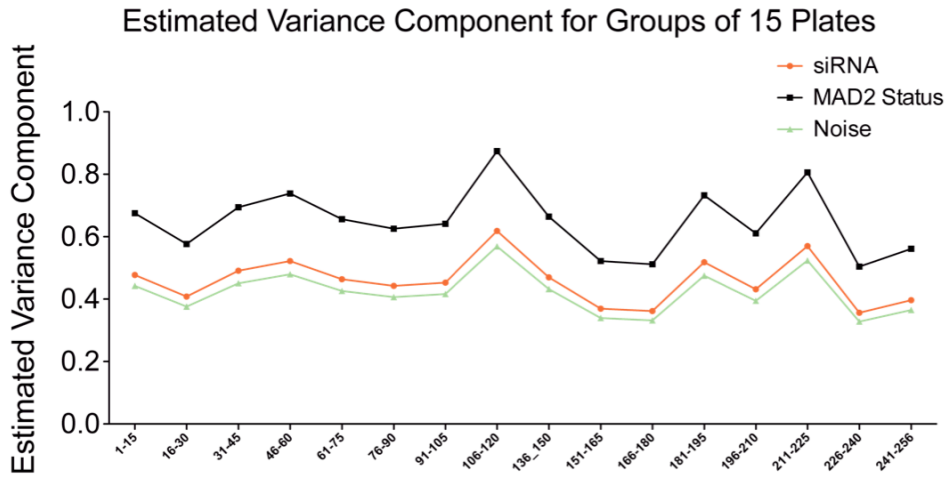

Figure 38 Usage of mixture models to assess noise factors

A) Graph of estimation of variance components in whole genome screen when analysing plates in groups of five. Plate groups where the mixture models failed to converge were excluded.

B) Graph of estimation of variance components in whole genome screen when analysing plates in groups of fifteen. Plate groups where the mixture models failed to converge were excluded. To speed up analysis, estimation of noise due to replicates was excluded as noise due to this term was much smaller compared to other terms.

Fitting the cell count data into the model, and applying a z-test at the level of p=0.05 across all plates, it was found that the minimal critical cell count difference in order to confidently identify a difference between the two cell lines was approximately 4707 cells.

The screen workflow was analysed to identify if any possible sources of variability such as “batch effects” may have contributed to this variance but no such artefacts were identified within our model, suggesting that the unknown noise was not contributed by any obvious breaks or pauses in the manner in which the screen was performed.

4.2.7 Retrospective power analysis of whole genome RNAi screen

A retrospective power analysis was performed. Observed power values were modelled (Figure 39A) using an idealised surviving cell number of 10000 (Figure 39B, based on the average cell number of control transfected cells in validation experiments) in the HCT116 diploid parental cell line and a critical cell number difference of 4707. The statistical power was 50% to detect an approximate 50% difference in cell number between the two screens. The screen appeared to be modestly powered to detect a large difference in cell number between the two cell lines (Power= 75% to detect ≈60% difference in cell number).

A

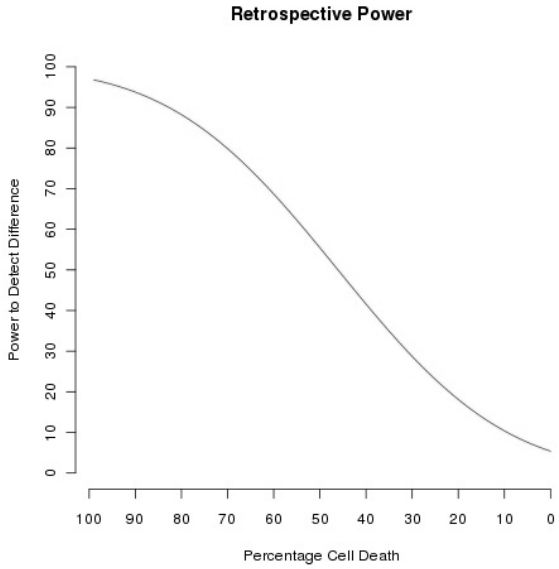

B

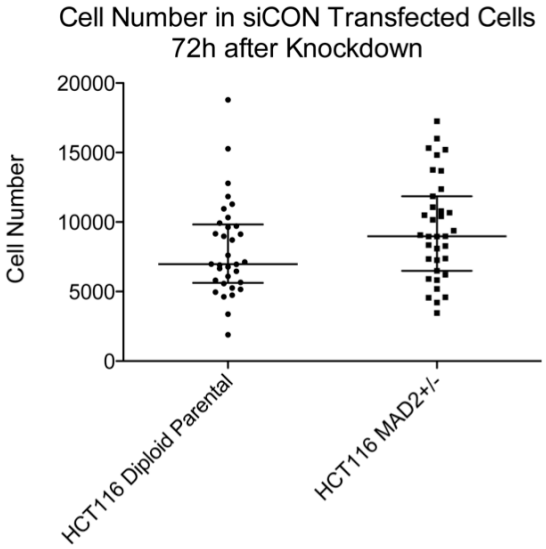

Figure 39 Retrospective power analysis of whole genome RNAi Screen and average cell number in control transfected cells

A) Graph of retrospective power analysis of whole genome RNAi Screen.

B) Scatter plot of cell number following 72h of siCON transfection in HCT116 diploid parental and *MAD2+/-* cell lines. Horizontal lines represent median and interquartile range.

4.3 Discussion

4.3.1 Summary of screen results

In this study I have attempted to use a synthetic lethal high throughput siRNA screen to identify pathways that are necessary for the survival of CIN+ cells. The screen did not identify candidate genes that are able to consistently display selective lethality in CIN+ cell lines compared to CIN- cell lines. 69 candidate genes were selected based on the criteria that these genes induced preferential cell death in HCT116 *MAD2+/-* cell line but not its diploid parental cell line. I was able to validate 17 of these genes as having on-target effects on cell viability in the *MAD2+/-* cell line but was unable to validate these genes as being selectively lethal towards CIN+ cell lines specifically compared to diploid isogenic and non-isogenic cells. A further 75 candidate genes were selected on the basis of being selectively lethal towards the HCT116 *MAD2+/-* cell line but not in three other cancer types. Again I was unable to validate these candidate genes as being preferentially lethal towards CIN+ cancer cells. Figure 40 summarises the candidate gene selection and validation process.

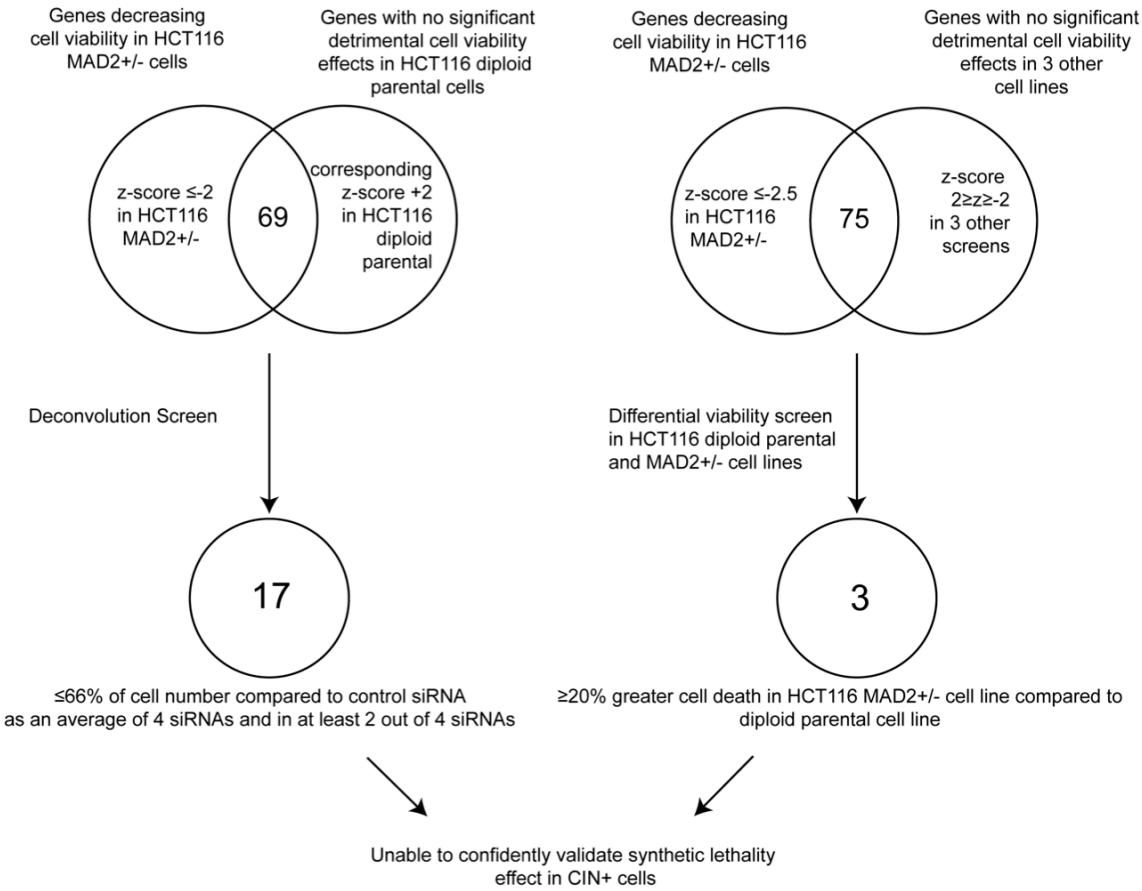

Figure 40 Workflow of candidate gene selection and validation

4.3.2 Estimation of noise component in genome wide siRNA screen and validation experiments

An attempt has been made to assign variance within our system to various components. Here, using mixed effects models; it is shown that there exists a component of variance unaccounted for that contributes approximately 30 to 50% of the total variance within the system within the parameters of the whole genome screen. I was unable to attribute this component to technical reasons such as “batch” effects.

Moreover, the critical cell count for the whole genome screen in order to confidently detect a difference between the two cell lines was approximately 5000 cells. On the basis that the cell number in control transfected cells range from about 7500 to 10000 cells (Figure 39B), this implies that in order to reliably observe a difference in cell lethality at the p=0.05 level, an approximate 50% reduction in *MAD2+/-* cell line viability and none in the diploid parental cell line needs to be observed.

4.3.3 Suitability of siRNA screening approach for synthetic lethality

I speculate that there may have been a variety of factors contributing to our inability to identify pathways required for survival of CIN+ cells. Firstly, the siRNA screening approach may not have been a suitable approach to identify synthetic lethal genes in an isogenic model of CIN+. Many RNAi screens for synthetic lethality in human cancer cell lines have been published. However, the majority of these published screens in human cell lines have either used shRNA (238, 246-251), (shRNA results in a longer duration of knockdown of target gene compared to siRNA (252)). Additionally, it has been reported candidate genes identified using shRNA screening may not be picked up

in similar siRNA screens (253), suggesting that the two techniques may produce different results, possibly due to factors such as technique of RNAi delivery into the cells or duration or magnitude of knockdown. There have been recent published siRNA synthetic lethal screens using isogenic cell lines, where the investigators have been able to identify and validate candidate genes, however they used endpoints of a longer duration post siRNA transfection such as 7 days (254) or 5 days (255). This suggests that following siRNA transfection; subtle differences in cell viability between isogenic cell lines may only become more apparent following a longer duration of gene silencing. There exists a published siRNA synthetic lethal screen with a 72-hour gene silencing endpoint, targeting cancer cells with activated K-ras (256), however the validated genes identified from that screen caused a two to three fold increase in cell death (measured using an assay for apoptosis) in the activated K-ras cell line compared to that without activated K-ras; a much greater difference in cell viability between the two cell lines compared to the cell viability effects of candidate gene knockdown observed in our screen. Unfortunately the authors did not report the cell number difference between the two isogenic cell lines following silencing of their validated candidate gene. The lack of published work using the siRNA synthetic lethal screening techniques combined with our datasets in isogenic cell line models suggest that pathway dependencies for survival in isogenic cell lines may be too subtle to be reliably detected.

4.3.4 Suitability of HCT116 *MAD2+/-* cell line as a model of CIN+ synthetic lethality

I cannot exclude the possibility that the model system that we used for our screens may have been flawed. Firstly, there is a small difference in proliferation rate between the HCT116 diploid parental and *MAD2+/-* cell line, where the *MAD2+/-* has a slower growth rate, resulting in a 10% difference in cell number at the end of the 72-hour time point when starting with the same initial cell number. The proportion of cells undergoing events such as DNA synthesis, cell septation, cell constriction, and enzymatic activity peaks is increased with an increased proliferation rate within a given time-frame (257). Therefore an increased proliferation rate may result in an increased susceptibility to the effects of a particular gene knockdown as a higher proportion of cells may require the use of that gene within the time frame of the experiment. Furthermore, HCT116 *MAD2+/-* cells may not faithfully re-capitulate CIN in human cancer. MAD2 is a SAC gene, however there may be limited evidence for checkpoint dysfunction in CIN tumours as *in vivo* mutations appear rare (Table 1) and *in vitro* demonstrations show that many CIN+ cell lines have a functional SAC (66, 76, 77). This suggests that SAC aberrations may not be the cause of CIN in the majority of tumours and the MAD2 deficient cell line may not recapitulate CIN as it exists in naturally occurring CIN+ tumours.

The variation analysis as presented in Figure 38 suggests that relative to the noise, the contribution of MAD2 status is far bigger than that of the contribution of siRNA whose effects appear to be obscured by the noise factor. The close ratio of siRNA variance to noise within our system could either mean 1) The noise within our system is too great,

leading to differences in cell number due to siRNA to be obscured by this noise. 2) The similarity of both cell lines results in cell number differences between the two cell lines post siRNA transfection to be subtle, and this is not able to overcome the noise inherent within the system.

4.3.5 The CIN model system and the technical challenges of siRNA screening may lead to yield poor validation rate

The CIN phenotype in the *MAD2+/-* cell line may have compounded other difficulties associated with siRNA transfection. siRNA transfection has been shown to induce broad gene expression changes and that is not likely to be attributable to off-target effects (258, 259). The CIN phenotype results in alterations in gene copy number and structure and these may affect gene dosage across the genome, that may differentially influence siRNA-induced gene expression changes between the CIN and non-CIN cell lines. Cell to cell variability within a cell population may result in low phenotypic penetrance (260) and this is likely to be compounded by the increased heterogeneity in a CIN cancer cell population. Such heterogeneity may result in difficulties reproducing phenotypes observed in the primary screen or resistance to cell death following gene silencing due to underlying genomic heterogeneity in the CIN cell line.

Finally, non CIN-specific technical challenges associated with the use of siRNA may have contributed to our problems in candidate gene validation. siRNA transfection reagents may display significant batch to batch effects (261) and this may have affected out ability to reproduce the differential phenotype observed in our primary screen in our validation experiments.

4.3.6 Comparison with screens performed in yeast to identify polyploidy and aneuploidy survival regulators

The screen was unable to confirm the findings of genome-wide screens performed in yeast to identify survival regulators of polyploid and aneuploid yeast cells (93, 127). We speculate that this may be due to a number of reasons. Firstly, our screen was set up to discover CIN specific survival pathways and not aneuploidy/polyploidy survival pathways. CIN reflects a dynamic state of changes of chromosome number and structure and this leads to a higher level of inter-cell heterogeneity. This may lead to inter-cell variation in dependency on certain pathways for survival. Why were polyploid/aneuploid survival pathways not identified in my screens? Although the *MAD2+/-* cells display an increase in aneuploidy compared to their diploid parental cell line, this only results in an increase in proportion of aneuploid cells in the total cell population from about 15% in the diploid parental cell line to approximately 25% in the *MAD2+/-* cells (164). Therefore there may be an insufficient proportion of aneuploid cells within the population for us to observe a significant difference in cell viability due to lack of phenotype penetrance in our siRNA screen.

Furthermore, the experiments conducted in the yeast model systems involved the stable overexpression of whole copies of chromosomes where else we performed a loss of function screen. Not only were the yeast experiments gain of function experiments, but the magnitude and stability of gene expression changes are likely to be lower in our RNAi screen due to the short time span of siRNA knockdown.

4.4 Conclusion

In conclusion, I was unable to identify any synthetic lethal survival regulators of CIN+ cancer cells. A noise component within the screen was identified that may contribute to about a third of the variance within the system. However, despite the noise within our system, the reproducibility of the phenotype observed with positive control siRNAs and good dynamic range of our output measurements imply that the screen was not flawed. Statistical estimations suggest that the screen was sufficiently powered (power=75%) to detect candidate genes resulting in approximately 60% more death within HCT116 *MAD2+/-* cell line compared to its diploid parental cell line.

In agreement with the previous chapter where it was shown that CIN+ cells are intrinsically multidrug resistant, I speculate that the adaptations acquired by these CIN+ cells in order to maintain or initiate CIN may lead to adaptations and compensations that render them less sensitive to perturbations of genetic pathways crucial for cell survival. Additionally, CIN may allow for redundancy in survival pathways to be generated within the cells via CIN-mediated increase in copies of beneficial genes. Therefore it is likely that identifying candidate genes resulting in at least 50% greater cell death in CIN+ cells will be challenging to identify. A more attractive way of targeting CIN may be to identify pathways involved in initiating or maintaining a CIN+ phenotype to in order to limit adaptation and phenotypic heterogeneity.

Chapter 5. Identification of novel ploidy regulators with relevance to CIN+ Colorectal Cancer

5.1 Introduction

In Chapter 3, I proposed that CIN+ cancer cells are intrinsically multidrug resistant. In the previous chapter, it has been discussed that the identification of CIN-specific lethality pathways may be challenging in the context of mammalian cancer cell synthetic lethality screens. Carrying on from this, I reasoned that improved understanding of mechanisms involved in the generation or maintenance of polyploidy that are tumour relevant may provide further insight into understanding CIN and may be exploited to limit CIN in cancer.

As discussed in section 1.3.4, polyploidy, tetraploidy and aneuploidy may appear to be a consequence of CIN due to missegregation of whole chromosomes but these phenotypes may also contribute to CIN. In order to identify putative tumour-relevant regulators of ploidy, cell cycle data from the whole genome siRNA screen performed in HCT116 cancer cell lines (as described in the Chapter 4) was combined with cell cycle data from other whole genome RNAi screens performed in this Institute. Using SNP array data from CRC cell lines provided by the Wellcome Trust Sanger Institute, the list of ploidy regulators obtained from the screens was filtered to regions of DNA copy number loss as these regions may contain genes that are lost in CIN+ tumours in order to maintain or initiate an increase in ploidy. The overlapping genes may allow the identification of novel ploidy regulators.

Data from the high-throughput RNAi screens presented in this chapter were made available from the High-Throughput Screening Facility (Michael Howell, Ming Jiang, Rachael Instrell and Becky Saunders) at the Cancer Research UK London Research Institute. The DNA copy number analysis was performed by David Endesfelder.

5.2 Results

5.2.1 Whole Genome RNAi screen identifies potential tumour relevant genes that are involved in the generation or maintenance of polyploidy

As described in Chapter 4, a high throughput loss of function screen using synthetic siRNA oligonucleotide pools from Dharmacon targeting 21122 genes was performed in the HCT116 cell line. Cells were stained with DAPI to enable the measurement of cell number and cell cycle profile data. The cell cycle profile data was used in this chapter to address whether loss of function of any of these genes resulted in an increase in the fraction of polyploid cells within the colorectal cancer (CRC) HCT116 cell line, a CIN-, near-diploid cancer cell line.

The HCT116 CRC cell line was transfected with 21122 siRNA pools in triplicate, each siRNA pool containing 4 different siRNA sequences. Cells were transfected in 96-well plates and were fixed 72 hours after transfection. Plates were then stained with DAPI, to allow a quantitative assessment of cellular DNA content and cell cycle profile following gene silencing.

The population of cells with DNA content greater than 4n (>4n -corresponding to aneuploid or polyploid cells and possibly tetraploid cells in S-phase) was determined for

each siRNA pool and the data were normalised and analysed as described in material and methods. Z-scores (scores measuring the standard deviations from the mean in normalised data) for the >4n data for each siRNA were obtained from this normalised data. A threshold of Z-scores of 2.5 or greater was used to define candidate siRNAs that induced polyploidy, yielding a total of 301 candidate genes whose gene silencing resulted in an increase in the >4n fraction of cells (Figure 41A).

Of the list of 301 candidate genes, I next wanted to investigate whether any of these genes are preferentially lost in CIN+ cancer cells. To address this, we used a dataset of single-nucleotide polymorphism comparative hybridisation data (SNP 6.0 Affymetrix) from the Wellcome Trust Sanger Institute for 20 CIN+ and 9 CIN- CRC cell lines (CIN+ status of cell lines defined by an increase in DNA index as in section 3.2.1) to identify genomic regions that were commonly altered in CIN+ colorectal cancer cells. Genomic regions that are consistently and stably lost at the DNA copy number level in CIN+ cancers compared to non-CIN cancers may reflect adaptations necessary for maintaining or initiating polyploidy, and these regions may contain dosage sensitive genes whose loss of function may contribute to polyploidy. Minimum consistent regions of genomic alteration between all cell lines were defined and assigned a score of significance based on both frequency and amplitude of aberration, adjusting for tumour baseline ploidy (see materials and methods for details). After controlling for multiple testing using a false discovery rate of 0.05, 2377 genes were identified that were contained within genomic regions that were lost in CIN+ cells relative to the median copy number (which approximates the ploidy) of the cell line compared to non-CIN cell lines (Figure 41B).

The list of 301 candidate genes whose silencing induces polyploidy were overlapped with the 2377 genes that are lost in CIN+ cell lines relative to median ploidy (Figure 41C). A total of 28 genes were in common between these two lists. This list of 28 genes did not represent a significant enrichment in either list. This may be due to two reasons: 1) Many genes may induce polyploidy when silenced but this loss may not be sustainable in cancer due to negative survival effects, and therefore are not stably lost in CIN+ CRC cell lines. 2) Not all genes that are lost at the copy number level in CIN+ CRC cell lines may be regulators of ploidy.

It was next investigated if there were any genes whose loss of function was able to induce polyploidy not only in CRC but also in cancer cells of different tissues of origin, but that were still preferentially lost in CIN+ cancer cell lines. To address this, we obtained >4n cell cycle data from three other whole genome RNAi screens assayed using the same methods as the HCT116 screen. These other screens were performed using cell lines originating from fibrosarcoma (HT1080), lung cancer (PC9) and renal cancer (RCC4). The >4n data from the HCT116 screen were re-normalised (as in materials and methods) and new Z-scores calculated so as to enable comparison with the Z-scores from the other 3 screens. Z-scores in the re-normalised HCT116 data displayed an increased value compared to Z-scores obtained using the original normalisation method. To identify candidate genes that were able to induce polyploidy in cancer cells of different tissue types, a threshold of at least 2.5 Z-scores (reflecting a lowered threshold in the case of the HCT116 screen, due to the increase in value of HCT116 z-scores upon renormalisation) in 3 or more different cancer cell lines was used. This was compared to the list of genes lost in CIN+ colorectal cancer cell lines to give 9 further candidate genes (Figure 41D). Of these 9 genes, 4 of them, KIF17,

KNTC2, MAD2L1, and RBX1 have known or putative roles in cell division (242, 262) (27, 263). This gave me the confidence that these methods enabled us to identify potential regulators of polyploidy in colorectal cancer.

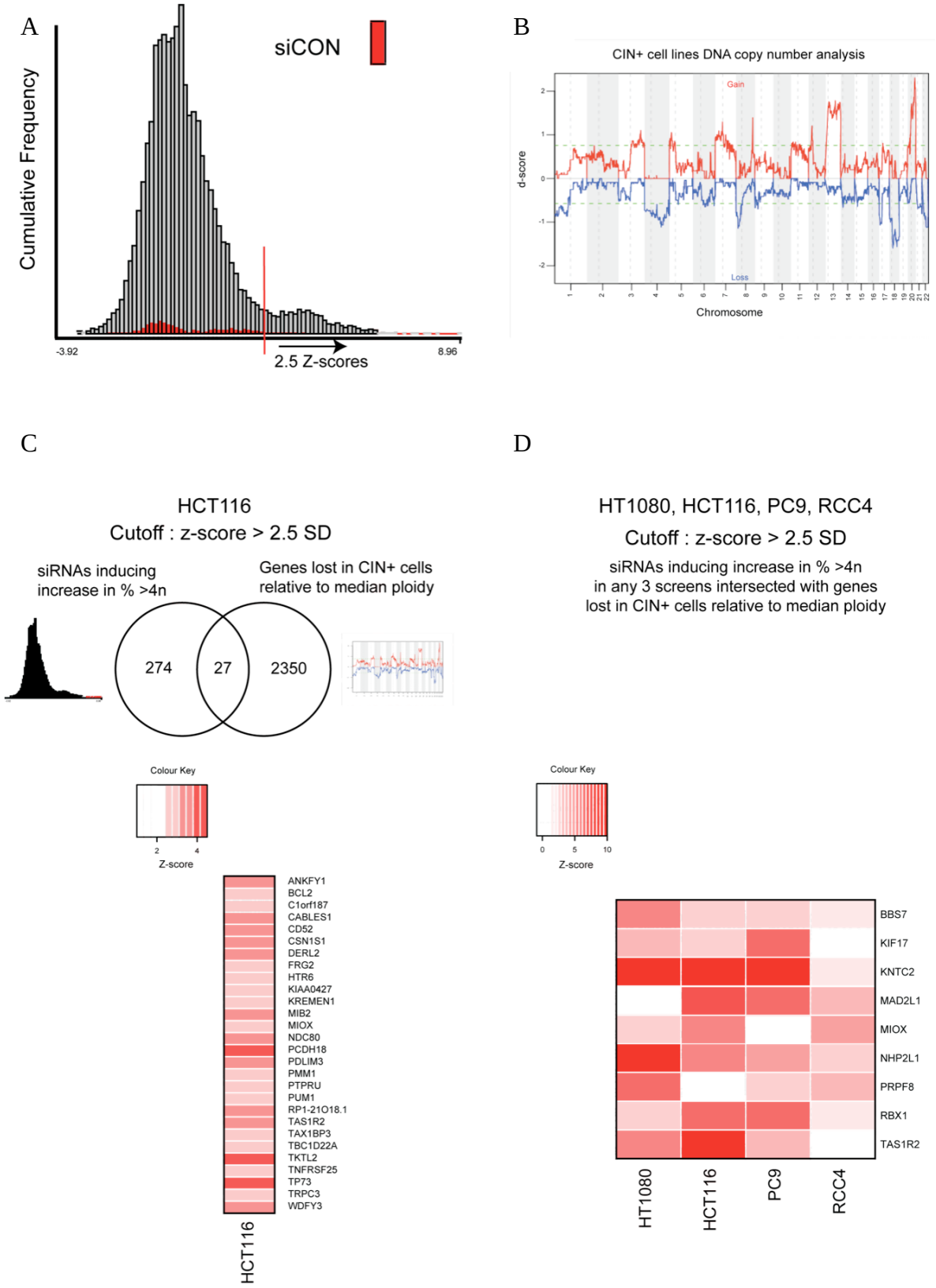

Figure 41 Cell cycle profile data from whole genome siRNA screens and overlapped with DNA copy number data in CIN+ CRC cell lines

A) Cumulative frequency plot of Z-scores for >4n data in HCT116 screen. A threshold of 2.5 Z-scores was chosen to select candidate genes for follow-up.
B) Q –Plot of SNP-CGH data indicating regions of loss or gain in copy number relative to median ploidy in CIN+ CRC cancer cell lines.
C) Heatmap of Z-scores of candidate genes selected from HCT116 screen that overlapped with list of genes that are lost relative to median ploidy in CIN+ cells
D) Heatmap of Z-scores of candidate genes selected from HCT116, HT1080, PC9 and RCC4 screens that overlapped with list of genes that are lost relative to median ploidy in CIN+ cells and appeared in at least 3 of those screens.

5.2.2 Validation of candidate genes for on-target effects

Candidate genes from the previous section, encoded in regions of copy number loss in CIN+ cells, and which had no previously described cell division function, were assessed for off-target effects. To address this, the high throughput screen assay was repeated in the HCT116 cell line using the four individual siRNAs that make up the Dharmacon SmartPool siRNAs for each gene of interest..

29 unique candidate genes (Figure 42A) were re-assayed. The percentage of >4n cells for each siRNA was normalised to non-targeting siRNA controls (siCON). A threshold of at least a two-fold increase in the percentage of >4n cells relative to siCON in at least 2 or more individual siRNAs for each gene of interest was considered an on-target effect. 13 siRNAs (Figure 42B) met this threshold.

A

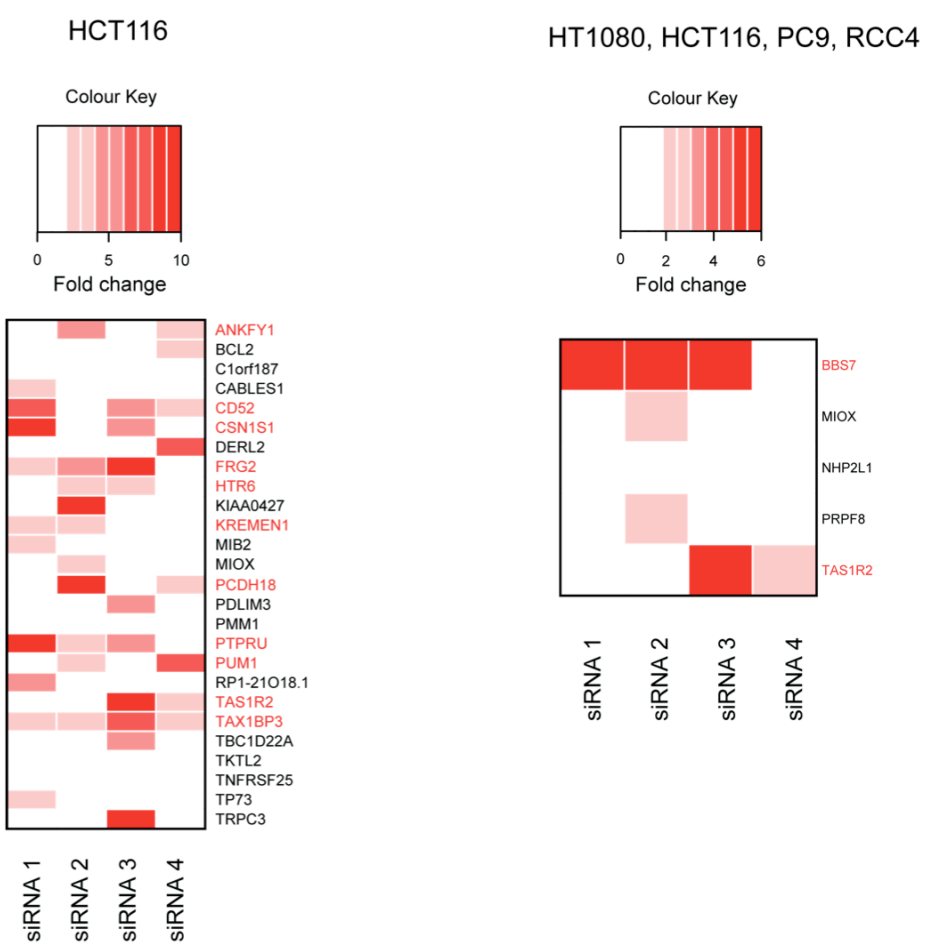

B

Gene Name
ANKFY1
BBS7
CD52
CSN1S1
FRG2
HTR6
IER3IP1
KREMEN1
PCDH18
PTPRU
PUM1
TAS1R2
TAX1BP3

Figure 42 Validation of candidate genes for off-target effects
A) Heatmap of fold change compared to siCON of >4n population of cells for single siRNAs for each candidate genes.
B) Table listing the candidate genes that caused at least a 2-fold increase relative to siCON in % of >4n cells in at least 2 out of 4 single siRNAs.

5.2.3 Live cell microscopy analysis reveals potential mechanisms for the generation of polyploid cells

Each of the 13 validated candidate genes were then analysed using live cell microscopy to identify potential mechanisms for the generation of polyploidy. siRNAs were transfected into a HCT116 cell line which stably expresses Histone 2B tagged with RFP (H2B-RFP) enabling visualisation of DNA, in order to allow the tracking of cells for mitotic defects using both phase contrast images of the cell and fluorescent images of the cellular chromatin. Cells were transfected for 48h with the siRNA of interest and then imaged every 3 minutes using the Deltavision imaging system for a total of 8 hours.

CD52 silencing induced a change in nuclear and cellular morphology to that which was spindle-like (Figure 43) with no obvious errors in mitosis or cytokinesis and was regarded as a false positive in my screen for the induction of polyploidy.

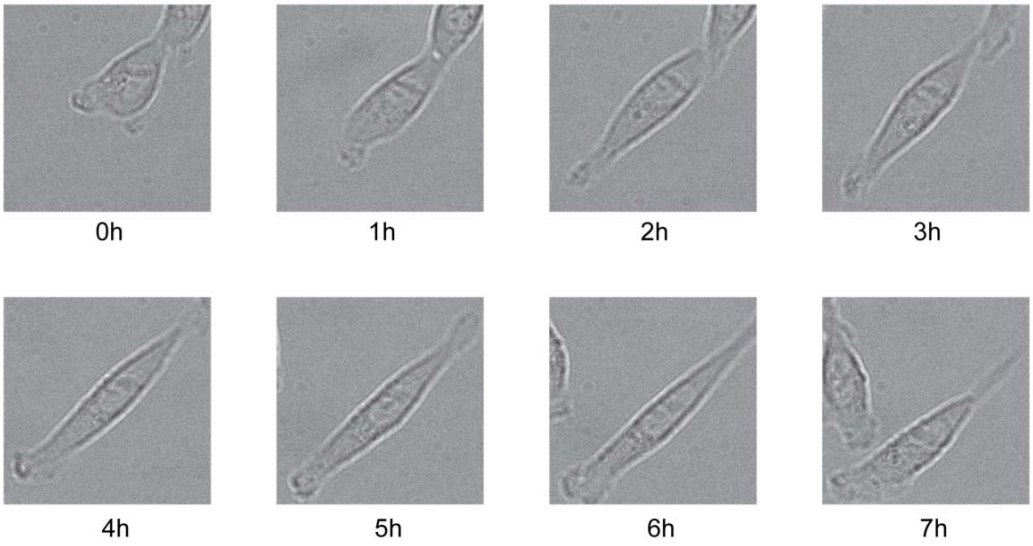

Figure 43 Representative time-lapse phase-contrast images following CD52 silencing in HCT116 cells

The percentage of cells entering mitosis was scored for each candidate gene (Figure 44A). Cells that increase ploidy without entering mitosis may reflect an increase in DNA content without cell division. None of the siRNAs appeared to induce a statistically significant increase in percentage of cells entering mitosis compared to siCON (Fisher's exact test). ANKFY1, IER3IPI, PTPRU and TAS1R2 all reduced the percentage of cells entering mitosis to less than 10% each over the duration of the movie. However only IER3IPI and PTPRU resulted in a significant decrease in percentage of cells entering mitosis ($p=0.018$ and 0.01 respectively, Fisher's exact test).

Candidate genes whose depletion did not result in a reduction of cells entering mitosis to less than 10% were further investigated. Cumulative frequency plots of the time each cell spends in mitosis post transfection were plotted for the remaining candidate genes. An extended time spent in mitosis may reflect mitotic errors and subsequent arrest. The lines for BBS7, FRG2, HTR6, PUM1 and TAX1BP3 both appeared to be shifted to the right compared to siCON transfected cells, indicating an increase in time each cell spends in mitosis (Figure 44B).

Next, numbers of mitotic slippages resulting in giant nuclei reformation or multinucleated cells were scored (Figure 45A), representing the numbers of polyploid cells being generated. BBS7, KREMEN1 and PCDH18 silencing led to an increase in giant nuclei interphase cells following mitotic slippage when compared to control transfected cells. FRG2, PUM1 and TAX1BP3 appeared to increase the proportion of multinucleated cells generated following mitotic slippage.

Lagging chromosomes and anaphase bridges are errors that can arise following merotelic kinetochore-microtubule attachments, in which one sister chromatid is

attached to microtubules originating from both centrosomes (45, 76). This can then lead to whole chromosome non-disjunction and/or structural chromosome damage, promoting the generation of CIN. Anaphase bridges, lagging chromosomes and multipolar divisions were scored following gene silencing (Figure 45B). BBS7, FRG2, PUM1 and TAX1BP3 appeared to induce higher rates of these errors compared to control transfected cells. Approximately 80% of cells that were silenced for PCDH18 underwent mitotic slippage and this may account for the decrease in lagging chromosomes/anaphase bridges and multipolar divisions being measured following silencing of this gene.

Representative images for the phenotypes scored are presented in Figure 46.

A

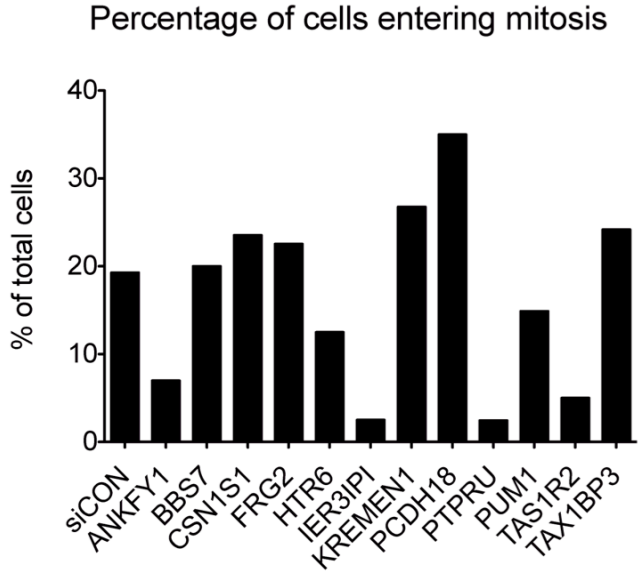

B

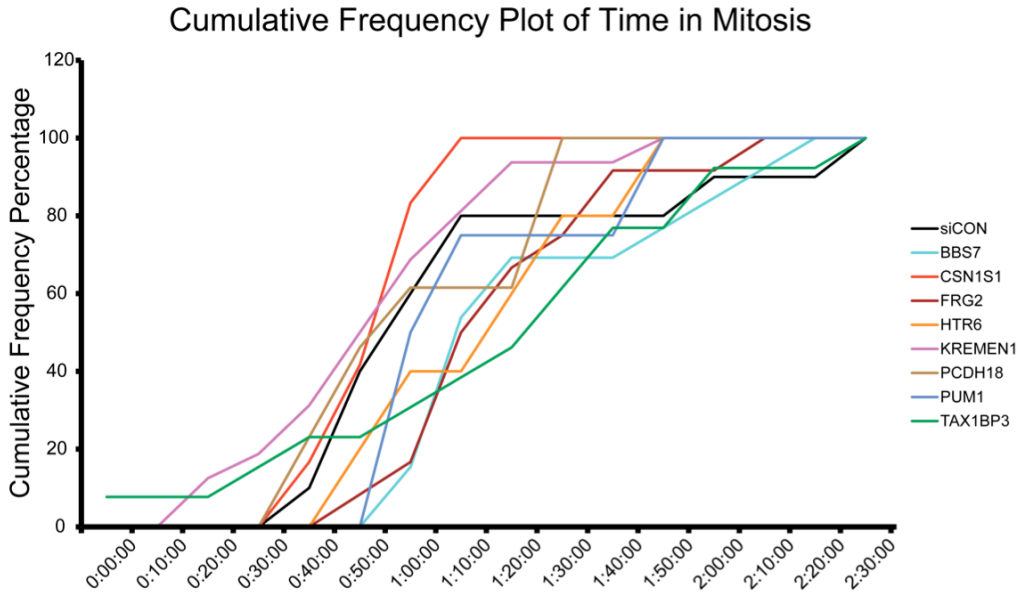

Figure 44 Graphs of percentage cells entering mitosis and time spent in mitosis
A) Barplot of percentage of cells entering mitosis.
B) Cumulative frequency graph of time each cell spends in mitosis.

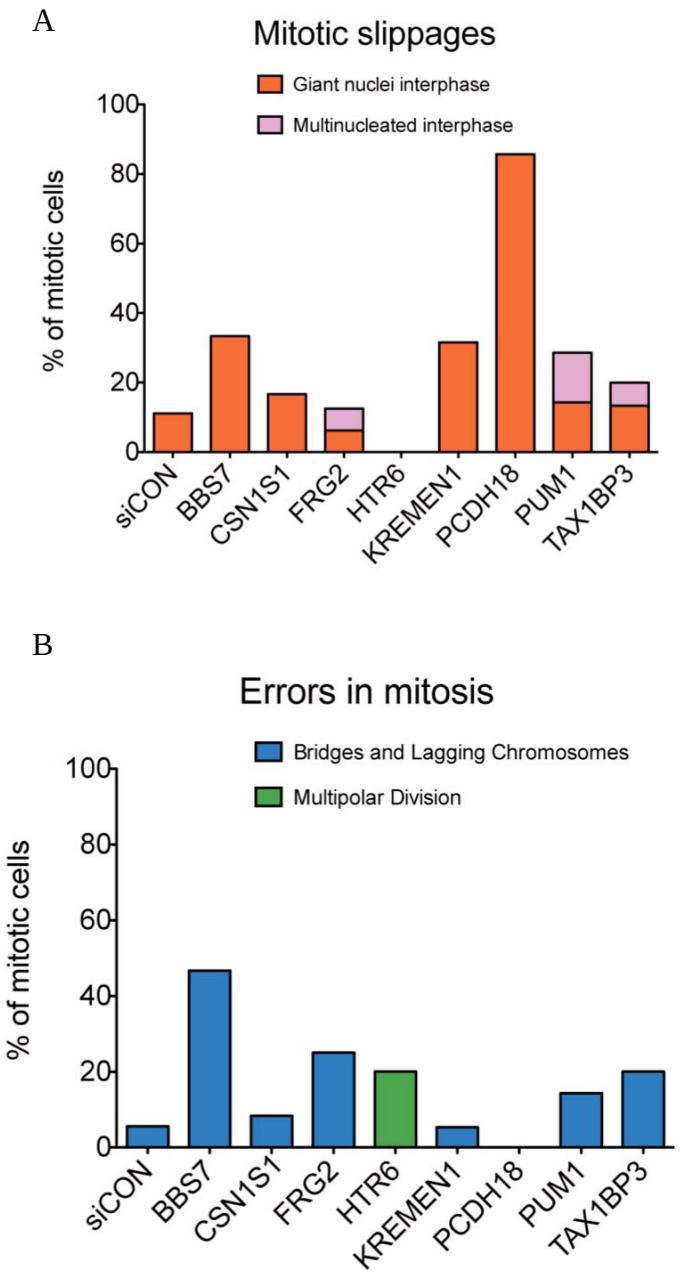

Figure 45 Percentage of mitotic errors in cells following candidate gene silencing
A) Barplot of percentage of mitotic cells slipping out of mitosis and forming giant nuclei or multinucleated interphase cells.
B) Barplot of percentage of mitotic cells demonstrating lagging chromosomes and anaphase bridges or multipolar divisions.

A

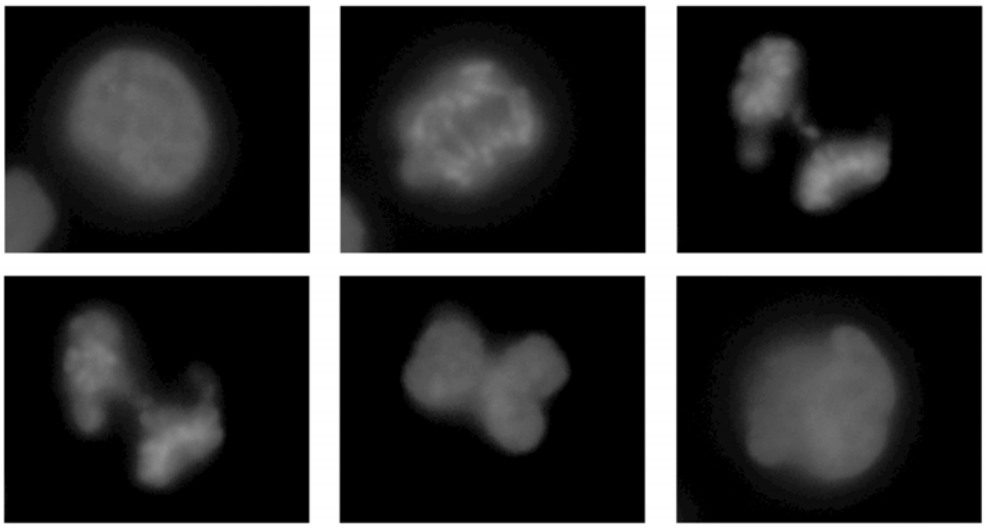

B

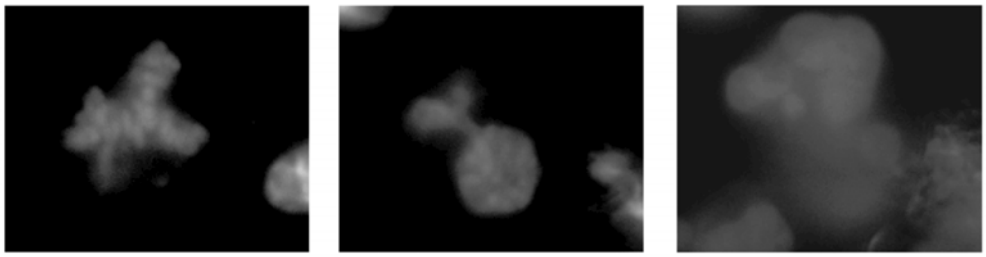

Figure 46 Representative images of mitotic errors
A) Representative images of lagging chromosomes and anaphase bridge formation followed by exit from mitotis to form a single polyploid nuclei following BBS7 silencing.
B) Representative images of anaphase bridge formation followed by exit from mitosis to form a multinucleated cell following TAX1BP3 silencing.

5.3 Discussion

In this study, 13 genes with no previously described function in cell division have been identified that may be relevant to the generation or maintenance of polyploidy in CIN cancer cell lines. A genome wide siRNA screen was used to identify genes that induce polyploidy in the near-diploid CRC cell line, HCT116 and cancer cell lines from other tissue types (HT1080, PC9, RCC4). I then focused on candidate genes that were in common with genes that are lost at the DNA copy number level in CIN relative to diploid colorectal cancer cell lines. This method allowed the identification of 28 candidate genes that are lost in CIN cancer cells and that result in polyploidy when silenced in HCT116 cancer cell lines and 9 genes that result in the same phenotype when silenced in cancer cell lines originating from other tissue types. This gave a total of 35 unique genes identified through the screen, of which 4 have described functions in cell division. 13 of these genes were deemed less likely to have off-target effects (Figure 47) as the phenotype was reproducible in at least 2 out of the 4 individual siRNA sequences making up the pooled siRNAs.

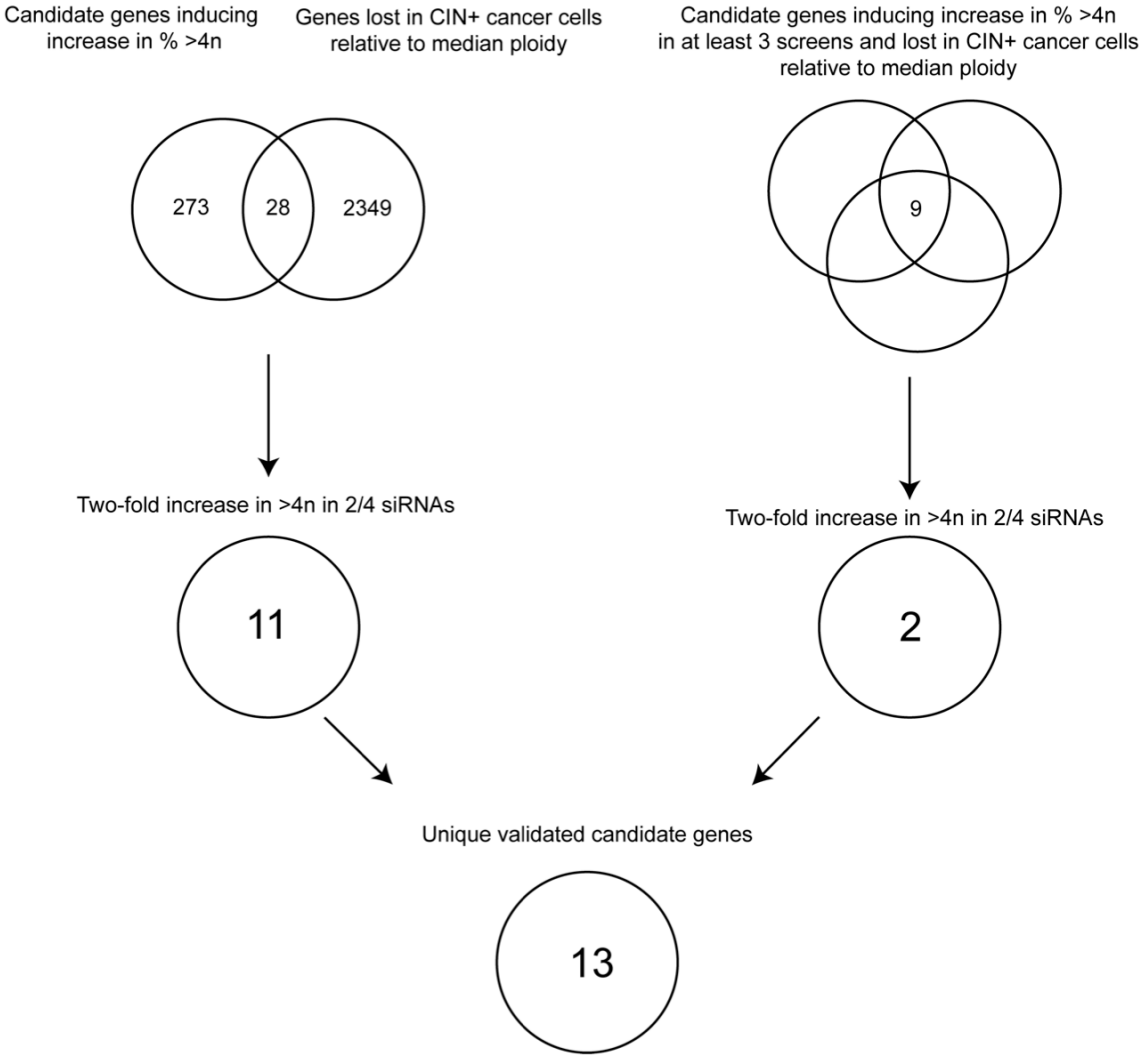

Figure 47 Workflow of candidate genes selection and validation

There appeared to be no common pathway to link these 13 candidate genes together in generating polyploidy. Further investigation by live cell microscopy and FACS suggested that polyploidy was induced by loss of function of these genes through various mechanisms. For 6 of these genes (BBS7, CSN1S1, KREMEN1, PCDH18, PUM1, TAX1BP3) loss of function appeared to cause an increase in mitotic slippage followed by giant nuclei formation or multinucleation compared to control transfected cells. PCDH18 in particular induced very high levels of mitotic slippage to form a mononucleate polyploid cell. Depletion of HTR6 appeared to result in multipolar divisions. FRG2 silencing appeared to induce a very modest increase in rates of mitotic errors compared to siCON transfected cells but we were not able to measure an increase in observable mechanisms of generation of polyploidy during the short time course of the live cell microscopy experiments. For four of these genes, there was a decrease in the number of cells entering mitosis following silencing of ANKFY1, IER3IPI PTPRU or TAS1R2. This may be a mechanism of polyploidy induction for these genes. CD52 appeared to be a false positive as it induced spindle-like morphological changes without any erros in mitosis or cytokinesis being observed.

Two of these genes (TAX1BP3 and KREMEN1) may induce polyploidy through deregulation of the Wnt/Beta-catenin signalling pathway. In the Wnt signalling pathway, Beta-catenin is constantly targeting for degradation by the Beta-catenin destruction complex via GSK3beta-mediated phosphorylation (264). Wnt signalling inhibits the destruction of Beta-catenin by interfering with GSK3beta-mediated phosphorylation and thus allows an increase in levels of Beta-catenin (265). With relevance to cell division, WNT/beta-catenin signalling has been shown to peak at

G2/M and Beta-catenin has been reported to localise to both interphase and mitotic centrosomes (266). Depletion of Beta-catenin has been reported to cause an increase in monopolar spindle formation and the failure of centrosomes to separate (267). Stabilisation of Beta-catenin (via mutations of GSK3beta phosphorylation sites, thus preventing degradaton of Beta-catenin) on the other hand, induces centrosome separation (266). TAX1BP3 (also known as TIP-1) has been shown to bind to Beta-catenin with high affinity and inhibit its transcriptional activity (268). Depletion of TAX1BP3 may therefore increase the levels of active Beta-catenin. KREMEN1 is a transmembrane coreceptor for Dickkopf-1, a negative regulator of Wnt signalling. KREMEN1 double knockout mice have been shown to have an increase in Wnt signalling (269). KREMEN1 down-regulation could therefore also result in an increase in active Beta-catenin via increased levels of Wnt that prevent degradation of Beta-catenin. I speculate that down-regulation of either TAX1BP3 or KREMEN1 may result in an increase in levels of active Beta-catenin and therefore cause disruptions in centrosome cohesion.

PUM1 encodes a PUF family RNA-binding protein, a regulator of posttranscriptional gene expression. Morris and colleagues (270) have previously shown that knockdown of PUM1 results in a decreased rate of mRNA decay of genes involved in the mitotic cell cycle such as Cyclin B1 and *CKS2*. In their study they did not observe a function for PUM1 in cell cycle progression (data not shown in study). In my data, I did not observe alterations in the amount of time that cells spend in mitosis, however, there appeared to be an increase in proportion of cells slipping through mitosis leading to giant nuclei and multinucleated interphases following knockdown of PUM1. However, it has been also shown that elevated levels of Cyclin B1 prevent cells from undergoing

mitotic slippage (271) and that CKS2 depletion concurrent with CKS1 depletion leads to mitotic slippage and polyploidy (272). Therefore elevated half-lives of Cyclin B1 and *CKS2* mRNA following PUM1 knockdown may not be the explanation for the increase in mitotic slippage and mitotic errors that we observed.

Loss of function of BBS7 has been shown to cause defects in the structure and functions of cilia (273) and mutations in this gene have been shown to affect the localisation and motility of IFT88/Polaris. In other studies, depletion of IFT88 has been shown to induce mitotic defects such as an increase in mitotic defects and delayed mitotic progression. This may be due to disruption of the spindle poles, an increase in chromosome misalignment and spindle misorientation (274). I speculate that depletion of BBS7 may lead to defects in proper localisation or function of IFT88. IFT88 and other IFT proteins localise to the spindle poles during mitosis and their disruption may cause defects in mitosis such as the ones we observed with an increase in mitotic errors. Interestingly, HTR6 has been reported to localise to cilia but the function or significance of its localisation is as yet unknown (275).

5.4 Conclusion

The identification of genes with known cell division functions and also novel genes that may be implicated in pathways that ensure proper mitotic segregation by overlapping our HTS screen data with data obtained from an analysis of SNP-CGH data in CIN and non-CIN CRC cell lines suggests the utility of our approach. Further work investigating the function of these genes and also genes that have no known mitotic function or are not implicated in any pathways maintaining mitotic fidelity may allow us to better understand the generation and maintenance of polyploidy in CIN cancer cells.

Chapter 6. CERT predicts chemotherapy benefit and mediates cytotoxic and polyploid-specific cancer cell death through autophagy induction

6.1 Introduction

The ceramide transporter CERT was identified through a multidrug sensitivity RNAi screen to enhance sensitivity to paclitaxel, cisplatin, 5-FU and doxorubicin when silenced from multiple cancer cell lines (12). Given that 1) CIN+ cells are intrinsically resistant to taxanes but the silencing of CERT results in taxane sensitisation, and 2) identifying pathways that are required for the specific survival of CIN+ cancer cells is challenging (Chapter 3 and Chapter 4), I reasoned that a clearer understanding of the molecular pathways responsible for cell death following CERT depletion and paclitaxel exposure may offer a broader insight into mechanisms regulating mitotic catastrophe and suggest therapeutic opportunities to specifically limit the development of chromosomally unstable cells.

Through parallel integrative genomics approaches combining transcriptomic analyses with RNAi-based functional genomics and live cell microscopy studies, I identified that CERT silencing resulted in multidrug sensitisation through the augmentation of LAMP2-dependent autophagic flux. This process results in the specific death of multinucleated cells following paclitaxel exposure and thus CERT targeting may serve as a rational approach to attempt to eliminate precursors of intra-tumour heterogeneity in cancer.

The work presented in this section has been published as a first author article (276) (see Appendix 8.4). Part of section 6.2.2 has been published as a first author article in (277) (see Appendix 8.5). Philip East performed the microarray analysis. In section 6.2.10 and section 6.2.12, analysis of CERT expression in cancer cell lines has been performed by Neil P. Jones, analysis of CERT expression data in breast cancer microarray datasets has been performed by Nicolai Juul Birkbak and analysis of CERT TMA data has been performed by David Endesfelder and Jil Sander with IHC staining and quantification performed by Patricia Gorman and Rebecca Roylance on samples (and corresponding patient data) provided by Valerie Speirs and Andrew Hanby.

6.2 Results

6.2.1 CERT depletion results in ceramide accumulation

CERT, identified in a paclitaxel-sensitisation RNAi screen (12), encodes a lipid transporter that transports long-chain ceramides (C_{14-20}) as well as short chain fluorescent ceramide analogues from the endoplasmic reticulum to the Golgi apparatus (135). I hypothesised that CERT silencing in the presence of paclitaxel might mimic the effect of ceramide exposure through the attenuation of ceramide transport from the ER to the Golgi and its subsequent conversion into sphingomyelin. Depletion of CERT by RNAi (siCERT) in HCT116 cells was confirmed to result in attenuation of ceramide transport with ceramide confined to membranous and diffuse cytoplasmic structures, in contrast to control transfected cells (siCON), in which ceramide is localised to Golgi-like punctate perinuclear regions (Figure 48A) (278).

To establish whether CERT depletion might induce alterations in ceramide levels that could be exacerbated by paclitaxel exposure, lipid extracts were analysed for their ceramide content by mass spectrometry from siCERT-transfected cells treated with vehicle or paclitaxel (25nM for 48 hours) compared to siCON transfected cells under identical conditions. Paclitaxel treatment of siCON transfected cells did not significantly increase total ceramide levels (Figure 48B). CERT depletion resulted in an increase in total ceramide levels relative to siCON transfected cells ($p=0.008$) and the combination of siCERT with paclitaxel treatment resulted in a greater increase in total cellular ceramide levels ($p=0.0001$) relative to siCON transfected cells. An increase in total ceramide accumulation occurs within the same timeframe as the marker of endoplasmic reticulum stress, CHOP, is detected in HCT116 cells under identical conditions (12).

A

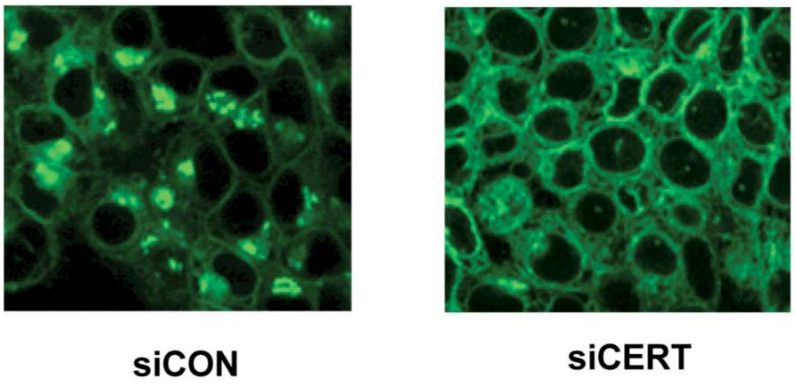

B

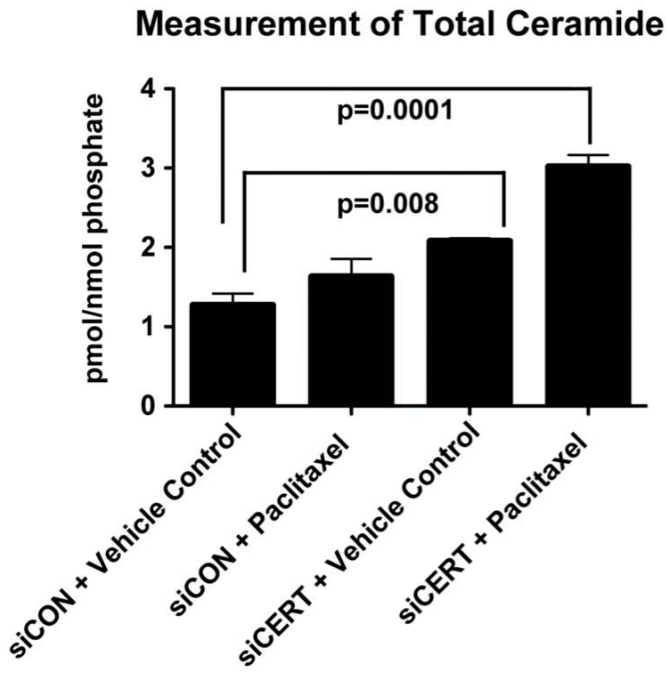

Figure 48 Validation of siRNA transfection and measurements of ceramide content of cells

A) Fluorescent C5-Ceramide was added to cells transfected with either siCON or siCERT and imaged 20 mins following exposure to drug.

B) Relative ceramide levels were measured using mass spectrometry. Graph shows ratio of total ceramide normalised to total phosphate within each condition in siCON/vehicle control, siCON/paclitaxel, siCERT/vehicle control and siCERT/paclitaxel. Error bars represent standard deviations across triplicate experiments for each condition.

6.2.2 Transcriptomic analysis reveals a CERT-specific response

I hypothesised that the CERT-specific paclitaxel sensitisation phenotype may be attributable to two mechanisms; the first readies the cell for paclitaxel-induced cell death following CERT silencing, the second mechanism might be attributable to a response derived from ceramide sequestration within the ER that acts synergistically to enhance cell death. I reasoned that through the identification of a CERT-specific and a possible ER-localised ceramide transcriptional response, mediators of this process might be identifiable.

First I addressed whether CERT depletion is associated with a specific transcriptional response that might inform upon the mechanism through which CERT silencing primes cells for paclitaxel induced death. Microarray expression analysis of HCT116 cells was used to identify genes differentially regulated following CERT depletion in the presence of ceramide, paclitaxel or DMSO vehicle control compared to the same treatments in siCON transfected cells. A common CERT-specific transcriptional response was identified (Figure 49). Variation in expression pattern between the triplicates may reflect the analysis of biological triplicates for each condition.

24 genes, including CERT, were selected for qPCR validation of gene expression changes following CERT silencing and vehicle control treatment (Figure 50A). I found that microarray profiles correlated closely with gene expression changes validated by qPCR (R=0.97) (published in (277), see Appendix 8.5) indicating the reliability of gene expression changes quantified by Affymetrix HuEx-1_0-st-v2 (Human Exon) array profiling (Figure 50B). Moreover, it has been previously reported that gene expression

fold changes <1.5 as determined using traditional microarray profiling, correlate poorly with qPCR assessments of gene expression (279, 280). Analysis of the correlation of exon array expression and qPCR data used in my study for gene expression fold changes <1.5 revealed a correlation coefficient of 0.84.

Reasons for the improved estimates of gene expression using the Affymetrix exon array analysis may include the use of multiple probes per exon allowing data to be collected from the whole gene and not just the 3' end, and the use of labelled cDNA, in contrast to other microarray platforms which use labelled cRNA. Labelled cDNA produces less cross hybridisation compared to labelled cRNA and may contribute to the high performance of the exon array platform (281). The high concordance of the exon array gene expression data with qPCR assessments of gene expression even at low fold changes gave me the confidence to further investigate these genes.

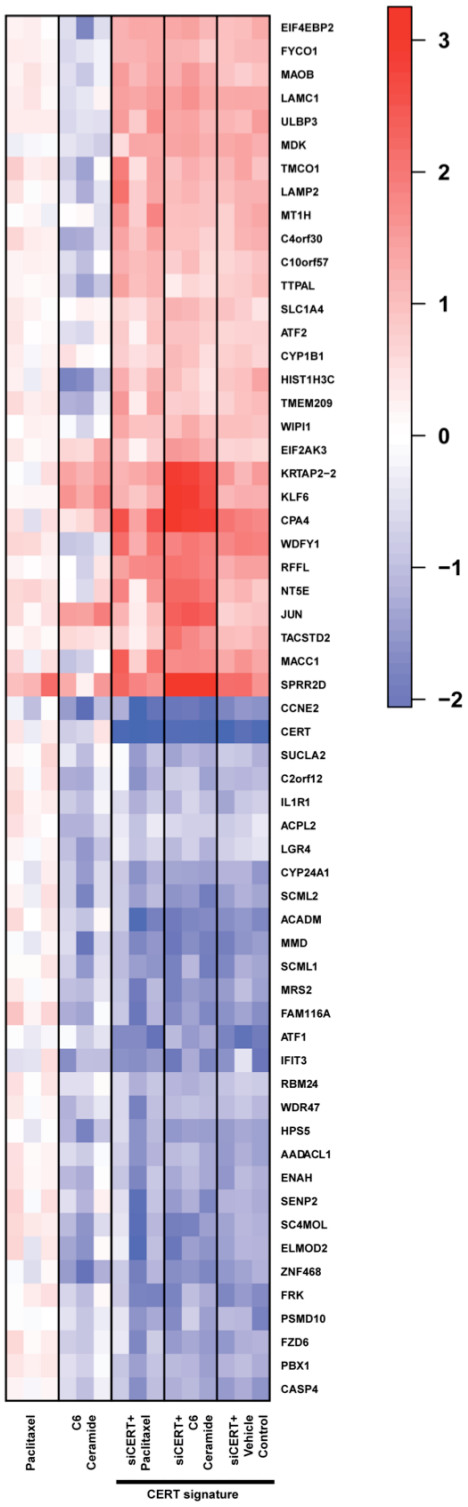

Figure 49 CERT gene expression signature
Heatmap of differentially expressed genes in HCT116 cells 8h after paclitaxel, C6-ceramide or vehicle control treatment, 48h following siCERT transfection. siCON transfected samples treated with paclitaxel or ceramide provided for comparison.

A

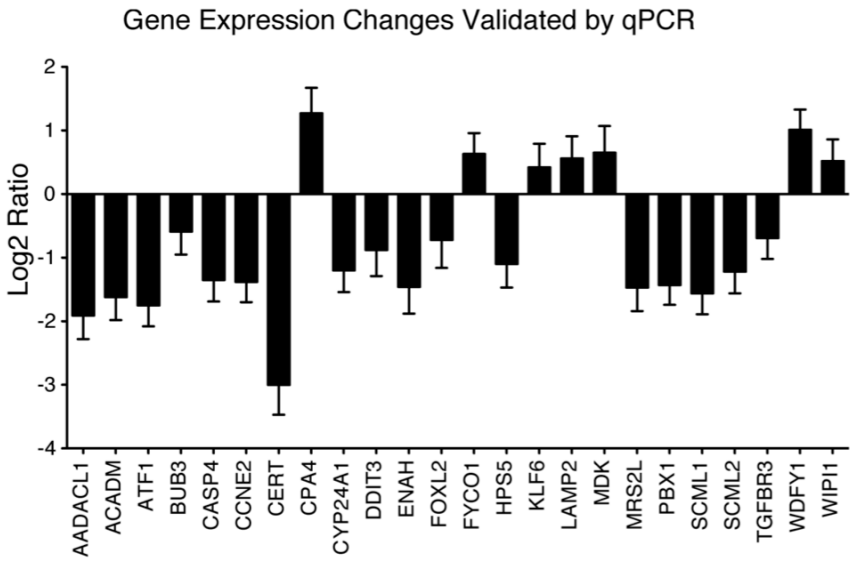

B

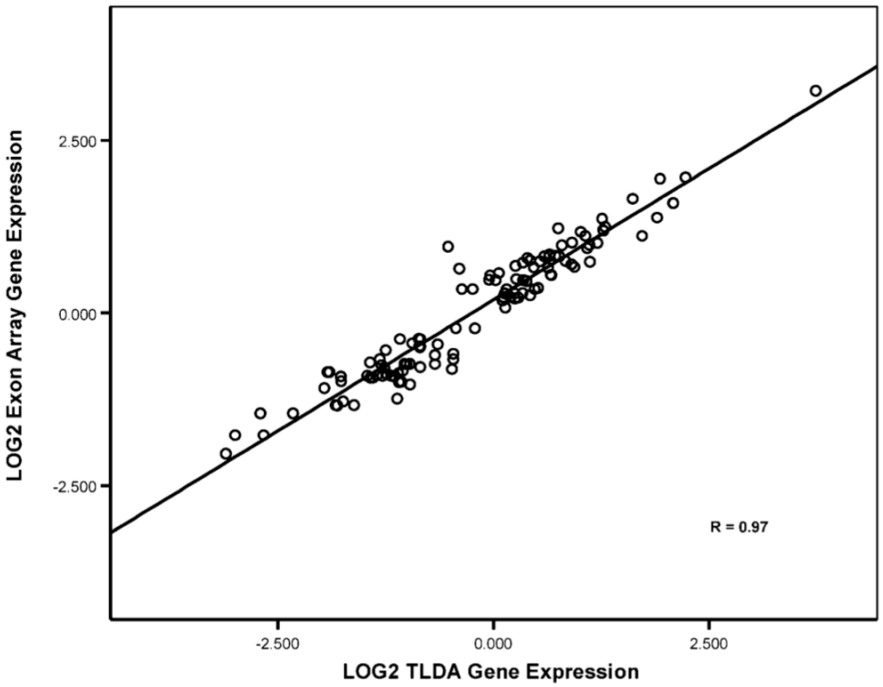

Figure 50 qPCR validation of microarray data
A) Graph of qPCR validation of 24 genes that are differentially expressed following CERT depletion. Error bars represent standard deviations across triplicate experiments. B) Linear regression model of relative gene expression changes quantified by exon array and TLDA gene profiling. Correlation coefficient = 0.97.

6.2.3 CERT depletion induces LAMP2 which is required for paclitaxel cell death

Gene expression changes following CERT depletion might prime cells for subsequent cell death initiated by paclitaxel. I reasoned that silencing the expression of these genes through RNAi might antagonise paclitaxel response and siCERT-specific paclitaxel sensitisation. To explore this possibility, seven genes (CPA4, FYCO1, KLF6, LAMP2, MDK, WDFY1, WIPI1), whose expression were induced following CERT depletion (and validated by qPCR), were silenced by siRNA in HCT116 cells and paclitaxel sensitivity was assessed. Two of the seven genes promoted paclitaxel resistance when silenced in HCT116 cells, LAMP2 (encoding a lysosomal membrane protein) (282) and CPA4 (a carboxypeptidase with unknown specific substrate) (Figure 51A). Induction of LAMP2 protein following CERT silencing and efficient knockdown of LAMP2 protein by RNAi were confirmed (Figure 51B). Real-time qPCR quantification using primers specific to the LAMP2a and to all LAMP2 splice variants revealed an increase in expression of LAMP2 and LAMP2A specifically (Figure 51C). To assess whether siCERT-mediated paclitaxel sensitisation was dependent upon LAMP2 expression, both CERT and LAMP2 were co-depleted and paclitaxel sensitivity was assessed. siLAMP2 abrogated the ability of siCERT to sensitise cells to paclitaxel exposure (Figure 51A). Co-silencing of both CERT and LAMP2 was confirmed by qPCR (Figure 51D) and antagonism of paclitaxel was confirmed for two separate siLAMP2 siRNA oligonucleotide sequences (Figure 51E).

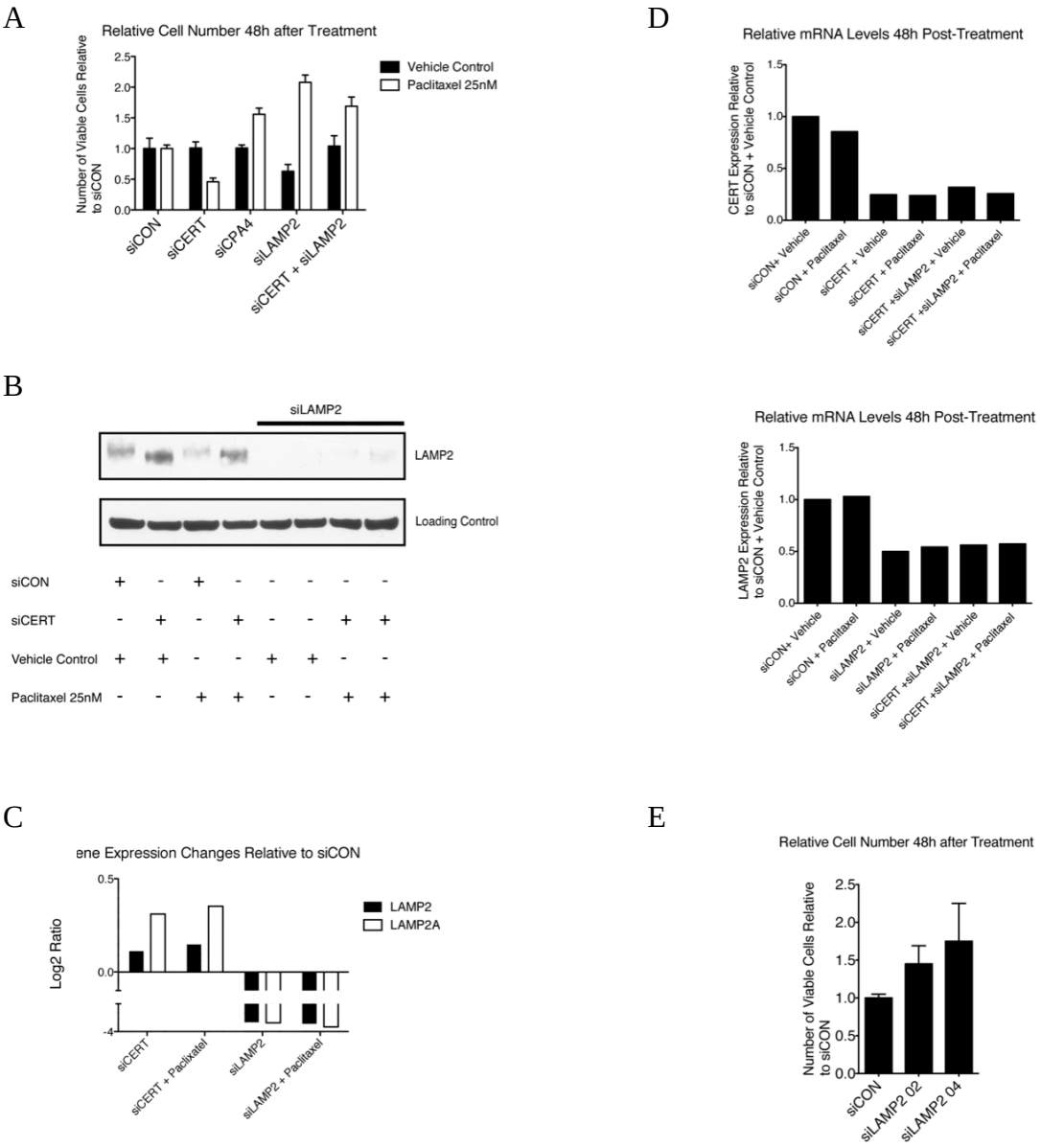

Figure 51 Investigation of pathways mediating paclitaxel-induced cell death following CERT silencing

A) Graph of relative cell number following transfection of siCON, siCERT, siCPA4, siLAMP2 or siCERT+siLAMP2 and vehicle control or paclitaxel treatment. Data were normalised to cell number in siCON/vehicle control or siCON/paclitaxel for paclitaxel treated experiments. Error bars represent standard deviations across 6 replicates.

B) Western blot analysis showing LAMP2 protein expression 24h after paclitaxel or vehicle control treatment following 48h of siCON or siCERT transfection.

C) Graph of qPCR assessment of gene expression of LAMP2 and LAMP2A specifically following CERT silencing.

D) Graph of relative expression levels of CERT (above) and LAMP2 (below) as measured using qPCR 48h post-treatment with paclitaxel or vehicle control following 48h of siRNA transfection.

E) Graph of relative cell number following transfection of siCON or individual siRNAs (siLAMP2 02 and siLAMP2 04) that make up the siLAMP2 siRNA pool and resulted in resistance to paclitaxel compared to siCON transfected cells. Data were normalised to cell number in siCON/vehicle control and siCON/paclitaxel for paclitaxel treated experiments. Error bars represent standard deviations across 6 replicates.

6.2.4 Ceramide treatment on the background of CERT silencing induces a specific transcriptional response

Previously it has been shown that CERT depletion attenuates the transport of exogenous ceramide from the ER to the Golgi and promotes an increase in cellular ceramide levels with paclitaxel. I hypothesised that the rise in cellular ceramide, restricted to the ER compartment following CERT depletion, might contribute to cellular cytotoxicity coordinated with a CERT-specific transcriptional response.

To investigate the impact of ceramide that is likely to be ER-restricted due to CERT silencing, on the cellular transcriptional response, I asked what gene sets were significantly altered in HCT116 cells treated with ceramide on a CERT depleted background, relative to ceramide treated siCON-transfected cells. The autophagy geneset (Figure 52A) was significantly altered following ceramide treatment of CERT depleted cells compared to ceramide treatment of HCT116 cells with proficient CERT transport ($p=3.5E-05$). CERT functions to transport ceramide from the ER to the Golgi, where it is subsequently converted to sphingomyelin. Silencing of CERT is therefore likely to restrict ceramide to the ER, and this accumulation of ceramide in the ER may explain the specific transcriptional autophagy response observed here.

6.2.5 CERT depletion and paclitaxel exposure initiates an autophagy response

Given the observations that 1) CERT depletion induces a rise in cellular ceramide in the presence of paclitaxel, 2) Ceramide treatment of CERT depleted cells results in an autophagic transcriptional response and 3) LAMP2, induced following CERT depletion,

can antagonise paclitaxel-cell death when silenced from cells, I addressed whether autophagy induction might occur following paclitaxel treatment of CERT depleted cells. Expression and lipidation of endogenous microtubule-associated protein light chain 3 (LC3) were studied in HCT116 cells following CERT silencing and paclitaxel exposure. LC3 is used as a marker of autophagy and is converted from LC3-I to LC3 during the formation of autophagosomes. Changes in levels of both LC3 species may reflect changes in autophagic flux. Following transfection of siCON and paclitaxel treatment, there was minimal change in LC3-I (unlipidated LC3) or LC3-II (lipidated LC3) levels compared to vehicle control-treated HCT116 cells (Figure 53). Similarly, CERT silencing in the absence of drug treatment did not significantly alter LC3-I or LC3-II levels. However, the combination of CERT silencing and paclitaxel treatment resulted in a reduction of both LC3-I and LC3-II, suggestive of autophagy flux induction. Consistent with the degradation of LC3 by lysosomal proteases, addition of the lysosomal protease inhibitor, leupeptin, resulted in the reappearance of LC3-I and LC3-II in siCERT cells treated with paclitaxel (Figure 54).

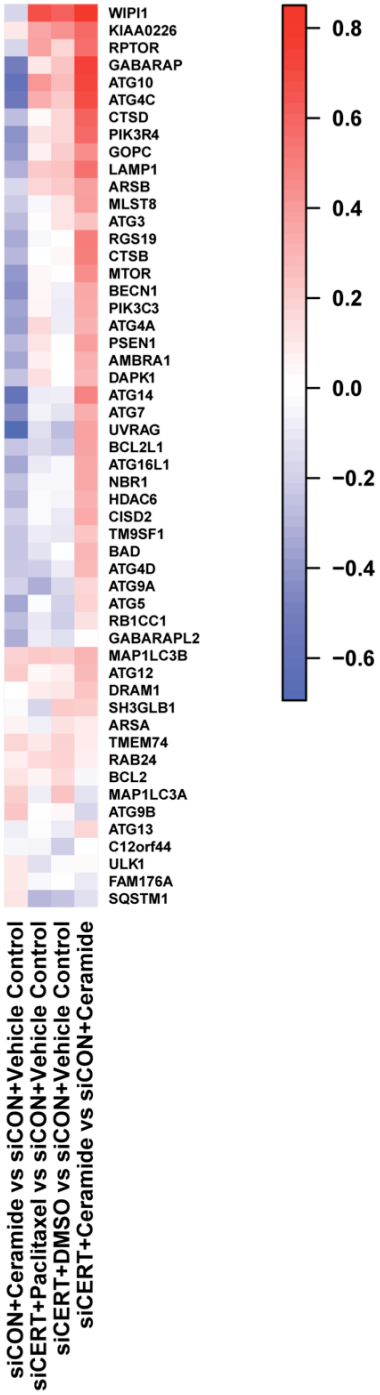

Figure 52 siCERT and ceramide mediates an autophagy transcriptional response
Heatmap of autophagy gene set (as defined using Metacore from GeneGo Inc.).

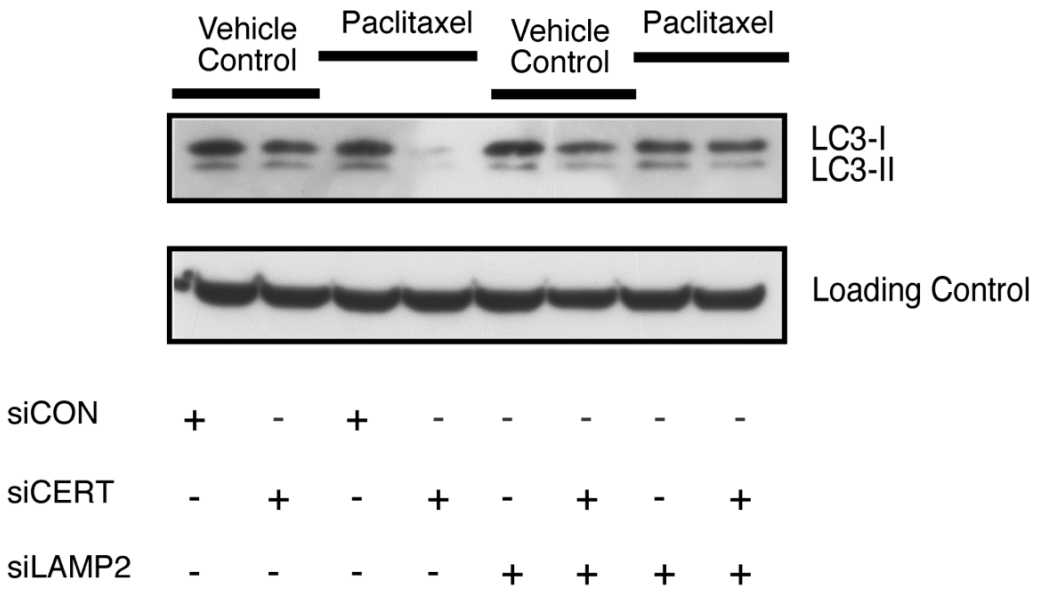

Figure 53 LC3I/II western blot analysis following CERT and LAMP2 silencing for 48h and 24h of paclitaxel exposure

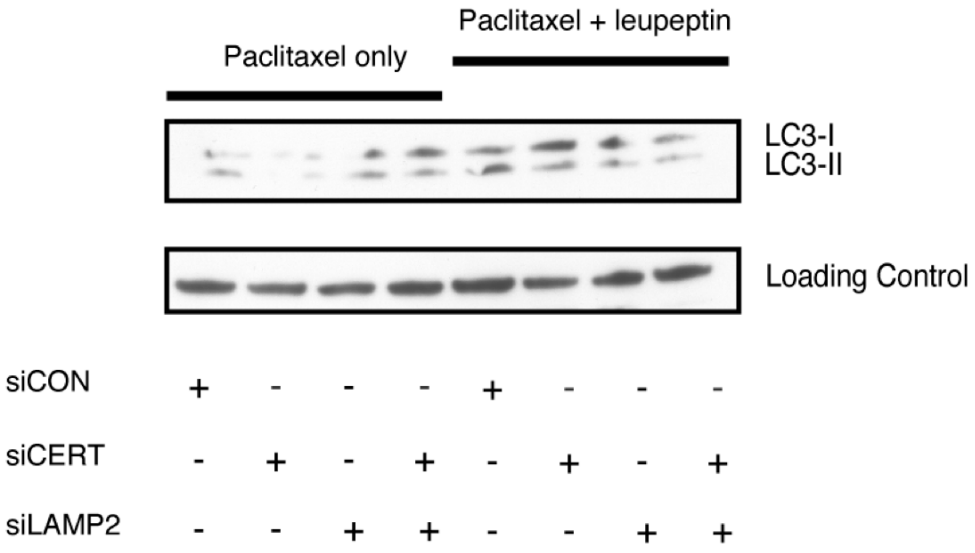

Figure 54 LC3I/II western blot analysis following siCON or CERT silencing for 48h and 24h of paclitaxel exposure in the presence of leupeptin protease inhibitor

6.2.6 CERT-mediated paclitaxel sensitisation is LAMP2 dependent

It has been proposed that the tethering of the autophagosome to the lysosomal membrane is a rate-limiting step that defines the life-span of autophagosomes (283). The expression of LAMP2, encoding a lysosomal membrane protein (282), is induced following CERT depletion and LAMP2 silencing antagonises paclitaxel sensitisation following CERT depletion. Given the reported role of the lysosome and lysosomal proteases in response to taxanes (153, 154), I speculated that the expression of LAMP2 following CERT depletion may contribute to paclitaxel-sensitisation through autophagic cell death. Supporting the role of LAMP2 in siCERT/paclitaxel induced autophagy response and LC3 degradation, LAMP2 silencing attenuated LC3 degradation following CERT and LAMP2 co-depletion (Figure 52B).

To investigate the timing of cell death relative to LC3 disappearance, cells were transfected with siCON or siCERT and treated with vehicle control or paclitaxel. Cells were assayed at 12h, 24h, 48h and 72h for apoptotic activity as measured by Caspase 3/7 activity (Figure 55) and for LC3-I and LC3-II expression. Maximal reduction of LC3-I and LC3-II following siCERT and Paclitaxel was observed at 12h with reappearance of both moieties by 72h. In contrast, maximal apoptotic activity of siCERT and siCON transfected cells was observed 36 hours later, at 48h following paclitaxel treatment. Taken together, these data suggest that increased autophagic flux precedes caspase activity following paclitaxel exposure of CERT depleted cells.

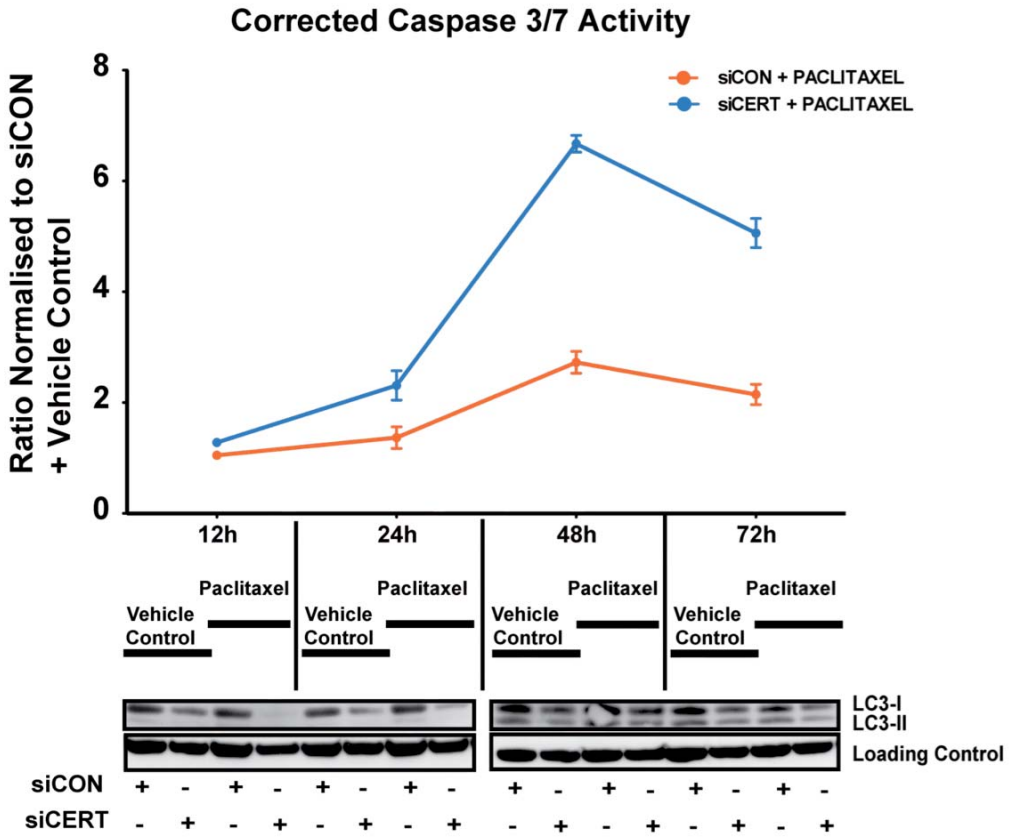

Figure 55 Autophagy response precedes apoptotic activity following CERT silencing and paclitaxel treatment
Graph showing corrected Caspase 3/7 activity of siCON/paclitaxel and siCERT/paclitaxel treated HCT116 cells normalised to siCON/vehicle control over 72h. Error bars represent standard deviations over 6 replicates per condition. Below the graph is a western blot analysis over the same time course showing LC3 expression following siCON or siCERT transfection with vehicle control or paclitaxel treatment.

6.2.7 CERT depletion induces localisation of LAMP2/LC3 and the accumulation of lysosomal structures in the presence of paclitaxel

The localisation of endogenous LAMP2 expression was addressed following CERT depletion in GFP-LC3-HEK293 (transformed Human Embryonic Kidney) cells, cells which stably express GFP-LC3, by fixed cell immunofluorescence in the presence of the lysosomal acidification inhibitor Bafilomycin A to prevent GFP-LC3 degradation. Endogenous LAMP2 intensity was elevated in siCERT/paclitaxel treated relative to siCON/paclitaxel GFP-LC3-HEK293 cells, and there was marked co-localisation of GFP-LC3 with LAMP2 (Figure 56A). These results suggest that CERT depletion induces paclitaxel sensitisation through a LAMP2-dependent mechanism that is associated with LAMP2/LC3 co-localisation and LC3 degradation. Next, lysosomal mass was estimated by quantifying LAMP2 intensity per spot. Depletion of CERT resulted in a significant increase in LAMP2 spot intensity (Mann-Whitney U, $p=0.015$). Co-depletion of LAMP2 significantly decreased this intensity (Mann-Whitney U, $p=0.0043$) (Figure 56B).

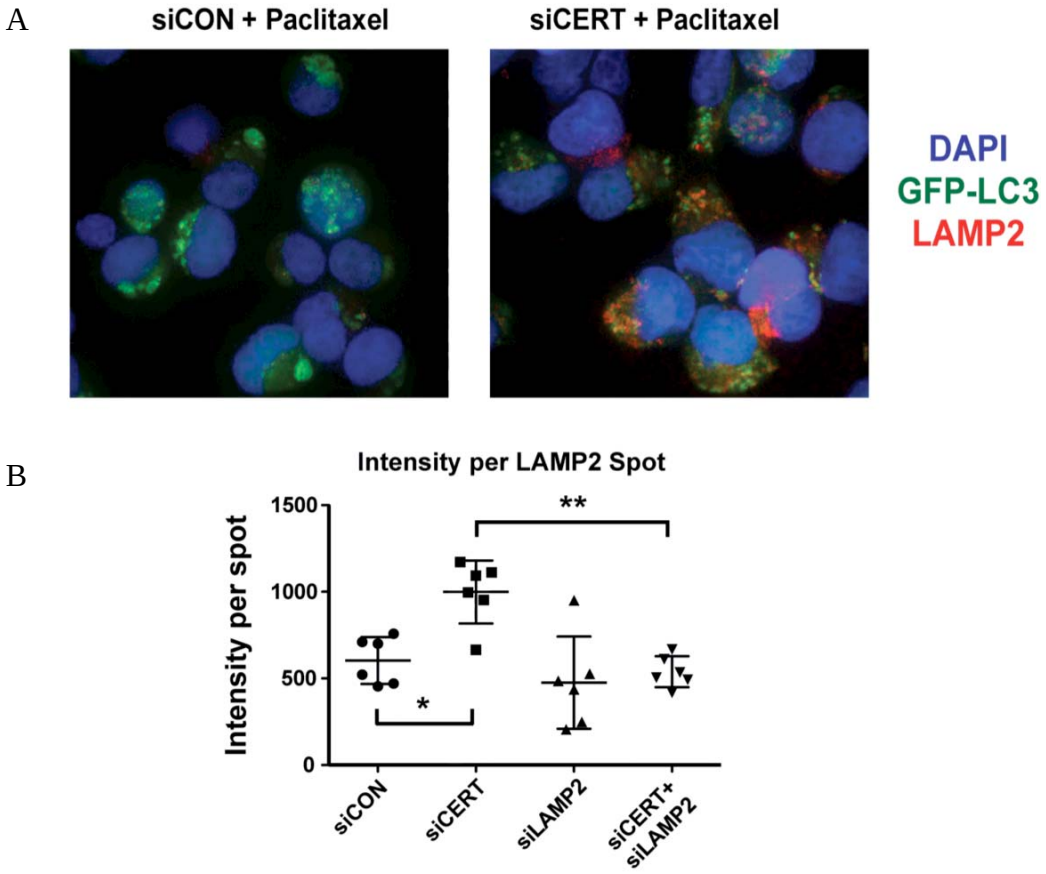

Figure 56 CERT depletion results in increased LAMP2 spot intensity as measured using immunofluorescence microscopy
A) Representative immunofluorescence microscopy images of siCON/paclitaxel and siCERT/paclitaxel cells in the presence of Bafilomycin A1. Blue corresponds to DAPI staining, green to GFP-LC3 and red to LAMP2.
B) Scatter plot of LAMP2 intensity per spot following siCON, siCERT, siLAMP2 or siCERT+siLAMP2 silencing and treatment with 25nM paclitaxel. Each dot represents a replicate well. Horizontal lines signify mean and standard deviations.

I asked whether specific changes to the cellular ultrastructure could be identified by electron microscopy (EM) analysis of siCERT/paclitaxel and siCON/paclitaxel treated cells (Figure 57). EM analysis revealed an increase in the number of cells with electron dense structures that may correspond to lysosomal or autophagosomal structures in siCERT/paclitaxel treated cells in contrast to siCON/paclitaxel treated cells (Figure 58: percentage of cells with electron dense structures with siCERT/paclitaxel: 75% n=24 vs siCON/paclitaxel: 44%, n=27, p=0.045, Fisher's Exact Test). In contrast, co-depletion of CERT and LAMP2 in the presence of paclitaxel significantly reduced the number of cells with these electron dense structures compared to siCERT/paclitaxel treated cells (siCERT/siLAMP2/Paclitaxel: 32% vs siCERT/Paclitaxel 75%, n=25 and n-24 respectively, p=0.004, Fisher's Exact Test).

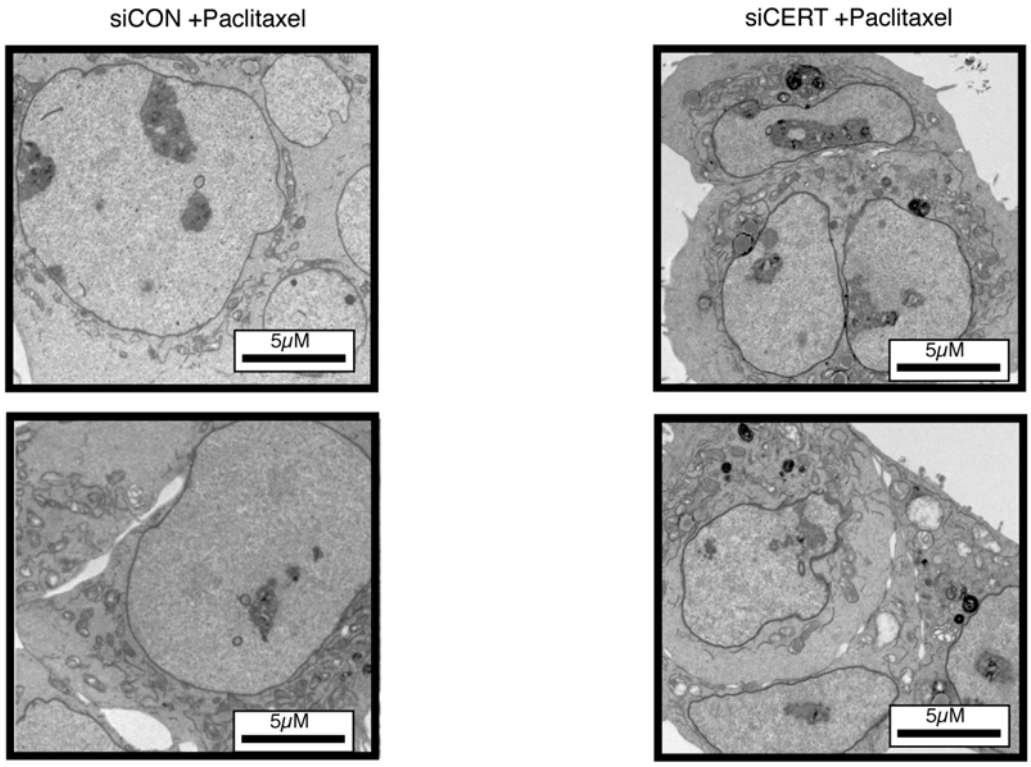

Figure 57 Representative transmission electron micrographs (TEM) of siCON/paclitaxel and siCERT/paclitaxel cells

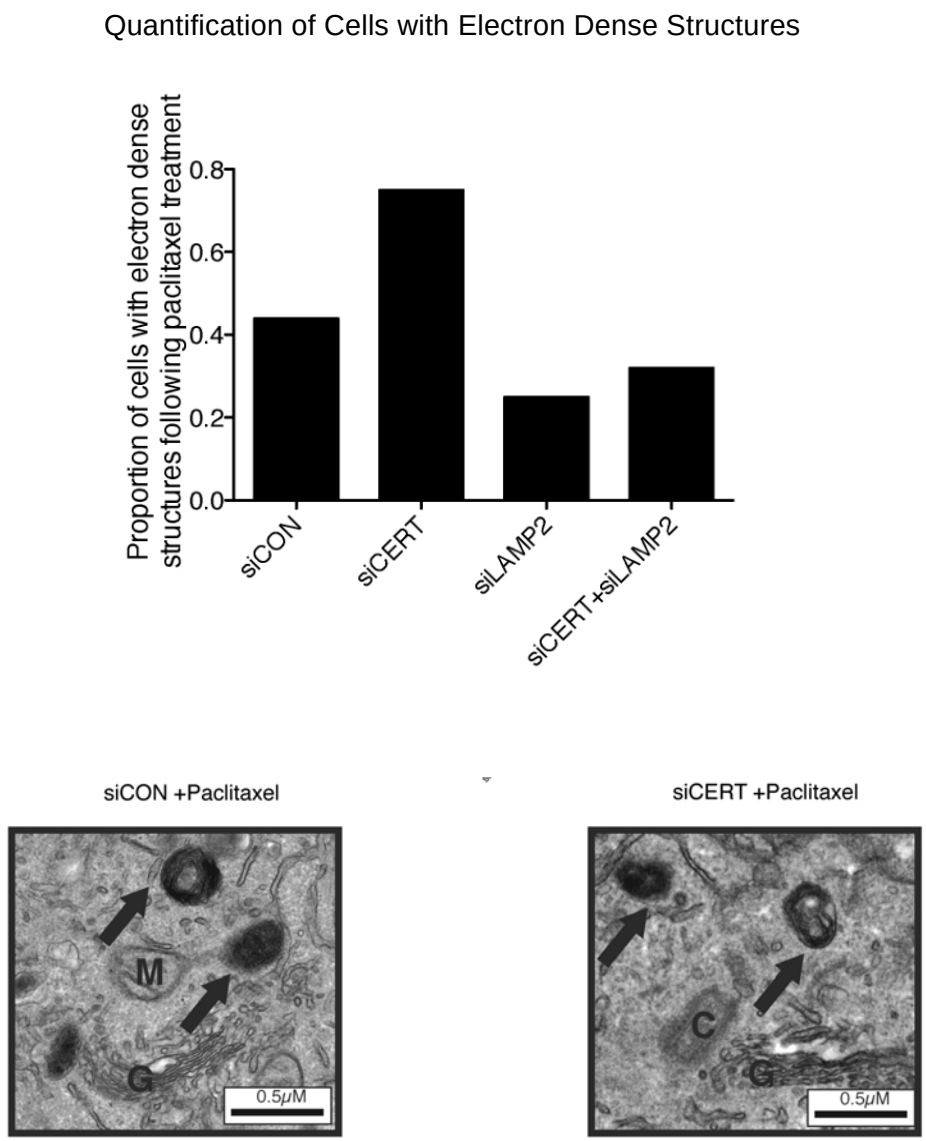

Figure 58 Electron dense structures appearing following CERT silencing were quantified

Graph of percentage of cells with electron dense structures following paclitaxel treatment and siCON, siCERT, siLAMP2 or siCERT and siLAMP2 transfection. Representative high magnification TEM images of siCON/paclitaxel and siCERT/paclitaxel cells, showing electron dense structures (arrow). N=nucleus, G=Golgi Apparatus, C=Centriole, M=Mitochondria.

6.2.8 Relationship of paclitaxel response with autophagy gene expression

To further explore the relationship of autophagy with paclitaxel response, I addressed whether silencing other components of the autophagy pathway might influence paclitaxel sensitivity. Silencing the majority of these genes resulted in significant cell death independent of taxane exposure. However, silencing of ATG7 induced paclitaxel resistance, indicating that a proximal member of the autophagy pathway may influence paclitaxel response (Figure 59A). Phenocopying LAMP2 silencing, co-depletion of both ATG7 and CERT significantly attenuated CERT-mediate cell death (Mann Whitney-U, p=0.002) (Figure 59B).

A

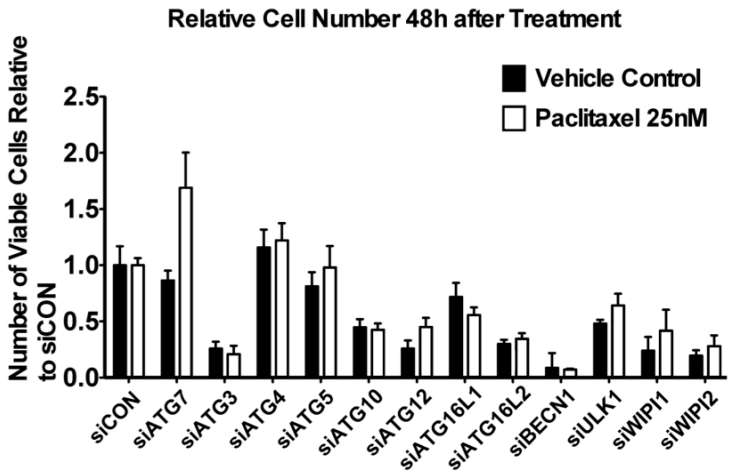

B

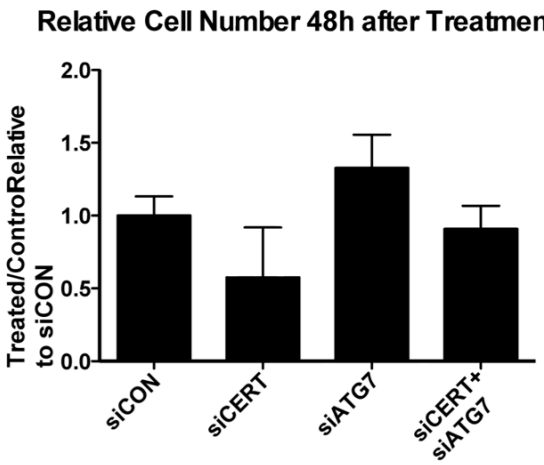

Figure 59 Assessment of relationship of paclitaxel response with autophagy gene expression

A) Graph of relative cell number following transfection of siCON or siRNAs targeting regulators of autophagy. Data were normalised to cell number in siCON/vehicle control or siCON/paclitaxel for paclitaxel treated experiments. Error bars represent standard deviations across six replicates per condition.

B) Graph of relative cell number in paclitaxel treated compared to vehicle control following transfection of siCON, siCERT, siATG7 or siCERT+siATG7. Treated/control ratio for siCON was set to 1. Error bars represent standard deviations across six replicates per condition.

6.2.9 CERT depletion promotes mitotic catastrophe that is LAMP2 dependent

I sought to establish the cell cycle fate of individual cells following paclitaxel treatment and CERT silencing, through live cell microscopy imaging of H2B-GFP labelled HCT116 cells during 48 hours of paclitaxel exposure. Paclitaxel treatment of siCON transfected cells promoted cell death following mitosis or during interphase following exposure to anti-mitotic agents as previously reported (76). CERT depletion induced two-fold more death events over 48 hours compared to control transfected cells following paclitaxel treatment, consistent with the drug-sensitising effect of CERT depletion (Figure 60A and B). The majority of death events following paclitaxel treatment of CERT depleted cells occurred during a multinucleated interphase resulting from an aberrant mitosis. Next, I sought to identify the role of LAMP2 in this process. Consistent with my previous observations (Figure 51A), co-depletion of LAMP2 with CERT reversed paclitaxel-sensitisation following 48 hours of paclitaxel exposure. Paclitaxel induced cell death was still observed in interphase cells but LAMP2 depletion abrogated the majority of mitotic and post-mitotic cell death events, with the majority of multinucleated cells surviving to the end of the observation period. Taken together, these data suggest that CERT depletion promotes the elimination of multinucleated polyploid cells following paclitaxel exposure that is abrogated by LAMP2 co-silencing.

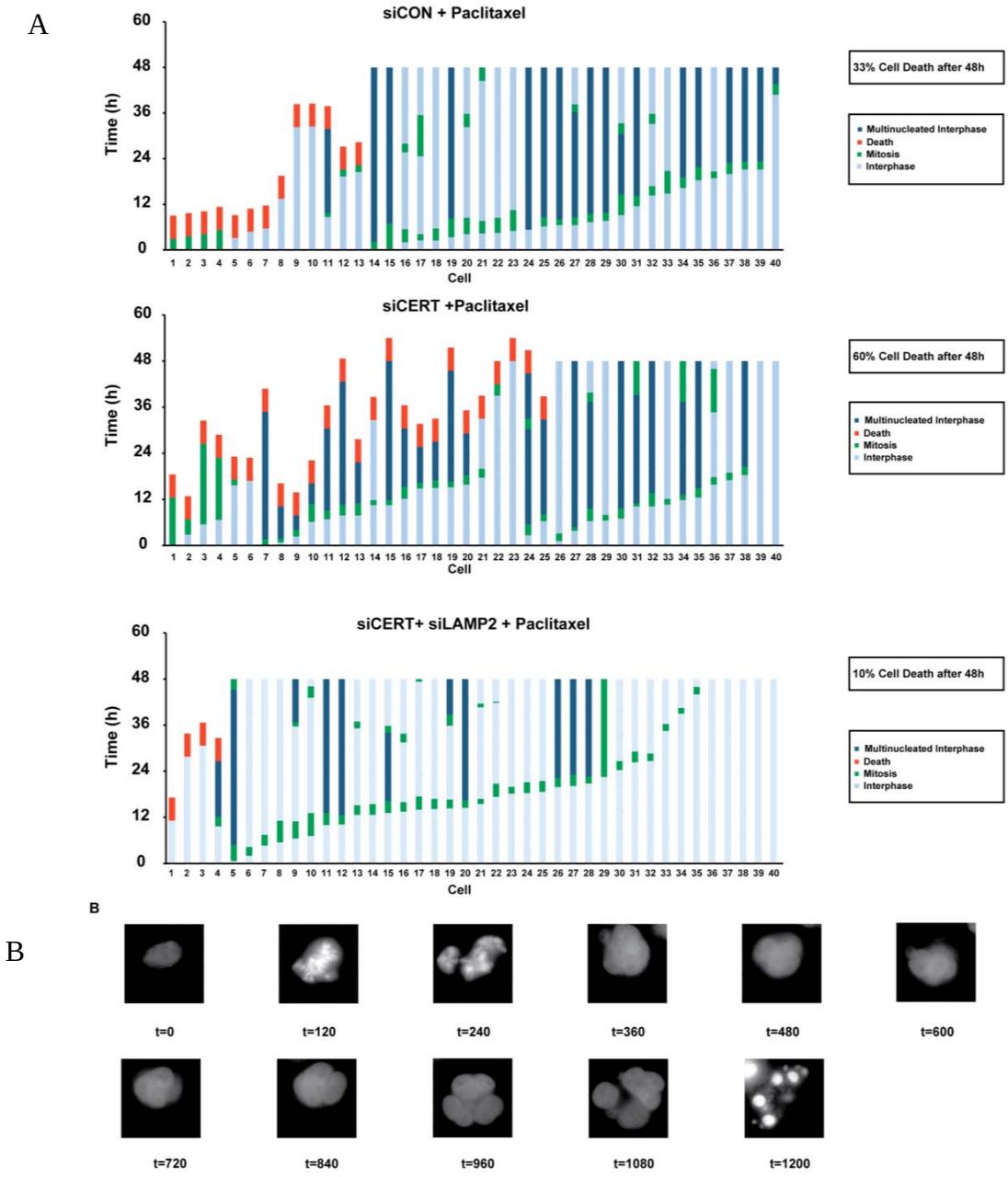

Figure 60 Live cell imaging and single cell fate analysis following CERT silencing and paclitaxel treatment

A) Graph of single cell fate analysis during paclitaxel exposure following transfection with siCON, siCERT, or siCERT and siLAMP2. Cells were individually tracked for 48h following paclitaxel treatment. Timing of entry into mitosis was scored from time from nuclear envelope breakdown (NEB) to reformation of nuclei.

B) Example of a time-lapse sequence (t=time in minutes) of a CERT depleted cell treated with paclitaxel over 1200 minutes following mitotic entry. Cell undergoes nuclear envelope breakdown (NEB) followed by an aberrant mitosis resulting in a multinucleated interphase and subsequently cell death.

6.2.10 CERT is overexpressed in HER2+ primary breast cancer

Work in this section has been contributed by Neil Jones, Nicolai Juul Birkbak, David Endesfelder, Jil Sander, Rebecca Roylance and Patricia Gorman.

The expression of CERT in a panel of cancer cell lines was determined by qPCR to attempt to identify cancer subtypes in which CERT expression may play a role (Figure 61A). Breast cancer cell lines appeared to have the broadest distribution of CERT expression. Analysis of four HER2+ and eight HER2- breast cancer cell lines revealed higher relative CERT expression in the HER2+ cell lines in comparison to HER2- cancer cell lines ($p=0.006$, t-test) (Figure 61A). 12 breast cancer datasets for which CERT expression was measured by microarray analysis were identified. CERT mRNA expression was significantly repressed in basal breast cancers ($p=1.41e-51$) relative to other intrinsic subtypes of breast cancer (Figure 61B). Next CERT protein expression was analysed in a Tissue Microarray (TMA) panel of 356 primary breast cancers of mixed ER/HER2 receptor subtype, tumour grade and nodal status (Table 7). CERT protein levels, determined by the quickscore (CERT protein intensity x percentage of cells positive) (173), appeared to be significantly elevated in HER2+ relative to HER2- primary breast cancers (Wilcoxon test $p=0.0009$) (Figure 62) (Representative images, Figure 63) with no significant difference between ER+ and ER2 subtypes ($p=0.0889$).

A

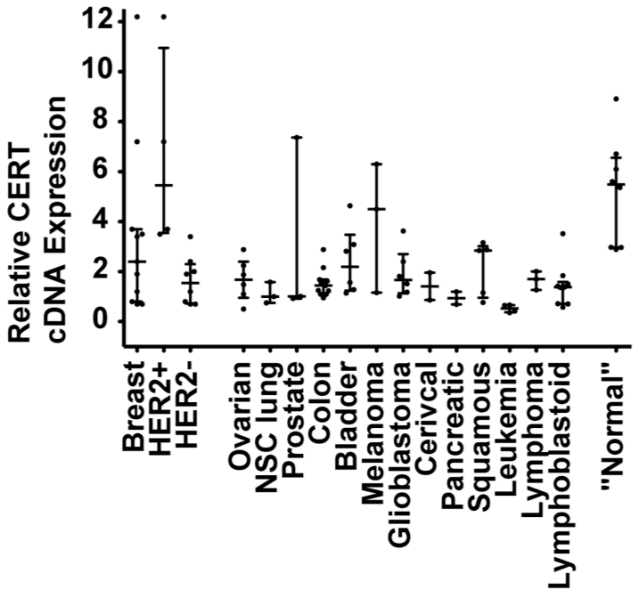

B

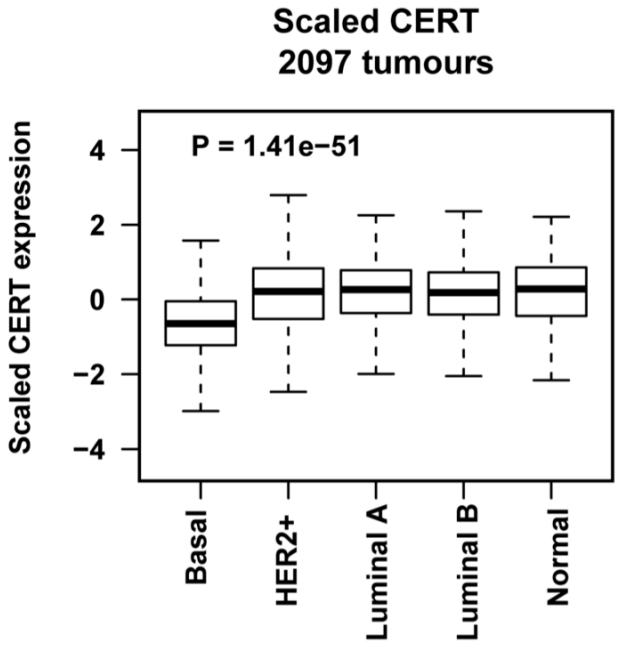

Figure 61 CERT mRNAis overexpressed in HER2+ primary breast cancer
A) Graph of relative CERT cDNA expression in cell lines of various tissue origins. Horizontal lines signify median and interquartile range.
B) Boxplot showing CERT expression in breast cancer divided into intrinsic subtypes in a meta-analysis across 12 datasets. The length of the whiskers was limited by maximal = 1.5 times the interquartile range.

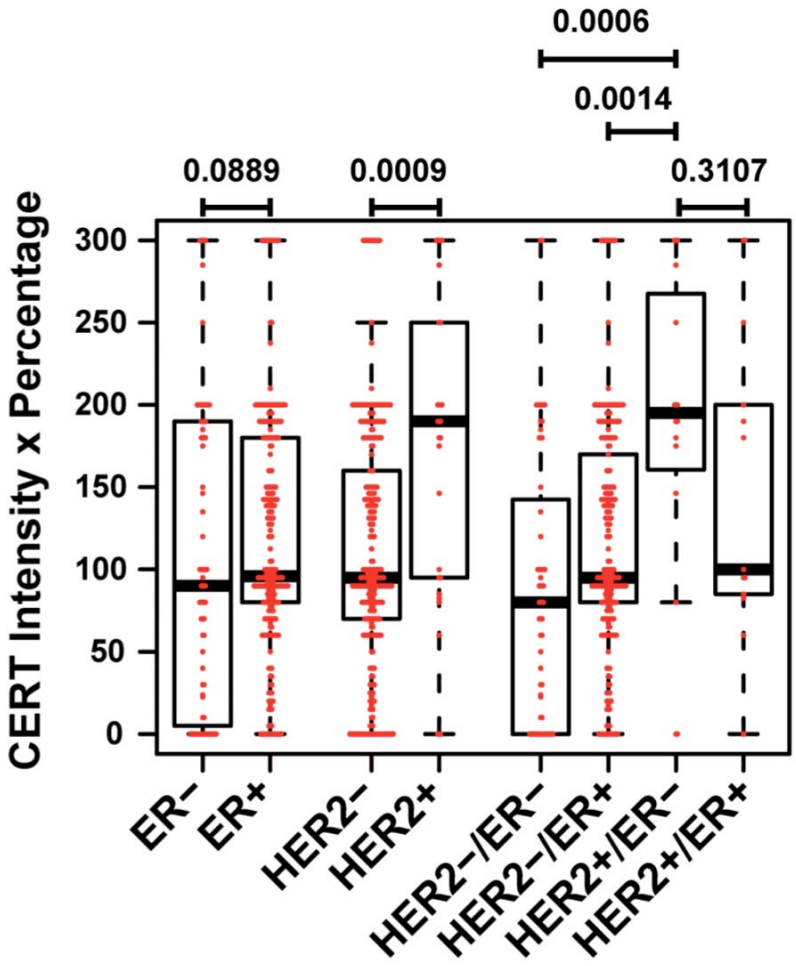

Figure 62 CERT protein expression in TMA Cohort
Graph demonstrates CERT protein intensity x percentage in a breast cancer TMA cohort of 356 primary breast cancers divided into various subtypes based on ER and HER2 receptor status.

	All Patients	**CERT low**	**CERT high**
	(n = 426)	**(n = 271)**	**(n = 102)**
Median Age (range)	58 (27 - 92)	58 (30 - 90)	59 (27 - 92)
Unknown	2	2	0
Median Size in mm (range)	20 (1 - 130)	19 (1 - 100)	20 (6 - 130)
Unknown	13	11	1
Grade, N(%)			
1	98 (23)	67 (25)	11 (11)
2	184 (43)	127 (47)	43 (42)
3	143 (34)	76 (28)	48 (47)
Unknown	1	1	0
Lymph Node Status, N(%)			
positive	215 (53)	125 (48)	63 (65)
negative	192 (47)	134 (52)	34 (35)
Unknown	19	12	5
Stage, N(%)			
T1: 0 – 2cm	246 (60)	163 (62)	54 (53)
T2: 2 – 5cm	149 (36)	90 (35)	39 (39)
T3: >5cm	18 (4)	7 (3)	8 (8)
Unknown	13	11	1
ER Status, N(%)			
positive	326 (78)	216 (80)	75 (74)
negative	92 (22)	54 (20)	27 (26)
Unknown	8	1	0
HER2 Status, N(%)			
positive	31 (7)	11 (4)	18 (18)
negative	393 (93)	258 (96)	84 (82)
Unknown	2	2	0

PR Status, N(%)			
positive	300 (79)	198 (78)	79 (79)
negative	80 (21)	57 (22)	21 (21)
Unknown	46	16	2
Chemotherapy, N(%)			
yes	149 (49)	100 (48)	41(49)
no	157 (51)	107 (52)	43 (51)
Unknown	120	64	18

Table 7 Demographic data of patients in breast cancer TMA cohort

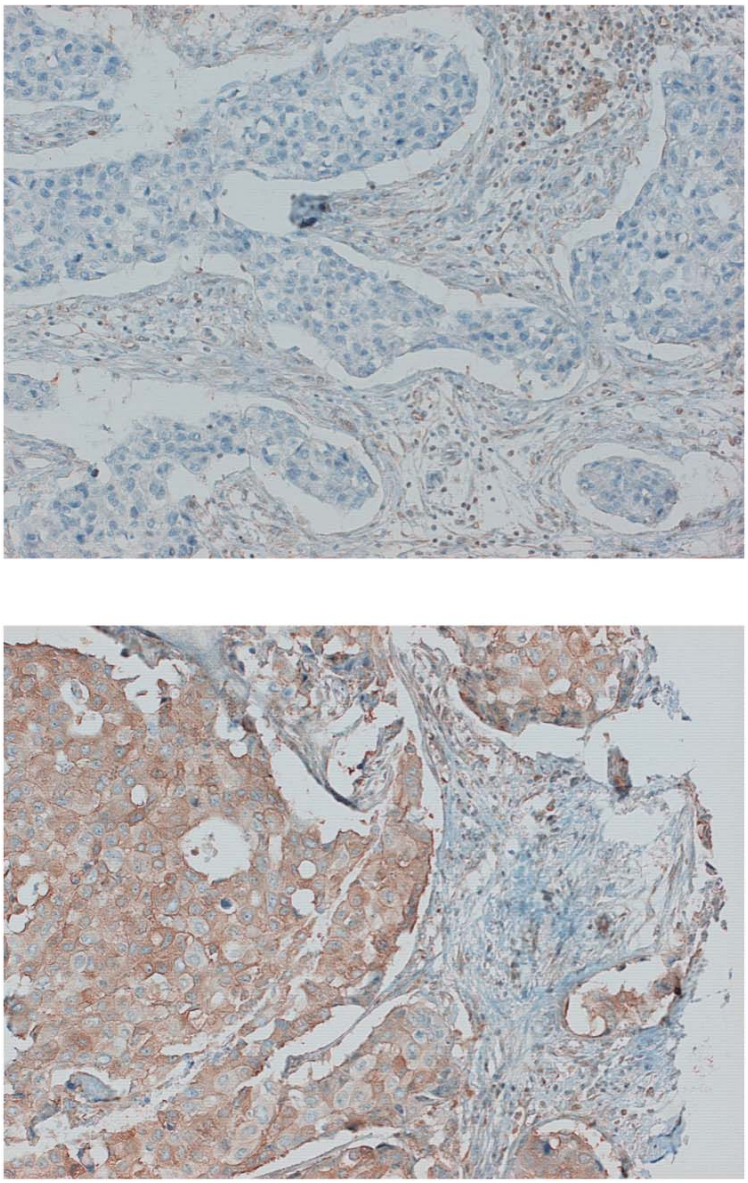

Figure 63 Representative IHC images for CERT expression.
(Above) Representative image showing a complete absence of CERT staining with benign breast tissue acting as internal control.
(Below) Representative image of CERT expression with a quickscore of 3.

6.2.11 CERT depletion sensitises HER2+ breast cancer cell lines to cytotoxics and induces autophagic flux

Given the observation that CERT was selectively over-expressed in HER2+ cell lines and HER2+ breast cancers, I assessed drug sensitivity in three HER2+ breast cancer cell lines, BT474, HCC1954 and SKBR3, following CERT silencing. CERT depletion resulted in multidrug sensitisation to clinically relevant cytotoxics, paclitaxel, doxorubicin and cisplatin (Figure 64). In order to establish whether CERT depletion and drug exposure was associated with enhanced autophagic flux, I analysed LC3-I/II expression in drug treated HCC1954 cells. CERT depletion in the HCC1954 cell line resulted in decreased levels of LC3-I and LC3-II following treatment with paclitaxel, cisplatin or doxorubicin when compared to siCON transfected cells (Figure 65A), suggesting that, concordant with the HCT116 analyses, increased autophagic flux occurs following CERT depletion and cytotoxic drug treatment in HER2+ breast cancer cells.

Next, the HCC1954 cell line was transfected with siCON, siCERT, siLAMP2 or siCERT and siLAMP2 and treated with either paclitaxel or doxorubicin, drugs widely used in the management of high-risk breast cancer in the adjuvant setting (Figure 65B). In all conditions, LAMP2 co-silencing resulted in a significant attenuation of CERT depletion-induced drug sensitisation (Mann-Whitney U, paclitaxel 50nM, $p=0.0087$, paclitaxel 500nM, $p=0.0043$, doxorubicin 250nM, $p=0.0087$, doxorubicin 1000nM, $p=0.015$). Finally, I assessed the efficacy of Trastuzumab, a monoclonal antibody targeting the HER2 receptor used in the treatment of HER2+ breast cancer. The HCC1954 cell line has been shown to be more resistant to Trastuzumab compared to

other HER2+ cell lines (284). CERT depletion resulted in Trastuzumab sensitisation (Figure 65C, Mann-Whitney, p=0.0087).

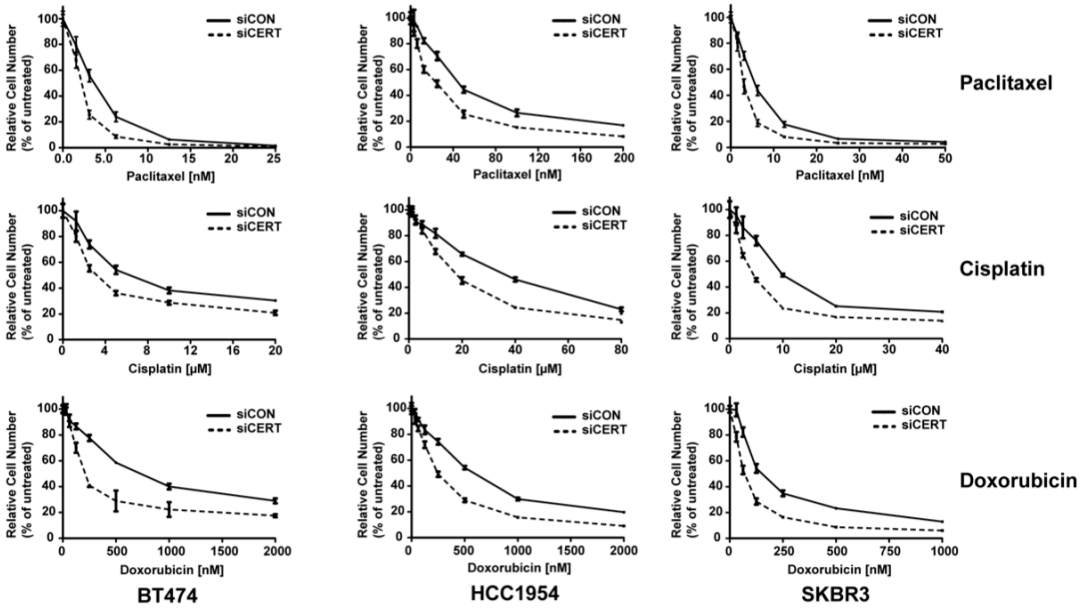

Figure 64 CERT silencing sensitises HER2+ breast cancer cell lines to various drugs and induces autophagic flux changes.
Graphs showing relative cell number compared to vehicle control of HER2+ breast cancer cell lines, BT474, HCC1954 and SKBR3 following either siCON or siCERT transfection and treatment with paclitaxel, cisplatin or doxorubicin.

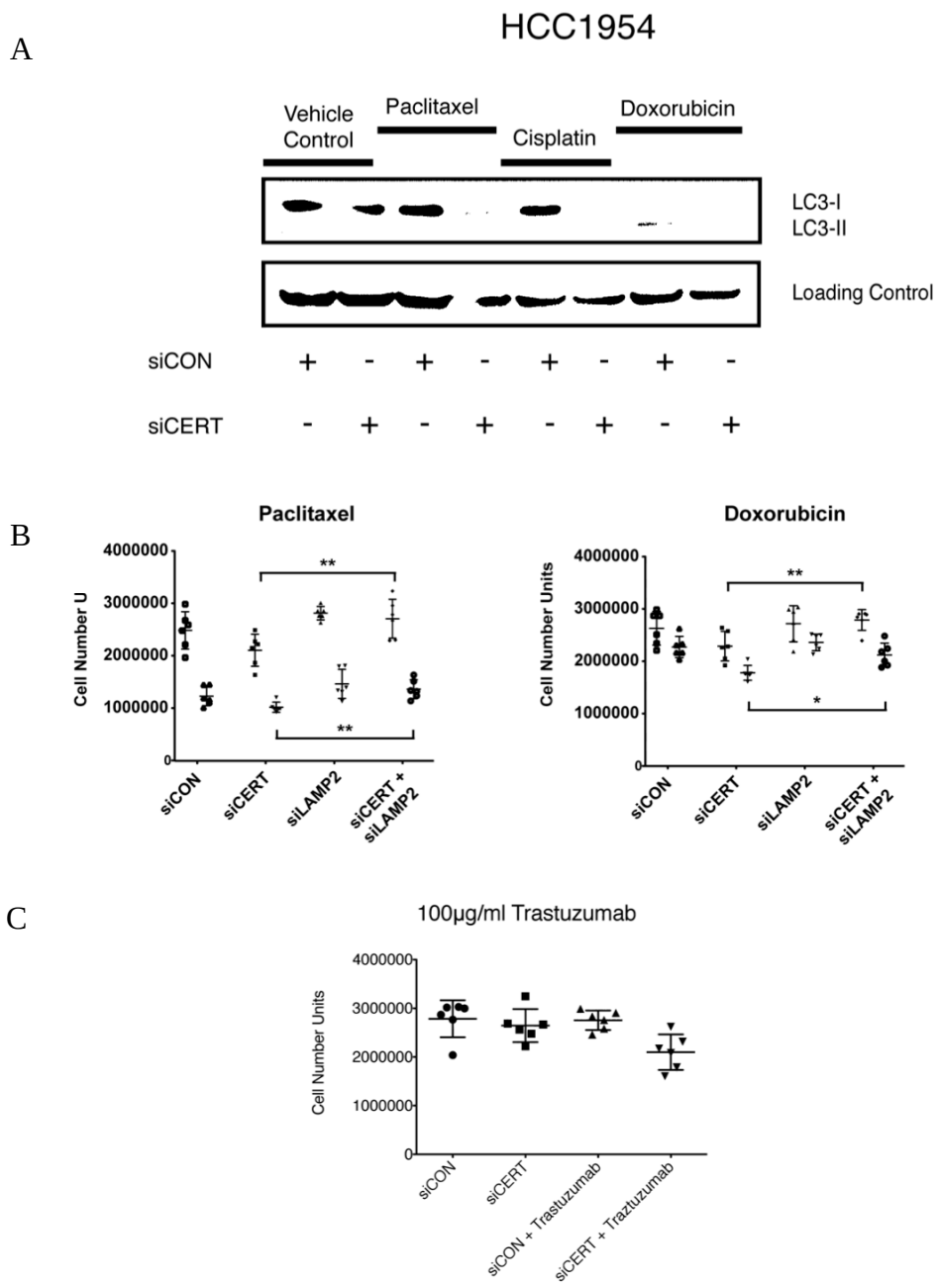

Figure 65 CERT silencing induces changes in autophagic flux in HCC1954 cells and sensitisation that is LAMP2-dependent in response to drug treatment

A) Western blot demonstrating LC3I and LC3-II expression in HCC1954 cells following 48h of CERT depletion followed by 24h of treatment with paclitaxel, cisplatin or doxorubicin.
B) Scatter plot of cell number (as measured by fluorescence activity) in paclitaxel treated (50nM and 500nM) (left) and doxorubicin treated (250nM and 1000nM) (right) HCC1954 cells following transfection with siCON, siCERT, siLAMP2 or siCERT and siLAMP2. Each dot represents a replicate well. Horizontal lines signify mean and standard deviations.
C) Scatter plot of cell number (as measured by fluorescence activity) in HCC1954 cells following transfection with siCON or siCERT and treatment with 100µg/ml Trastuzumab or vehicle control. Each dot represents a replicate well. Horizontal lines signify mean and standard deviations.

6.2.12 CERT expression is associated with survival outcome in patients with primary breast cancer treated with adjuvant chemotherapy.

Survival analysis in this section has been contributed by David Endesfelder and Jil Sander.

According to data from my laboratory, CERT silencing alone appears to have little impact on cancer cell viability, but sensitises cells to multiple clinically relevant cytotoxics in parallel with enhanced autophagic flux. Therefore, I wanted to address whether low CERT expression might be associated with improved clinical outcome, particularly in primary breast cancers treated with adjuvant chemotherapy. First, it was addressed whether CERT expression was associated with survival outcome (breast cancer specific survival (BCSS)) in the 356 primary breast cancer TMA cohort. A maximally selected rank statistic (174) was used to derive a threshold for separating tumours into cohorts of low and high CERT expression based on survival outcome. This method selects an optimal threshold for prediction, but avoids the erroneous reporting of overoptimistic low p-values by adjusting for the multiple test problem inherent in the selection of the threshold. A CERT quickscore threshold of <175 and >175 was obtained for separating tumours into low and high CERT expression respectively. Significantly poorer breast cancer outcome was observed across all patients with primary breast cancers with a CERT quick score >175 compared to patients with a CERT quick score <175 (HR 2.2 95% CI 1.3-3.6, p=0.003) (Figure 66A). A similar relationship was observed when the analysis was restricted to HER2+ breast cancer patients only (Figure 66B, p=0.035 HR 6.81). This association was confirmed for

relapse free survival in a meta-analysis of 1861 patients with primary breast cancer using the publicly available Kaplan-Meier meta-analysis tool (285) (Figure 66C) HR 1.2 (1.1-1.4 p=0.027).

CERT silencing alone has limited or no effect on cancer cell viability, but induces autophagy flux and enhanced cell death only in combination with multiple cytotoxics with different mechanisms of action. It was investigated whether the relationship of low CERT expression with significantly improved outcome was observed when patients were stratified by use of adjuvant chemotherapy. Consistent with a role for CERT in augmenting drug sensitivity when repressed, low CERT expression in the 356 patient TMA cohort was associated with significantly improved outcome in patients treated with adjuvant chemotherapy (Figure 66D, n=134 HR 2.2 1.2-5.5 p=0.014). In contrast, in a similarly powered analysis of 150 patients who did not receive adjuvant chemotherapy from within this cohort, there was no such significant association of low CERT expression with improved outcome (Figure 66E). Consistent with the drug sensitising phenotype associated with CERT silencing, these data suggest that CERT expression may predict outcome specifically in patients with primary breast cancer receiving chemotherapy. Finally, in a robust multivariate cox regression model using data from the TMA cohort of 356 patients with primary breast cancer, when known breast cancer histopathological prognostic markers are considered, the association of CERT expression with survival acts as a significant independent prognostic variable (Table 8).

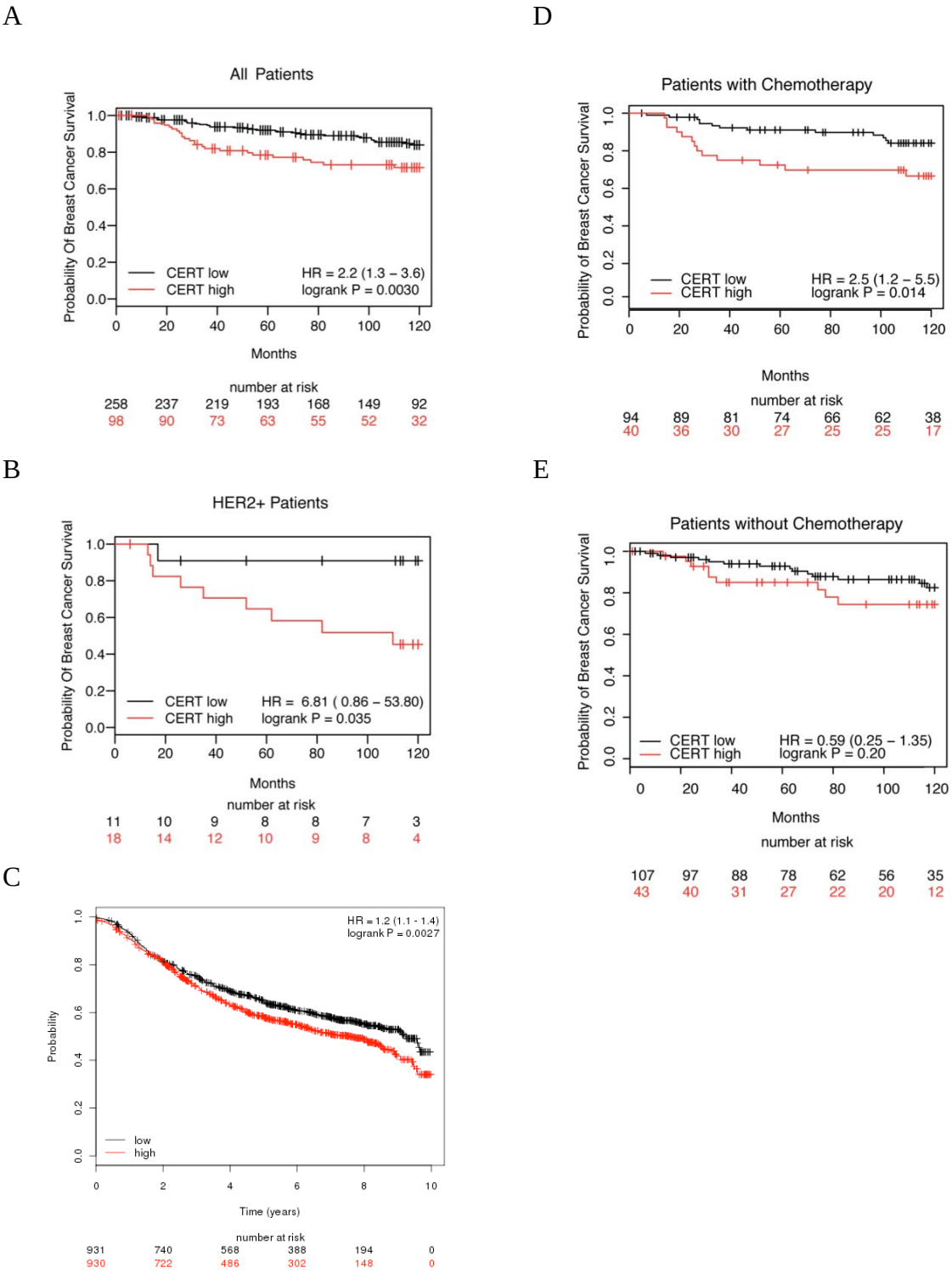

Figure 66 CERT expression is associated with survival outcome in patients with primary breast cancer treated with adjuvant chemotherapy

A) Kaplan-Meier analysis of high CERT expression compared to tumours with low CERT expression (Quickscore >175 vs <175).
B) Kaplan-Meier analysis of high CERT expression compared to tumours with low CERT expression (Quickscore >175 vs <175) restricted to HER2+ breast cancer patients (n=29) within the same cohort of 356 patients.
C) Kaplan-Meier analysis of high CERT expression compared to tumours with low CERT expression within 1861 patients with 10-year relapse-free survival data available using online kmplot.com tool that uses gene expression data and survival information of 1908 patients downloaded from GEO (Affymetrix HGU133A and HGU133+2 microarrays).
D) Kaplan-Meier analysis of high CERT expression compared to tumours with low CERT expression (Quickscore >175 vs <175) restricted to patients treated with adjuvant chemotheraphy (n=134) within the same cohort of 356 patients.
E) Kaplan-Meier analysis of high CERT expression compared to tumours with low CERT expression (Quickscore >175 vs <175) restricted to patients treated without adjuvant chemotheraphy (n=150) within the same cohort of 356 patients.

	log(HR)	HR	se(log(HR))	P Value
Size in mm	0.02005	1.020	0.0084	0.017
Grade 2	1.66957	5.310	1.0356	0.110
Grade 3	2.87047	17.65	1.0224	0.005
Node positive	0.49507	1.64	0.3477	0.150
CERT	0.00365	1.004	0.0017	0.030

Table 8 Multivariate analysis of prognostic predictors including CERT expression in breast cancer TMA cohort

6.3 Discussion

It has been previously demonstrated that reduced CERT expression forms part of a functional metagene that is predictive of pathological complete response to paclitaxel/doxorubicin combination chemotherapy in breast cancer (286). In order to explore how CERT depletion might mediate its drug sensitisation effect, I investigated how CERT silencing results in paclitaxel sensitisation using transcriptomic and functional genomics based approaches. I find that CERT depletion and paclitaxel exposure accelerates autophagic flux in both colon and breast cancer models and results in LAMP2-dependent death of multinucleated cells following paclitaxel exposure, observed through single cell fate tracking experiments by live cell microscopy.

Accumulating evidence supports the importance of autophagy in the response to cytotoxic drug or radiation therapy that may enhance death or augment cancer cell viability (287-290). Lysosomal activity has also been implicated in the paclitaxel response. The lysosomal enzymes GBA1 and GBA3 was previously identified by our laboratory as regulators of paclitaxel sensitivity and microtubule stabilising drugs initiate lysosomal cathepsin B activation and release, inhibition of which promotes resistance to this class of drug (153).

Transcriptomic analysis identified that an autophagy gene module is significantly enriched following CERT silencing and ceramide treatment. This gene signature may reflect the accumulation of ceramide within the ER. Through this analysis I suggest an explanation for the synergistic activities of CERT depletion and paclitaxel exposure that provides a molecular basis for the elimination of multinucleated polyploid cells resulting from an aberrant mitosis. I speculate that expression of LAMP2 primes the cell

for completion of the autophagic process but on its own LAMP2 expression is insufficient to drive cell death. This process may depend on CERT depletion with drug exposure that promotes a greater rise in ER-restricted cellular ceramide resulting in the expression of an autophagy gene module, in agreement with previous reports of autophagy initiation by ceramide (291, 292) and autophagy regulation by transcriptional dependent mechanisms (293). Consistent with the requirement for both CERT depletion and drug treatment for the induction and completion of autophagy, I observed co-localisation of LAMP2 and LC3 in the presence of lysosomal inhibitors in HEK293 cells as well as a potent reduction of both LC3-I and LC3-II in CERT depleted cells treated with paclitaxel. The requirement for LAMP2 in the synergistic interaction between siCERT and drug sensitisation was demonstrated through abrogation of the siCERT sensitising phenotype following LAMP2 silencing in both paclitaxel and doxorubicin treated HER2+ HCC1954 cells.

Studies suggest that multinucleation may be a precursor of mononucleate aneuploidy/polyploidy and CIN (98-100). Autophagic flux and the consequent cell death of multinucleated cells following paclitaxel exposure is dependent upon LAMP2 induction following CERT depletion, suggesting a rational approach for limiting the development of CIN in cancer. Recently, Amon and colleagues demonstrated that aneuploid cells display an increased susceptibility to compounds that interfere with protein folding and trisomic MEFs displayed increased LC3 lipidation relative to wild-type MEFs, that was further enhanced following treatment with the aneuploidy-specific agent, AICAR (129). These data are strikingly similar to our observations demonstrating that CERT depletion and paclitaxel treatment induces the unfolded protein response (12), autophagic flux and as demonstrated using live cell microscopy,

the specific death of cells that have undergone an aberrant mitosis or entered a multinucleated state.

CERT was established to be relatively over-expressed in HER2+ breast cancer. I provide evidence for the ability of CERT silencing to sensitise HER2+ breast cancer cell lines to paclitaxel, doxorubicin, cisplatin and Trastuzumab and demonstrate that cytotoxic multidrug sensitisation is associated with accelerated autophagic flux. Consistent with a role for LAMP2 induction in the multidrug sensitisation phenotype, LAMP2 co-silencing attenuates doxorubicin sensitisation following CERT depletion in the HER2+ HCC1954 breast cancer cell line. As HER2 positivity is also associated with CIN (294), CERT targeting may provide a mechanisms to improve patient outcome in those with HER+ by allowing the targeting of aneuploid cells via a LAMP2-dependent pathway.

Furthermore, CERT expression defines a population of patients with breast cancer with divergent survival outcomes in multivariate analysis. Additionally, consistent with the drug sensitising phenotype following CERT silencing, low expression of CERT appears to predict improved outcome in patients treated with adjuvant chemotherapy. Prospective validation of the potential role for CERT in predicting outcome following adjuvant chemotherapy in breast cancer is in progress.

This chapter has focused mainly on the effect of CERT silencing on paclitaxel sensitisation. However, previous findings have shown that CERT silencing results in sensitisation to non-mitotic targeting drugs such as 5-FU, cisplatin and doxorubicin (12) and I observed that CERT silencing induces changes in autophagic flux following treatment with cisplatin and doxorubicin in HER2+ breast cancer cells. Taken together,

these findings suggest that changes in autophagic flux following CERT silencing and drug treatment may also play a role in sensitisation to these drugs. Further work is needed to investigate the role of LAMP2 in this process and to study the timing of cell death following exposure to these drugs.

6.4 Conclusion

Taken together, these results suggest that there may be therapeutic potential in the targeting of CERT to augment autophagy and the death of multinucleated cells in order to limit the initiation of chromosomal instability, intra-tumour heterogeneity and chemotherapy resistance. These studies also suggest that an increase in autophagic flux may act to selectively target cells that have undergone an aberrant mitosis or that undergo an increase in ploidy due to mitotic slippage into a multinucleated interphase state. Furthermore, these data also implies that cell death following mitotic catastrophe may be coupled to autophagy and lysosomal activity. Further understanding of the coupling of death following and aberrant mitosis and autophagic-lysosomal activity may provide further insight into the targeting of CIN+ cancer cells for death.

Chapter 7. Discussion

The causes and consequences of aneuploidy and CIN have been an intriguing part of cancer research ever since von Hansemann reported abnormal mitotic figures in cancer cells and Boveri postulated that aneuploidy may promote cancer (295). It has been established for some time now that patients with CIN+ tumours have a worse prognosis (198, 200, 296) compared to those with diploid or near-diploid tumours.

In 2000, it was proposed that aneuploid cells are able to acquire multidrug resistance at a high rate due to having a high chromosome reassortment rate that confers genetic variation and an evolutionary advantage in the face of selection pressure (11). More recently, our laboratory has shown that CIN+ cells are intrinsically taxane resistant (12, 297). Further examining the link between CIN and intrinsic taxane resistance, my laboratory proposed that CIN+ cancer cells overexpress a set of genes termed the microtubule-stabilising (MTS) gene signature, genes that are repressed following MTS treatment (14), that enables them to survive down-regulation of these genes that occurs following MTS treatment. A similar link was not seen with the non-MTS-targeting cytotoxic, 5-FU. Together with work demonstrating that aneuploid tumours across different tissue types overexpress the CIN70 gene signature (59), this demonstrated that there exists stable gene expression changes in CIN+ cancer cells that enable these cancer cells to be intrinsically taxane resistant. As taxanes function by arresting cells in mitosis and inducing cell death by mitotic catastrophe, this may reflect the property of CIN+ cancer cells to escape proper mitotic surveillance.

Work performed in aneuploid and polyploid yeast (93, 127) suggest that adaptations are required to tolerate abnormal numbers of chromosomes. It has also been proposed that

CIN cells acquire adaptations that enable them to tolerate chromosome missegregations (66). Taken together, it suggests that there indeed exist pathways that are required for survival in CIN+ cancer cells. Indeed, Roschke and colleagues (4, 123) defined several anticancer agents that had preferential activity in cancer cells with more structurally complex chromosomes. Recently, Tang and colleagues proposed that aneuploid cells are more sensitive to energy and protein stress induced by AICAR and 17-AAG treatment (129) and extended their results to a panel of 5 CIN+ and 5 CIN- cell lines.

In my thesis, I set out to identify pathways that are required for the survival of CIN+ human cancer cells in an attempt to both further understand CIN and to provide means to limit the acquisition of CIN in human cancer. In chapter 3, I performed a kinase inhibitor and cytotoxic agent screen to identify compounds that may be selectively lethal in CIN+ cells. I used a large panel (18 CIN+ and 9 CIN-) of CRC cell lines in my studies to allow for the interrogation of a genetically diverse panel of CIN+ and CIN- cell lines with many compounds. Although I was unable to identify a single agent that was selectively lethal towards the CIN+ cancer cells, I demonstrated that CIN+ cancer cells were intrinsically resistant to these compounds of many different mechanisms of action, including 17-AAG and AICAR. Further examining the link between intrinsic multidrug resistance with CIN and polyploidy, I treated two isogenic models of CIN, HCT116 *MAD2+/-* and HCT116 *PTTG1-/-* cell lines, and HCT116 isogenic models of tetraploidy, with the kinase inhibitors and cytotoxic agents. Here, my work suggests that the intrinsic drug resistance phenotype is associated with increased CIN but not increased ploidy. The short time course of my experiments suggested that drug resistance phenotype that I observed was unlikely to be due to adaptive drug resistance. A possible explanation for my findings would be that even at low numbers of cells

(4000 non-clonally derived cells per cell line were plated prior to drug exposure) there may exist sufficient heterogeneity in the CIN+ cancer cell population to enable sub-populations of the cancer cells to survive. An alternative hypothesis would be that cell lines that have acquired CIN also become intrinsically resistant to external stressors, and this may reflect survival adaptations to tolerate CIN, also known as a CIN survival state.

In chapter 4, I discussed my efforts to identify CIN survival pathways using a functional genomics approach. Whole genome RNAi screens were performed in HCT116 diploid parental and HCT116 *MAD2+/-* cell lines. Candidate genes were identified that caused a reduction in cell viability in both cell lines but none appeared to consistently result in greater cell lethality in the CIN+ cancer cell line over the CIN- cell line. While I was unable to identify a CIN survival regulator that consistently targeted CIN+ cancer cells for death, statistical analysis revealed that the RNAi screens may have been sufficiently powered to identify candidate genes resulting in large difference in cell viability between the CIN+ and CIN- cancer cell lines (Power ≈ 75% to detect ≈ 60% difference in cell death). The failure to identify a CIN survival gene may be due to a number of reasons: 1) The isogenic cell lines are too genetically similar in order to enable the identification of a candidate gene that results in a great reduction in cell viability of one cell line but not the other. The lack of published whole genome siRNA screens for synthetic lethality using isogenic cell lines may support this argument. 2) There may not exist a single CIN survival pathway that results in a great reduction in cell viability when silenced in CIN+ cancer cells. This may reflect a dependency on multiple pathways for the survival of CIN+ cancer cells, therefore the disruption of just one pathway may be compensated for by the others.

Supporting the idea that the genome wide screens were not technically flawed, in chapter 5, using cell cycle profile data from the same HCT116 screen as performed in chapter 4, I identified both known and novel ploidy regulators that corresponded to regions of stable genomic loss in CIN+ cancer cell lines. Confirmation and evaluation of the phenotypic changes was performed using light cell microscopy. As it may be challenging to selectively target survival pathways of CIN+ cancer cells in order to induce lethality, an alternative approach to overcoming CIN in cancer may be to limit the acquisition of CIN by targeting ploidy regulators. The novel regulators of ploidy identified here may help achieve that aim although work is needed to further characterise the functions of the genes identified.

Previously, my laboratory demonstrated that CERT when silenced mediates sensitivity to drugs with differing mechanisms of action (12), however the mechanisms of the drug sensitisation were not understood. Further investigation of this pathway was performed as 1) It is a drug sensitivity pathway that may be exploited to induce death in cancer cells including CIN+ cancer cells and 2) CERT depletion results in taxane sensitisation. As CIN+ cells are intrinsically resistant to taxanes, further understanding of the CERT pathway may allow us to understand cell death downstream of mitotic catastrophe and may provide insight into sensitising CIN+ cells to MTS agents. I showed that combination of CERT silencing and drug treatment resulted in changes to autophagic flux. While it has been previously shown that ceramide and ER-stress induction can result in an up-regulation of autophagy, I showed that CERT silencing induced the expression of the lysosomal membrane protein, LAMP2 (that mediates autophagosome-lysosome fusion(298), that was required for the drug sensitisation phenotype following CERT silencing. LAMP2 was not up-regulated by ceramide nor was its expression

altered by the addition of paclitaxel to CERT silencing, suggesting that its change in expression was specific to CERT down-regulation and not due to changes in autophagic flux due to ceramide or ER-stress induced autophagy. I demonstrated that cell death following CERT silencing and paclitaxel treatment is often preceded by an abnormal mitosis and a multinucleated interphase state and by silencing LAMP2, multinucleated cell death was avoided. This may suggest that cells may be sensitive to changes in autophagic flux or lysosomal structure during a mitotic arrest, especially since transcription is halted during mitosis. Alternatively, cells in multinucleated interphase following mitotic slippage may be sensitive to CERT and LAMP2 expression. Interestingly this may link with work demonstrating that changes in lysosomal membrane activity synergise with taxane activity (299) further suggesting that cell death associated with mitotic arrest may be lysosomal dependent.

In conclusion, my work has helped to demonstrate that CIN+ cancer cells are intrinsically more resistant to perturbations of many different pathways compared to CIN- cancer cells. Whilst it is conceivable that the survival and drug resistant properties of a CIN cancer cell population may be consequence of its genetic heterogeneity, an alternative and perhaps more compelling hypothesis is that in order to tolerate CIN a cell must evolve into a survival state that indirectly confers drug resistance. I was not able to identify a survival regulator of CIN+ using an isogenic whole genome RNAi screening model, however, my screen appeared to be sufficiently powered to detect large differences in cell viability. The negative result obtained may reflect the fact that there may not exist a dependency on just a single pathway for survival in CIN+ cancer. However, I have identified novel regulators of ploidy using a functional genomics approach. Finally, my work has helped to provide insight into the mechanisms

regulating drug sensitisation following CERT depletion and possibly indicates that increased autophagic flux or lysosomal activity may be lethal to cells arrested in mitosis or multinucleated cells. This may be exploited to specifically target polyploid cells.

Reference List

1. Ding L, Ellis MJ, Li S, Larson DE, Chen K, Wallis JW, et al. Genome remodelling in a basal-like breast cancer metastasis and xenograft. Nature. 2010 Apr 15;464(7291):999-1005.
2. Shah SP, Morin RD, Khattra J, Prentice L, Pugh T, Burleigh A, et al. Mutational evolution in a lobular breast tumour profiled at single nucleotide resolution. Nature. 2009 Oct 8;461(7265):809-13.
3. Lengauer C, Kinzler KW, Vogelstein B. Genetic instability in colorectal cancers. Nature. 1997 Apr 10;386(6625):623-7.
4. Roschke AV, Tonon G, Gehlhaus KS, McTyre N, Bussey KJ, Lababidi S, et al. Karyotypic complexity of the NCI-60 drug-screening panel. Cancer Res. 2003 Dec 15;63(24):8634-47.
5. Lee AJX, Kolesnick R, Swanton C. RNAi-mediated functional analysis of pathways influencing cancer cell drug resistance. Expert Reviews in Molecular Medicine. 2009;11(1).
6. Lee AJX, Endesfelder D, Rowan AJ, Walther A, Birkbak NJ, Futreal PA, et al. Chromosomal Instability Confers Intrinsic Multidrug Resistance. Cancer Research. 2011 March 1, 2011;71(5):1858-70.
7. Longley DB, Johnston PG. Molecular mechanisms of drug resistance. J Pathol. 2005 Jan;205(2):275-92.
8. Downward J. RNA interference-based functional genomics in cancer research - an introduction. Oncogene. 2000;23(51):8334-5.
9. Nobili S, Landini I, Giglioni B, Mini E. Pharmacological strategies for overcoming multidrug resistance. Curr Drug Targets. 2006 Jul;7(7):861-79.
10. Szakacs G, Paterson JK, Ludwig JA, Booth-Genthe C, Gottesman MM. Targeting multidrug resistance in cancer. Nat Rev Drug Discov. 2006 Mar;5(3):219-34.
11. Duesberg P, Stindl R, Hehlmann R. Explaining the high mutation rates of cancer cells to drug and multidrug resistance by chromosome reassortments that are catalyzed by aneuploidy. Proc Natl Acad Sci U S A. 2000 Dec 19;97(26):14295-300.
12. Swanton C, Marani M, Pardo O, Warne PH, Kelly G, Sahai E, et al. Regulators of mitotic arrest and ceramide metabolism are determinants of sensitivity to paclitaxel and other chemotherapeutic drugs. Cancer Cell. 2007 Jun;11(6):498-512.
13. Sudo T, Nitta M, Saya H, Ueno NT. Dependence of Paclitaxel Sensitivity on a Functional Spindle Assembly Checkpoint. Cancer Res. 2004 April 1, 2004;64(7):2502-8.
14. Swanton C, Nicke B, Schuett M, Eklund AC, Ng C, Li Q, et al. Chromosomal instability determines taxane response. Proceedings of the National Academy of Sciences. 2009 May 26, 2009;106(21):8671-6.
15. Morgan DO. The cell cycle: principles of control: Published by New Science Press in association with Oxford University Press; 2007.
16. Koshland D, Strunnikov A. Mitotic chromosome condensation. Annu Rev Cell Dev Biol. 1996;12:305-33.
17. Blow JJ, Tanaka TU. The chromosome cycle: coordinating replication and segregation. Second in the cycles review series. EMBO Rep. 2005 Nov;6(11):1028-34.
18. Uhlmann F, Nasmyth K. Cohesion between sister chromatids must be established during DNA replication. Curr Biol. 1998 Oct 8;8(20):1095-101.

19. Atherton-Fessler S, Liu F, Gabrielli B, Lee MS, Peng CY, Piwnica-Worms H. Cell cycle regulation of the p34cdc2 inhibitory kinases. Mol Biol Cell. 1994 Sep;5(9):989-1001.
20. Ducommun B, Brambilla P, Felix MA, Franza BR, Jr., Karsenti E, Draetta G. cdc2 phosphorylation is required for its interaction with cyclin. EMBO J. 1991 Nov;10(11):3311-9.
21. Fisher RP, Morgan DO. A novel cyclin associates with MO15/CDK7 to form the CDK-activating kinase. Cell. 1994 Aug 26;78(4):713-24.
22. Larochelle S, Merrick KA, Terret ME, Wohlbold L, Barboza NM, Zhang C, et al. Requirements for Cdk7 in the assembly of Cdk1/cyclin B and activation of Cdk2 revealed by chemical genetics in human cells. Mol Cell. 2007 Mar 23;25(6):839-50.
23. Strausfeld U, Labbe JC, Fesquet D, Cavadore JC, Picard A, Sadhu K, et al. Dephosphorylation and activation of a p34cdc2/cyclin B complex in vitro by human CDC25 protein. Nature. 1991 May 16;351(6323):242-5.
24. Timofeev O, Cizmecioglu O, Settele F, Kempf T, Hoffmann I. Cdc25 Phosphatases Are Required for Timely Assembly of CDK1-Cyclin B at the G2/M Transition. Journal of Biological Chemistry. 2010 May 28, 2010;285(22):16978-90.
25. Kimura K, Hirano M, Kobayashi R, Hirano T. Phosphorylation and activation of 13S condensin by Cdc2 in vitro. Science. 1998 Oct 16;282(5388):487-90.
26. Heald R, McKeon F. Mutations of phosphorylation sites in lamin A that prevent nuclear lamina disassembly in mitosis. Cell. 1990 May 18;61(4):579-89.
27. Musacchio A, Salmon ED. The spindle-assembly checkpoint in space and time. Nat Rev Mol Cell Biol. 2007 May;8(5):379-93.
28. Tanaka TU, Stark MJR, Tanaka K. Kinetochore capture and bi-orientation on the mitotic spindle. Nat Rev Mol Cell Biol. [10.1038/nrm1764]. 2005;6(12):929-42.
29. Winey M, Mamay CL, O'Toole ET, Mastronarde DN, Giddings TH, Jr., McDonald KL, et al. Three-dimensional ultrastructural analysis of the Saccharomyces cerevisiae mitotic spindle. J Cell Biol. 1995 Jun;129(6):1601-15.
30. Hayden JH, Bowser SS, Rieder CL. Kinetochores capture astral microtubules during chromosome attachment to the mitotic spindle: direct visualization in live newt lung cells. The Journal of Cell Biology. 1990 September 1, 1990;111(3):1039-45.
31. Maiato H, DeLuca J, Salmon ED, Earnshaw WC. The dynamic kinetochore-microtubule interface. J Cell Sci. 2004 Nov 1;117(Pt 23):5461-77.
32. Peters J-M. The anaphase promoting complex/cyclosome: a machine designed to destroy. Nat Rev Mol Cell Biol. [10.1038/nrm1988]. 2006;7(9):644-56.
33. Uhlmann F, Lottspeich F, Nasmyth K. Sister-chromatid separation at anaphase onset is promoted by cleavage of the cohesin subunit Scc1. Nature. 1999 Jul 1;400(6739):37-42.
34. Stegmeier F, Amon A. Closing mitosis: the functions of the Cdc14 phosphatase and its regulation. Annu Rev Genet. 2004;38:203-32.
35. Clute P, Pines J. Temporal and spatial control of cyclin B1 destruction in metaphase. Nat Cell Biol. [10.1038/10049]. 1999;1(2):82-7.
36. Hauf S, Cole RW, LaTerra S, Zimmer C, Schnapp G, Walter R, et al. The small molecule Hesperadin reveals a role for Aurora B in correcting kinetochore,Äìmicrotubule attachment and in maintaining the spindle assembly checkpoint. The Journal of Cell Biology. 2003 April 28, 2003;161(2):281-94.
37. Tanaka TU, Rachidi N, Janke C, Pereira G, Galova M, Schiebel E, et al. Evidence that the Ipl1-Sli15 (Aurora kinase-INCENP) complex promotes chromosome

bi-orientation by altering kinetochore-spindle pole connections. Cell. 2002 Feb 8;108(3):317-29.
38. Cheeseman IM, Anderson S, Jwa M, Green EM, Kang J, Yates JR, 3rd, et al. Phospho-regulation of kinetochore-microtubule attachments by the Aurora kinase Ipl1p. Cell. 2002 Oct 18;111(2):163-72.
39. Gregan J, Polakova S, Zhang L, Toli -N¯rrelykke IM, Cimini D. Merotelic kinetochore attachment: causes and effects. Trends in Cell Biology. 2011;21(6):374-81.
40. Chen R-H, Shevchenko A, Mann M, Murray AW. Spindle Checkpoint Protein Xmad1 Recruits Xmad2 to Unattached Kinetochores. The Journal of Cell Biology. 1998 October 19, 1998;143(2):283-95.
41. Chen R-H, Waters JC, Salmon ED, Murray AW. Association of Spindle Assembly Checkpoint Component XMAD2 with Unattached Kinetochores. Science. 1996 October 11, 1996;274(5285):242-6.
42. Sudakin V, Chan GKT, Yen TJ. Checkpoint inhibition of the APC/C in HeLa cells is mediated by a complex of BUBR1, BUB3, CDC20, and MAD2. J Cell Biol. 2001 September 3, 2001;154(5):925-36.
43. Morrow CJ, Tighe A, Johnson VL, Scott MIF, Ditchfield C, Taylor SS. Bub1 and aurora B cooperate to maintain BubR1-mediated inhibition of APC/CCdc20. Journal of Cell Science. 2005 August 15, 2005;118(16):3639-52.
44. Nicklas RB, Ward SC, Gorbsky GJ. Kinetochore chemistry is sensitive to tension and may link mitotic forces to a cell cycle checkpoint. J Cell Biol. 1995 Aug;130(4):929-39.
45. Cimini D, Howell B, Maddox P, Khodjakov A, Degrassi F, Salmon ED. Merotelic Kinetochore Orientation Is a Major Mechanism of Aneuploidy in Mitotic Mammalian Tissue Cells. The Journal of Cell Biology. 2001 April 30, 2001;153(3):517-28.
46. Blagosklonny MV. Mitotic arrest and cell fate: why and how mitotic inhibition of transcription drives mutually exclusive events. Cell Cycle. 2007 Jan 1;6(1):70-4.
47. Smith J, Tho LM, Xu N, Gillespie DA. The ATM-Chk2 and ATR-Chk1 pathways in DNA damage signaling and cancer. Adv Cancer Res. 2010;108:73-112.
48. Peng CY, Graves PR, Thoma RS, Wu Z, Shaw AS, Piwnica-Worms H. Mitotic and G2 checkpoint control: regulation of 14-3-3 protein binding by phosphorylation of Cdc25C on serine-216. Science. 1997 Sep 5;277(5331):1501-5.
49. Wang H, Liu D, Wang Y, Qin J, Elledge SJ. Pds1 phosphorylation in response to DNA damage is essential for its DNA damage checkpoint function. Genes Dev. 2001 Jun 1;15(11):1361-72.
50. Agarwal R, Tang Z, Yu H, Cohen-Fix O. Two distinct pathways for inhibiting pds1 ubiquitination in response to DNA damage. J Biol Chem. 2003 Nov 7;278(45):45027-33.
51. Lengauer C, Kinzler KW, Vogelstein B. Genetic instabilities in human cancers. Nature. 1998 Dec 17;396(6712):643-9.
52. Venkitaraman AR. Chromosomal instability in cancer: causality and interdependence. Cell Cycle. 2007 Oct 1;6(19):2341-3.
53. Lothe RA, Peltomaki P, Meling GI, Aaltonen LA, Nystrom-Lahti M, Pylkkanen L, et al. Genomic instability in colorectal cancer: relationship to clinicopathological variables and family history. Cancer Res. 1993 Dec 15;53(24):5849-52.

54. Thibodeau SN, French AJ, Cunningham JM, Tester D, Burgart LJ, Roche PC, et al. Microsatellite instability in colorectal cancer: different mutator phenotypes and the principal involvement of hMLH1. Cancer Res. 1998 Apr 15;58(8):1713-8.
55. Walther A, Houlston R, Tomlinson I. Association between chromosomal instability and prognosis in colorectal cancer: a meta-analysis. Gut. 2008 Mar 27.
56. Hiddemann W, Schumann J, Andreef M, Barlogie B, Herman CJ, Leif RC, et al. Convention on nomenclature for DNA cytometry. Cancer Genetics and Cytogenetics. 1984;13(2):181-3.
57. Walther A, Johnstone E, Swanton C, Midgley R, Tomlinson I, Kerr D. Genetic prognostic and predictive markers in colorectal cancer. Nat Rev Cancer. 2009 Jul;9(7):489-99.
58. Kronenwett U, Huwendiek Sr, Ostring C, Portwood N, Roblick UJ, Pawitan Y, et al. Improved Grading of Breast Adenocarcinomas Based on Genomic Instability. Cancer Research. 2004 February 1, 2004;64(3):904-9.
59. Carter SL, Eklund AC, Kohane IS, Harris LN, Szallasi Z. A signature of chromosomal instability inferred from gene expression profiles predicts clinical outcome in multiple human cancers. Nat Genet. 2006 Sep;38(9):1043-8.
60. Birkbak NJ, Eklund AC, Li Q, McClelland SE, Endesfelder D, Tan P, et al. Paradoxical Relationship between Chromosomal Instability and Survival Outcome in Cancer. Cancer Research. 2011 May 15, 2011;71(10):3447-52.
61. Chin S, Teschendorff A, Marioni J, Wang Y, Barbosa-Morais N, Thorne N, et al. High-resolution aCGH and expression profiling identifies a novel genomic subtype of ER negative breast cancer. Genome Biology. 2007;8(10):R215.
62. Lingle WL, Barrett SL, Negron VC, D'Assoro AB, Boeneman K, Liu W, et al. Centrosome amplification drives chromosomal instability in breast tumor development. Proc Natl Acad Sci U S A. 2002 Feb 19;99(4):1978-83.
63. Greenman CD, Bignell G, Butler A, Edkins S, Hinton J, Beare D, et al. PICNIC: an algorithm to predict absolute allelic copy number variation with microarray cancer data. Biostatistics. 2010 Jan;11(1):164-75.
64. Colella S, Yau C, Taylor JM, Mirza G, Butler H, Clouston P, et al. QuantiSNP: an Objective Bayes Hidden-Markov Model to detect and accurately map copy number variation using SNP genotyping data. Nucleic Acids Res. 2007;35(6):2013-25.
65. Habermann JK, Doering J, Hautaniemi S, Roblick UJ, Bundgen NK, Nicorici D, et al. The gene expression signature of genomic instability in breast cancer is an independent predictor of clinical outcome. Int J Cancer. 2009 Apr 1;124(7):1552-64.
66. Thompson SL, Compton DA. Examining the link between chromosomal instability and aneuploidy in human cells. J Cell Biol. 2008 February 25, 2008;180(4):665-72.
67. Wang Q, Moyret-Lalle C, Couzon F, Surbiguet-Clippe C, Saurin JC, Lorca T, et al. Alterations of anaphase-promoting complex genes in human colon cancer cells. Oncogene. 2003 Mar 13;22(10):1486-90.
68. Sarafan-Vasseur N, Lamy A, Bourguignon J, Le Pessot F, Hieter P, Sesboue R, et al. Overexpression of B-type cyclins alters chromosomal segregation. Oncogene. 2002 Mar 27;21(13):2051-7.
69. Cahill DP. Mutations of mitotic checkpoint genes in human cancers. Nature. [10.1038/32688]. 1998;392:300-3.

70. Michel LS. MAD2 haplo-insufficiency causes premature anaphase and chromosome instability in mammalian cells. Nature. [10.1038/35053094]. 2001;409:355-9.
71. Tsukasaki K, Miller CW, Greenspun E, Eshaghian S, Kawabata H, Fujimoto T, et al. Mutations in the mitotic check point gene, MAD1L1, in human cancers. Oncogene. 2001 May 31;20(25):3301-5.
72. Burum-Auensen E, DeAngelis PM, Schj¯lberg AR, R¯islien J, MjÂland O, Clausen OPF. Reduced level of the spindle checkpoint protein BUB1B is associated with aneuploidy in colorectal cancers. Cell Proliferation. 2008;41(4):645-59.
73. Cleveland DW, Mao Y, Sullivan KF. Centromeres and kinetochores: from epigenetics to mitotic checkpoint signaling. Cell. 2003 Feb 21;112(4):407-21.
74. Janssen A, Kops GJPL, Medema RH. Elevating the frequency of chromosome mis-segregation as a strategy to kill tumor cells. Proceedings of the National Academy of Sciences. 2009 November 10, 2009;106(45):19108-13.
75. Sotillo R, Schvartzman J-M, Socci ND, Benezra R. Mad2-induced chromosome instability leads to lung tumour relapse after oncogene withdrawal. Nature. 2010;464(7287):436-40.
76. Gascoigne KE, Taylor SS. Cancer Cells Display Profound Intra- and Interline Variation following Prolonged Exposure to Antimitotic Drugs. Cancer Cell. 2008;14(2):111-22.
77. Tighe A, Johnson VL, Albertella M, Taylor SS. Aneuploid colon cancer cells have a robust spindle checkpoint. EMBO Rep. 2001 Jul;2(7):609-14.
78. Cancer Genome Project. [Internet] Cambridge, UK: Wellcome Trust Sanger Institute; 2010 [updated 2010 Dec 20; cited 2010 Dec 23]; Available from: http://www.sanger.ac.uk/genetics/CGP.
79. Cheeseman IM, Desai A. Molecular architecture of the kinetochore-microtubule interface. Nat Rev Mol Cell Biol. 2008;9(1):33-46.
80. Jallepalli PV, Waizenegger IC, Bunz F, Langer S, Speicher MR, Peters JM, et al. Securin is required for chromosomal stability in human cells. Cell. 2001 May 18;105(4):445-57.
81. Ogbagabriel S, Fernando M, Waldman FM, Bose S, Heaney AP. Securin is overexpressed in breast cancer. Mod Pathol. 2005;18(7):985-90.
82. Hagting A, Den Elzen N, Vodermaier HC, Waizenegger IC, Peters JM, Pines J. Human securin proteolysis is controlled by the spindle checkpoint and reveals when the APC/C switches from activation by Cdc20 to Cdh1. J Cell Biol. 2002 Jun 24;157(7):1125-37.
83. Brinkley BR, Goepfert TM. Supernumerary centrosomes and cancer: Boveri's hypothesis resurrected. Cell Motil Cytoskeleton. 1998;41(4):281-8.
84. Pihan GA, Purohit A, Wallace J, Malhotra R, Liotta L, Doxsey SJ. Centrosome Defects Can Account for Cellular and Genetic Changes That Characterize Prostate Cancer Progression. Cancer Res. 2001 March 1, 2001;61(5):2212-9.
85. Sakakura C, Hagiwara A, Yasuoka R, Fujita Y, Nakanishi M, Masuda K, et al. Tumour-amplified kinase BTAK is amplified and overexpressed in gastric cancers with possible involvement in aneuploid formation. Br J Cancer. 2001 Mar 23;84(6):824-31.
86. Meraldi P, Honda R, Nigg EA. Aurora-A overexpression reveals tetraploidization as a major route to centrosome amplification in p53-/- cells. EMBO J. [10.1093/emboj/21.4.483]. 2002;21:483-92.

87. Zhou H, Kuang J, Zhong L, Kuo WL, Gray JW, Sahin A, et al. Tumour amplified kinase STK15/BTAK induces centrosome amplification, aneuploidy and transformation. Nat Genet. 1998 Oct;20(2):189-93.
88. Wang X, Zhou YX, Qiao W, Tominaga Y, Ouchi M, Ouchi T, et al. Overexpression of aurora kinase A in mouse mammary epithelium induces genetic instability preceding mammary tumor formation. Oncogene. 2006;25(54):7148-58.
89. Ganem NJ, Godinho SA, Pellman D. A mechanism linking extra centrosomes to chromosomal instability. Nature. 2009 Jul 9;460(7252):278-82.
90. Duncan AW, Taylor MH, Hickey RD, Hanlon Newell AE, Lenzi ML, Olson SB, et al. The ploidy conveyor of mature hepatocytes as a source of genetic variation. Nature. 2010 Oct 7;467(7316):707-10.
91. Bakhoum SF, Thompson SL, Manning AL, Compton DA. Genome stability is ensured by temporal control of kinetochore-microtubule dynamics. Nature Cell Biol. 2008;11:27-35.
92. Mayer TU, Kapoor TM, Haggarty SJ, King RW, Schreiber SL, Mitchison TJ. Small molecule inhibitor of mitotic spindle bipolarity identified in a phenotype-based screen. Science. 1999 Oct 29;286(5441):971-4.
93. Storchova Z, Breneman A, Cande J, Dunn J, Burbank K, O'Toole E, et al. Genome-wide genetic analysis of polyploidy in yeast. Nature. 2006 Oct 5;443(7111):541-7.
94. Mayer VW, Aguilera A. High levels of chromosome instability in polyploids of Saccharomyces cerevisiae. Mutat Res. 1990 Aug;231(2):177-86.
95. Fukasawa K, Vande Woude G. Synergy between the Mos/mitogen-activated protein kinase pathway and loss of p53 function in transformation and chromosome instability. Mol Cell Biol. 1997 January 1, 1997;17(1):506-18.
96. Wu Q, Sahasrabudhe RM, Luo LZ, Lewis DW, Gollin SM, Saunders WS. Deficiency in myosin light-chain phosphorylation causes cytokinesis failure and multipolarity in cancer cells. Oncogene. 2010;29(29):4183-93.
97. Davies AH, Barrett I, Pambid MR, Hu K, Stratford AL, Freeman S, et al. YB-1 evokes susceptibility to cancer through cytokinesis failure, mitotic dysfunction and HER2 amplification. Oncogene. 2011 Mar 21.
98. Shi Q, King RW. Chromosome nondisjunction yields tetraploid rather than aneuploid cells in human cell lines. Nature. 2005 Oct 13;437(7061):1038-42.
99. Tatsuka M, Katayama H, Ota T, Tanaka T, Odashima S, Suzuki F, et al. Multinuclearity and Increased Ploidy Caused by Overexpression of the Aurora- and Ipl1-like Midbody-associated Protein Mitotic Kinase in Human Cancer Cells. Cancer Research. 1998 November 1, 1998;58(21):4811-6.
100. Fujiwara T, Bandi M, Nitta M, Ivanova EV, Bronson RT, Pellman D. Cytokinesis failure generating tetraploids promotes tumorigenesis in p53-null cells. Nature. 2005 Oct 13;437(7061):1043-7.
101. Sheffer M, Bacolod MD, Zuk O, Giardina SF, Pincas H, Barany F, et al. Association of survival and disease progression with chromosomal instability: A genomic exploration of colorectal cancer. Proceedings of the National Academy of Sciences. 2009 April 28, 2009;106(17):7131-6.
102. Cahill DP, Kinzler KW, Vogelstein B, Lengauer C. Genetic instability and darwinian selection in tumours. Trends in Cell Biology. 1999;9(12):M57-M60.
103. Nicholson JM, Duesberg P. On the karyotypic origin and evolution of cancer cells. Cancer Genetics and Cytogenetics. 2009;194(2):96-110.

104. Chandhok NS, Pellman D. A little CIN may cost a lot: revisiting aneuploidy and cancer. Current Opinion in Genetics & Development. 2009;19(1):74-81.
105. Roylance R, Endesfelder D, Gorman P, Burrell RA, Sander J, Tomlinson I, et al. Relationship of Extreme Chromosomal Instability with Long-term Survival in a Retrospective Analysis of Primary Breast Cancer. Cancer Epidemiology Biomarkers & Prevention. 2011 October 1, 2011;20(10):2183-94.
106. Nowell P. The clonal evolution of tumor cell populations. Science. 1976 October 1, 1976;194(4260):23-8.
107. Anderson K, Lutz C, van Delft FW, Bateman CM, Guo Y, Colman SM, et al. Genetic variegation of clonal architecture and propagating cells in leukaemia. Nature. 2011 Jan 20;469(7330):356-61.
108. Weaver BAA, Silk AD, Montagna C, Verdier-Pinard P, Cleveland DW. Aneuploidy Acts Both Oncogenically and as a Tumor Suppressor. Cancer Cell. [doi: DOI: 10.1016/j.ccr.2006.12.003]. 2007;11(1):25-36.
109. Hanks S, Coleman K, Reid S, Plaja A, Firth H, Fitzpatrick D, et al. Constitutional aneuploidy and cancer predisposition caused by biallelic mutations in BUB1B. Nat Genet. 2004 Nov;36(11):1159-61.
110. Rancati G, Pavelka N, Fleharty B, Noll A, Trimble R, Walton K, et al. Aneuploidy underlies rapid adaptive evolution of yeast cells deprived of a conserved cytokinesis motor. Cell. 2008 Nov 28;135(5):879-93.
111. Schiff PB, Fant J, Horwitz SB. Promotion of microtubule assembly in vitro by taxol. Nature. 1979 Feb 22;277(5698):665-7.
112. Schiff PB, Horwitz SB. Taxol stabilizes microtubules in mouse fibroblast cells. Proc Natl Acad Sci U S A. 1980 Mar;77(3):1561-5.
113. Vogel C, Kienitz A, Hofmann I, Muller R, Bastians H. Crosstalk of the mitotic spindle assembly checkpoint with p53 to prevent polyploidy. Oncogene. 2004;23(41):6845-53.
114. Roberts JR, Allison DC, Donehower RC, Rowinsky EK. Development of polyploidization in taxol-resistant human leukemia cells in vitro. Cancer Res. 1990 Feb 1;50(3):710-6.
115. Kops GJ, Foltz DR, Cleveland DW. Lethality to human cancer cells through massive chromosome loss by inhibition of the mitotic checkpoint. Proc Natl Acad Sci USA. [10.1073/pnas.0401142101]. 2004;101:8699-704.
116. Whitehurst AW, Bodemann BO, Cardenas J, Ferguson D, Girard L, Peyton M, et al. Synthetic lethal screen identification of chemosensitizer loci in cancer cells. Nature. 2007 Apr 12;446(7137):815-9.
117. Weingarten MD, Lockwood AH, Hwo SY, Kirschner MW. A protein factor essential for microtubule assembly. Proc Natl Acad Sci U S A. 1975 May;72(5):1858-62.
118. Rouzier R, Rajan R, Wagner P, Hess KR, Gold DL, Stec J, et al. Microtubule-associated protein tau: a marker of paclitaxel sensitivity in breast cancer. Proc Natl Acad Sci U S A. 2005 Jun 7;102(23):8315-20.
119. Muller HJ. THE RELATION OF RECOMBINATION TO MUTATIONAL ADVANCE. Mutat Res. 1964 May;106:2-9.
120. Lynch M, B√ºrger R, Butcher D, Gabriel W. The Mutational Meltdown in Asexual Populations. Journal of Heredity. 1993 September 1, 1993;84(5):339-44.

121. Allen JM, Light JE, Perotti MA, Braig HR, Reed DL. Mutational Meltdown in Primary Endosymbionts: Selection Limits Muller's Ratchet. PLoS ONE. 2009;4(3):e4969.
122. Kops GJPL, Foltz DR, Cleveland DW. Lethality to human cancer cells through massive chromosome loss by inhibition of the mitotic checkpoint. Proceedings of the National Academy of Sciences of the United States of America. 2004 June 8, 2004;101(23):8699-704.
123. Roschke AV, Kirsch IR. Targeting cancer cells by exploiting karyotypic complexity and chromosomal instability. Cell Cycle. 2005 May;4(5):679-82.
124. Torres EM, Williams BR, Amon A. Aneuploidy: cells losing their balance. Genetics. 2008 Jun;179(2):737-46.
125. Williams BR, Prabhu VR, Hunter KE, Glazier CM, Whittaker CA, Housman DE, et al. Aneuploidy Affects Proliferation and Spontaneous Immortalization in Mammalian Cells. Science. 2008 October 31, 2008;322(5902):703-9.
126. Segal DJ, McCoy EE. Studies on Down's syndrome in tissue culture. I. Growth rates protein contents of fibroblast cultures. Journal of Cellular Physiology. 1974;83(1):85-90.
127. Torres EM, Sokolsky T, Tucker CM, Chan LY, Boselli M, Dunham MJ, et al. Effects of aneuploidy on cellular physiology and cell division in haploid yeast. Science. 2007 Aug 17;317(5840):916-24.
128. Pavelka N, Rancati G, Zhu J, Bradford WD, Saraf A, Florens L, et al. Aneuploidy confers quantitative proteome changes and phenotypic variation in budding yeast. Nature. 2010 Nov 11;468(7321):321-5.
129. Tang Y-C, Williams BR, Siegel JJ, Amon A. Identification of Aneuploidy-Selective Antiproliferation Compounds. Cell. [doi: DOI: 10.1016/j.cell.2011.01.017]. 2011;144(4):499-512.
130. Ogretmen B, Hannun YA. Biologically active sphingolipids in cancer pathogenesis and treatment. Nat Rev Cancer. 2004 Aug;4(8):604-16.
131. Obeid LM, Linardic CM, Karolak LA, Hannun YA. Programmed cell death induced by ceramide. Science. 1993 Mar 19;259(5102):1769-71.
132. Pettus BJ, Chalfant CE, Hannun YA. Ceramide in apoptosis: an overview and current perspectives. Biochim Biophys Acta. 2002 Dec 30;1585(2-3):114-25.
133. Kolesnick R. The therapeutic potential of modulating the ceramide/sphingomyelin pathway. J Clin Invest. 2002 Jul;110(1):3-8.
134. Juul N, Szallasi Z, Eklund AC, Li Q, Burrell RA, Gerlinger M, et al. Assessment of an RNA interference screen-derived mitotic and ceramide pathway metagene as a predictor of response to neoadjuvant paclitaxel for primary triple-negative breast cancer: a retrospective analysis of five clinical trials. Lancet Oncol. 2010 Apr;11(4):358-65.
135. Hanada K, Kumagai K, Yasuda S, Miura Y, Kawano M, Fukasawa M, et al. Molecular machinery for non-vesicular trafficking of ceramide. Nature. 2003 Dec 18;426(6968):803-9.
136. Raya A, Revert-Ros F, Martinez-Martinez P, Navarro S, Rosell√≥ E, Vieites Ba, et al. Goodpasture Antigen-binding Protein, the Kinase That Phosphorylates the Goodpasture Antigen, Is an Alternatively Spliced Variant Implicated in Autoimmune Pathogenesis. Journal of Biological Chemistry. 2000 December 22, 2000;275(51):40392-9.

137. Ponting CP, Aravind L. START: a lipid-binding domain in StAR, HD-ZIP and signalling proteins. Trends in Biochemical Sciences. [doi: 10.1016/S0968-0004(99)01362-6]. 1999;24(4):130-2.
138. Funakoshi T, Yasuda S, Fukasawa M, Nishijima M, Hanada K. Reconstitution of ATP- and Cytosol-dependent Transport of de Novo Synthesized Ceramide to the Site of Sphingomyelin Synthesis in Semi-intact Cells. Journal of Biological Chemistry. 2000 September 29, 2000;275(39):29938-45.
139. Hannun YA, Obeid LM. Principles of bioactive lipid signalling: lessons from sphingolipids. Nat Rev Mol Cell Biol. 2008;9(2):139-50.
140. Itoh M, Kitano T, Watanabe M, Kondo T, Yabu T, Taguchi Y, et al. Possible Role of Ceramide as an Indicator of Chemoresistance: Decrease of the Ceramide Content via Activation of Glucosylceramide Synthase and Sphingomyelin Synthase in Chemoresistant Leukemia. Clin Cancer Res. 2003 January 1, 2003;9(1):415-23.
141. Liu X, Elojeimy S, Turner LS, Mahdy AE, Zeidan YH, Bielawska A, et al. Acid ceramidase inhibition: a novel target for cancer therapy. Front Biosci. 2008;13:2293-8.
142. Dawson K, Toone WM, Jones N, Wilkinson CRM. Loss of Regulators of Vacuolar ATPase Function and Ceramide Synthesis Results in Multidrug Sensitivity in Schizosaccharomyces pombe. Eukaryotic Cell. 2008 June 1, 2008;7(6):926-37.
143. Min J, Mesika A, Sivaguru M, Van Veldhoven PP, Alexander H, Futerman AH, et al. (Dihydro)ceramide Synthase 1 Regulated Sensitivity to Cisplatin Is Associated with the Activation of p38 Mitogen-Activated Protein Kinase and Is Abrogated by Sphingosine Kinase 1. Molecular Cancer Research. 2007 August 2007;5(8):801-12.
144. Gouaze V, Liu Y-Y, Prickett CS, Yu JY, Giuliano AE, Cabot MC. Glucosylceramide Synthase Blockade Down-Regulates P-Glycoprotein and Resensitizes Multidrug-Resistant Breast Cancer Cells to Anticancer Drugs. Cancer Res. 2005 May 1, 2005;65(9):3861-7.
145. Scarlatti F, Bauvy C, Ventruti A, Sala G, Cluzeaud F, Vandewalle A, et al. Ceramide-mediated macroautophagy involves inhibition of protein kinase B and up-regulation of beclin 1. J Biol Chem. 2004 Apr 30;279(18):18384-91.
146. Yorimitsu T, Nair U, Yang Z, Klionsky DJ. Endoplasmic reticulum stress triggers autophagy. J Biol Chem. 2006 Oct 6;281(40):30299-304.
147. Bernales S, McDonald KL, Walter P. Autophagy counterbalances endoplasmic reticulum expansion during the unfolded protein response. PLoS Biol. 2006 Nov;4(12):e423.
148. Guenther GG, Peralta ER, Rosales KR, Wong SY, Siskind LJ, Edinger AL. Ceramide starves cells to death by downregulating nutrient transporter proteins. Proc Natl Acad Sci U S A. 2008 Nov 11;105(45):17402-7.
149. Mizushima N. Autophagy: process and function. Genes & Development. 2007 November 15, 2007;21(22):2861-73.
150. Eskelinen EL. Maturation of autophagic vacuoles in Mammalian cells. Autophagy. 2005 Apr;1(1):1-10.
151. Levine B, Yuan J. Autophagy in cell death: an innocent convict? J Clin Invest. 2005 Oct;115(10):2679-88.
152. Kroemer G, Levine B. Autophagic cell death: the story of a misnomer. Nat Rev Mol Cell Biol. 2008 Dec;9(12):1004-10.
153. Broker LE, Huisman C, Span SW, Rodriguez JA, Kruyt FA, Giaccone G. Cathepsin B mediates caspase-independent cell death induced by microtubule

stabilizing agents in non-small cell lung cancer cells. Cancer Res. 2004 Jan 1;64(1):27-30.
154. Groth-Pedersen L, Ostenfeld MS, Hoyer-Hansen M, Nylandsted J, Jaattela M. Vincristine induces dramatic lysosomal changes and sensitizes cancer cells to lysosome-destabilizing siramesine. Cancer Res. 2007 Mar 1;67(5):2217-25.
155. Glasspool RM, Teodoridis JM, Brown R. Epigenetics as a mechanism driving polygenic clinical drug resistance. Br J Cancer. 2006 Apr 24;94(8):1087-92.
156. Duesberg P, Stindl R, Hehlmann R. Origin of multidrug resistance in cells with and without multidrug resistance genes: Chromosome reassortments catalyzed by aneuploidy. Proceedings of the National Academy of Sciences of the United States of America. 2001 September 25, 2001;98(20):11283-8.
157. Woodford-Richens KL, Rowan AJ, Gorman P, Halford S, Bicknell DC, Wasan HS, et al. SMAD4 mutations in colorectal cancer probably occur before chromosomal instability, but after divergence of the microsatellite instability pathway. Proceedings of the National Academy of Sciences of the United States of America. 2001 August 14, 2001;98(17):9719-23.
158. Gaasenbeek M, Howarth K, Rowan AJ, Gorman PA, Jones A, Chaplin T, et al. Combined Array-Comparative Genomic Hybridization and Single-Nucleotide Polymorphism-Loss of Heterozygosity Analysis Reveals Complex Changes and Multiple Forms of Chromosomal Instability in Colorectal Cancers. Cancer Res. 2006 April 1, 2006;66(7):3471-9.
159. Abdel-Rahman WM, Katsura K, Rens W, Gorman PA, Sheer D, Bicknell D, et al. Spectral karyotyping suggests additional subsets of colorectal cancers characterized by pattern of chromosome rearrangement. Proceedings of the National Academy of Sciences of the United States of America. 2001 February 27, 2001;98(5):2538-43.
160. Liu Y, Bodmer WF. Analysis of P53 mutations and their expression in 56 colorectal cancer cell lines. Proceedings of the National Academy of Sciences of the United States of America. 2006 January 24, 2006;103(4):976-81.
161. Rowan AJ, Lamlum H, Ilyas M, Wheeler J, Straub J, Papadopoulou A, et al. APC mutations in sporadic colorectal tumors: A mutational "hotspot" and interdependence of the "two hits". Proceedings of the National Academy of Sciences of the United States of America. 2000 March 28, 2000;97(7):3352-7.
162. Ilyas M, Tomlinson IPM, Rowan A, Pignatelli M, Bodmer WF. Beta-Catenin mutations in cell lines established from human colorectal cancers. Proceedings of the National Academy of Sciences of the United States of America. 1997 September 16, 1997;94(19):10330-4.
163. Samuels Y, Diaz Jr LA, Schmidt-Kittler O, Cummins JM, DeLong L, Cheong I, et al. Mutant PIK3CA promotes cell growth and invasion of human cancer cells. Cancer Cell. 2005;7(6):561-73.
164. Michel LS, Liberal V, Chatterjee A, Kirchwegger R, Pasche B, Gerald W, et al. MAD2 haplo-insufficiency causes premature anaphase and chromosome instability in mammalian cells. Nature. 2001 Jan 18;409(6818):355-9.
165. Inhibitor Libraries and Pathway Panels. [Internet] Darmstadt, Germany: Merck KGaA; 2010 [cited 2010 Dec 23]; Available from: http://www.emdchemicals.com/life-science-research/inhibitor-libraries-and-pathway-panels/c_bKSb.s1O9nQAAAEitTV5hDHD#docs.

166. Matthias Kahm GH, Hella Lichtenberg-Fraté, Jost Ludwig, Maik Kschischo. grofit: Fitting Biological Growth Curves with R. Journal of Statistical Software. 2010;33(7).
167. Parmar MK, Torri V, Stewart L. Extracting summary statistics to perform meta-analyses of the published literature for survival endpoints. Stat Med. 1998 Dec 30;17(24):2815-34.
168. Anderson MJ. Permutation tests for univariate or multivariate analysis of variance and regression. Canadian Journal of Fisheries and Aquatic Sciences. 2001;58:626-39.
169. Irizarry RA, Hobbs B, Collin F, Beazer-Barclay YD, Antonellis KJ, Scherf U, et al. Exploration, normalization, and summaries of high density oligonucleotide array probe level data. Biostatistics. 2003 Apr;4(2):249-64.
170. Gentleman RC, Carey VJ, Bates DM, Bolstad B, Dettling M, Dudoit S, et al. Bioconductor: open software development for computational biology and bioinformatics. Genome Biol. 2004;5(10):R80.
171. Subramanian A, Tamayo P, Mootha VK, Mukherjee S, Ebert BL, Gillette MA, et al. Gene set enrichment analysis: A knowledge-based approach for interpreting genome-wide expression profiles. Proceedings of the National Academy of Sciences of the United States of America. 2005 October 25, 2005;102(43):15545-50.
172. Mootha VK, Lindgren CM, Eriksson KF, Subramanian A, Sihag S, Lehar J, et al. PGC-1alpha-responsive genes involved in oxidative phosphorylation are coordinately downregulated in human diabetes. Nat Genet. 2003 Jul;34(3):267-73.
173. Detre S, Saclani Jotti G, Dowsett M. A "quickscore" method for immunohistochemical semiquantitation: validation for oestrogen receptor in breast carcinomas. J Clin Pathol. 1995 Sep;48(9):876-8.
174. Hothorn T, Lausen B. On the exact distribution of maximally selected rank statistics. Comput Stat Data Anal. 2003;43(2):121-37.
175. Hothorn T, Lausen B. Maximally Selected Rank Statistics in R. R News. 2002;2(1):3-5.
176. Chin K, DeVries S, Fridlyand J, Spellman PT, Roydasgupta R, Kuo WL, et al. Genomic and transcriptional aberrations linked to breast cancer pathophysiologies. Cancer Cell. 2006 Dec;10(6):529-41.
177. Desmedt C, Haibe-Kains B, Wirapati P, Buyse M, Larsimont D, Bontempi G, et al. Biological processes associated with breast cancer clinical outcome depend on the molecular subtypes. Clin Cancer Res. 2008 Aug 15;14(16):5158-65.
178. Lu X, Wang ZC, Iglehart JD, Zhang X, Richardson AL. Predicting features of breast cancer with gene expression patterns. Breast Cancer Res Treat. 2008 Mar;108(2):191-201.
179. Minn AJ, Gupta GP, Siegel PM, Bos PD, Shu W, Giri DD, et al. Genes that mediate breast cancer metastasis to lung. Nature. 2005 Jul 28;436(7050):518-24.
180. Pawitan Y, Bjohle J, Amler L, Borg AL, Egyhazi S, Hall P, et al. Gene expression profiling spares early breast cancer patients from adjuvant therapy: derived and validated in two population-based cohorts. Breast Cancer Res. 2005;7(6):R953-64.
181. Sotiriou C, Wirapati P, Loi S, Harris A, Fox S, Smeds J, et al. Gene expression profiling in breast cancer: understanding the molecular basis of histologic grade to improve prognosis. J Natl Cancer Inst. 2006 Feb 15;98(4):262-72.

182. Wang Y, Klijn JG, Zhang Y, Sieuwerts AM, Look MP, Yang F, et al. Gene-expression profiles to predict distant metastasis of lymph-node-negative primary breast cancer. Lancet. 2005 Feb 19-25;365(9460):671-9.
183. Andre F, Job B, Dessen P, Tordai A, Michiels S, Liedtke C, et al. Molecular characterization of breast cancer with high-resolution oligonucleotide comparative genomic hybridization array. Clin Cancer Res. 2009 Jan 15;15(2):441-51.
184. Hess KR, Anderson K, Symmans WF, Valero V, Ibrahim N, Mejia JA, et al. Pharmacogenomic predictor of sensitivity to preoperative chemotherapy with paclitaxel and fluorouracil, doxorubicin, and cyclophosphamide in breast cancer. J Clin Oncol. 2006 Sep 10;24(26):4236-44.
185. Miller LD, Smeds J, George J, Vega VB, Vergara L, Ploner A, et al. An expression signature for p53 status in human breast cancer predicts mutation status, transcriptional effects, and patient survival. Proc Natl Acad Sci U S A. 2005 Sep 20;102(38):13550-5.
186. Li Y, Zou L, Li Q, Haibe-Kains B, Tian R, Desmedt C, et al. Amplification of LAPTM4B and YWHAZ contributes to chemotherapy resistance and recurrence of breast cancer. Nat Med. 2010 Feb;16(2):214-8.
187. http://www.ncbi.nlm.nih.gov/projects/geo/query/acc.cgi?acc=GSE2109.
188. Baker DJ, Jeganathan KB, Cameron JD, Thompson M, Juneja S, Kopecka A, et al. BubR1 insufficiency causes early onset of aging-associated phenotypes and infertility in mice. Nat Genet. 2004 Jul;36(7):744-9.
189. Benjamini Y, Hochberg Y. Controlling the False Discovery Rate: A Practical and Powerful Approach to Multiple Testing. Journal of the Royal Statistical Society Series B (Methodological). 1995;57(1):289-300.
190. Petit E, Milano G, Levi F, Thyss A, Bailleul F, Schneider M. Circadian rhythm-varying plasma concentration of 5-fluorouracil during a five-day continuous venous infusion at a constant rate in cancer patients. Cancer Res. 1988 Mar 15;48(6):1676-9.
191. Harris BE, Song R, Soong SJ, Diasio RB. Relationship between dihydropyrimidine dehydrogenase activity and plasma 5-fluorouracil levels with evidence for circadian variation of enzyme activity and plasma drug levels in cancer patients receiving 5-fluorouracil by protracted continuous infusion. Cancer Res. 1990 Jan 1;50(1):197-201.
192. Barratt PL, Seymour MT, Stenning SP, Georgiades I, Walker C, Birbeck K, et al. DNA markers predicting benefit from adjuvant fluorouracil in patients with colon cancer: a molecular study. Lancet. 2002 Nov 2;360(9343):1381-91.
193. Sinicrope FA, Rego RL, Halling KC, Foster N, Sargent DJ, La Plant B, et al. Prognostic impact of microsatellite instability and DNA ploidy in human colon carcinoma patients. Gastroenterology. 2006 Sep;131(3):729-37.
194. Ahnen DJ, Feigl P, Quan G, Fenoglio-Preiser C, Lovato LC, Bunn PA, Jr., et al. Ki-ras mutation and p53 overexpression predict the clinical behavior of colorectal cancer: a Southwest Oncology Group study. Cancer Res. 1998 Mar 15;58(6):1149-58.
195. Gill S, Loprinzi CL, Sargent DJ, Thome SD, Alberts SR, Haller DG, et al. Pooled analysis of fluorouracil-based adjuvant therapy for stage II and III colon cancer: who benefits and by how much? J Clin Oncol. 2004 May 15;22(10):1797-806.
196. Baretton G, Gille J, Oevermann E, Lohrs U. Flow-cytometric analysis of the DNA-content in paraffin-embedded tissue from colorectal carcinomas and its prognostic significance. Virchows Arch B Cell Pathol Incl Mol Pathol. 1991;60(2):123-31.

197. Berczi C, Bocsi J, Bartha I, Math J, Balazs G. Prognostic value of DNA ploidy status in patients with rectal cancer. Anticancer Res. 2002 Nov-Dec;22(6B):3737-41.
198. Chang KJ, Enker WE, Melamed M. Influence of tumor cell DNA ploidy on the natural history of rectal cancer. Am J Surg. 1987 Feb;153(2):184-8.
199. Chapman MA, Hardcastle JD, Armitage NC. Five-year prospective study of DNA tumor ploidy and colorectal cancer survival. Cancer. 1995 Aug 1;76(3):383-7.
200. Emdin SO, Stenling R, Roos G. Prognostic value of DNA content in colorectal carcinoma. A flow cytometric study with some methodologic aspects. Cancer. 1987 Sep 15;60(6):1282-7.
201. Geido E, Sciutto A, Rubagotti A, Oliani C, Monaco R, Risio M, et al. Combined DNA flow cytometry and sorting with k-ras2 mutation spectrum analysis and the prognosis of human sporadic colorectal cancer. Cytometry. 2002 Aug 15;50(4):216-24.
202. Harlow SP, Eriksen BL, Poggensee L, Chmiel JS, Scarpelli DG, Murad T, et al. Prognostic implications of proliferative activity and DNA aneuploidy in Astler-Coller Dukes stage C colonic adenocarcinomas. Cancer Res. 1991 May 1;51(9):2403-9.
203. Heimann TM, Miller F, Martinelli G, Mester J, Kurtz RJ, Szporn A, et al. Significance of DNA content abnormalities in small rectal cancers. Am J Surg. 1990 Feb;159(2):199-202; discussion -3.
204. Jass JR, Mukawa K, Goh HS, Love SB, Capellaro D. Clinical importance of DNA content in rectal cancer measured by flow cytometry. J Clin Pathol. 1989 Mar;42(3):254-9.
205. Jones DJ, Moore M, Schofield PF. Prognostic significance of DNA ploidy in colorectal cancer: a prospective flow cytometric study. Br J Surg. 1988 Jan;75(1):28-33.
206. Karelia NH, Patel DD, Desai NS, Mehta HV, Yadav PK, Patel SM, et al. Prognostic significance of DNA aneuploidy and p21 ras oncoprotein expression in colorectal cancer and their role in the determination of treatment modalities. Int J Biol Markers. 2001 Apr-Jun;16(2):97-104.
207. Kay EW, Mulcahy HE, Curran B, O'Donoghue DP, Leader M. An image analysis study of DNA content in early colorectal cancer. Eur J Cancer. 1996 Apr;32A(4):612-6.
208. Kokal WA, Gardine RL, Sheibani K, Morris PL, Prager E, Zak IW, et al. Tumor DNA content in resectable, primary colorectal carcinoma. Ann Surg. 1989 Feb;209(2):188-93.
209. Lanza G, Gafa R, Santini A, Maestri I, Dubini A, Gilli G, et al. Prognostic significance of DNA ploidy in patients with stage II and stage III colon carcinoma: a prospective flow cytometric study. Cancer. 1998 Jan 1;82(1):49-59.
210. Offerhaus GJ, De Feyter EP, Cornelisse CJ, Tersmette KW, Floyd J, Kern SE, et al. The relationship of DNA aneuploidy to molecular genetic alterations in colorectal carcinoma. Gastroenterology. 1992 May;102(5):1612-9.
211. Purdie CA, Piris J. Histopathological grade, mucinous differentiation and DNA ploidy in relation to prognosis in colorectal carcinoma. Histopathology. 2000 Feb;36(2):121-6.
212. Risques RA, Moreno V, Marcuello E, Petriz J, Cancelas JA, Sancho FJ, et al. Redefining the significance of aneuploidy in the prognostic assessment of colorectal cancer. Lab Invest. 2001 Mar;81(3):307-15.
213. Robey-Cafferty SS, el-Naggar AK, Grignon DJ, Cleary KR, Ro JY. Histologic parameters and DNA ploidy as predictors of survival in stage B adenocarcinoma of colon and rectum. Mod Pathol. 1990 May;3(3):261-6.

214. Sinicrope FA, Hart J, Hsu HA, Lemoine M, Michelassi F, Stephens LC. Apoptotic and mitotic indices predict survival rates in lymph node-negative colon carcinomas. Clin Cancer Res. 1999 Jul;5(7):1793-804.
215. Sun XF, Carstensen JM, Stal O, Zhang H, Nilsson E, Sjodahl R, et al. Prognostic significance of p53 expression in relation to DNA ploidy in colorectal adenocarcinoma. Virchows Arch A Pathol Anat Histopathol. 1993;423(6):443-8.
216. Tang R, Ho YS, You YT, Hsu KC, Chen JS, Changchien CR, et al. Prognostic evaluation of DNA flow cytometric and histopathologic parameters of colorectal cancer. Cancer. 1995 Nov 15;76(10):1724-30.
217. Tonouchi H, Matsumoto K, Kinoshita T, Itoh H, Suzuki H. Prognostic value of DNA ploidy patterns of colorectal adenocarcinoma: univariate and multivariate analysis. Dig Surg. 1998;15(6):687-92.
218. Tsuchiya A, Ando Y, Ishii Y, Yoshida T, Abe R. Flow cytometric DNA analysis in Japanese colorectal cancer. A multivariate analysis. Eur J Surg Oncol. 1992 Dec;18(6):585-90.
219. Venkatesh KS, Weingart DJ, Ramanujam PJ. Comparison of double and single parameters in DNA analysis for staging and as a prognostic indicator in patients with colon and rectal carcinoma. Dis Colon Rectum. 1994 Nov;37(11):1142-7.
220. Visscher DW, Zarbo RJ, Ma CK, Sakr WA, Crissman JD. Flow cytometric DNA and clinicopathologic analysis of Dukes' A&B colonic adenocarcinomas: a retrospective study. Mod Pathol. 1990 Nov;3(6):709-12.
221. Zoras OI, Curti G, Cooke TG, Vlachonikolis IG, Forster G, McArdle CS, et al. Prognostic value of ploidy of primary tumour and nodal secondaries in colorectal cancers. Surg Oncol. 1994 Dec;3(6):345-9.
222. Baretton GB, Vogt M, Muller C, Diebold J, Schneiderbanger K, Schmidt M, et al. Prognostic significance of p53 expression, chromosome 17 copy number, and DNA ploidy in non-metastasized colorectal carcinomas (stages IB and II). Scand J Gastroenterol. 1996 May;31(5):481-9.
223. Bottger TC, Gabbert HE, Stockle M, Wellek S, Hils R, Heintz A, et al. DNA image cytometry: a prognostic tool in rectal cancer? Dis Colon Rectum. 1992 May;35(5):436-43.
224. Chen HS, Sheen-Chen SM, Lu CC. DNA index and S-phase fraction in curative resection of colorectal adenocarcinoma: analysis of prognosis and current trends. World J Surg. 2002 May;26(5):626-30.
225. Cosimelli M, D'Agnano I, Tedesco M, D'Angelo C, Botti C, Giannarelli D, et al. The role of multiploidy as unfavorable prognostic variable in colorectal cancer. Anticancer Res. 1998 May-Jun;18(3B):1957-65.
226. Hixon C, Furlong J, Silbergleit A. Flow cytometry in colon cancer: does flow cytometric cell cycle analysis help predict for short-term recurrence in patients with colorectal carcinoma? J Natl Med Assoc. 1995 Nov;87(11):803-6.
227. Lammering G, Taher MM, Gruenagel HH, Borchard F, Porschen R. Alteration of DNA ploidy status and cell proliferation induced by preoperative radiotherapy is a prognostic factor in rectal cancer. Clin Cancer Res. 2000 Aug;6(8):3215-21.
228. Michel P, Paresy M, Lepessot F, Hellot MF, Paillot B, Scotte M, et al. Pre-operative kinetic parameter determination of colorectal adenocarcinomas. Prognostic significance. Eur J Gastroenterol Hepatol. 2000 Mar;12(3):275-80.

229. Moran MR, Rothenberger DA, Gallo RA, Goldberg SM, James EC. Multifactorial analysis of local recurrences in rectal cancer, including DNA ploidy studies: a predictive model. World J Surg. 1993 Nov-Dec;17(6):801-5.
230. Sampedro A, Salas-Bustamante A, Lopez-Artimez M, Garcia-Muniz JL, Urdiales G. Cell cycle flow cytometric analysis in the diagnosis and management of colorectal carcinoma. Anal Quant Cytol Histol. 1999 Aug;21(4):347-52.
231. Tomoda H, Kakeji Y, Furusawa M. Prognostic significance of flow cytometric analysis of DNA content in colorectal cancer: a prospective study. J Surg Oncol. 1993 Jul;53(3):144-8.
232. Albe X, Vassilakos P, Helfer-Guarnori K, Givel JC, de Quay N, Suardet L, et al. Independent prognostic value of ploidy in colorectal cancer. A prospective study using image cytometry. Cancer. 1990 Sep 15;66(6):1168-75.
233. Vermeulen SJ, Chen TR, Speleman F, Nollet F, Van Roy FM, Mareel MM. Did the Four Human Cancer Cell Lines DLD-1, HCT-15, HCT-8, and HRT-18 Originate from One and the Same Patient? Cancer Genetics and Cytogenetics. 1998;107(1):76-9.
234. Chen TR, Dorotinsky CS, McGuire LJ, Macy ML, Hay RJ. DLD-1 and HCT-15 cell lines derived separately from colorectal carcinomas have totally different chromosome changes but the same genetic origin. Cancer Genetics and Cytogenetics. [doi: 10.1016/0165-4608(94)00225-Z]. 1995;81(2):103-8.
235. Melcher R, Steinlein C, Feichtinger W, Muller CR, Menzel T, Luhrs H, et al. Spectral karyotyping of the human colon cancer cell lines SW480 and SW620. Cytogenet Cell Genet. 2000;88(1-2):145-52.
236. Jeganathan K, Malureanu L, Baker DJ, Abraham SC, van Deursen JM. Bub1 mediates cell death in response to chromosome missegregation and acts to suppress spontaneous tumorigenesis. The Journal of Cell Biology. 2007 October 22, 2007;179(2):255-67.
237. Thompson SL, Compton DA. Proliferation of aneuploid human cells is limited by a p53-dependent mechanism. The Journal of Cell Biology. 2010 February 8, 2010;188(3):369-81.
238. Luo J, Emanuele MJ, Li D, Creighton CJ, Schlabach MR, Westbrook TF, et al. A genome-wide RNAi screen identifies multiple synthetic lethal interactions with the Ras oncogene. Cell. 2009 May 29;137(5):835-48.
239. Ngo VN, Davis RE, Lamy L, Yu X, Zhao H, Lenz G, et al. A loss-of-function RNA interference screen for molecular targets in cancer. Nature. 2006 May 4;441(7089):106-10.
240. Schlabach MR, Luo J, Solimini NL, Hu G, Xu Q, Li MZ, et al. Cancer proliferation gene discovery through functional genomics. Science. 2008 Feb 1;319(5863):620-4.
241. http://www.ttplabtech.com/products/acumen/index.html.
242. Martin-Lluesma S, Stucke VM, Nigg EA. Role of Hec1 in Spindle Checkpoint Signaling and Kinetochore Recruitment of Mad1/Mad2. Science. 2002 September 27, 2002;297(5590):2267-70.
243. Jiang M, Instrell R, Saunders B, Berven H, Howell M. Tales from an academic RNAi screening facility; FAQs. Brief Funct Genomics. 2011 Apr 28.
244. Venables, W. Ripley B. Modern Applied Statistics with S (4ed.): Springer Verlag; 2002.
245. Wood S. Generalized Additive Models: An Introduction with R : Chapman and Hall / CRC; 2006.

246. Bommi-Reddy A, Almeciga I, Sawyer J, Geisen C, Li W, Harlow E, et al. Kinase requirements in human cells: III. Altered kinase requirements in VHL-/- cancer cells detected in a pilot synthetic lethal screen. Proc Natl Acad Sci U S A. 2008 Oct 28;105(43):16484-9.
247. Potratz JC, Saunders DN, Wai DH, Ng TL, McKinney SE, Carboni JM, et al. Synthetic lethality screens reveal RPS6 and MST1R as modifiers of insulin-like growth factor-1 receptor inhibitor activity in childhood sarcomas. Cancer Res. 2010 Nov 1;70(21):8770-81.
248. Wang Y, Ngo VN, Marani M, Yang Y, Wright G, Staudt LM, et al. Critical role for transcriptional repressor Snail2 in transformation by oncogenic RAS in colorectal carcinoma cells. Oncogene. 2010 Aug 19;29(33):4658-70.
249. Barbie DA, Tamayo P, Boehm JS, Kim SY, Moody SE, Dunn IF, et al. Systematic RNA interference reveals that oncogenic KRAS-driven cancers require TBK1. Nature. 2009 Nov 5;462(7269):108-12.
250. Scholl C, Frohling S, Dunn IF, Schinzel AC, Barbie DA, Kim SY, et al. Synthetic lethal interaction between oncogenic KRAS dependency and STK33 suppression in human cancer cells. Cell. 2009 May 29;137(5):821-34.
251. Kim SY, Dunn IF, Firestein R, Gupta P, Wardwell L, Repich K, et al. CK1epsilon is required for breast cancers dependent on beta-catenin activity. PLoS ONE. 2010;5(2):e8979.
252. Rao DD, Vorhies JS, Senzer N, Nemunaitis J. siRNA vs. shRNA: Similarities and differences. Advanced Drug Delivery Reviews. [doi: 10.1016/j.addr.2009.04.004]. 2009;61(9):746-59.
253. Babij C, Zhang Y, Kurzeja RJ, Munzli A, Shehabeldin A, Fernando M, et al. STK33 Kinase Activity is Non-Essential in KRAS-Dependent Cancer Cells. Cancer Research. 2011 July 8, 2011.
254. Martin SA, Hewish M, Sims D, Lord CJ, Ashworth A. Parallel High-Throughput RNA Interference Screens Identify PINK1 as a Potential Therapeutic Target for the Treatment of DNA Mismatch Repair,ÄìDeficient Cancers. Cancer Research. 2011 March 1, 2011;71(5):1836-48.
255. Hattori H, Skoulidis F, Russell P, Venkitaraman AR. Context dependence of checkpoint kinase 1 as a therapeutic target for pancreatic cancers deficient in the BRCA2 tumor suppressor. Mol Cancer Ther. 2011 Apr;10(4):670-8.
256. Sarthy AV, Morgan-Lappe SE, Zakula D, Vernetti L, Schurdak M, Packer JC, et al. Survivin depletion preferentially reduces the survival of activated K-Ras-transformed cells. Mol Cancer Ther. 2007 Jan;6(1):269-76.
257. Gilbert P, Collier PJ, Brown MR. Influence of growth rate on susceptibility to antimicrobial agents: biofilms, cell cycle, dormancy, and stringent response. Antimicrob Agents Chemother. 1990 Oct;34(10):1865-8.
258. Persengiev SP, Zhu X, Green MR. Nonspecific, concentration-dependent stimulation and repression of mammalian gene expression by small interfering RNAs (siRNAs). RNA. 2004 Jan;10(1):12-8.
259. Jackson AL, Bartz SR, Schelter J, Kobayashi SV, Burchard J, Mao M, et al. Expression profiling reveals off-target gene regulation by RNAi. Nat Biotechnol. 2003 Jun;21(6):635-7.
260. Sacher R, Stergiou L, Pelkmans L. Lessons from genetics: interpreting complex phenotypes in RNAi screens. Curr Opin Cell Biol. 2008 Aug;20(4):483-9.

261. Erfle H, Neumann B, Liebel U, Rogers P, Held M, Walter T, et al. Reverse transfection on cell arrays for high content screening microscopy. Nat Protocols. [10.1038/nprot.2006.483]. 2007;2(2):392-9.
262. Jaulin F, Kreitzer G. KIF17 stabilizes microtubules and contributes to epithelial morphogenesis by acting at MT plus ends with EB1 and APC. J Cell Biol. 2010 Aug 9;190(3):443-60.
263. Sasagawa Y, Urano T, Kohara Y, Takahashi H, Higashitani A. Caenorhabditis elegans RBX1 is essential for meiosis, mitotic chromosomal condensation and segregation, and cytokinesis. Genes Cells. 2003 Nov;8(11):857-72.
264. Rubinfeld B, Albert I, Porfiri E, Fiol C, Munemitsu S, Polakis P. Binding of GSK3beta to the APC-beta-catenin complex and regulation of complex assembly. Science. 1996 May 17;272(5264):1023-6.
265. Gordon MD, Nusse R. Wnt Signaling: Multiple Pathways, Multiple Receptors, and Multiple Transcription Factors. Journal of Biological Chemistry. 2006 August 11, 2006;281(32):22429-33.
266. Bahmanyar S, Kaplan DD, Deluca JG, Giddings TH, Jr., O'Toole ET, Winey M, et al. beta-Catenin is a Nek2 substrate involved in centrosome separation. Genes Dev. 2008 Jan 1;22(1):91-105.
267. Kaplan DD, Meigs TE, Kelly P, Casey PJ. Identification of a role for beta-catenin in the establishment of a bipolar mitotic spindle. J Biol Chem. 2004 Mar 19;279(12):10829-32.
268. Zhang J, Yan X, Shi C, Yang X, Guo Y, Tian C, et al. Structural basis of beta-catenin recognition by Tax-interacting protein-1. J Mol Biol. 2008 Dec 5;384(1):255-63.
269. Ellwanger K, Saito H, Clement-Lacroix P, Maltry N, Niedermeyer J, Lee WK, et al. Targeted disruption of the Wnt regulator Kremen induces limb defects and high bone density. Mol Cell Biol. 2008 Aug;28(15):4875-82.
270. Morris AR, Mukherjee N, Keene JD. Ribonomic analysis of human Pum1 reveals cis-trans conservation across species despite evolution of diverse mRNA target sets. Mol Cell Biol. 2008 Jun;28(12):4093-103.
271. Brito DA, Rieder CL. Mitotic checkpoint slippage in humans occurs via cyclin B destruction in the presence of an active checkpoint. Curr Biol. 2006 Jun 20;16(12):1194-200.
272. Martinsson-Ahlzen HS, Liberal V, Grunenfelder B, Chaves SR, Spruck CH, Reed SI. Cyclin-dependent kinase-associated proteins Cks1 and Cks2 are essential during early embryogenesis and for cell cycle progression in somatic cells. Mol Cell Biol. 2008 Sep;28(18):5698-709.
273. Blacque OE, Reardon MJ, Li C, McCarthy J, Mahjoub MR, Ansley SJ, et al. Loss of C. elegans BBS-7 and BBS-8 protein function results in cilia defects and compromised intraflagellar transport. Genes Dev. 2004 Jul 1;18(13):1630-42.
274. Delaval B, Bright A, Lawson ND, Doxsey S. The cilia protein IFT88 is required for spindle orientation in mitosis. Nat Cell Biol. [10.1038/ncb2202]. 2011;13(4):461-8.
275. Berbari NF, Johnson AD, Lewis JS, Askwith CC, Mykytyn K. Identification of Ciliary Localization Sequences within the Third Intracellular Loop of G Protein-coupled Receptors. Mol Biol Cell. 2008 April 1, 2008;19(4):1540-7.
276. Lee AJX, Roylance R, Sander J, Gorman P, Endesfelder D, Kschischo M, et al. CERT depletion predicts chemotherapy benefit and mediates cytotoxic and polyploid-

specific cancer cell death through autophagy induction. The Journal of Pathology. [10.1002/path.2998]. 2012;226(3):482-94.
277. Lee AJX, East P, Pepper S, Nicke B, Szallasi Z, Eklund AC, et al. Concordance of exon array and real-time PCR assessment of gene expression following cancer cell cytotoxic drug exposure. Cell Cycle. 2008 Dec 15;7(24):3947-8.
278. Toth B, Balla A, Ma H, Knight ZA, Shokat KM, Balla T. Phosphatidylinositol 4-kinase IIIbeta regulates the transport of ceramide between the endoplasmic reticulum and Golgi. J Biol Chem. 2006 Nov 24;281(47):36369-77.
279. Dallas PB, Gottardo NG, Firth MJ, Beesley AH, Hoffmann K, Terry PA, et al. Gene expression levels assessed by oligonucleotide microarray analysis and quantitative real-time RT-PCR -- how well do they correlate? BMC Genomics. 2005;6:59.
280. Morey JS, Ryan JC, Van Dolah FM. Microarray validation: factors influencing correlation between oligonucleotide microarrays and real-time PCR. Biol Proced Online. 2006;8:175-93.
281. Eklund AC, Turner LR, Chen P, Jensen RV, deFeo G, Kopf-Sill AR, et al. Replacing cRNA targets with cDNA reduces microarray cross-hybridization. Nat Biotechnol. 2006 Sep;24(9):1071-3.
282. Saftig P, Beertsen W, Eskelinen EL. LAMP-2: a control step for phagosome and autophagosome maturation. Autophagy. 2008 May 16;4(4):510-2.
283. Mehrpour M, Esclatine A, Beau I, Codogno P. Overview of macroautophagy regulation in mammalian cells. Cell Res. 2010 Jul;20(7):748-62.
284. Sahin O, Frohlich H, Lobke C, Korf U, Burmester S, Majety M, et al. Modeling ERBB receptor-regulated G1/S transition to find novel targets for de novo trastuzumab resistance. BMC Systems Biology. 2009;3(1):1.
285. Gyorffy B, Lanczky A, Eklund AC, Denkert C, Budczies J, Li Q, et al. An online survival analysis tool to rapidly assess the effect of 22,277 genes on breast cancer prognosis using microarray data of 1,809 patients. Breast Cancer Res Treat. 2010 Oct;123(3):725-31.
286. Juul N, Szallasi Z, Eklund AC, Li Q, Burrell RA, Gerlinger M, et al. Assessment of an RNA interference screen-derived mitotic and ceramide pathway metagene as a predictor of response to neoadjuvant paclitaxel for primary triple-negative breast cancer: a retrospective analysis of five clinical trials. The Lancet Oncology. 2010;11(4):358-65.
287. Demasters G, Di X, Newsham I, Shiu R, Gewirtz DA. Potentiation of radiation sensitivity in breast tumor cells by the vitamin D3 analogue, EB 1089, through promotion of autophagy and interference with proliferative recovery. Mol Cancer Ther. 2006 Nov;5(11):2786-97.
288. Gewirtz DA, Hilliker ML, Wilson EN. Promotion of autophagy as a mechanism for radiation sensitization of breast tumor cells. Radiother Oncol. 2009 Sep;92(3):323-8.
289. Hoyer-Hansen M, Jaattela M. Autophagy: an emerging target for cancer therapy. Autophagy. 2008 Jul 1;4(5):574-80.
290. de Bruin EC, Medema JP. Apoptosis and non-apoptotic deaths in cancer development and treatment response. Cancer Treat Rev. 2008 Dec;34(8):737-49.
291. Spassieva SD, Mullen TD, Townsend DM, Obeid LM. Disruption of ceramide synthesis by CerS2 down-regulation leads to autophagy and the unfolded protein response. Biochem J. 2009 Sep 3.

292. Daido S, Kanzawa T, Yamamoto A, Takeuchi H, Kondo Y, Kondo S. Pivotal role of the cell death factor BNIP3 in ceramide-induced autophagic cell death in malignant glioma cells. Cancer Res. 2004 Jun 15;64(12):4286-93.
293. Settembre C, Di Malta C, Polito VA, Arencibia MG, Vetrini F, Erdin S, et al. TFEB Links Autophagy to Lysosomal Biogenesis. Science. 2011 June 17, 2011;332(6036):1429-33.
294. Ellsworth RE, Ellsworth DL, Patney HL, Deyarmin B, Love B, Hooke JA, et al. Amplification of HER2 is a marker for global genomic instability. BMC Cancer. 2008;8:297.
295. Holland AJ, Cleveland DW. Boveri revisited: chromosomal instability, aneuploidy and tumorigenesis. Nat Rev Mol Cell Biol. [10.1038/nrm2718]. 2009;10(7):478-87.
296. Wolley RC, Schreiber K, Koss LG, Karas M, Sherman A. DNA distribution in human colon carcinomas and its relationship to clinical behavior. J Natl Cancer Inst. 1982 Jul;69(1):15-22.
297. Bouchet BP, Bertholon J, Falette N, Audoynaud C, Lamblot C, Puisieux A, et al. Paclitaxel resistance in untransformed human mammary epithelial cells is associated with an aneuploidy-prone phenotype. Br J Cancer. 2007;97(9):1218-24.
298. Eskelinen E-L, Illert AL, Tanaka Y, Schwarzmann G, Blanz J, von Figura K, et al. Role of LAMP-2 in Lysosome Biogenesis and Autophagy. Mol Biol Cell. 2002 September 1, 2002;13(9):3355-68.
299. Impens F, Van Damme P, Demol H, Van Damme J, Vandekerckhove J, Gevaert K. Mechanistic insight into taxol-induced cell death. Oncogene. 2008.